Universitat Politècnica de València
Departamento de Máquinas y Motores Térmicos


Doctoral Thesis

# Influence of inter-jet spacing on the diesel spray formation and combustion

*Presented by:*
Tomás Enrique Montiel Prieto

*Supervised by:*
Dr. Raúl Payri Marín

*in fulfillment of the requirements for the degree of*
Doctor of Philosophy

Valencia, March 2022

Ph.D. Thesis

# Influence of inter-jet spacing on the diesel spray formation and combustion


Written by: Mr. Tomás Enrique Montiel Prieto
Supervised by: Dr. Raúl Payri Marín


*Examination committee:*

Chairman: Dr. José María García Oliver
Secretary: Dr. María del Pilar Dorado Pérez
Member: Dr. Walter Martín Vera-Tudela Fajardo

*Reviewing board:*

Dr. Luigi Alloca
Dr. Angelo Onorati
Dr. Walter Martín Vera-Tudela Fajardo

Valencia, March 2022

## Abstract

The growing public aversion to internal combustion engines has led to a strong desire to shift towards renewable and cleaner energy sources. However, it is still hard to replace petroleum-derived liquid fuels as the primary energy source, mainly due to their plenty of availability, reliability, and affordability. Then, efforts have to come from the research community to increase the efficiency of these engines for the benefit of society.

Regarding diesel engines, one implemented technique has been to increase the number of outlet holes of the injector and reduce their diameters, enhancing the air/fuel mixing process. Nevertheless, as the number of holes in the nozzle increases, so does the proximity between them, leading to a reduction in the space available for each jet to develop without interacting with the neighbor sprays. This interaction could affect the combustion event, and its implications have not been entirely defined.

Thus, the present thesis aimed to analyze the influence of inter-jet spacing on the injection development and enhance the methodology employed in the institute to study injection events of multi-holes injectors, accounting for the interactions between jets.

To this end, two diesel injectors with six outlet orifices were manufactured by Continental with identical design, except for the geometric distribution of the outlet holes of each nozzle, as they were specifically allocated to study the influence of inter-jet spacing on the injection event. Concretely, the first injector allowed the study of the development of an isolated spray on one side and a spray with an inter-jet spacing of 30° on the other side during the same injection event. Moreover, the second injector has two additional orifices distributions, so a total of three inter-jet spacing configurations (30° - 36° - 45°) were compared to the performance of the isolated spray (spacing = 120°). Additionally, a novel optical window and high-temperature ceramic mirror were successfully tested.

The results were grouped into analyses under non-reactive and reactive environments. The experiments under a non-reactive environment were mainly done to assess the similarity or variance in performance due to fabrication differences between the injectors, finding that the inter-jet spacing did not affect the injection event under non-reactive conditions.

Then, the studies focused on the injection event under a reactive environment, analyzing the influence of inter-jet spacing on the ignition delay, lift-off length, and soot formation.

Regarding the ignition delay, sprays with neighbor jets tended to have

equal or slightly smaller ignition delay values under poor mixing and ignition conditions (low rail pressure, chamber temperature, or chamber density conditions). On the other hand, the opposite effect was generally observed as the boundary conditions were overall increased, with equal or higher ignition delay values within sprays with neighbor jets, compared to that of the isolated spray. Nonetheless, no clear trend was defined, with complex interactions and multiple factors simultaneously affecting the ignition event.

On the lift-off length, the results showed that after certain proximity between sprays is reached, the interaction between the jets becomes a predominant factor in their behavior, and the lift-off length is considerably reduced. Moreover, as the inter-jet spacing increases, the performance gradually approaches that obtained from the isolated spray. Plausibly, closely spaced sprays entrain a higher amount of hot combustion products and radicals. Then, the entrained gas with a higher temperature could trigger autoignition near the nozzle, reducing the lift-off length. Lastly, a novel regression for the lift-off length was developed, which accounted for the effect of the proximity between sprays.

Respecting the soot formation, the sprays with closely spaced neighbor jets (30° and 36°) generally had higher optical thickness KL and peak soot mass values for a given boundary condition when compared to the development of the isolated spray. These trends are in line with the lift-off length results observed, in which the closely spaced jets had a shorter lift-off length due to (plausibly) hot gases re-entrainment. This shortening would deteriorate the air/fuel mixing process and, consequently, combustion happens in richer mixture conditions that are suitable for soot formation. On the other hand, the impact of the inter-jet spacing was smaller as the boundary conditions promoting soot formation were enhanced, that is, increasing the ambient density, ambient temperature, or reducing the rail pressure.

Additionally, the influence of the chamber temperature, chamber density, and rail pressure on the spray behavior was assessed. The observed impact of these parameters on the spray followed the trends found in the literature and served to validate the consistency of the work done.

## Resumen

La creciente aversión pública contra los motores de combustión interna ha llevado a un fuerte deseo de cambio hacia fuentes de energía renovables y más limpias. Sin embargo, todavía es difícil reemplazar los combustibles líquidos derivados del petróleo como fuente primaria de energía, principalmente debido a su gran disponibilidad, confiabilidad, y asequibilidad. Por lo tanto, la comunidad científica debe mantener los esfuerzos para aumentar la eficiencia de estos motores en beneficio de la sociedad.

Con respecto a los motores diésel, una técnica implementada ha sido aumentar el número de orificios de salida del inyector y reducir sus diámetros, mejorando el proceso de mezcla aire/combustible. Sin embargo, a medida que aumenta el número de orificios en la boquilla, también aumenta la proximidad entre ellos, lo que lleva a una reducción en el espacio disponible para que cada chorro se desarrolle sin interactuar con los chorros adyacentes. Esta interacción podría afectar el evento de combustión y sus implicaciones no se han definido por completo.

De esta manera, la presente tesis tuvo como objetivo analizar la influencia del espaciamiento entre chorros en el desarrollo de la inyección, y mejorar la metodología empleada en el instituto para estudiar el chorro en inyectores multi-orificios, teniendo en cuenta las interacciones entre chorros.

Con este objetivo, Continental fabricó dos inyectores diésel idénticos excepto por la distribución geométrica de los orificios de salida de cada boquilla, ya que se destinaron específicamente a estudiar la influencia del espaciamiento entre chorros en el evento de inyección. Concretamente, el primer inyector permitió estudiar, durante el mismo evento de inyección, el desarrollo de un chorro aislado en un lado de la boquilla y, en la cara opuesta, cinco chorros con un espaciamiento entre ellos de 30°. Por otro lado, el segundo inyector tiene dos distribuciones de orificios adicionales, por lo que un total de tres configuraciones de espaciado entre chorros (30° - 36° - 45°) fueron comparadas con el rendimiento del chorro aislado (espaciado = 120°). Además, se probaron con éxito una nueva ventana óptica y un espejo de cerámica de alta temperatura.

Los resultados se agruparon en análisis en entorno no reactivo y reactivo. Los experimentos en el entorno no reactivo se realizaron principalmente para evaluar la similitud o la variación en el rendimiento debido a las diferencias de fabricación entre los inyectores, encontrando que el espaciado entre chorros no afectó el evento de inyección en dichas condiciones.

Luego, los estudios se centraron en el desarrollo del chorro en un entorno reactivo, analizando la influencia del espaciado entre chorros en el retraso de

la ignición, la longitud de levantamiento de llama, y la formación de hollín.

Con respecto al retraso de la ignición, los chorros con chorros vecinos tendieron a tener valores de retraso de la ignición iguales o ligeramente inferiores a los del chorro aislado en condiciones pobres de contorno (baja presión del raíl, temperatura, o densidad de la cámara). Por otro lado, el efecto contrario se observó al aumentar los valores de las condiciones de contorno, con valores de retraso de la ignición iguales o más altos para los chorros con chorros vecinos. No obstante, no se observó una tendencia clara, con interacciones complejas y múltiples factores afectando simultáneamente el evento de ignición.

Sobre la longitud de levantamiento de llama, los resultados mostraron que al alcanzar cierta proximidad entre los chorros, la interacción entre ellos se convierte en un factor predominante en su comportamiento, y dicha longitud se reduce considerablemente. Por otro lado, a medida que aumentaba el espaciado entre chorros, la longitud se aproximaba gradualmente a la obtenida con el chorro aislado. Posiblemente, los chorros con poco espaciado entre ellos engloben una mayor cantidad de productos de combustión calientes. Consecuentemente, el gas englobado posee una temperatura más alta y podría desencadenar una autoignición cerca de la boquilla, reduciendo la longitud de levantamiento de llama. Por último, se desarrolló una nueva regresión para la longitud de levantamiento de llama, teniendo en cuenta el efecto de la proximidad entre chorros.

En cuanto a la formación de hollín, los chorros con menor espaciado con sus chorros vecinos (30° y 36°) generalmente tuvieron mayor espesor óptico KL y valores máximos de masa de hollín para una condición de contorno dada, en comparación con el desarrollo del chorro aislado. Estas tendencias están en línea con los resultados de la longitud de levantamiento de llama observados, en los que los chorros estrechamente espaciados tuevieron una longitud más corta debido (posiblemente) al englobamiento de gases calientes. Esta reducción deterioraría el proceso de mezcla de aire/combustible y, en consecuencia, la combustión ocurriría en condiciones de mezcla más ricas que son propicias para la formación de hollín. Por otro lado, el impacto del espaciado entre chorros fue menor a medida que se mejoraron las condiciones de contorno que promueven la formación de hollín, es decir, aumentando la densidad y temperatura de la cámara, o reduciendo la presión del raíl.

Adicionalmente, se evaluó la influencia de la temperatura de la cámara, la densidad de la cámara y la presión del raíl en el desarrollo de la inyección. El impacto de estos parámetros sobre el chorro siguió las tendencias encontradas en la literatura y sirvió para validar la consistencia del trabajo realizado.

## Resum

La creixent aversió pública contra els motors de combustió interna ha portat a un fort desig de canvi cap a fonts d'energia renovables i més netes. Tot i això, encara és difícil substituir els combustibles líquids derivats del petroli com a font primària d'energia, principalment per la seva gran disponibilitat, seguretat, i assequibilitat. Per tant, la comunitat científica ha de mantenir la investigació per tal d'augmentar l'eficiència d'aquests motors en benefici de la societat.

Pel que fa als motors dièsel, una tècnica implementada ha estat augmentar el nombre d'orificis de sortida de l'injector i reduir els seus diàmetres, millorant el procés de barreja aire/combustible. No obstant això, a mesura que augmenta el nombre d'orificis a la tovera, també augmenta la proximitat entre ells, fet que porta a una reducció a l'espai disponible perquè cada raig es desenvolupi sense interactuar amb els dolls adjacents. Aquesta interacció podria afectar l'esdeveniment de la combustió i les seves implicacions no s'han definit del tot.

D'aquesta manera, aquesta tesi va tenir com a objectiu analitzar la influència de l'espaiament entre dolls en el desenvolupament de la injecció, i millorar la metodologia emprada a l'institut per a estudiar els esdeveniments d'injecció d'injectors de múltiples orificis, tenint en compte les interaccions entre dolls.

Amb aquest objectiu, Continental va fabricar dos injectors dièsel amb idèntic disseny intern excepte per la distribució geomètrica dels orificis de sortida de cada tovera, ja que es van destinar específicament a estudiar la influència de l'espaiament entre dolls a l'esdeveniment d'injecció. Concretament, el primer injector va permetre estudiar, durant el mateix esdeveniment d'injecció, el desenvolupament d'un raig solitari en un costat del tovera i, a la cara oposada, cinc raigs amb un espai entre ells de 30°. D'altra banda, el segon injector té dues distribucions d'orificis addicionals, aconseguint que un total de tres configuracions d'espaiat entre dolls (30°-36°-45°) es compararen amb el rendiment del raig solitari (espaiat = 120°). A més, es van provar amb èxit una nova finestra òptica i un mirall de ceràmica d'alta temperatura.

Els resultats es van agrupar en anàlisi en entorn no reactiu i anàlisi en entorn reactiu.. Els experiments a l'entorn no reactiu es van realitzar principalment per tal d'avaluar la similitud o la variació en el rendiment a causa de les diferències de fabricació entre els injectors, trobant que l'espaiat entre dolls no afecta l'esdeveniment d'injecció en aquestes condicions.

Després, els estudis es van centrar en el desenvolupament del raig en un entorn reactiu, analitzant la influència de l'espaiat entre dolls en el retard de

la ignició, la longitud d'aixecament de flama, i la formació de sutge.

Pel que fa al retard de la ignició, els dolls amb dolls adjacents van tendir a tenir valors de retard de la ignició iguals o lleugerament inferiors als del raig solitari en condicions pobres de contorn (baixa pressió del rail, temperatura, o densitat de la càmera). D'altra banda, l'efecte contrari es va observar augmentant els valors de les condicions de contorn, amb valors de retard de la ignició iguals o més alts per als dolls amb dolls adjacents. Tot i això, no es va apreciar un efecte constant, amb interaccions complexes i múltiples factors afectant simultàniament l'esdeveniment d'ignició.

Sobre la longitud d'aixecament de flama, els resultats van mostrar que en assolir certa proximitat entre els dolls, la interacció entre ells es converteix en un factor predominant en el seu comportament, reduint-se considerablement aquesta longitud. D'altra banda, a mesura que augmentava l'espaiat entre dolls, la longitud s'aproximava gradualment a l'obtinguda amb el raig solitari. Possiblement, els raigs amb poc espaiat entre ells englobin una major quantitat de productes de combustió calents. Per tant, el gas englobat té una temperatura més alta i podria desencadenar una autoignició a prop del tovera, reduint la longitud d'aixecament de flama. Finalment, es va desenvolupar una nova regressió per a la longitud d'aixecament de flama, tenint en compte l'efecte de la proximitat entre dolls.

Quant a la formació de sutge, els raigs amb menor espaiat amb els seus raigs adjacents (30° i 36°) generalment van tenir més gruix òptic KL i valors màxims de massa de sutge per a una condició de contorn donada, en comparació amb el desenvolupament del raig solitari. Aquestes tendències estan aliniades amb els resultats de la longitud d'aixecament de flama observats, en què els dolls estretament espaiats van tenir una longitud més curta degut (possiblement) a l'englobament de gasos calents. Aquesta reducció deterioraria el procés de barreja d'aire/combustible i, en per tant, la combustió ocorreria en condicions de mescla més riques que són propícies per a la formació de sutge. D'altra banda, l'impacte de l'espaiat entre dolls va ser menor a mesura que es van millorar les condicions de contorn que promouen la formació de sutge, és a dir, augmentant la densitat i la temperatura de la cambra, o reduint la pressió del rail.

Addicionalment, es va avaluar la influència de la temperatura de la càmera, la densitat de la càmera i la pressió del rail en el desenvolupament de la injecció. L'impacte d'aquests paràmetres sobre el raig va seguir les tendències trobades a la literatura i va servir per validar la consistència del treball realitzat.

*"Isn't it funny how day by day nothing changes, but when you look back, everything is different."*
- C.S. Lewis

*A mis padres.*

## Acknowledgments

I want to start by honoring the key role of my lovely wife, Coco, throughout these research years. Her constant support and love made it possible to achieve the numerous requirements established to get to this latest stage of the Ph.D. I feel very, very fortunate to have her as my life companion.

I'm also deeply thankful to my parents for the love, care, and education they gave me (and my nine brothers). If I'm writing these lines, it is only because of the sacrifices they made for my development. I know I'll never be able to repay them; I hope to replicate at least some of my role models' virtues. Additionally, the long-distance periodical calls with my brothers were always encouraging, so thank you all for those moments.

Regarding CMT, I would like to thank my supervisor Raúl Payri for his constant guidance. His extensive knowledge about the injection-combustion event always admired me. However, I believe the soft skills I learned from him are equally (or more) valuable: His quick problem-solving, project, and group management abilities were always top class. I also appreciate the assistance from the lecturers of the department. Jaime, Marco, Pedro, Javi, and Gabriela all assisted me at some point during the Ph.D.

I can't forget the technicians within the department, Omar and José Enrique, as their support was crucial in setting up the test rigs employed during the experimental measurements. Also, a big thank you to Amparo and Haby in the administrative department. Not all heroes wear capes.

This Ph.D. has also allowed me to have numerous great teammates and friends. When I first arrived, Alberto and Abián, part of the old guard, were my office companions. Naturally, we became friends. Thanks for all the knowledge, fun, and advice shared daily. I also relish the memories with other old guard Ph.D. students, Vico, Jesús, Mary, Mario, Santi, and Armando, the good old days. They all finished their objectives, but my current teammates are second to none.

Kike and Lucas started with me, together with María, who I grew particularly fond of. By the way, I must thank her for all the assistance on the never-ending administrative paperwork. A year later, César joined the team, and it is no secret how close friends we have become. Thanks for all, man. As if it wasn't enough, two old friends and roommates in Venezuela arrived at CMT: Ibra and Sebas, very lucky to have them back. Even though in different departments, the comrade inevitably remained; So many Ronaldos along the way.

Also, my new office teammates and friends, Rami and Victor, have made

daily life quite nice. Finally, I'm also thankful for my friends at the optical techniques department: Felipe, Alba, and Frank. Fantastic people, and I wish we would have developed our friendship earlier in the Ph.D.

I also had the opportunity to meet lovely people during my internship in FHNW, Switzerland. Kai Herrmann permanently provided assistance and attention throughout the exchange, ensuring that I always had everything I needed on a technical and personal aspect. Additionally, Bruno, Pascal, and Dario were always kind and helpful when setting up the experiments. Additionally, I feel lucky to have stayed at Sabine's place, with excellent moments with her and her family, especially Gregory.

Additionally, I want to express my gratitude to Generalitat Valenciana and European Social Fund for the financial support provided through the research grant (ACIF/2018/122).

My last acknowledgment happens to be the most important. I want to thank God. First, I believe all the amazing people mentioned in previous lines were put in my life by Him, so thank you for that: You knocked it out of the park. On the other hand, I also believe that He gave me the strength to reach any ability or achievement I might have acquired throughout this stage (or any stage), and for that, I'm very grateful.

# Contents

# List of Figures

# List of Tables

# Nomenclature

**Acronyms**

| | |
|---|---|
| AHRR | Apparent Heat Release Rate. |
| ASOE | After start of energizing. |
| ASOI | After start of injection. |
| CFD | Computational Fluid Dynamics. |
| CV | Control volume. |
| DBI | Diffused back-illumination. |
| ECN | Engine Combustion Network. |
| EGR | Exhaust Gas Cecirculation. |
| ET | Energizing time. |
| ICE | Internal combustion engine. |
| ID | Ignition delay. |
| IRDCI | Injection Rate Discharge Curve Indicator. |
| LED | Light-emitting diode. |
| LOL | Lift-off length. |
| Ox | Oxygen concentration. |
| ROI | Rate of injection. |
| RSD | Relative standard deviation. |
| SOI | Start of injection. |
| SSI | Second stage ignition. |
| TDC | Top Dead Center. |
| UV | Ultra violet. |

## Greek symbols

| | |
|---|---|
| $\alpha_{sa}$ | Scattering to absorption ratio. |
| $\Delta P$ | Difference between the rail and the back pressure. |
| $\Delta u_f$ | Variation of fuel flow velocity. |
| $\lambda$ | LED wavelength. |
| $\rho$ | Chamber density. |
| $\rho_f$ | Fuel density. |
| $\rho_{soot}$ | Soot density. |
| $\theta$ | Spray spreading angle. |
| $\varepsilon$ | Angular deflection of a ray. |
| $\varpi$ | Surface of the control volume. |

## Latin symbols

| | |
|---|---|
| $\dot{m}_t$ | Theoretical mass flow rate. |
| $\dot{M}$ | Momentum flux. |
| $\dot{m}$ | Mass flow rate. |
| $\overline{D}_o$ | Average outlet diameter. |
| $a_f$ | Speed of sound in the fuel. |
| $A_o$ | Outlet area of the nozzle. |
| $A_{eff}$ | Effective area. |
| $A_{pixel}$ | Pixel area. |
| $C_d$ | Discharge coefficient. |
| $C_M$ | Momentum coefficient. |
| $C_v$ | Velocity coefficient. |
| $D_o$ | Nozzle outlet diameter. |
| $F$ | Force. |
| $f$ | Focal distance. |
| $f_v$ | Soot volume fraction. |
| $I_0$ | Pixel intensity of the background image. |
| $I_{camzero}$ | Pixel intensity of the digital black of the camera. |
| $I_{off}$ | Pixel intensity of the image with LED-off. |
| $I_{on}$ | Pixel intensity of the image with LED-on. |
| $K$ | Dimensional extinction coefficient. |
| $k - factor$ | Orifice conicity factor. |
| $k_e$ | Dimensionless extinction coefficient. |

| | |
|---|---|
| $k_{GD}$ | Gladstone-Dale coefficient. |
| $k_{adjust}$ | Mass scaling factor. |
| $KL$ | Optical thickness related to soot. |
| $KL_{max}$ | Maximum measurable KL. |
| $L$ | Optical path length. |
| $LL$ | Liquid length. |
| $m_{int}$ | Mass integrated from the signal. |
| $m_{soot,\,pixel}$ | Projected soot mass in a pixel. |
| $m_{soot}$ | Soot mass. |
| $n$ | Refractive index. |
| $n_0$ | Refractive index of the surroundings. |
| $n_s$ | Complex refractive index of the soot particles. |
| $O_x$ | Oxygen concentration. |
| $p$ | Pressure (general). |
| $p_0$ | Ambient pressure. |
| $P_b$ | Back pressure. |
| $P_r$ | Rail pressure. |
| $p_{cv}$ | Control volume pressure. |
| $S$ | Spray penetration. |
| $T$ | Chamber temperature. |
| $t$ | Time. |
| $T_0$ | Ambient temperature. |
| $t_b$ | Breakup time. |
| $T_f$ | Fuel temperature. |
| $T_{cv}$ | Control volume temperature. |
| $u$ | Velocity. |
| $u_t$ | Theoretical discharge velocity. |
| $u_{eff}$ | Effective velocity. |
| $u_f$ | Fuel velocity. |
| $V$ | Volume (general). |

# Chapter 1

# Introduction

## 1.1 General context

The rise in popularity of internal combustion engines and the growing environmental awareness have led to the creation of emissions and fuel economy legislation that have been increasingly restrictive throughout the years [1, 2]. These events have motivated researchers to continuously search for improvements in multiple areas of the internal combustion (IC) engine, leading to a notable increase in their efficiency [3–5].

On the other hand, there is a public aversion against these engines, a sentiment driven by politically charged statements, isolated emission scandals, and a lack of data-driven press releases. Nevertheless, the plenty availability, reliability, and affordability of petroleum-derived liquid fuels have set the internal combustion engine (ICE) as the undisputed leader to almost entirely power the current transport of goods and people, essential elements of modern society. Moreover, stationary combustion engines (i.e., generators in power generation facilities) have also been established as a must-have to promote current living standards.

In particular, there are several factors as to why the internal combustion engine should remain highly relevant for the foreseeable future:

- Internal combustion engines have become highly efficient in terms of pollutant emissions, reducing their production levels down a thousandfold in the last decades. Putting it into perspective, particulate emissions

from tire and brake wear are now a more significant scientific cause of concern than engine particulate emissions [6].

- The standard of living has dramatically increased in the last decades. A key element in this development has been the availability of petroleum-derived liquid fuels as an affordable energy source, especially for developing markets. Moreover, the globalization phenomenon has been greatly enhanced by the worldwide transportation infrastructure, which is heavily reliant on internal combustion engines. It would require years of work and massive economic, social, and environmental costs to dismantle this infrastructure completely.

- For light-duty vehicles, alternatives to replace internal combustion engines face environmental and economic challenges, and many problems need to be addressed for significant growth to happen. For instance, battery electric vehicles (BEVs) are not "zero emissions" as long as the upstream production and distribution of electricity generate $CO_2$. Moreover, a considerable amount of energy is required to obtain the raw materials that compose the batteries. Additionally, the toxicity issue related to the battery end-of-cycle needs to be properly addressed [7].

- Furthermore, the percentage of greenhouse gases (GHG) emitted from road transportation remains at around 12% according to the latest breakdown of emissions by sectors and sub-sectors (Figure 1.1) [8]. Thus, a massive complete change to electric vehicles could amount to a global reduction of 12% in GHG emissions at most, assuming that the batteries are produced and charged from energy sources without $CO_2$ emissions, a challenging task.

- Alternatives in heavy-duty transportation (trucks, trains, airplanes) also have these and additional obstacles, which is why little discussion is seen on this area. In particular, the charging times for such massive batteries would not be suitable, and the driving range would also be limited [7, 9].

It is then reasonable that oil remains as the highest source of energy consumption, as seen in Figure 1.2 [10], despite the marketing campaign against this source of energy. Moreover, the share of energy produced from oil has remained relatively stable since 2015 at around 33%. Furthermore, around 60% of this fossil oil is destined for internal combustion engines.

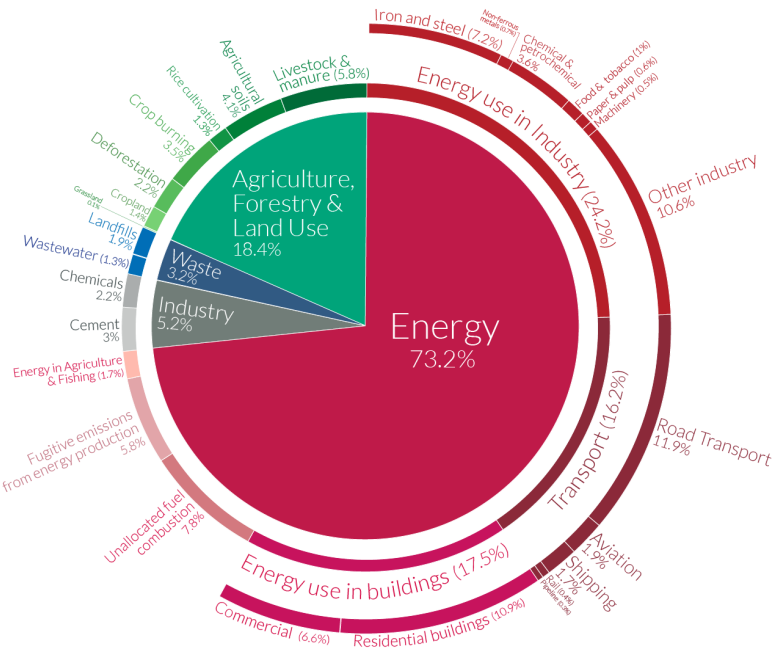


*Figure 1.1: Global greenhouse gas emissions by sector [8].*

On the other hand, it can also be seen that energy coming from renewable sources is seeing rapid growth. However, renewables still only supply a small fraction of the current energy needs (around 5%).

Thus, a situation is set in which there is a strong desire of shifting towards renewable and cleaner energy sources, but it is still hard to replace oil as the primary source of energy. In this sense, as long as demand remains high, efforts have to come from the research community to increase the efficiency of internal combustion engines for the benefit of society.

Regarding the diesel engines, a critical area of study has been the diesel spray injection process, as the air/fuel mixing process has been acknowledged as a critical factor to reduce pollutant emissions during the combustion development [11, 12]. On this matter, numerous techniques have been analyzed and implemented, such as increasing the injection pressure [13–16], employing multiple injection strategies [17–20], improvements of the nozzle geometry [21–23], and so on.

Respecting the nozzle geometry trends, a technique of particular interest for this work is the implementation of injectors with multiple outlet-orifices in the nozzle [24]. In this sense, increasing the number of outlet holes has

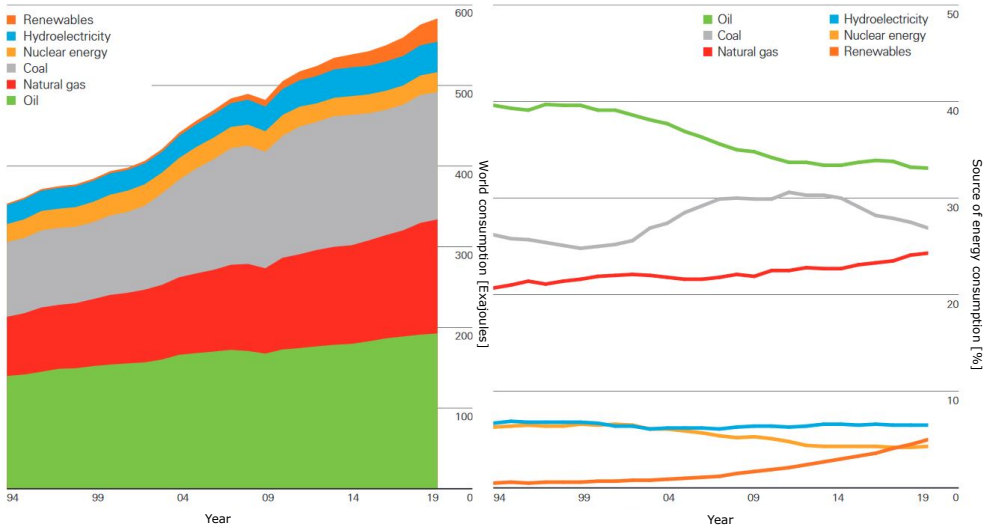


*Figure 1.2: Evolution of the energy consumption by source around the world, in Exajoules (left) and share percentage (right) [10].*

allowed them to have smaller diameters, leading to smaller droplet sizes and enlarging the liquid-gas contact surface. This phenomenon generally leads to more homogeneous mixtures, enhancing the combustion event.

Nevertheless, as the number of holes in the nozzle increases, so does the proximity between them, leading to a reduction in the space available for each jet to develop without interacting with the neighbor sprays. Then, increasing the number of holes presents a trade-off between improving the air entrainment through smaller orifices diameter and providing a larger volume of air between the sprays. In this sense, as the sprays come closer to each other, jet-to-jet interaction could significantly affect the combustion process. This phenomenon is a matter of interest among the research community, and its implications have not been entirely defined [25, 26].

Moreover, many of these works were performed in real diesel engines [27, 28], in which minor modifications were done to gain optical access to the combustion chamber. These studies are important for engine calibration, as the combustion process is carried out under real engine volume and boundary conditions, although these conditions are not entirely controlled or known.

On the other hand, the fundamental analysis through optically accessible test rigs has allowed the visualization of the combustion process in a simplified

and nearly quiescent environment with controlled boundary conditions [29]. Furthermore, a larger optical access is available compared to an engine, easing the implementation of optical diagnostics. Thus, high-fidelity experiments can be performed, focusing on specific parameters to have a greater understanding of the topic of interest [30–32]. Then, these results served as a valuable database to validate models through Computational Fluid Dynamics (CFD), a crucial tool to reduce testing times and production costs. Thus, an optically accessible test rig was employed to obtain most of the results presented in this study.

## 1.2 Objectives and methodology

The current work was developed within the Injection-Combustion group of CMT-Motores Térmicos institute [33]. Over the years, the group has mainly focused on analyzing the isolated spray development by employing single-orifice injectors[34–38]. These studies have allowed for a deep fundamental understanding of the injection and combustion process of the spray.

Moreover, injectors with a single hole give more flexibility on implementing the numerous optical diagnostics techniques, as the injection process can be recorded from different angles without another spray interfering on the field of view of the spray of interest. On the other hand, the visualization of multi-hole nozzles is commonly performed through a single optical access, increasing the complexity of the optical setup.

Nevertheless, injectors with multiple outlet holes have become a standard in the industry, which involves many adjacent jets. The research group is well aware of this trend and has thus done various works with multi-hole injectors [30, 39–41].

However, the analysis is not as developed as with isolated sprays, and the interaction between sprays has not been thoroughly studied. This pattern is also observed in the research community: while comprehensive studies on isolated sprays are readily available, the interaction between jets and its effect on the combustion process has not been entirely defined.

Thus, the current thesis was proposed from the necessity of enhancing the methodology (optical techniques, materials, and image processing) employed to analyze injection events of multi-holes injectors and account for the interactions between jets. Moreover, robust experimental data accounting for the interaction between neighbor sprays was required to enhance a 1-D model capable of predicting the mixing, evaporation, and combustion development during the injection process [42, 43].

Then, the present work focuses on three central objectives:

- To contribute to the current fundamental understanding of the effect of the interactions between closely spaced jets on the diesel spray development.
- To strengthen the experimental procedure employed to measure injection events of multi-holes injectors in optically accessible test rigs, accounting for the interactions between jets.
- To provide a database of results, with a wide range of boundary conditions, for model validation.

To this end, two diesel injectors with six outlet orifices were manufactured by Continental with identical design, except for the geometric distribution of the outlet holes of each nozzle, as they were specifically allocated to study the influence of inter-jet spacing. Concretely, the first injector allowed the study of the development of an isolated spray and sprays with an inter-jet spacing of 30° during the same injection event. Moreover, the second injector has two additional orifices distributions, so a total of three inter-jet spacing configurations (30° - 36° - 45°) were compared to the performance of the isolated spray, maintaining the boundary conditions.

Additionally, the optical elements and test rigs available in the institute were employed to analyze various characteristics of the injection event. Specifically, the measurements campaign can be grouped into three sections:

- Hydraulic characterization of the orifices of the injectors, to compare their internal flow behavior.
- Sprays characterization in non-reactive evaporative conditions, visualizing the spray development under various inter-jet spacing configurations.
- Sprays characterization in a reactive environment, comparing the combustion process under several inter-jet spacing configurations.

The hydraulic characterization consisted of measurements of the rate of injection and momentum flux of the injectors. Afterward, the visualization of the spray under a non-reactive environment was done employing the MIE scattering and double-pass schlieren techniques. Both of these campaigns were done to compare the behavior of each injector before the combustion analysis

and review any change in behavior due to differences in the functionality of the injectors.

Lastly, the effect of inter-jet spacing on the combustion process was analyzed. To this end, the following high-speed visualizations in the reactive environment were obtained:

- Ignition delay and lift-off length, with the OH* chemiluminescence optical technique.
- Initial soot appearance, with the natural luminosity optical technique.
- Soot formation, with the soot Diffuse Back-Illumination (DBI) optical technique.

These results were obtained for each inter-jet spacing configuration, along with a wide range of boundary conditions.

## 1.3 Thesis outline

The following work has been divided into seven chapters.

In **chapter 1**, a brief description of the general context surrounding internal combustion engines and diesel injectors is made. Additionally, the main objectives are presented, as well as the methodology employed to achieve them.

**Chapter 2** reviews the theoretical concepts that are relevant to the scope of this work, which could serve to have a better understanding of the obtained results. Specifically, the chapter details the injection and mixing process of the spray and the following combustion process. Moreover, a summary of the relevant works related to jet-to-jet interactions is presented.

**Chapter 3** describes the injectors and facilities employed throughout the measurements, including the implementation of a novel window of the test rig to allow the DBI measurements of multi-hole injectors. The chapter also contains a description of the optical techniques and image processing methodology used.

**Chapter 4** presents the results obtained in a non-reactive environment. First, the results of the hydraulic characterization of the injectors are depicted, that is, the time-resolved rate of injection and momentum flux results. Additionally, various hydraulic coefficients are obtained to compare the performance of each injector and orifice properly. Then, the results from the non-reactive visualizations are detailed, comparing the development of the

sprays in terms of the liquid length and spray penetration for several inter-jet spacing.

In **chapter 5**, a detailed analysis of the development of the spray in a reactive atmosphere is presented. Specifically, a comparison of the performance of each inter-jet spacing configuration is made in terms of ignition delay and lift-off length. Moreover, a novel empirical correlation was developed for the lift-off length considering the influence of inter-jet spacing.

**Chapter 6** contains the results from the soot measurement campaign. These measurements represent the second and final experimental campaign under a reactive environment. The experiments employed the novel window, which allowed the implementation of the DBI technique on multi-orifices injectors.

Lastly, **chapter 7** summarizes the work carried out, focusing on the main achievements and conclusions. In addition, various ideas are proposed as future projects to continue and further contribute to understanding the influence of inter-jet spacing on the combustion process.

# References


[1] Johnson, Timothy. "Vehicular Emissions in Review". In: *SAE International Journal of Engines* 9.2 (2016), pp. 1258–1275. DOI: 10.4271/2016-01-0919.

[2] European Comittee for Standardization. *Regulation EC No 595/2009*. 2009.

[3] Claßen, Johannes et al. "Statistically supported real driving emission calibration: Using cycle generation to provide vehicle-specific and statistically representative test scenarios for Euro 7". In: *International Journal of Engine Research* 21.10 (2020), pp. 1783–1799. DOI: 10.1177/1468087420935221.

[4] Altenschmidt, Frank; Banzhaf, Gerald; Kraus, Eberhard; and Loll, Steffen. "The SI-engine - at the end of its development?" In: *16th Conference The Working Process of the Internal Combustion Engine*. Ed. by Helmut Eichlseder; and Andreas Wimmer. Graz: Verlag der Technischen Universität Graz, 2017, pp. 35–49.

[5] Lapuerta, Magín; Ramos, Ángel; Fernández-Rodríguez, David; and González-García, Inmaculada. "High-pressure versus low-pressure exhaust gas recirculation in a Euro 6 diesel engine with lean-NOx trap: Effectiveness to reduce NOx emissions". In: *International Journal of Engine Research* 20.1 (2019), pp. 155–163. DOI: 10.1177/1468087418817447.

[6] Grigoratos, Theodoros; Gustafsson, Mats; Eriksson, Olle; and Martini, Giorgio. "Experimental investigation of tread wear and particle emission from tyres with different treadwear marking". In: *Atmospheric Environment* 182.March (2018), pp. 200–212. DOI: 10.1016/j.atmosenv.2018.03.049.

[7] Kalghatgi, Gautam. "Is it really the end of internal combustion engines and petroleum in transport?" In: *Applied Energy* 225.April (2018), pp. 965–974. DOI: 10.1016/j.apenergy.2018.05.076.

[8] Ritchie, Hannah; and Roser, Max. *Emissions by sector*. 2020.

[9] Reitz, R. D. et al. "IJER editorial: The future of the internal combustion engine". In: *International Journal of Engine Research* 21.1 (2020), pp. 3–10. DOI: 10.1177/1468087419877990.

[10] BP. *Statistical Review of World Energy*. 2020.

[11] Musculus, Mark P B; Miles, Paul C; and Pickett, Lyle M. *Conceptual models for partially premixed low-temperature diesel combustion.* Vol. 39. 2-3. Elsevier Ltd, 2013, pp. 246–283. DOI: 10.1016/j.pecs.2012.09.001.

[12] Han, Sangwook; Kim, Jaeheun; and Bae, Choongsik. "Effect of air-fuel mixing quality on characteristics of conventional and low temperature diesel combustion". In: *Applied Energy* 119 (2014), pp. 454–466. DOI: 10.1016/j.apenergy.2013.12.045.

[13] Nishida, Keiya; Jingyu, Zhu; Xianyin, Leng; and He, Zhixia. "Effects of micro-hole nozzle and ultra-high injection pressure on air entrainment, liquid penetration, flame lift-off and soot formation of diesel spray flame". In: *International Journal of Engine Research* 18.1-2 (2017), pp. 51–65.

[14] Wang, Xiangang; Huang, Zuohua; Zhang, Wu; Abiola, Olawole; and Nishida, Keiya. "Effects of ultra-high injection pressure and micro-hole nozzle on flame structure and soot formation of impinging diesel spray". In: *Applied Energy* 88.5 (2011), pp. 1620–1628. DOI: 10.1016/j.apenergy.2010.11.035.

[15] Jia, Tao Ming; Li, Guo Xiu; Yu, Yu Song; and Xu, Yang Jie. "Effects of ultra-high injection pressure on penetration characteristics of diesel spray and a two-mode leading edge shock wave". In: *Experimental Thermal and Fluid Science* 79 (2016), pp. 126–133. DOI: 10.1016/j.expthermflusci.2016.07.006.

[16] Xu, Qinglin et al. "Diesel Spray Characterization at Ultra-High Injection Pressure of DENSO 250 MPa Common Rail Fuel Injection System". In: *SAE Technical Paper*. SAE International, 2017. DOI: 10.4271/2017-01-0821.

[17] O'Connor, Jacqueline; Musculus, Mark P B; and Pickett, Lyle M. "Effect of post injections on mixture preparation and unburned hydrocarbon emissions in a heavy-duty diesel engine". In: *Combustion and Flame* 170 (2016), pp. 111–123. DOI: 10.1016/j.combustflame.2016.03.031.

[18] Lee, Jinwoo; Jeon, Jinwoog; Park, Jungseo; and Bae, Choongsik. "Effect of Multiple Injection Strategies on Emission and Combustion Characteristics in a Single Cylinder Direct-Injection Optical Engine". In: *SAE Technical Paper 2009-01-1354* (2010). DOI: 10.4271/2009-01-1354.

[19] Mingfa, Yao; Hu, Wang; Zunqing, Zheng; and Yan, Yue. "Experimental Study of Multiple Injections and Coupling Effects of Multi-Injection and EGR in a HD Diesel Engine". In: *SAE Technical Paper 2009-01-2807* (2009). DOI: 10.4271/2009-01-2807.

[20] Payri, Francisco; Benajes, Jesus; Pastor, Jose Vicente; and Molina, Santiago. "Influence of the Post-Injection Pattern on Performance, Soot and NOx Emissions in a HD Diesel Engine". In: *SAE Technical Paper 2002-01-0502* (2002). DOI: 10.4271/2002-01-0502.

[21] Hulkkonen, Tuomo; Sarjovaara, Teemu; Kaario, Ossi; Hamalainen, Ismo; and Larmi, Martti. "Experimental Study of Conical Diesel Nozzle Orifice Geometry". In: *Atomization and Sprays* 25.6 (2015), pp. 519–538. DOI: 10.1615/AtomizSpr.2015010383.

[22] Payri, Raul; Viera, Juan Pablo; Gopalakrishnan, Venkatesh; and Szymkowicz, Patrick G. "The effect of nozzle geometry over internal flow and spray formation for three different fuels". In: *Fuel* 183 (2016), pp. 20–33. DOI: 10.1016/j.fuel.2016.06.041.

[23] Shi, J et al. "Using LES and x - ray imaging to understand the influence of injection hole geometry on Diesel spray formation". In: *THIESEL 2016 Conference on Thermo- and Fluid Dynamic Processes in Diesel EnginesConference on Thermo and Fluid Dynamic* (2016), pp. 1–21.

[24] Sayin, Cenk; Gumus, Metin; and Canakci, Mustafa. "Influence of injector hole number on the performance and emissions of a di diesel engine fueled with biodiesel-diesel fuel blends". In: *Applied Thermal Engineering* 61.2 (2013), pp. 121–128. DOI: 10.1016/j.applthermaleng.2013.07.038.

[25] Zhou, L. Y. et al. "Measurements and analyses on the transient discharge coefficient of each nozzle hole of multi-hole diesel injector". In: *Sensors and Actuators, A: Physical* 244 (2016), pp. 198–205. DOI: 10.1016/j.sna.2016.04.017.

[26] Aori, Gele; Hung, David L S; and Zhang, Ming. "Effect of Nozzle Configuration on Macroscopic Spray Characteristics of Multi-Hole Fuel Injectors Under Superheated Conditions". In: *Atomization and Sprays* 26.5 (2016), pp. 439–462. DOI: 10.1615/AtomizSpr.2015011990.

[27] Rusly, Alvin M.; Le, Minh K.; Kook, Sanghoon; and Hawkes, Evatt R. "The shortening of lift-off length associated with jet-wall and jet-jet interaction in a small-bore optical diesel engine". In: *Fuel* 125 (2014), pp. 1–14. DOI: 10.1016/j.fuel.2014.02.004.

[28] Chartier, Clément; Aronsson, Ulf; Andersson, Öivind; Egnell, Rolf; and Johansson, Bengt. "Influence of jet-jet interactions on the lift-off length in an optical heavy-duty di diesel engine". In: *Fuel* 112 (2013), pp. 311–318. DOI: 10.1016/j.fuel.2013.05.021.

[29] Baert, Rik S G et al. "Design and operation of a high pressure, high temperature cell for HD diesel spray diagnostics: guidelines and results". In: *SAE paper 2009-01-0649* 4970 (2009). DOI: 10.4271/2009-01-0649.

[30] Bardi, Michele. "Partial needle lift and injection rate shape effect on the formation and combustion of the Diesel spray". PhD thesis. Valencia (Spain): Universitat Politècnica de València, 2014. DOI: 10.4995/Thesis/10251/37374.

[31] Viera, Juan Pablo. "Experimental study of the effect of nozzle geometry on the performance of direct-injection diesel sprays for three different fuels". PhD thesis. 2017. DOI: 10.4995/Thesis/10251/81857.

[32] Viera, Alberto. "Effect of multiple injection strategies on the diesel spray formation and combustion using optical diagnostics". PhD thesis. Universitat Politècnica de València, 2019. DOI: 10.4995/Thesis/10251/123954.

[33] CMT. *Official website: https://www.cmt.upv.es, accessed on 15-12-2021.*

[34] Desantes, Jose Maria; García-Oliver, José Maria; García, Antonio; and Xuan, Tiemin. "Optical study on characteristics of non-reacting and reacting diesel spray with different strategies of split injection". In: *International Journal of Engine Research* 301 (2018). DOI: 10.1177/1468087418773012.

[35] Xuan, Tiemin. "Optical investigations on diesel spray dynamics and inflame soot formation". PhD thesis. Universitat Politècnica de València, 2017. DOI: 10.4995/Thesis/10251/94626.

[36] Payri, Raul; Gimeno, Jaime; Cuisano, Julio; and Arco, Javier. "Hydraulic characterization of diesel engine single-hole injectors". In: *Fuel* 180 (2016), pp. 357–366. DOI: 10.1016/j.fuel.2016.03.083.

[37] Benajes, Jesus; Payri, Raul; Bardi, Michele; and Martí-aldaraví, Pedro. "Experimental characterization of diesel ignition and lift-off length using a single-hole ECN injector". In: *Applied Thermal Engineering* 58.1-2 (2013), pp. 554–563. DOI: 10.1016/j.applthermaleng.2013.04.044.

[38] Payri, Raul; Salvador, Francisco Javier; Gimeno, Jaime; and Peraza, Jesús E. "Experimental study of the injection conditions influence over n-dodecane and diesel sprays with two ECN single-hole nozzles. Part II: Reactive atmosphere". In: *Energy Conversion and Management* 126 (2016), pp. 1157–1167. DOI: 10.1016/j.enconman.2016.07.079.

[39] Giraldo, Jhoan S.; Payri, Raul; Marti-Aldaravi, Pedro; and Montiel, Tomas. "Effect of high injection pressures and ambient gas properties over the macroscopic characteristics of the diesel spray on multi-hole nozzles". In: *Atomization and Sprays* 28.12 (2018), pp. 1145–1160. DOI: 10.1615/AtomizSpr.2019029651.

[40] Payri, Raul; Salvador, Francisco Javier; Manin, Julien; and Viera, Alberto. "Diesel ignition delay and lift-off length through different methodologies using a multi-hole injector". In: *Applied Energy* 162 (2016), pp. 541–550. DOI: 10.1016/j.apenergy.2015.10.118.

[41] Payri, Raul; Gimeno, Jaime; Bardi, Michele; and Plazas, Alejandro Hernan. "Study liquid length penetration results obtained with a direct acting piezo electric injector". In: *Applied Energy* 106.JUNE (2013), pp. 152–162. DOI: 10.1016/j.apenergy.2013.01.027.

[42] Pastor, Jose Vicente; Lopez, Jose Javier; Garcia-Oliver, Jose Maria; and Pastor, Jose Manuel. "A 1D model for the description of mixing-controlled inert diesel sprays". In: *Fuel* 87.13-14 (2008), pp. 2871–2885. DOI: 10.1016/j.fuel.2008.04.017.

[43] Desantes, Jose Maria; Pastor, Jose Vicente; Garcia-Oliver, Jose Maria; and Pastor, Jose Manuel. "A 1D model for the description of mixing-controlled reacting diesel sprays". In: *Combustion and Flame* 156.1 (2009), pp. 234–249. DOI: 10.1016/j.combustflame.2008.10.008.

# Chapter 2

# Fundamentals of the diesel injection process

## 2.1 Introduction

A comprehensive understanding of the fundamental behavior of the spray during the injection process has been a crucial element of the improvements reached in the efficiency of internal combustion engines.

In this sense, the following sections summarize the theoretical concepts of injection of the diesel spray related to this work. On the other hand, comprehensive works that contain a complete and well-established review of the results obtained in the field are readily available [1–5].

## 2.2 Types of internal combustion engines

Internal combustion engines generate energy from the combustion of petroleum-derived fuels. This process occurs in a chamber within the equipment (cylinder), hence the "internal" attribute.

Internal combustion engines (ICEs) can be classified by the combustion thermodynamic cycle. The two most popular cycles in ICEs are the diesel and otto, setting the principles of diesel (Figure 2.1) and gasoline (Figure 2.2) engines, respectively. As the name implies, each of them is driven by a different type of fuel.

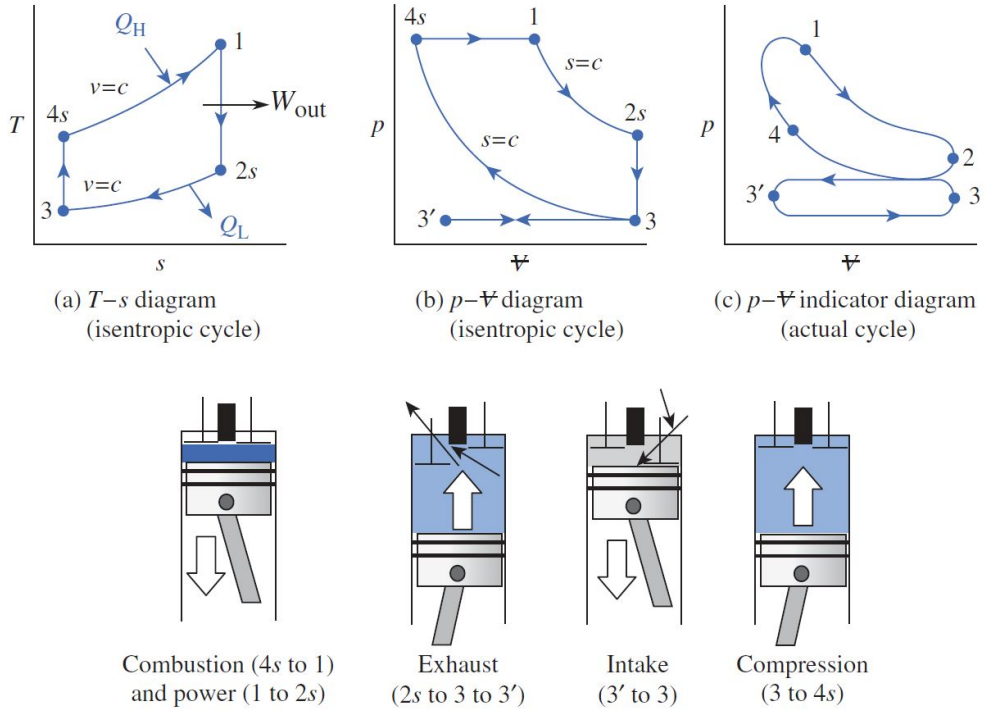


(a) $T-s$ diagram (isentropic cycle)

(b) $p-\forall$ diagram (isentropic cycle)

(c) $p-\forall$ indicator diagram (actual cycle)

*Figure 2.1: Operation of a four-stroke diesel cycle engine [6].*

Other main differences between these types of engines are:

- **The formation of the air-fuel mixture.** In diesel engines, the fuel is directly injected into the combustion chamber, filled by air when the piston is near the Top Dead Center (TDC). It is then an heterogeneous combustion with an excess of air, in which combustion occurs where the proper air-fuel mixture conditions are achieved. In gasoline engines, a stoichiometric air-fuel mixture has traditionally been created prior to its admission to the combustion chamber (indirect injection), producing a homogeneous charge. Nevertheless, newer technologies are allowing for gasoline direct injection inside the cylinder.

- **The ignition technique.** In gasoline engines, the air-fuel mixture is ignited by an electric arc from a spark plug when the piston is near the Top Dead Center, which is why they are also called spark ignition engines. On the other hand, in diesel engines, the temperature and

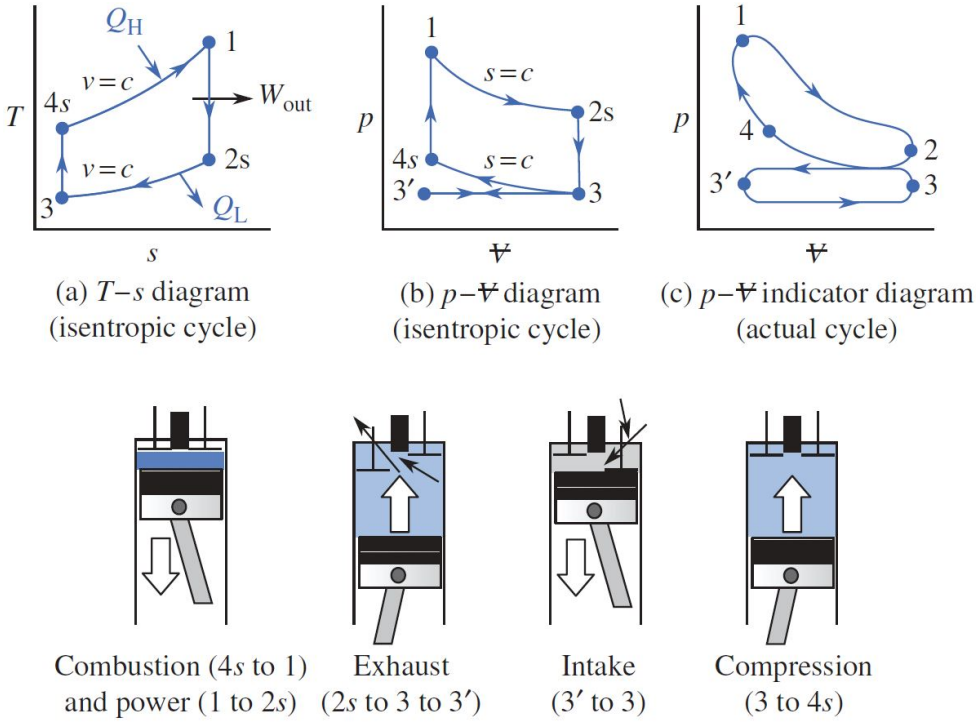


*Figure 2.2: Operation of a four-stroke Otto cycle engine [6].*

pressure of the combustion chamber rise to the point where self-ignition of the air-fuel mixture develops near the TDC. Hence, these types of engines are also known as Compression-ignition engines.

Thus, the efficiency of compression-ignition engines is more reliant on the injection and air-fuel mixture process. Consequently, understanding these phenomena has been essential for the improvements achieved in fuel consumption economy and reducing pollutant emissions of this engine type. In the following sections, the fuel spray injection and mixing processes are detailed.

## 2.3 The diesel injector

From now on, this work will focus on the specific area of study of this thesis, that is, the diesel injection process.

First, it is convenient to detail the diesel injector and its working principle. The main components of a typical injector are depicted in Figure 2.3. Initially, high-pressure fuel is delivered to the injector (fuel delivery system is detailed in section 3.2) and distributed in two lines. Part of the fuel is sent to the nozzle of the injector, and another is directed to the control volume.

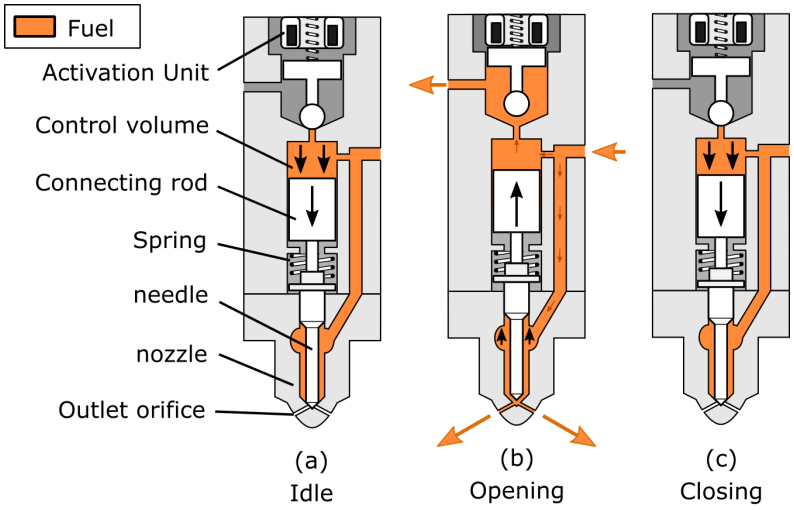


*Figure 2.3: Working principle of the diesel injector [7].*

In an idle state, the fuel located in the nozzle creates a pressure pushing the needle upwards, and, likewise, the fuel in the control volume applies the same pressure downwards (Figure 2.3.a). As the surface area in the control volume is more extensive than in the nozzle, a greater force is applied downwards, which, together with the force from the spring, pushes down the needle and seals the outlet orifices, preventing any injection.

To start the injection, an electric pulse is sent to the activation unit. Notably, the injectors can be classified by the activation unit they use: solenoid or piezoelectric injectors. A magnetic field is generated in solenoid injectors to pull upwards the ball-shaped valve that seals the control volume. Consequently, the pressure in the control volume drops as the fuel flows to the adjacent camera through its outlet orifice (Figure 2.3.b). Then, the force pushing the needle from the nozzle is enough to move the needle upwards, enabling the start of injection through the now accessible outlet orifices.

Towards the end of injection, the electric pulse (and the resultant magnetic field) is stopped, enabling the valve to go back to its idle placement. Then, the

pressure is restored in the control volume, and the needle is pushed downwards, sealing the outlet-orifices and ending the injection (Figure 2.3.c).

For piezoelectric injectors, the working principle is similar, but the solenoid is replaced by piezoelectric crystals that compress or expand in tune with the electric pulse received, unsealing or sealing the outlet orifice of the control volume [8]. This type of injector offers a better hydraulic response as the piezoelectric can act directly on the needle, without the need of the connecting-rod (Figure 2.4) [9–12]. Thus, the dynamic response is enhanced [13, 14], achieving better control of the injections timings.

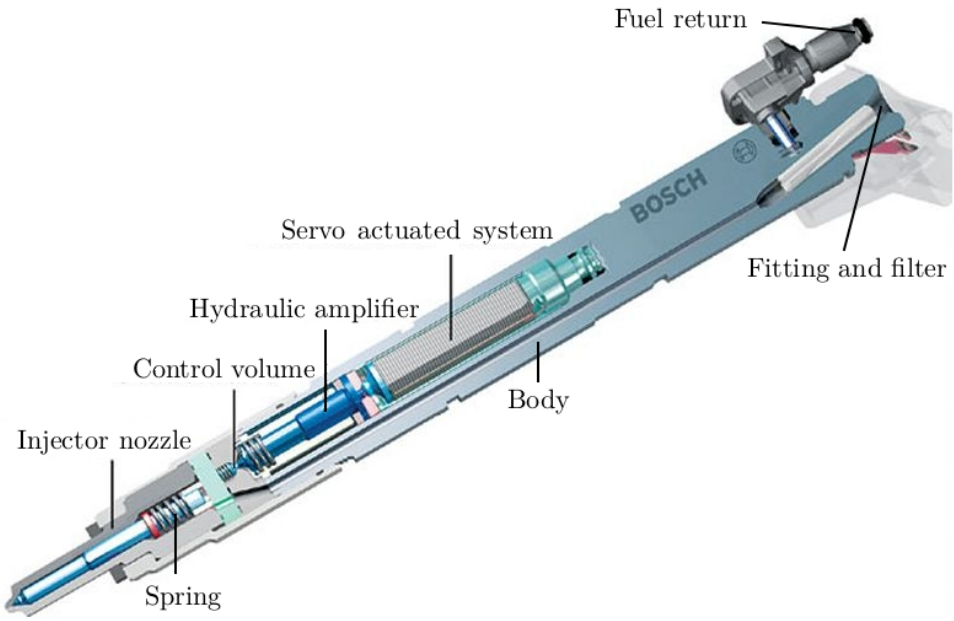


*Figure 2.4: Piezoelectric-driven diesel injector [15].*

Lastly, another critical aspect of the injector is the geometry of its nozzle and outlet orifices, as it is closely related to the development of the spray and subsequent efficiency of the combustion [16–20].

## 2.4 The development of the diesel spray

The present section describes the formation and development of the diesel spray. Specifically, the subsections will follow the fuel trajectory going from

the inside of the injector up to the combustion and diffusive flame. Throughout the review, a parameter will be more or less described depending on its relation with the current work, although proper references to other detailed studies are constantly provided.

### 2.4.1 Internal flow characterization

Section section 2.3 described the general working principle of a diesel injector and how the fuel reaches the outlet orifices. Nevertheless, the fuel suffers from losses throughout its trajectory from the feeding line down to the nozzle. This section serves as a summary of more detailed works [7, 15] in respect of the internal hydraulic behavior of the fuel.

The overall efficiency of the injector in delivering the fuel can be accounted with the Bernoulli equation. Assuming a stationary fuel upstream of the injector, the equation results in:

$$\frac{P_r}{\rho_f} = \frac{P_b}{\rho_f} + \frac{1}{2} \cdot u_t^2 \tag{2.1}$$

In which $P_r$ refers to the rail pressure, $P_b$ the discharge pressure, $\Delta P$ the difference between $P_r$ and $P_b$, $\rho_f$ the fuel density, and $u_t$ the theoretical discharge velocity. Then, the discharge velocity can be computed as:

$$u_t = \sqrt{\frac{2 \cdot \Delta P}{\rho_f}} \tag{2.2}$$

Finally, the theoretical mass flow rate ($\dot{m}_t$) can be calculated from this velocity and the geometrical dimensions of the orifice. Assuming that the fuel completely fills the cross-sectional area of the hole ($A_o$) throughout its trajectory:

$$\dot{m}_t = A_o \cdot \rho_f \cdot u_t \tag{2.3}$$

On the other hand, the real mass flow rate ($\dot{m}$) can be obtained experimentally [21, 22], which is done of this work, and the methodology is explained in subsection 3.3.1. Then, the theoretical mass flow can be compared to the real mass flow. This relation is represented by the discharge coefficient ($C_d$), a parameter widely employed to assess the efficiency of the injector in delivering the fuel [23–27]. Specifically, the discharge coefficient is computed as follows:

$$C_d = \frac{\dot{m}}{\dot{m}_t} = \frac{\dot{m}}{A_o\sqrt{2 \cdot \rho_f \cdot \Delta P}} \tag{2.4}$$

Another parameter used to account for the losses in the fuel delivery is the effective area ($A_{eff}$) of the orifice, that is, the homogeneous area of the fuel inside the orifice (Figure 2.5.right), equivalent in magnitude to the real non-uniform distribution along the hole (Figure 2.5.left).

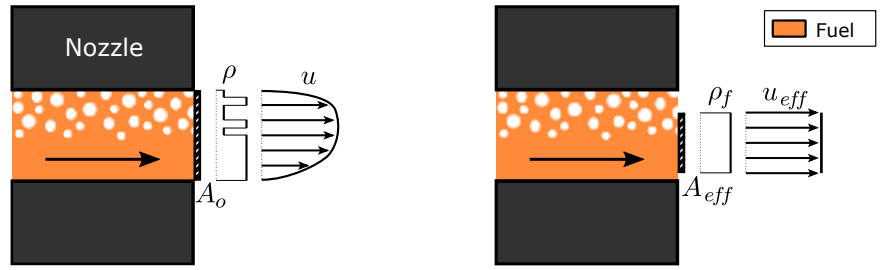


*Figure 2.5: Flow distribution outside of the orifice and equivalent simplified model [7].*

Then, the mass flow can be expressed in terms of the effective area [7]:

$$\dot{m} = A_{eff} \cdot \rho_f \cdot u_{eff} \tag{2.5}$$

Moreover, it is also possible to relate the effective area with the momentum flux ($\dot{M}$), another parameter employed to characterize the hydraulic behavior of the spray. This parameter can also be obtained experimentally, and the corresponding methodology is described in [7]:

$$\dot{M} = A_{eff} \cdot \rho_f \cdot u_{eff}^2 \tag{2.6}$$

Lastly, Equation 2.5 and Equation 2.6 are employed to obtain the effective velocity ($u_{eff}$) and effective area at the outlet hole [7]:

$$u_{eff} = \frac{\dot{M}}{\dot{m}} \tag{2.7}$$

$$A_{eff} = \frac{\dot{m}^2}{\rho_f \cdot \dot{M}} \tag{2.8}$$

As previously stated, $\dot{m}$ and $\dot{M}$ are obtained experimentally, so $A_{eff}$ can be computed. This parameter is frequently employed in computational models [28, 29], as it accounts for the losses due to cavitation in the nozzle, hydraulic flip, and non-uniform velocity [7, 19, 30–33].

### 2.4.2 Combustion phases

This section provides a summary of the general phases of the injection and combustion process. Afterward, a detailed description of the events occurring in each phase is provided.

Figure 2.6 plots the development of the injection rate in time and its relation with the evolution of the apparent heat release rate (AHRR) in the combustion chamber.

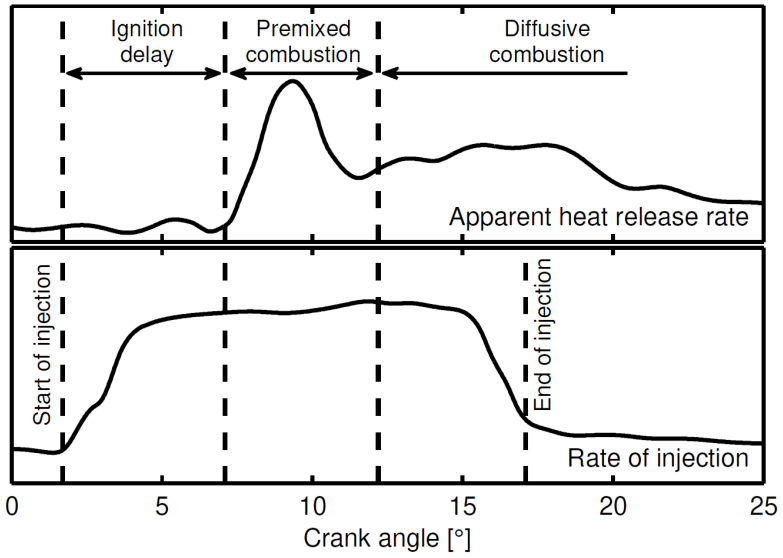


*Figure 2.6: Temporal relationship between the fuel mass flow rate and the apparent heat release rate (AHRR) [34].*

The development seen in Figure 2.6 can be divided in the following events [1–4, 35]:

- **Start of injection.** This parameter accounts for the hydraulic delay of the injection, that is, the elapsed time between the start of energizing of the injector and the actual start of injection (SOI) through the outlet

orifices of the nozzle. This delay is mainly related to the internal mechanism of the injector, although the injection conditions have some effect as well.

- **Ignition delay.** This phase is thoughtfully described in subsection 2.4.3. In summary, this event begins at the start of injection and includes the atomization, air entrainment, and evaporation phenomena occurring during the air-fuel mixing process; and the initial chemical reactions of low intensity. This phase ends prior to the high-intensity exothermic reaction.

- **Premixed combustion.** This stage is defined by the autoignition of the mixture that reached flammability conditions in the previous phase. During this period, a steep increase and peak of heat released is observed [36], which was typically reflected in the noise of old diesel engines.

  Moreover, the high temperatures reached in this phase cause pollutants emissions, so numerous studies have been done to find techniques to control this phenomenon. For instance, pilot injections are now employed to pre-heat the camera and shorten the ignition delay of the main injection, thus limiting the peak of heat release and temperature reached inside the chamber and subsequent $NO_x$ without incurring in large penalties of soot formation [37–40].

- **Diffusive combustion.** After the transient autoignition of the initial flammable mixture finalizes, a more stable stage begins, known as diffusive combustion. This period is characterized by a mixing-controlled process, as the air-fuel mixture is fluently ignited as long as the injection continues. In long injections, a relatively stable heat release and flame are reached. This flame is known as the diffusive flame and is described in subsection 2.4.6.

- **End of injection.** This phase starts shortly after the end of energizing (EOE), when the fuel injection stops. During this period, a rapid decrease of the heat release occurs as the last available mixture ignites, completing the combustion process.

### 2.4.3 Liquid length

The air-fuel mixing process is depicted in Figure 2.7 and can be grouped into three events: injection, atomization, and evaporation. As previously described, the injection process leads up to the fuel emerging from the outlet

orifice at the objective pressure, defining the creation of the fuel spray. Once the fuel is ejected from the injector, an interaction begins between the mentioned fuel and the surrounding gas in the chamber.

As the spray develops, it faces high-density and high-temperature air, which promotes the breakup of the fuel molecules into droplets, a process known as atomization. Then, the surrounding air is entrained by the fuel droplets, establishing the air-fuel mixture. As the mixture moves forward, a heat exchange process is continuously developing between the air and the fuel droplets, in which the latter rises to high enough temperatures to reach evaporation.

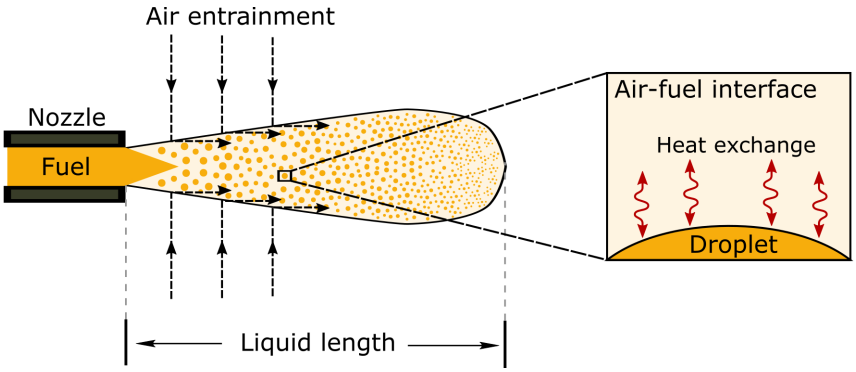


*Figure 2.7: Air-fuel mixing process [34].*

The distance between the nozzle tip and the location at which the fuel completely evaporates is known as the liquid length (LL) of the fuel. This is an important parameter since it indicates how much space is required for a proper mixture to develop prior to the combustion. The influence on the LL of the boundary conditions analyzed in this work are contained in the equation Equation 2.1, proposed by Payri et al. [41]. Other authors propose slightly different exponents but the general trends are constantly the same:

$$LL \propto D_o^{1.08} \cdot \rho^{-0.51} \cdot T^{-1.7} \cdot \Delta P^{-0.015} \tag{2.9}$$

It can be seen that increasing the chamber density ($\rho$), enlarging the chamber temperature ($T$), or decreasing the orifice diameter, generates a reduction of the liquid length, as these changes enhance the atomization and evaporation processes [32, 42–44].

On the other hand, variations on the rail or discharge pressure do not considerably affect the liquid length, as reflected in the low $\Delta P$ coefficient. In this sense, an increase of the rail pressure enhances the spray evaporation but also the spray velocity. Hence, a balance is made in which one phenomenon enlarges and the other shrinks the liquid length, resulting in an overall negligible effect [42–45].

### 2.4.4 Spray penetration

The liquid length accounts for the distance needed by the fuel jet to vaporize completely. Nevertheless, the spray continues to move forward in its vapor phase, and the parameter to account for this development is the spray penetration. An illustrative example depicting the temporal evolution of these parameters is presented in Figure 2.8.

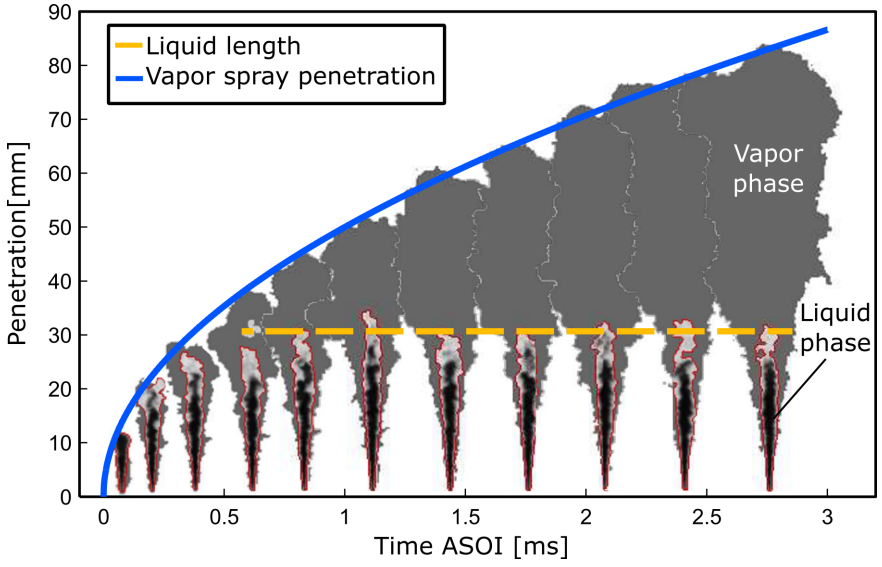


*Figure 2.8: Temporal evolution of the liquid and vapor spray penetration.*

Specifically, the spray penetration is defined as the distance between the nozzle tip and the furthest point of the spray structure, as graphically depicted in Figure 2.9.

The spray penetration has been a key macroscopic parameter of interest since it is directly associated with the mixing process. In particular, the penetration is dependent on the momentum exchange rate ($\dot{M}$) between the spray and the surrounding gas. Moreover, characterizing the spray penetration

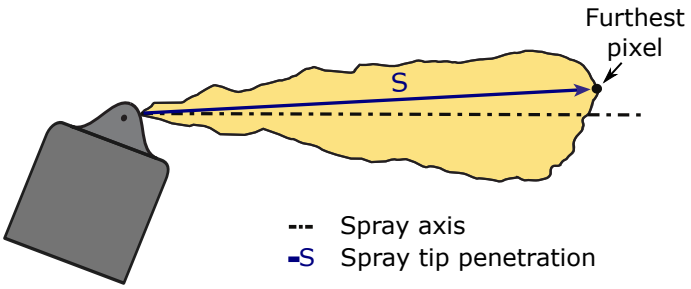


*Figure 2.9: Spray penetration definition.*

has served to assess the combustion chamber dimensions and piston movement properly.

Through numerous experimental campaigns, the development of the spray penetration has been defined in detail [7, 46–51]. In this regard, it is generally accepted that the spray follows two temporal behaviors, and the transition between these stages occurs at the breakup time ($t_b$)[47, 49].

Before the breakup time, the penetration follows a linear correlation with time ($t$), although recent visualizations near the nozzle tip at a very high acquisition rate have noted a parabolic relation with time in the very first few millimeters after the start of injection [41, 52, 53].

After the breakup time, these studies have found the spray penetration ($S$) to be proportional to the square root of the time, adjusting to the following correlation:

$$S \propto \rho^{-1/4} \cdot \dot{M}^{1/4} \cdot tan\,(\theta/2)^{-1/2} \cdot t^{1/2} \tag{2.10}$$

In which $\rho$ represents the chamber density and $\theta$ is the spray spreading angle [54–57]. Moreover, the spray penetration can also be expressed in terms of the difference between the injection/rail pressure and the chamber pressure ($\Delta P$), and the diameter orifice ($D_o$) [7, 34], as detailed in Equation 2.11.

$$S \propto \rho^{-1/4} \cdot \Delta P^{1/4} \cdot tan\,(\theta/2)^{-1/2} \cdot D_o^{1/2} \cdot t^{1/2} \tag{2.11}$$

### 2.4.5 Ignition delay

The elapsed time between the start of injection and the start of combustion (autoignition) is known as the ignition delay, and the events leading up to the ignition can be divided into three groups.

Before describing each of them, it is worth noting that during the combustion event, chemical reactions produce molecules in a transient high-energy state, which then move to a lower energy level emitting light during the process [58]. Formally, this process is known as chemiluminescence and can be used to track the ignition development.

As mentioned, three phenomenon leading to the combustion can be disguised [59, 60]:

- **Physical induction.** This phase includes the events described in subsection 2.4.3, that is, the fuel atomization and the following hot air entrainment. Then, the fuel starts to vaporize through the heat exchange with the air, causing a temporal reduction of the chamber temperature as the fuel absorbs the heat. This phenomenon temporally inhibits any chemical reaction, but the temperature rises again as the mixture travels forwards. Then, the fuel reaches flammability conditions, leading to the first stage ignition.

- **First stage ignition.** This period begins with low-intensity chemical reactions occurring between the oxygen and the fuel, leading to the first noticeable chemiluminescence and rise of the pressure chamber. CH radicals appear during these reactions and are thus considered appropriate markers of the first stage ignition. This phase is also known as the cool flames stage [61] because of the relatively low amount of heat released and chemiluminescence intensity of the flame.

  These reactions develop under a rich air-fuel mixture with an equivalent ratio ranging between three and four, releasing a small amount of energy that gradually increases the chamber pressure and temperature. Consequently, this increase further enhances the consumption of the premixed fuel, up until a point when an abrupt and high-intensity exothermic reaction occurs, which marks the start of the second stage ignition.

- **Second stage ignition.** The chemical reactions happening during the first stage ignition lead to favorable mixture conditions for the subsequent autoignition to occur. Specifically, the temperature rises to a level in which the dissociation of hydrogen peroxide dominates the chemical reactions [2, 60]. This dissociation produces high heat release, activating the premixed burn and second stage ignition (SSI).

  The appearance of OH radicals marks this stage, as they appear under high-temperature stoichiometric combustion [62]. On the other hand, the ignition delay is technically defined as the elapsed time between the

start of injection and the start of the second stage ignition. Then, the ignition delay can be computed by measuring the appearance of OH radicals chemiluminescence [63–66].

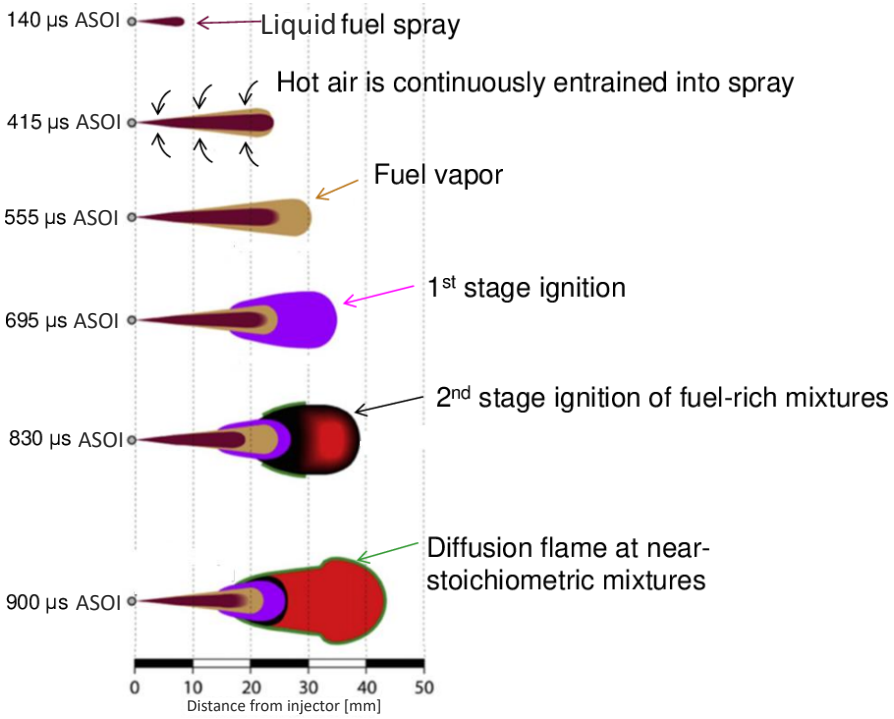


*Figure 2.10: Representative time sequence of diesel direct-injection ignition [67].*

During the combustion occurring in the SSI, the combustion chamber reaches a high temperature, promoting nitrogen oxides ($NO_X$) emissions. Thus, researchers have put great effort into understanding the mechanism leading to premixed combustion. On this matter, the length of the ignition delay (ID) has been found to affect the heat release and peak of temperature reached during the premixed combustion. Thus, boundaries conditions affecting this value have been analyzed and are summarized in the Equation 2.12 [61, 68, 69]:

$$ID \propto \exp\left(\frac{A}{T}\right) \cdot \rho^{-1.3} \cdot \Delta P^{-0.17} \cdot O_2\%^{-0.8} \tag{2.12}$$

In which $A$ represents the global activation energy of reactions and $O_2\%$ the oxygen concentration in the combustion chamber. It can be observed that an increase of either the chamber temperature, chamber density, difference between rail and chamber pressure, or oxygen concentration, results in a reduction of the ignition delay. These trends have been observed and explained in detailed in numerous works [61, 64, 68–73].

### 2.4.6 Diffusive flame

Near the peak of the heat release rate of the premixed combustion Figure 2.6, a transition to a more stable stage begins [74], known as the diffusive combustion. Around this moment, a diffusive flame emerges at the spray front and propagates upwards and up to a certain distance of the nozzle of the injector. The length separating the nozzle and the start of the diffusive flame is known as the lift-off length (LOL) [63, 68, 69, 75–77].

Figure 2.11 depicts the structure of the diffusive flame, as proposed by Dec [78]. This flame model serves as a guide to depict the fuel trajectory along the flame [35, 79]:

- As recently mentioned, the lift-off length marks the start of the diffusive flame. The lift-off length can be established either before or after the liquid fully evaporates and mixes. In both cases, the structure of the flame relies on the momentum provided by the injection of fuel, as it drives the mixing process that generates the diffusive flame, which is why it is defined as a mixing-controlled event.
- The existing air-fuel mix near the liquid length is known for being rich in fuel concentration. Thus, the following flame zone is characterized for hosting rich combustion and its products, such as soot precursors, unburned fuel, and partial combustion products. This rich reaction zone comprises the core of the diffusive flame and leads up to the flame front.
- The temperature of these products increases as they move towards the flame front, promoting the production of soot particles that merge into bigger molecules [80]. As these partial products reach the flame front, they are oxidized by the available oxygen, producing most of the energy of the diffusive flame. On the other hand, at high temperatures, the available oxygen promotes the formation of nitrogen oxides [81].

It can be observed in Figure 2.11 that the lift-off length is set before the fuel fully atomizes; that is, the lift-off length is shorter than the liquid

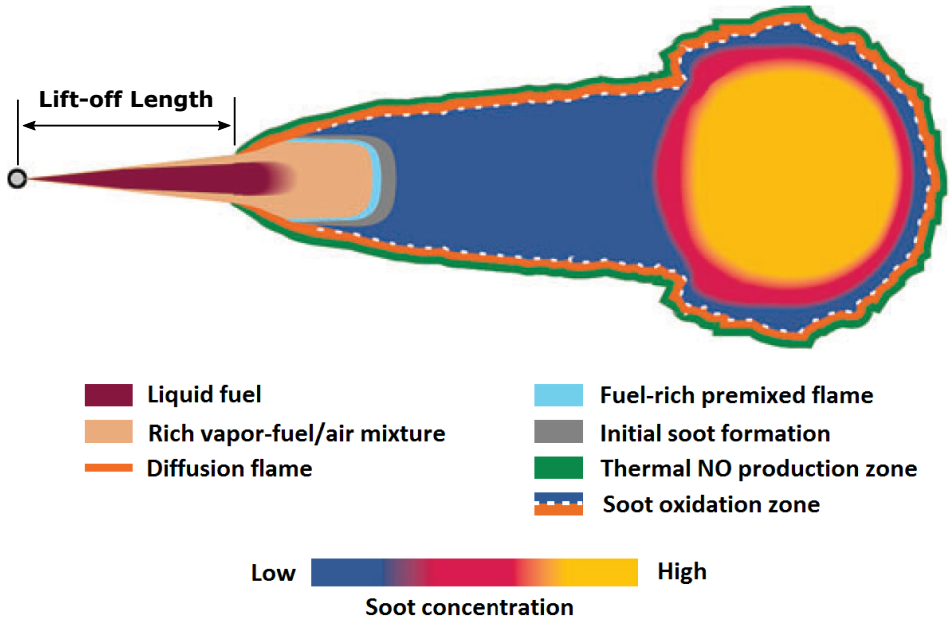


*Figure 2.11: Structure of the diffusive flame [34].*

length. Nevertheless, the lift-off length can be larger than the liquid length [63], especially for small holes diameters [82, 83], such as the nozzle orifices employed in this work. Then, there would be more space for the initial air entrainment, with a leaner air/fuel mixture reaching the ignition zone. Then, the enhanced air/fuel ratio would reduce the partial combustion products and soot precursors appearance, and possibly the soot produced [63].

Thus, the lift-off length serves as indicative of the space available for the fuel to mix with the air properly and have better combustion. Consequently, this parameter has been studied in detail, including the influence of the boundary conditions on its value [61, 63, 68, 69, 75–77].

In Equation 5.2, the main boundary conditions affecting the lift-off length are depicted [68, 69]:

$$LOL \propto T^a \cdot \rho^b \cdot {u_t}^c \cdot {O_2\%}^d \tag{2.13}$$

In which $u_t$ refers to the theoretical velocity of the fuel at the nozzle exit, calculated by the equation[68]:

$$u_t = \sqrt{2\frac{\Delta P}{\rho_f}} \tag{2.14}$$

Lastly, the influence of each parameter is reflected on the Table 5.2, which contains the coefficients obtained by Siebers; and Higgins [63] and Benajes et al. [68] for the Equation 5.2, and are representative of the trends observed in the numerous works regarding the lift-off length.

*Table 2.1: Coefficients obtained for the lift-off length correlation.*

| | $a$ | $b$ | $c$ | $d$ |
|---|---|---|---|---|
| Benajes et al. [68] | -3.89 | -1 | 0.54 | -1 |
| Siebers; and Higgins [63] | -3.74 | -0.85 | 1 | -1 |

### 2.4.7 Inter-jet spacing

Regarding the diesel injection event, injectors with multiple holes have been established as one of the numerous techniques employed in modern diesel engines to reduce their emissions [84] and improve the fuel consumption economy. In this sense, increasing the number of outlet holes has allowed for a smaller diameter, leading to more homogeneous mixtures and smaller droplet sizes, enlarging the liquid-gas contact surface. These phenomena have enhanced the injection event [85], as the mixing process is crucial for the combustion efficiency [86].

Nevertheless, as the number of holes in the nozzle increases, the spacing between them decreases, leading to a reduction in the space available for each jet development without interacting with the neighbor sprays (Figure 2.12). Then, increasing the number of holes presents a trade-off between improving the air entrainment through smaller orifices diameter and providing a larger volume of air between the sprays. In this sense, as the sprays come closer to each other, jet-to-jet interactions could significantly affect the combustion process.

This phenomenon is a matter of interest among the research community, as its implications have not been entirely defined [87, 88]. In this work, the inter-jet spacing is defined as the angle, in degrees, between a spray axis and that of its neighbor jet.

Rusly et al. [89] investigated the development of wall-interacting jets and jet-jet interaction in a small-bore optical diesel engine. They found that,

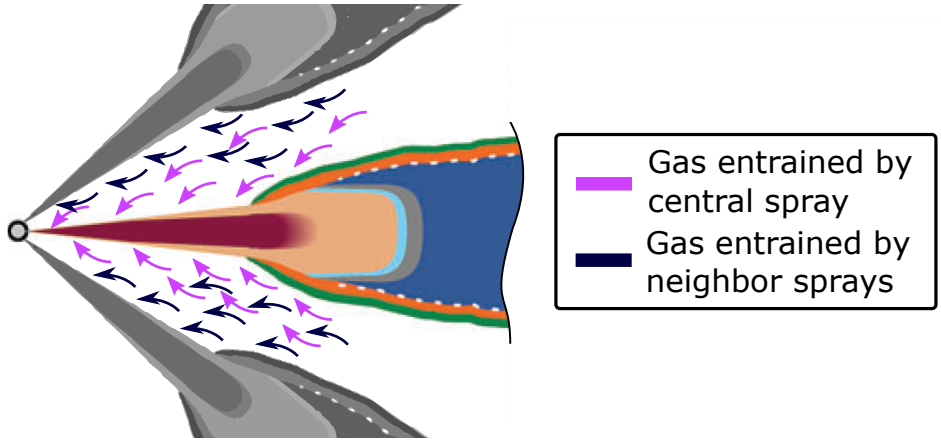


*Figure 2.12: Air entrainment in neighbor sprays.*

for narrow inter-jet spacing, the impact of jet-jet interaction on the lift-off length and natural soot luminosity is more significant than the effect of the re-entrainment from the jet-wall interaction. To avoid an increase in soot formation, the authors suggested the implementation of split injections and larger bowl diameter, as well as increasing the inter-jet spacing to reduce the high-temperature gas re-entrainment and shorten the lift-off length. Similar results were found by Le et al. [90].

Chartier et al. [91] conducted lift-off measurements in an optical heavy-duty diesel engine, using various hardware configurations in order to investigate the influence of jet-to-jet interactions on the lift-off length. They indicated that burned gases from neighbor jets are entrained in the lift-off region, shortening the lift-off length. They also stated that this phenomenon gained importance when reducing the inter-jet spacing.

Additionally, the authors found a strong interaction between the chamber gas temperature and the spacing between jets. Specifically, their results stated that, for closer inter-jet spacing, the chamber temperature had a considerably lower influence on the lift-off length variations, in contrast with its impact for larger inter-jet spacing configurations. A plausible explanation noted by the authors is that the local gas temperature experienced by the jet, at close inter-jet conditions, is dominated by the re-entrained burned gas.

Moreover, Lequien et al. [92] studied the liquid length under reacting conditions in an optical heavy-duty diesel engine. The authors noticed a shorter

liquid length penetration for the spray with maximum inter-jet spacing, finding that the hot gas reservoirs formed by the combustion products near the lift-off area were not strongly influencing the liquid length. Moreover, the authors attributed this trend to the cooling effect of the surrounding jets.

The mentioned works were performed in real diesel engines, in which minor modifications were done to gain optical access to the combustion chamber. These studies are essential for engine calibration, as the combustion process is carried out under real engine volume and boundary conditions, although these conditions are not entirely controlled or known.

On the other hand, the fundamental analysis through optically accessible test rigs has allowed the visualization of the combustion process in a simplified and nearly quiescent environment with controlled boundary conditions. Bazyn and Koci [93] analyzed the lift-off length for several jet spacing configurations in an optically accessible test rig with a large chamber volume compared to the space within an engine combustion chamber. They also found that, as the inter-jet spacing decreased, so did the lift off-length. Nevertheless, the authors found that these variations only appeared below a threshold proximity between jets (around 36°). For spacing values above the threshold level, the sprays had a behavior similar to that of a single jet.

Although some investigations regarding the effect of inter-jet spacing on combustion have been done, its influence is not entirely defined, as most works have been qualitative studies. Furthermore, the majority of the investigations were carried out in real diesel engines.

In contrast, an optically accessible vessel with high-pressure and high-temperature capabilities is employed in this work to study the combustion development under various inter-jet spacing configurations, obtaining both qualitative and quantitative results. This test rig can develop a nearly quiescent environment while simulating the conditions found in the combustion chamber of current compression ignition engines in terms of temperature, pressure, and oxygen concentration.

## References

[1] Payri, Francisco; and Desantes, Jose Maria. *Motores de combustion interna alternativos*. Editorial Universitat Politecnica de Valencia, 2011.

[2] Heywood, John B. *Internal Combustion Engine Fundamentals*. Vol. 21. 1988, p. 930.

[3] Taylor, Charles Fayette. *The internal-combustion engine in theory and practice*. 2nd ed. Cambridge: MIT Press, 1989.

[4] Garcia-Oliver, Jose Maria. "Aportaciones al estudio del proceso de combustión turbulenta de chorros en motores Diesel de inyección directa". PhD thesis. Valencia: E.T.S. Ingenieros Industriales. Universidad Politécnica de Valencia, 2004.

[5] Armas, Octavio. "Diagnóstico experimental del proceso de combustión en motores Diesel de inyección directa". PhD thesis. Valencia: E.T.S. Ingenieros Industriales. Universidad Politécnica de Valencia, 1998.

[6] Balmer, Robert T. *Vapor and Gas Power Cycles*. 2011, pp. 447–534. DOI: 10.1016/b978-0-12-374996-3.00013-0.

[7] Gimeno, Jaime. "Desarrollo y aplicación de la medida de flujo de cantidad de movimiento de un chorro Diesel". PhD thesis. E.T.S. Ingenieros Industriales, Universidad Politécnica de Valencia, 2008. DOI: 10.4995/Thesis/10251/8306.

[8] Chaplya, Pavel M; Mitrovic, Milan; Carman, Gregory P; and Straub, Friedrich K. "Durability properties of piezoelectric stack actuators under combined electromechanical loading". In: *Journal of Applied Physics* 100.12 (2006), p. 124111. DOI: 10.1063/1.2407269.

[9] Payri, Raul; Gimeno, Jaime; Mata, Carmen; and Viera, Alberto. "Rate of injection measurements of a direct-acting piezoelectric injector for different operating temperatures". In: *Energy Conversion and Management* 154 (2018), pp. 387–393. DOI: 10.1016/j.enconman.2017.11.029.

[10] Bardi, Michele. "Partial needle lift and injection rate shape effect on the formation and combustion of the Diesel spray". PhD thesis. Valencia (Spain): Universitat Politècnica de València, 2014. DOI: 10.4995/Thesis/10251/37374.

[11] Viera, Juan Pablo et al. "Linking instantaneous rate of injection to X-ray needle lift measurements for a direct-acting piezoelectric injector". In: *Energy Conversion and Management* 112 (2016), pp. 350–358. DOI: 10.1016/j.enconman.2016.01.038.

[12] Payri, Raul; Gimeno, Jaime; Viera, Juan Pablo; and Plazas, Alejandro Hernan. "Needle lift profile influence on the vapor phase penetration for a prototype diesel direct acting piezoelectric injector". In: *Fuel* 113 (2013), pp. 257–265. DOI: 10.1016/j.fuel.2013.05.057.

[13] Lee, J W et al. "Effect of piezo-driven and solenoid-driven needle opening of common-rail diesel injectors on internal nozzle flow and spray development". In: *International Journal of Engine Research* 7.6 (2006), pp. 489–502. DOI: 10.1243/14680874JER00806.

[14] Suh, Hyun Kyu; Park, Sung Wook; and Lee, Chang Sik. "Effect of piezo-driven injection system on the macroscopic and microscopic atomization characteristics of diesel fuel spray". In: *Fuel* 86.17-18 (2007), pp. 2833–2845. DOI: 10.1016/j.fuel.2007.03.015.

[15] Carreres, Marcos. "Thermal Effects Influence on the Diesel Injector Perfomance through a Combined 1D Modelling and Experimental Approach". PhD thesis. Universitat Politècnica de València, 2016. DOI: 10.4995/Thesis/10251/73066.

[16] Kastengren, Alan L et al. "Engine Combustion Network (ECN): Measurements of Nozzle Geometry and Hydraulic Behavior". In: *Atomization and Sprays* 22.12 (2012), pp. 1011–1052. DOI: 10 . 1615 / AtomizSpr.2013006309.

[17] Bermúdez, Vicente; Payri, Raul; Salvador, Francisco Javier; and Plazas, Alejandro Hernan. "Study of the influence of nozzle seat type on injection rate and spray behavior". In: *ImechE. Journal of automobile engineering* 219.5 (2005), pp. 677–689. DOI: 10.1243/095440705X28303.

[18] Benajes, Jesus; Pastor, Jose Vicente; Payri, Raul; and Plazas, Alejandro Hernan. "Analysis of the influence of Diesel nozzle geometry in the Injection Rate characteristic". In: *Journal of Fluids Engineering* 126.1 (2004), pp. 63–71. DOI: 10.1115/1.1637636.

[19] Payri, Raul; Garcia-Oliver, Jose Maria; Salvador, Francisco Javier; and Gimeno, Jaime. "Using spray momentum flux measurements to understand the influence of diesel nozzle geometry on spray characteristics". In: *Fuel* 84.5 (2005), pp. 551–561. DOI: 10.1016/j.fuel.2004.10.009.

[20] Viera, Juan Pablo. "Experimental study of the effect of nozzle geometry on the performance of direct-injection diesel sprays for three different fuels". PhD thesis. 2017. DOI: 10.4995/Thesis/10251/81857.

[21] Bosch, Wilhelm. "The Fuel Rate Indicator: A New Measuring Instrument for Display of the Characteristics of Individual Injection". In: *SAE Technical Paper 660749* (1966). DOI: 10.4271/660749.

[22] Salvador, Francisco Javier; Gimeno, Jaime; Carreres, Marcos; and Crialesi-Esposito, Marco. "Fuel temperature influence on the performance of a last generation common-rail diesel ballistic injector. Part I: Experimental mass flow rate measurements and discussion". In: *Energy Conversion and Management* 114 (2016), pp. 364–375. DOI: 10.1016/j.enconman.2016.02.042.

[23] Payri, Raul; Martí-Aldavarí, Pedro; Montiel, Tomas; and Viera, Alberto. "Influence of aging of a diesel injector on multiple injection strategies". In: *Applied Thermal Engineering* 181.August (2020), p. 115891. DOI: 10.1016/j.applthermaleng.2020.115891.

[24] Essien, S.; Archibong-Eso, A.; and Lao, L. "Discharge coefficient of high viscosity liquids through nozzles". In: *Experimental Thermal and Fluid Science* 103.January (2019), pp. 1–8. DOI: 10.1016/j.expthermflusci.2019.01.004.

[25] Payri, Raul; Hardy, Gilles; Gimeno, Jaime; and Bautista, Abian. "Analysis of counterbore effect in five diesel common rail injectors". In: *Experimental Thermal and Fluid Science* 107.February (2019), pp. 69–78. DOI: 10.1016/j.expthermflusci.2019.05.008.

[26] Fox, T A; and Stark, J. "Discharge coefficients for miniature fuel injectors". In: *Aerospace Engineering* 203.1 (1989), pp. 75–78. DOI: 10.1243/PIME_PROC_1989_203_056_01.

[27] Salvador, Francisco Javier. "Estudio teórico experimental de la influencia de la geometría de toberas de inyección Diésel sobre las características del flujo interno y del chorro". PhD thesis. Valencia: E.T.S. Ingenieros Industriales. Universidad Politécnica de Valencia, 2003.

[28] Desantes, Jose Maria; Pastor, Jose Vicente; Garcia-Oliver, Jose Maria; and Pastor, Jose Manuel. "A 1D model for the description of mixing-controlled reacting diesel sprays". In: *Combustion and Flame* 156.1 (2009), pp. 234–249. DOI: 10.1016/j.combustflame.2008.10.008.

[29] Pastor, Jose Vicente; Lopez, Jose Javier; Garcia-Oliver, Jose Maria; and Pastor, Jose Manuel. "A 1D model for the description of mixing-controlled inert diesel sprays". In: *Fuel* 87.13-14 (2008), pp. 2871–2885. DOI: 10.1016/j.fuel.2008.04.017.

[30] Desantes, Jose Maria; Salvador, Francisco Javier; Carreres, Marcos; and Martínez-López, Jorge. "Large-eddy simulation analysis of the influence of the needle lift on the cavitation in diesel injector nozzles". In: *Proceedings of the Institution of Mechanical Engineers, Part D: Journal of Automobile Engineering* 229.4 (2014), pp. 407–423. DOI: 10.1177/0954407014542627.

[31] Salvador, Francisco Javier; Martínez-López, Jorge; Caballer, M.; and De Alfonso, C. "Study of the influence of the needle lift on the internal flow and cavitation phenomenon in diesel injector nozzles by CFD using RANS methods". In: *Energy Conversion and Management* 66 (2013), pp. 246–256. DOI: 10.1016/j.enconman.2012.10.011.

[32] Martínez-López, Jorge. "Estudio computacional de la influencia del levantamiento de aguja sobre el flujo interno y el fenómeno de la cavitación en toberas de inyección Diesel". PhD thesis. Valencia: Universitat Politecnica de Valencia, 2013.

[33] Salvador, Francisco Javier; De la Morena, Joaquin; Crialesi-Esposito, Marco; and Martínez-López, Jorge. "Comparative study of the internal flow in diesel injection nozzles at cavitating conditions at different needle lifts with steady and transient simulations approaches". In: *Proceedings of the Institution of Mechanical Engineers, Part D: Journal of Automobile Engineering* 232.8 (2018), pp. 1060–1078. DOI: 10.1177/0954407017725672.

[34] Viera, Alberto. "Effect of multiple injection strategies on the diesel spray formation and combustion using optical diagnostics". PhD thesis. Universitat Politècnica de València, 2019. DOI: 10.4995/Thesis/10251/123954.

[35] Molina, Santiago. "Influencia de los parámetros de inyección y la recirculación de gases de escape sobre el proceso de combustión en un motor diesel". PhD thesis. Barcelona, 2005.

[36] Alkidas, A C. "On the Premixed Combustion in a Direct-Injection Diesel Engine". In: *Journal of Engineering for Gas Turbines and Power* 109.2 (1987), pp. 187–192. DOI: 10.1115/1.3240023.

[37] Carlucci, Paolo; Ficarella, Antonio; and Laforgia, Domenico. "Effects on combustion and emissions of early and pilot fuel injections in diesel engines". In: *International Journal of Engine Research* 6.1 (2005), pp. 43–60. DOI: 10.1243/146808705X7301.

[38] Badami, M; Millo, Federico; and D'Amato, D D. "Experimental investigation on soot and NOx formation in a DI common rail diesel engine with pilot injection". In: *SAE Technical Paper 2001-01-0657* (2001). DOI: 10.4271/2001-01-0657.

[39] Mingfa, Yao; Hu, Wang; Zunqing, Zheng; and Yan, Yue. "Experimental Study of Multiple Injections and Coupling Effects of Multi-Injection and EGR in a HD Diesel Engine". In: *SAE Technical Paper 2009-01-2807* (2009). DOI: 10.4271/2009-01-2807.

[40] Binde, Andreas; Busch, Stephen; Velji, Amin; and Wagner, Uwe. "Soot and NO x Reduction by Spatially Separated Pilot Injection". In: *SAE International Journal of Engines* 5.3 (2012), pp. 1242–1259. DOI: 10.4271/2012-01-1159.

[41] Payri, Raul; Bracho, Gabriela; Marti-Aldaravi, Pedro; and Viera, Alberto. "Near field visualization of diesel spray for different nozzle inclination angles in non-vaporizing conditions". In: *Atomization and Sprays* 27.3 (2017), pp. 251–267. DOI: 10.1615/AtomizSpr.2017017949.

[42] Siebers, Dennis L. "Scaling liquid-phase fuel penetration in diesel sprays based on mixing-limited vaporization". In: *SAE Technical Paper 1999-01-0528* (1999). DOI: 10.4271/1999-01-0528.

[43] Siebers, Dennis L. "Liquid-Phase Fuel Penetration in Diesel Sprays". In: *SAE Technical Paper 980809* (1998), pp. 1–23. DOI: 10.4271/980809.

[44] Payri, Raul; Gimeno, Jaime; Bardi, Michele; and Plazas, Alejandro Hernan. "Study liquid length penetration results obtained with a direct acting piezo electric injector". In: *Applied Energy* 106.JUNE (2013), pp. 152–162. DOI: 10.1016/j.apenergy.2013.01.027.

[45] Payri, Raul; Gimeno, Jaime; Bracho, Gabriela; and Vaquerizo, Daniel. "Study of liquid and vapor phase behavior on Diesel sprays for heavy duty engine nozzles". In: *Applied Thermal Engineering* 107 (2016), pp. 365–378. DOI: 10.1016/j.applthermaleng.2016.06.159.

[46] Payri, Francisco; Bermúdez, Vicente; Payri, Raul; and Salvador, Francisco Javier. "The influence of cavitation on the internal flow and the spray characteristics in diesel injection nozzles". In: *Fuel* 83.4-5 (2004), pp. 419–431. DOI: 10.1016/j.fuel.2003.09.010.

[47] Naber, Jeffrey D; and Siebers, Dennis L. "Effects of Gas Density and Vaporization on Penetration and Dispersion of Diesel Sprays". In: *SAE Paper 960034*. Vol. 105. 412. Society of Automotive Engineers, Inc., Warrendale, Pennsylvania, USA, 1996, pp. 82–111. DOI: 10.4271/960034.

[48] Wan, Yuepeng; and Peters, Norbert. "Scaling of spray penetration with evaporation". In: *Atomization and Sprays* 9.2 (1999), pp. 111–132. DOI: 10.1615/AtomizSpr.v9.i2.10.

[49] Hiroyasu, Hiroyuki; and Arai, Masataka. "Structures of Fuel Sprays in Diesel Engines". In: *SAE Technical Paper 900475*. 1990. DOI: 10.4271/900475.

[50] Correas, David. "Estudio teórico-experimental del chorro libre Diesel isotermo". PhD thesis. Valencia: E.T.S. Ingenieros Industriales. Universidad Politécnica de Valencia, 1998.

[51] Giraldo Valderrama, Jhoan Sebastián. "Macroscopic and microscopic characterization of non-reacting diesel sprays at low and very high injection pressures". PhD thesis. Universitat Politècnica de València, 2018.

[52] Manin, Julien; Bardi, Michele; Pickett, Lyle M; Dahms, R. N.; and Oefelein, J. C. "Microscopic investigation of the atomization and mixing processes of diesel sprays injected into high pressure and temperature environments". In: *Fuel* 134 (2014), pp. 531–543. DOI: 10.1016/j.fuel.2014.05.060.

[53] Manin, J.; Bardi, M.; Pickett, L. M.; and Payri, R. "Boundary condition and fuel composition effects on injection processes of high-pressure sprays at the microscopic level". In: *International Journal of Multiphase Flow* 83 (2016), pp. 267–278. DOI: 10.1016/j.ijmultiphaseflow.2015.12.001.

[54] Jung, Yongjin; Manin, Julien; Skeen, Scott A; and Pickett, Lyle M. "Measurement of Liquid and Vapor Penetration of Diesel Sprays with a Variation in Spreading Angle". In: *SAE Technical Paper 2015-01-0946* (2015). DOI: 10.4271/2015-01-0946.

[55] Payri, Raul; Molina, Santiago; Salvador, Francisco Javier; and Gimeno, Jaime. "A study of the relation between nozzle geometry, internal flow and sprays characteristics in diesel fuel injection systems". In: *KSME International Journal* 18.7 (2004), pp. 1222–1235. DOI: 10.1007/BF02983297.

[56] Delacourt, E; Desmet, B; and Besson, B. "Characterisation of very high pressure Diesel sprays using digital imaging techniques". In: *Fuel* 84.7-8 (2005), pp. 859–867. DOI: 10.1016/j.fuel.2004.12.003.

[57] Wu, K J; Su, C C; Steinberger, R L; Santavicca, D A; and Bracco, Frediano V. "Measurements of the spray angle of atomizing jets". In: *Journal of fluids Engineering* 105.4 (1983), pp. 406–410. DOI: 10.1115/1.3241019.

[58] Gaydon, A G. *The Spectroscopy of Flames*. Springer Netherlands, 1974. DOI: 10.1007/978-94-009-5720-6.

[59] Higgins, Brian; Siebers, Dennis L; and Aradi, Allen. "Diesel-Spray Ignition and Premixed-Burn Behavior". In: *SAE Technical Paper 2000-01-0940* (2000). DOI: 10.4271/2000-01-0940.

[60] Westbrook, C K et al. "The effects of pressure, temperature, and concentration on the reactivity of alkanes: Experiments and modeling in a rapid compression machine". In: *International Symposium on Combustion* 27.1 (1998), pp. 371–378. DOI: 10.1016/S0082-0784(98)80425-6.

[61] Pickett, Lyle M.; Siebers, Dennis L.; and Idicheria, Cherian A. "Relationship Between Ignition Processes and the Lift-Off Length of Diesel Fuel Jets". In: *SAE Paper 2005-01-3843* 724 (2005). DOI: 10.4271/2005-01-3843.

[62] Dec, John E; and Espey, Christoph. "Chemiluminescence Imaging of Autoignition in a DI Diesel Engine". In: *SAE Technical Paper 982685* 724 (1998). DOI: 10.4271/982685.

[63] Siebers, Dennis L; and Higgins, Brian. "Flame Lift-Off on Direct-Injection Diesel Sprays Under Quiescent Conditions". In: *SAE Technical Paper 2001-01-0530* 724 (2001).

[64] Payri, Raul; Viera, Juan Pablo; Pei, Yuanjiang; and Som, Sibendu. "Experimental and numerical study of lift-off length and ignition delay of a two-component diesel surrogate". In: *Fuel* 158 (2015), pp. 957–967. DOI: 10.1016/j.fuel.2014.11.072.

[65] Jakob, Markus et al. "Simultaneous high-speed visualization of soot luminosity and OH * chemiluminescence of alternative-fuel combustion in a HSDI diesel engine under realistic operating conditions". In: *Combustion and Flame* 159.7 (2012), pp. 2516–2529. DOI: 10.1016/j.combustflame.2012.03.004.

[66] Pastor, José V.; García, A.; Micó, C.; and García-Carrero, Alba A. "Experimental study of influence of Liquefied Petroleum Gas addition in Hydrotreated Vegetable Oil fuel on ignition delay, flame lift off length and soot emission under diesel-like conditions". In: *Fuel* 260.July 2019 (2020), p. 116377. DOI: 10.1016/j.fuel.2019.116377.

[67] Knox, Benjamin W. "End-of-Injection Effects on Diesel Spray Combustion". PhD thesis. Georgia Institute of Technology, 2016.

[68] Benajes, Jesus; Payri, Raul; Bardi, Michele; and Martí-aldaraví, Pedro. "Experimental characterization of diesel ignition and lift-off length using a single-hole ECN injector". In: *Applied Thermal Engineering* 58.1-2 (2013), pp. 554–563. DOI: 10.1016/j.applthermaleng.2013.04.044.

[69] Payri, Raul; Salvador, Francisco Javier; Manin, Julien; and Viera, Alberto. "Diesel ignition delay and lift-off length through different methodologies using a multi-hole injector". In: *Applied Energy* 162 (2016), pp. 541–550. DOI: 10.1016/j.apenergy.2015.10.118.

[70] Kobori, S; Kamimoto, T; and Aradi, A A. "A study of ignition delay of diesel fuel sprays". In: *International Journal of Engine Research* 1.29 (2000), pp. 29–39. DOI: 10.1243/1468087001545245.

[71] Bruneaux, Gilles. "Development of optical diagnostics techniques to correlate mixing and auto-ignition processes in high pressure diesel jets". In: *Oil and Gas Science and Technology* 63.4 (2008), pp. 461–477. DOI: 10.2516/ogst:2008031.

[72] Lillo, Peter M; Pickett, Lyle M; Persson, Helena; Andersson, Oivind; and Kook, Sanghoon. "Diesel Spray Ignition Detection and Spatial/Temporal Correction". In: *SAE Paper 2012-01-1239* (2012), pp. 1–21. DOI: 10.4271/2012-01-1239.

[73] Payri, Raul; Viera, Juan Pablo; Gopalakrishnan, Venkatesh; and Szymkowicz, Patrick G. "The effect of nozzle geometry over ignition delay and flame lift-off of reacting direct-injection sprays for three different fuels". In: *Fuel* 199 (2017), pp. 76–90. DOI: 10.1016/j.fuel.2017.02.075.

[74] Dec, John E; and Coy, Edward B. "OH Radical Imaging in a DI Diesel Engine and the Structure of the Early Diffusion Flame". In: 412 (1996). DOI: 10.4271/960831.

[75] Higgins, Brian; and Siebers, Dennis L. "Measurement of the Flame Lift-Off Location on DI Diesel Sprays Using OH Chemiluminescence". In: *SAE Technical Paper 2001-01-0918* (2001).

[76] Pickett, Lyle M; Kook, Sanghoon; Persson, Helena; and Andersson, Öivind. "Diesel fuel jet lift-off stabilization in the presence of laser-induced plasma ignition". In: *Proceedings of the Combustion Institute* 32 (2009), pp. 2793–2800. DOI: 10.1016/j.proci.2008.06.082.

[77] Taskiran, Ozgur Oguz; and Ergeneman, Metin. "Effect of nozzle dimensions and fuel type on flame lift-off length". In: *Fuel* 115 (2014), pp. 833–840. DOI: 10.1016/j.fuel.2013.03.005.

[78] Dec, John E. "A Conceptual Model of DI Diesel Combustion Based on Laser-Sheet Imaging". In: *SAE Technical Paper 970873* (1997). DOI: 10.4271/970873.

[79] Flynn, P et al. "Diesel combustion: an integrated view combining laser diagnostics, chemical kinetics, and empirical validation". In: *SAE Paper 1999-01-0509* 724 (1999).

[80] Xi, Jun; and Zhong, Bei Jing. "Soot in diesel combustion systems". In: *Chemical Engineering and Technology* 29.6 (2006), pp. 665–673. DOI: 10.1002/ceat.200600016.

[81] Dec, John E; and Canaan, Robert E. "PLIF Imaging of NO Formation in a DI Diesel Engine". In: *SAE Technical Paper 980147* (1998). DOI: 10.4271/980147.

[82] Nishida, Keiya; Jingyu, Zhu; Xianyin, Leng; and He, Zhixia. "Effects of micro-hole nozzle and ultra-high injection pressure on air entrainment, liquid penetration, flame lift-off and soot formation of diesel spray flame". In: *International Journal of Engine Research* 18.1-2 (2017), pp. 51–65.

[83] Payri, Raul; Bracho, Gabriela; Martí-Aldaraví, Pedro; and Viera, Alberto. "Nozzle geometry size influence on reactive spray development: from Spray B to heavy duty applications". In: *SAE Technical Paper 2017-01-0846* (2017), p. 12. DOI: 10.4271/2017-01-0846.

[84] Sayin, Cenk; Gumus, Metin; and Canakci, Mustafa. "Influence of injector hole number on the performance and emissions of a di diesel engine fueled with biodiesel-diesel fuel blends". In: *Applied Thermal Engineering* 61.2 (2013), pp. 121–128. DOI: 10.1016/j.applthermaleng.2013.07.038.

[85] Lahane, Subhash; and Subramanian, K. A. "Impact of nozzle holes configuration on fuel spray, wall impingement and NOx emission of a diesel engine for biodiesel-diesel blend (B20)". In: *Applied Thermal Engineering* 64.1-2 (2014), pp. 307–314. DOI: 10.1016/j.applthermaleng.2013.12.048.

[86] Han, Sangwook; Kim, Jaeheun; and Bae, Choongsik. "Effect of air-fuel mixing quality on characteristics of conventional and low temperature diesel combustion". In: *Applied Energy* 119 (2014), pp. 454–466. DOI: 10.1016/j.apenergy.2013.12.045.

[87] Zhou, L. Y. et al. "Measurements and analyses on the transient discharge coefficient of each nozzle hole of multi-hole diesel injector". In: *Sensors and Actuators, A: Physical* 244 (2016), pp. 198–205. DOI: 10.1016/j.sna.2016.04.017.

[88] Aori, Gele; Hung, David L S; and Zhang, Ming. "Effect of Nozzle Configuration on Macroscopic Spray Characteristics of Multi-Hole Fuel Injectors Under Superheated Conditions". In: *Atomization and Sprays* 26.5 (2016), pp. 439–462. DOI: 10.1615/AtomizSpr.2015011990.

[89] Rusly, Alvin M.; Le, Minh K.; Kook, Sanghoon; and Hawkes, Evatt R. "The shortening of lift-off length associated with jet-wall and jet-jet interaction in a small-bore optical diesel engine". In: *Fuel* 125 (2014), pp. 1–14. DOI: 10.1016/j.fuel.2014.02.004.

[90] Le, Minh K. et al. "Effect of jet-jet interactions on soot formation in a small-bore diesel engine". In: *Proceedings of the Combustion Institute* 36.3 (2017), pp. 3559–3566. DOI: 10.1016/j.proci.2016.07.025.

[91] Chartier, Clément; Aronsson, Ulf; Andersson, Öivind; Egnell, Rolf; and Johansson, Bengt. "Influence of jet-jet interactions on the lift-off length in an optical heavy-duty di diesel engine". In: *Fuel* 112 (2013), pp. 311–318. DOI: 10.1016/j.fuel.2013.05.021.

[92] Lequien, Guillaume et al. "Effect of jet-jet interactions on the liquid fuel penetration in an optical heavy-duty di diesel engine". In: *SAE Technical Papers* 2 (2013). DOI: 10.4271/2013-01-1615.

[93] Bazyn, Tim; and Koci, Chad. "The Effect of Jet Spacing on the Combustion Characteristics of Diesel Sprays". In: *THIESEL 2014 Conference on Thermo- and Fluid Dynamic Processes in Direct Injection Engines*. 2014, pp. 1–19.

# Chapter 3

# Materials and methods

## 3.1 Introduction

The current chapter details the equipment and methods used throughout the experiments, which were done entirely within the CMT-Motores Térmicos institute. First, the injection system is described. Then, the chapter continues with a description of the test rigs and post-processing employed for the hydraulic characterization of the sprays. Lastly, the chapter presents the test rig and optical set-ups used for the visualization campaigns and the subsequent image processing methodologies.

## 3.2 Injection system

### 3.2.1 Fuel delivery system

The fuel feeding system is depicted in Figure 3.1. Initially, fuel is retrieved from the tank and sent through a purger to take out the air, followed by a filter to remove particles and impurities contained in the fuel. Then, the required combustible goes inside the CP3 pump, where its pressure is raised to the desired injection pressure and sent to the common-rail and contained.

Afterward, the pressurized fuel is directed through a high-pressure line to a second common-rail, which serves two purposes: further reducing the pressure variations of the fuel due to the pump cycles [1, 2], and complying with Engine Combustion Network (ECN) standards [3] of common-rail dimensions and distance from the injector. Specifically, the common-rail (volume= 22 $cm^3$,

length = 28 cm) is connected to the injector through a rigid high-pressure line (inside/outside diameter = 2.4/6 mm, length 24 cm). Lastly, the returning fuel from the pump and the first common-rail is directed through a heat exchanger to control its temperature, and then sent back to the purger.

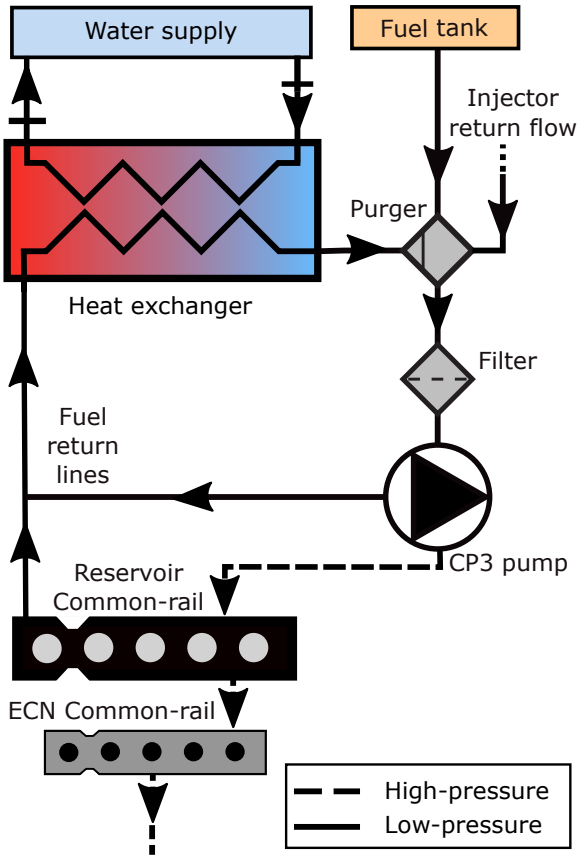


*Figure 3.1: Fuel delivery system diagram.*

Commercially available diesel was employed, and the general properties at ambient conditions are depicted in Table 3.1.

### 3.2.2 Diesel injectors

The injectors employed throughout the experiments were the piezo common-rail type 5 from Continental [4]. Both of them have identical designs, except for the distribution of the outlet holes of the nozzle. Concretely, different outlet

*Table 3.1: Fuel general properties at 313 K and 101 KPa.*

| **Density** $[Kg/m^3]$ | **Viscosity** $[mm^2/s]$ | **Surface tension** $[N/m]$ | **Boiling point** $[K]$ | **Cetane number** [-] | $C_{p,liq}$ $[J/kgK]$ |
|---|---|---|---|---|---|
| 825 | 2.34 | 0.021 | 450-520 | 51 | 2002 |

orifices configurations were established (Figure 3.2) as they were specifically manufactured to study the influence of the inter-jet spacing.

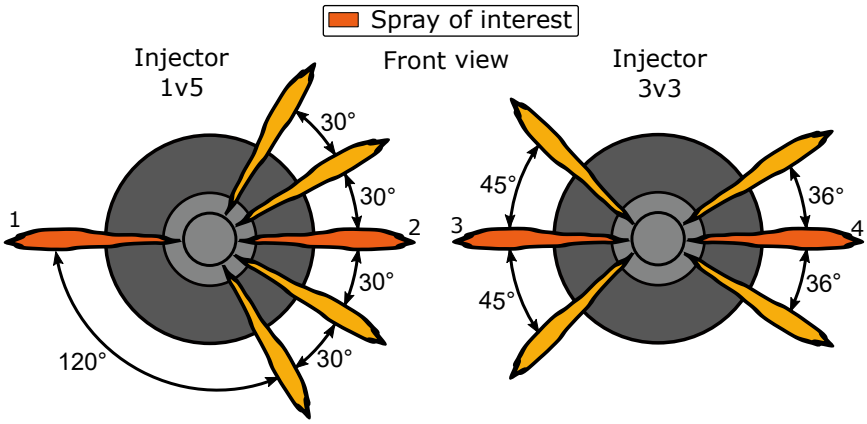


*Figure 3.2: Geometric distribution of the outlet holes (front view).*

The nozzle of the injector 1v5 has an outlet hole to one side, which was taken as the reference isolated spray (inter-jet spacing of 120°), and five orifices to the other side with a spacing between jets of 30°, representing an injector of 12 equally distributed holes. On the other hand, the injector 3v3 has three holes on each side, in which one set has an inter-jet spacing of 36° and the other of 45°, emulating an injector with 10 and 8 holes, respectively. Both injectors can manage up to 250 MPa of injection pressure.

In this work, the sprays of interest are enumerated and highlighted in dark orange. These are the isolated spray and the sprays in the center of each configuration, ensuring the presence of neighbor jets. A side view illustrating the height angle is depicted in Figure 3.3.

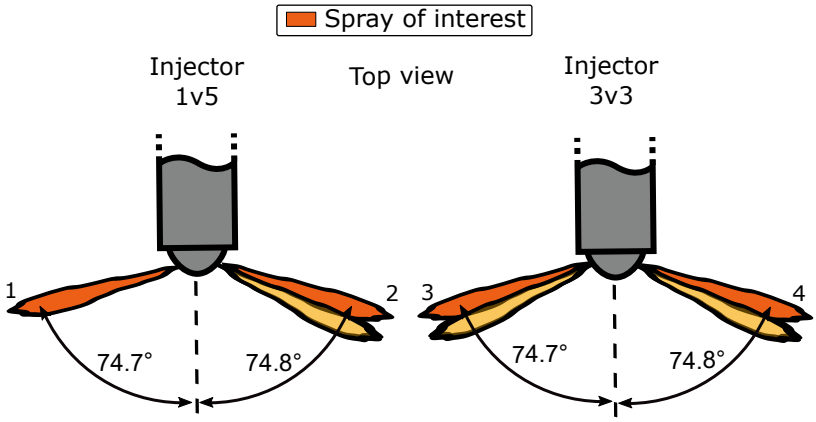


*Figure 3.3: Geometric distribution of the outlet holes (side view).*

Moreover, the geometry of each nozzle and hole of interest is presented in Table 3.2 and Table 3.3, respectively.

*Table 3.2: Geometry of the nozzle of each injector.*

| **Parameter** | **1v5 injector** | **3v3 injector** | **Units** |
|---|---|---|---|
| Number of orifices | 6 | 6 | - |
| Degree of hydro-erosion | 7.7 | 7.7 | % |
| Avg. height angle | 74.8 | 74.8 | degrees |
| Avg. *k–factor* | 5.3 | 5.1 | - |
| Avg. outlet diameter ($\overline{D}_o$) | 90.7 | 91.5 | µm |
| Nominal flow rate | 313* | 322* | mL min$^{-1}$ |

* At 10 MPa of injection pressure.

*Table 3.3: Geometry of the holes of interest.*

| **Orifice** | **1** | **2** | **3** | **4** |
|---|---|---|---|---|
| Outlet diameter [$\mu m$] | 90.9 | 90.1 | 91.3 | 90.5 |
| Height angle [°] | 74.7 | 74.8 | 74.7 | 74.8 |
| K-factor [-] | 5.1 | 5.3 | 5.0 | 5.3 |

In particular, Table 3.3 shows the high resemblance between the orifices of interest, excluding their geometric shape as a possible cause of considerable

variations in performance. For instance, the difference in hole diameter was under 1.3% between any pair of orifices of interest.

Furthermore, orifices with high k-factor [5] were fabricated given that increasing the conicity inhibits cavitation appearance inside the nozzle orifices [6, 7]. The manufacturer provided the geometry of the injector.

## 3.3 Hydraulic Characterization

### 3.3.1 Rate of injection

Figure 3.4 depicts a diagram of the injection rate discharge curve indicator (IRDCI), the test rig employed for the rate of injection measurements.

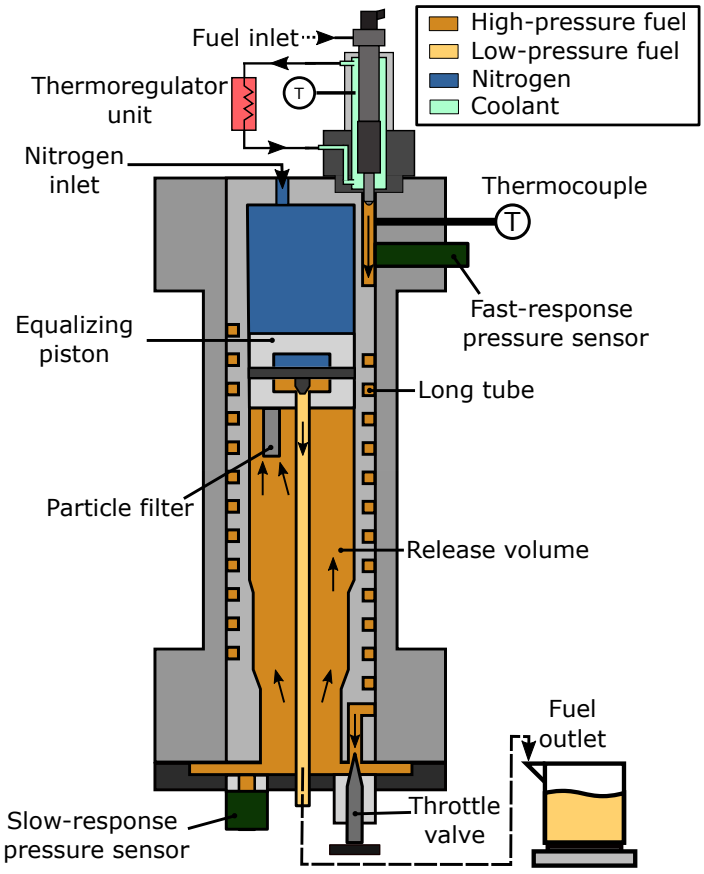


*Figure 3.4: Rate of injection test rig diagram.*

The injector is immersed in circulating coolant (ethylene glycol at 30 % pumped at a rate of 60 L/min) to take its temperature up to 363 K. This proceeding is essential, as the performance of a piezoelectric injector dramatically depends on its working temperature [8].

The rate of injection (ROI) measurements were done applying the Bosch long-tube methodology [9]. When fuel is injected into the measurement tube, a pressure wave is generated. The fast-response pressure sensor, a piezoelectric transducer, captures the pressure variation caused by the injection event. From the signal, it is possible to calculate the instantaneous mass flow rate through the following steps [10]:

- The injection event generates a pressure difference reflected on the pressure wave. The trajectory of the pressure wave is detailed by Payri et al. [4], and this pressure variation can be computed with the Allievi equation, which is valid for a simple pressure wave in steady flows [11]:

$$\Delta p = \rho_f \cdot a_f \cdot u_f \tag{3.1}$$

  In which $\Delta p$ is the pressure increase due to the injection (measured by the piezoelectric sensor), $\rho_f$ is the density of the fuel, $a_f$ is the speed of sound in the fuel, and $u_f$ is the velocity of the fuel in the section.

- The fuel density and speed of sound were computed based on the fuel and boundary conditions employed. Specifically, these variables were obtained with the correlation developed by Payri et al. [12] for commercial diesel, the fuel employed throughout this study:

$$\begin{aligned}(a_f, \rho_f) = {} & k_1 + k_2\,(T_{cv} - T_0) + k_3\,(p_{cv} - p_0) \\ & + k_4\,(p_{cv} - p_0)^2 + k_5\,(T_{cv} - T_0)^2 + k_6 (p_{cv} - p_0)(T_{cv} - T_0)\end{aligned} \tag{3.2}$$

  Where $T_0$ and $p_0$ represent the chamber temperature (298 K) and pressure (0.1 MPa), respectively. On the other hand, $T_{cv}$ and $p_{cv}$ are the temperature and pressure in the control volume and are measured by the thermocouple and the slow-response pressure sensor, respectively. Lastly, the $K_s$ coefficients are listed in Table 3.4.

*Table 3.4: Coefficients employed to compute the fuel density and speed of sound [12].*

| - | $a_f$ [m s$^{-1}$] | $\rho_f$ [kg m$^{-3}$] |
|---|---|---|
| $k1$ | 1363.05 | 835.698 |
| $k2$ | -3.11349 | -0.6280 |
| $k3$ | 4.1751 | 0.4914 |
| $k4$ | -0.006968 | -0.000705 |
| $k5$ | 0 | 0.000737 |
| $k6$ | 0.009401 | 0.001036 |

- With Equation 3.1 and Equation 3.2, it is possible to obtain both $u_f$ and $\rho_f$. Moreover, considering the cylindrical shape of the long tube, the cross-sectional section of the control volume ($A_t$) can be computed. Lastly, the mass flow rate ($\dot{m}$) can be obtained by the continuity equation:

$$\dot{m} = \rho_f \cdot A_t \cdot \Delta u_f \tag{3.3}$$

  Combining Equation 3.1 and Equation 3.3, $\dot{m}$ can also be expressed in terms of $\Delta p$:

$$\dot{m} = \frac{A_t}{a_f} \Delta p \tag{3.4}$$

  This process is continuously done at each moment of the injection, and a temporal signal of the mass flow rate is obtained (Figure 3.5).

  After the initial transitory phase, a stable flow is set; and every temporal value of this steady state is averaged into the final injection rate flow $\dot{m}$. Moreover, the signal can be integrated to determine the total injected mass.

On the other hand, the pressure difference induced by the injection event unseals the IRDCI exit, letting out an amount of mass equivalent to the mass injected. The outlet mass is deposited on a downstream scale and compared to the injected mass measured by the piezoelectric sensor [10].

This comparison is important given that the injected mass measured through the piezoelectric sensor is subject to some uncertainties, such as cycle-to-cycle variations, temperature, and speed of sound variations along the fuel

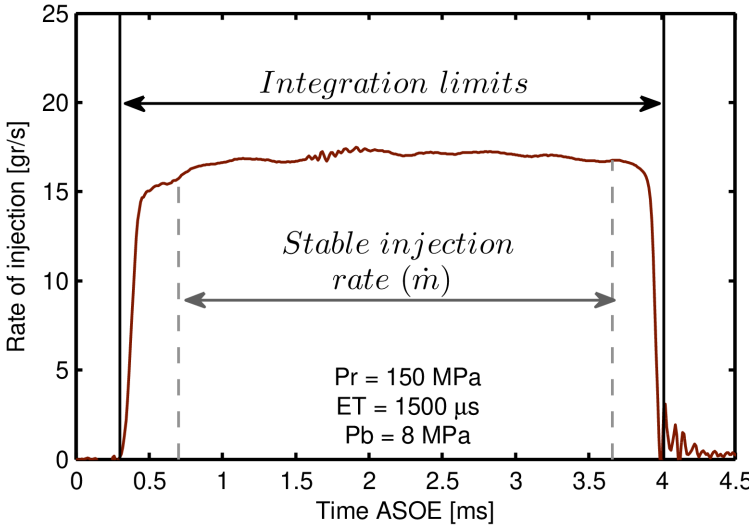


*Figure 3.5: Rate of injection curve.*

trajectory, among others. Thus, there could be a difference when compared to the mass value measured by the scale.

Therefore, a methodology developed in the laboratory is used to account for these variations, which has been widely employed in various works [8, 10, 13–15]. In particular, a scaling factor is computed by taking the ratio between the injected mass measured through the scale and that from the integrated signal, as detailed in Equation 3.5:

$$k_{adjust} = \frac{m_{scale}}{m_{int}} \tag{3.5}$$

To minimize measuring errors and uncertainties, 50 cycles of each test point were made and averaged into a final signal (Figure 3.6). Then, the signal is corrected to account for the cumulative phenomenon [13].

Finally, shot-to-shot dispersion is evaluated through the relative standard deviation of the stabilized injection rate.

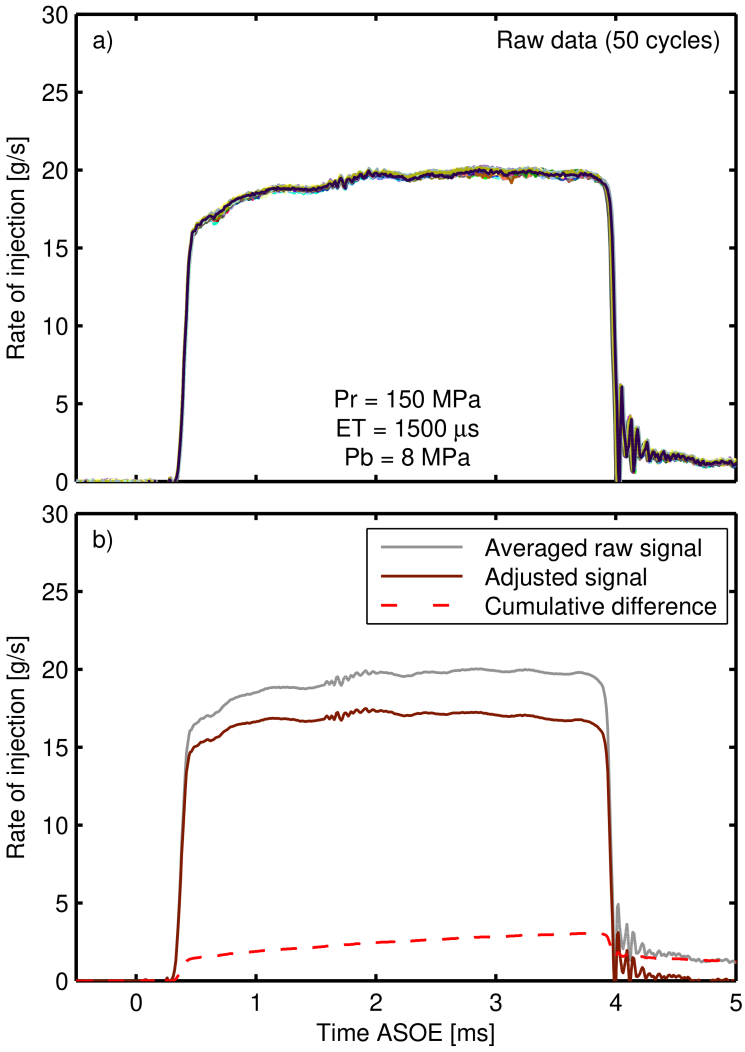


*Figure 3.6: Process to obtain the final rate of injection curve.*

### 3.3.2 Momentum Flux

Momentum flux measurements were done to assess the status of the outlet orifices of the injector, as this technique allowed the study of each hole of the nozzle individually. In Figure 3.7, part of the used equipment is shown.

High-pressure fuel is delivered to the injector, which is subject to the same refrigerating system detailed in the rate of injection section. Within the cham-

ber, the hole of interest is faced to the pressure sensor. This pressure sensor is mounted on the sensor holder and employed to measure the impact force of the spray during the injection.

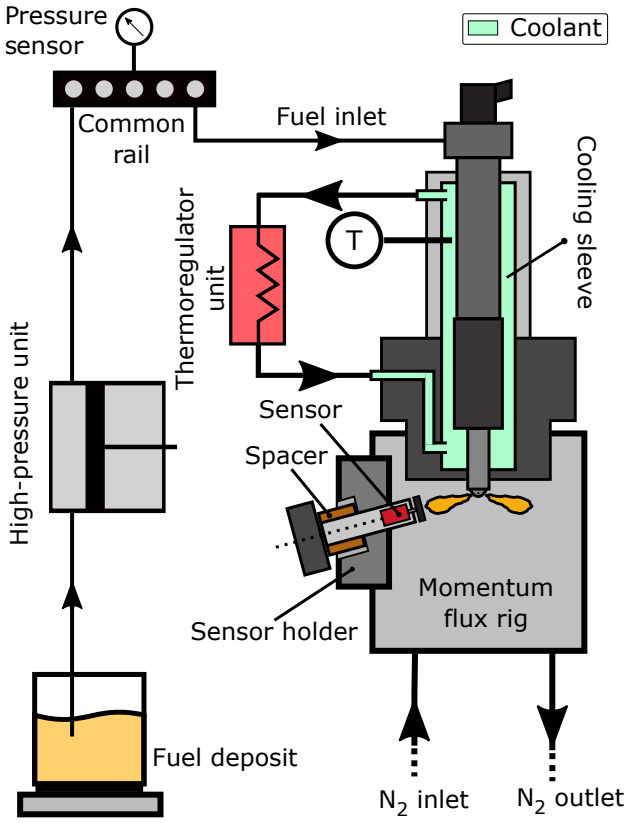


*Figure 3.7: Momentum flux test rig schematic diagram.*

Additionally, spacers are used to separate the sensor from the nozzle tip at a convenient distance. To do so, an equilibrium was found in which the sensor was kept close enough to ensure the entire jet was obtained and far enough to avoid interference from the neighbor jets [6]. Also, the chamber pressure was controlled through valves connected to a pressurized nitrogen tank. Moreover, the holder was perpendicularly aligned to the spray, as depicted in Figure 3.8.

Shortly after the injection starts, the fuel spray reaches the pressure sensor. This sensor captures the temporal evolution of the impact force ($F$) received from the spray. From this measurement, it is possible to obtain the momentum flux of the spray, assuming the following conditions [14, 16]:

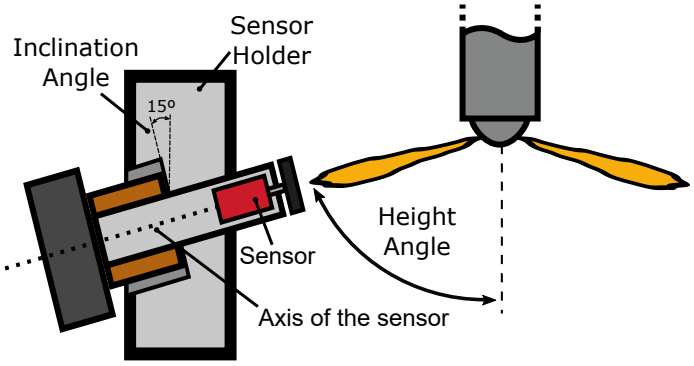


*Figure 3.8: Sensor alignment in the momentum flux test rig.*

- The gravity force is much smaller than the impact force ($F$), thus negligible.
- The fuel spray direction is aligned with the axis of the piezoelectric sensor. In other words, the spray perpendicularly impacts the surface of the sensor.
- The direction of the nitrogen that will be entrained by the spray and the direction of the fuel after impacting the surface of the sensor are perpendicular to the axis of the sensor and the movement of the spray. Then, the axial component of the force produced by these flows is negligible.
- The chamber pressure is constant and uniform along the spray trajectory.

Then, it is possible to relate the impact force to the momentum flux ($\dot{M}$) by applying the law of momentum conservation in a control volume adjacent to the pressure sensor (such as the one depicted in purple dashed lines in Figure 3.9):

$$F = \frac{\partial}{\partial t} \int_{CV} \rho \, u \, d\varpi \, + \, \dot{M} \tag{3.6}$$

In which $\rho$ and $u$ are the air-fuel mixture density and velocity, respectively. $d\varpi$ represents the surface of the sensor that the fuel impacts. For long enough injections, the mixture flow stabilizes, and the first element of the right-side of Equation 3.6 becomes negligible.

Therefore, during the stationary phase of injection, Equation 3.6 can be simplified to:

$$F = \dot{M} \tag{3.7}$$

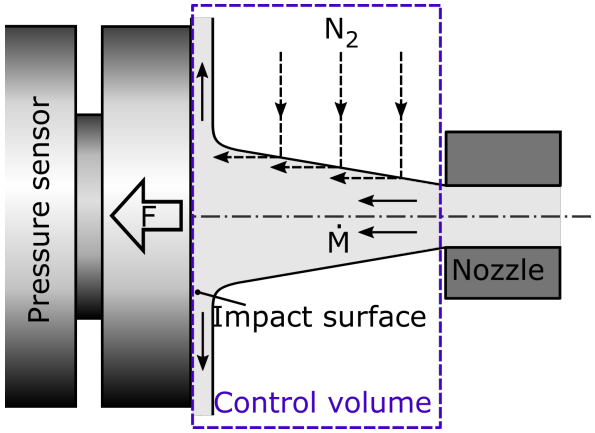


*Figure 3.9: Momentum flux computation principle [6].*

Thus, the impact force of the spray translates into a direct measurement of the stable momentum flux of the spray (Figure 3.10).

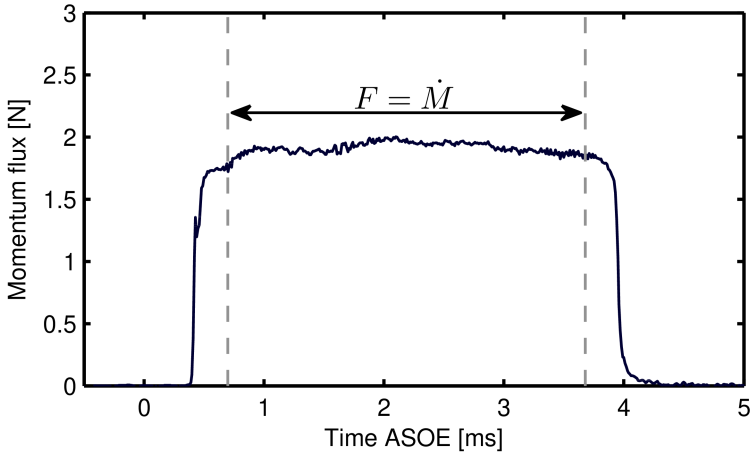


*Figure 3.10: Momentum Flux signal.*

50 cycles of each test point were made and averaged into a final signal. Then, the signal is corrected to account for the cumulative phenomenon also present in the momentum flux vessel [13] (Figure 3.11).

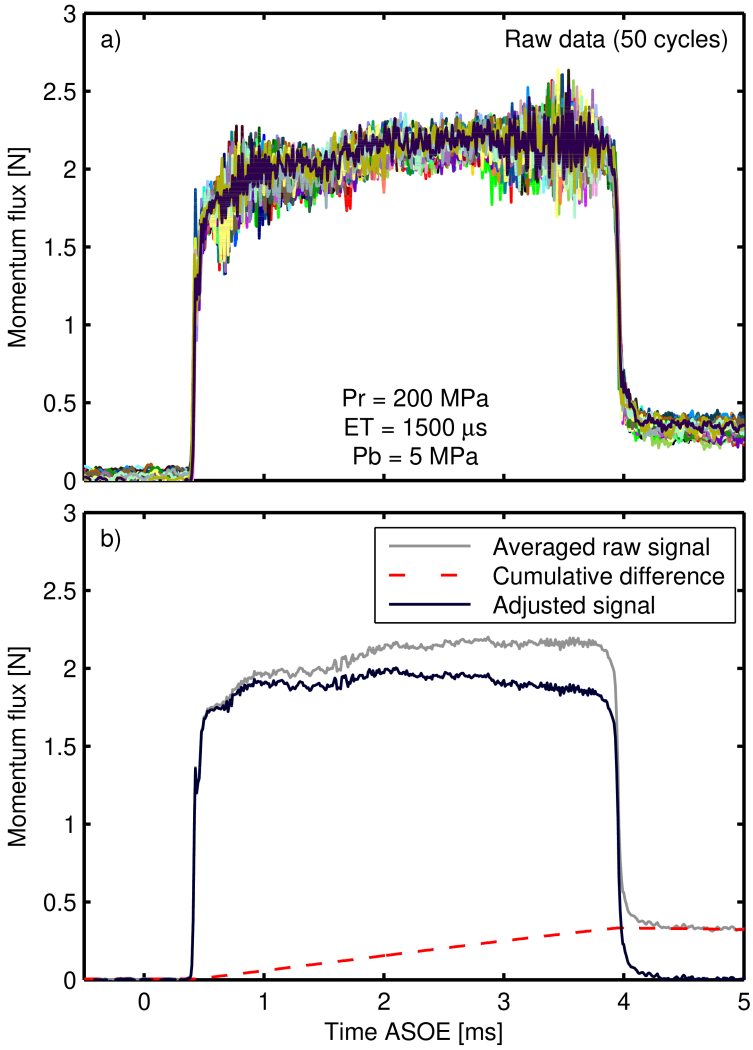


*Figure 3.11: Treatment of the signal of Momentum Flux.*

It can be seen that the deviations between each cycle are greater when contrasted to that of the injection rate experiments. This contrast could be due to the bigger turbulence and acoustic waves produced by the air-fuel mixture in the momentum test rig, resulting in larger noise in the signal captured

by the sensor [14]. Nevertheless, the uncertainty is reduced by performing numerous repetitions, and shot-to-shot dispersion is evaluated through the relative standard deviation of the stable momentum flux.

### 3.3.3 Hydraulic coefficients

The hydraulic characterization measurements detailed in section 3.3.2 and section 3.3.2 serve to obtain both the momentum flux ($\dot{M}$) and the rate of injection flow ($\dot{m}$), respectively.

From those parameters, it is possible to obtain various hydraulic coefficients, which are useful to have a normalized evaluation of the performance of each injector.

Recalling from section 2.4.1, the discharge coefficient ($C_d$) can be computed by Equation 3.8:

$$C_d = \frac{\dot{m}}{\dot{m}_t} = \frac{\dot{m}}{A_o\sqrt{2 \cdot \rho_f \cdot \Delta P}} \tag{3.8}$$

In which $A_o$ represents the cross-sectional area of the hole, $\rho_f$ the density of the fuel (computed by Equation 3.2) and $\Delta P$ the difference between the injection and back pressure.

This coefficient is frequently used to evaluate the flow going throughout the orifices of the injector [4, 5, 17–19], as it compares how much of the maximum theoretical flow ($\dot{m}_t$) is flowing through them. Then, $\dot{m}_t$ is computed assuming a flow with a cross-sectional area equivalent to that of the outlet orifice and a velocity equal to the maximum theoretical velocity (Equation 5.3).

As with the mass flow rate, it is possible to obtain an adimensional coefficient that compares the experimental momentum flux to the maximum theoretical value ($\dot{M}_t$). This parameter is known as the momentum coefficient ($C_M$):

$$C_M = \frac{\dot{M}}{\dot{M}_t} = \frac{\dot{m}}{A_o \cdot \rho_f \cdot u_t^2} = \frac{\dot{M}}{2 \cdot A_o \cdot \Delta P} \tag{3.9}$$

Lastly, the performance in terms of the real outlet velocity of the flow can also be evaluated. To do so, the velocity coefficient ($C_v$) is calculated to compare the real velocity to the maximum theoretical one:

$$C_v = \frac{u_{eff}}{u_t} = \frac{u_{eff}}{\sqrt{2 \cdot \Delta P/\rho_f}} \tag{3.10}$$

In which $u_{eff}$ is computed with the Equation 2.7.

## 3.4 High-temperature and high-pressure test rig

After measuring the hydraulic performance of each injector and orifice, the remaining experimental measurements in this work were made in a High-temperature and high-pressure test rig depicted in Figure 3.12.

*Figure 3.12: High-pressure and high-temperature test rig.*

Within the combustion chamber of the test rig, it is possible to reproduce real engine thermodynamic conditions, as it can reach temperatures and pressures up to 1100 K and 15 MPa, respectively. Additionally, the test rig has the attribute of maintaining nearly quiescent and steady conditions within the chamber, allowing to test an extensive range of boundary conditions and multiple repetitions without incurring in alterations of the chamber conditions due to long testing periods [20, 21].

### 3.4.1 Gas supply

A notable characteristic of the test rig is that it has a constant flow system throughout the combustion chamber. Specifically, the ambient gas is constantly renovating, maintaining the boundary conditions of pressure and temperature. Thus, it is possible to make numerous repetitions of an injection test point in a relatively short amount of time (e.g., an injection every 4 seconds).

Figure 3.13 depicts the setup employed to run the test rig, and it serves to explain how the gas is fed at the desired conditions.

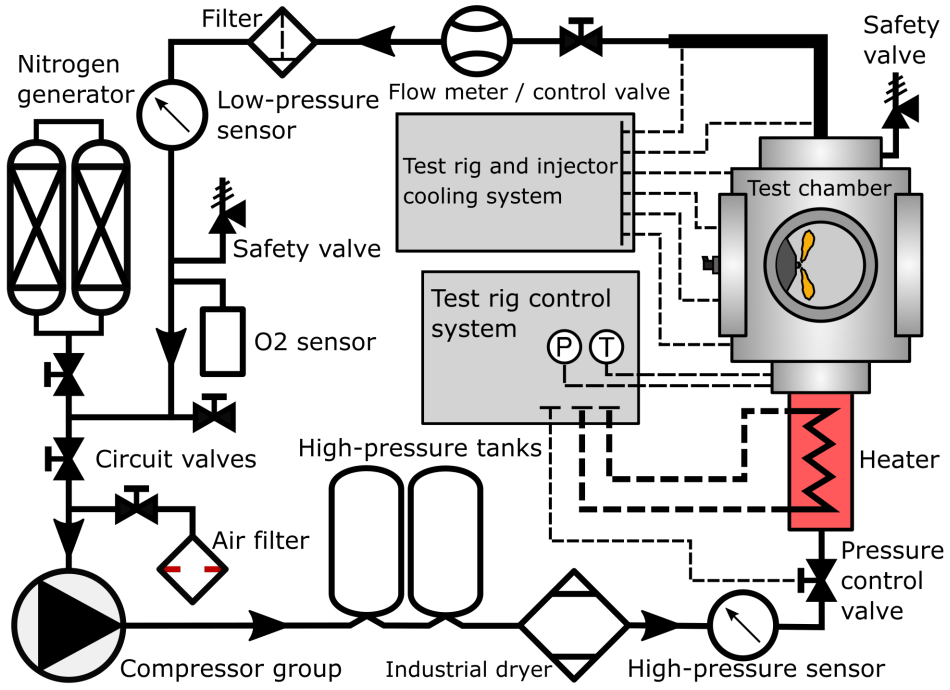


*Figure 3.13: Air supply lines for the high-temperature and high-pressure test rig.*

Specifically, the test rig can operate in an open or closed-loop configuration. The ambient air inlet valve is fully open in the open-loop format, and the nitrogen inlet valve is closed. Thus, the gas flowing through the circuit is pure ambient air.

The closed-loop configuration is employed to set the percentage of oxygen of the gas entering the test chamber below 21%, making it viable to emulate

the proportion of oxygen found in exhaust gas recirculation (EGR) techniques. Moreover, it is possible to completely close the ambient air inlet valve and send pure nitrogen through the test rig. Then, the absence of oxygen allows to make non-reactive evaporative measurements and study the development of the spray in an inert atmosphere.

After defining the gas composition, it is sent through a compressor group to raise its pressure to 15 MPa. Then, the gas is contained in high-pressure tanks, readily available to flow to the test chamber. Before entering the test chamber, the high-pressure gas goes through an industrial dryer to reduce its humidity, followed by a pressure control valve employed to set the gas pressure at the desired value. Lastly, the gas goes through a 40 kW electric heating system which is in charge of getting the gas to the objective temperature.

Afterward, the gas enters the test chamber, where the injection event occurs. A valve placed downstream of the test rig controls the outlet flow of the chamber to maintain a constant pressure flow.

## 3.5 Optical diagnostic techniques

The following section describes the optical setups employed on the high-temperature and high-pressure test rig.

### 3.5.1 MIE Scattering

The MIE-scattering optical technique is frequently used for the visualization of the liquid phase of the spray [22–24]. Accordingly, it was applied in this work to compute the distance required by the spray to fully evaporate (liquid length) under non-reacting conditions.

To do so, the optical setup depicted in Figure 3.14 was employed. First, a continuous light is provided by two 150 W quartz-halogen illuminators (Dolan-Jenner PL800) and directed to the sprays. Then, part of this light is reflected on the liquid droplets of the jets, a process known as light scattering. Finally, the scattered light is captured by the high-speed camera (Photron FastCam SA-X2). Images were recorded at a frequency of 54000 fps, with an image resolution of 640 x 532 pixels, in which 6.24 pixels corresponded to 1 millimeter.

Even though it is not the main focus of the study, these measurements partially characterize the behavior of the spray under non-reacting conditions and any alteration due to inter-jet spacing variations. Furthermore, these experiments allowed timing the start of injection (SOI) and comparing this parameter between the orifices of interest. Moreover, it could be possible

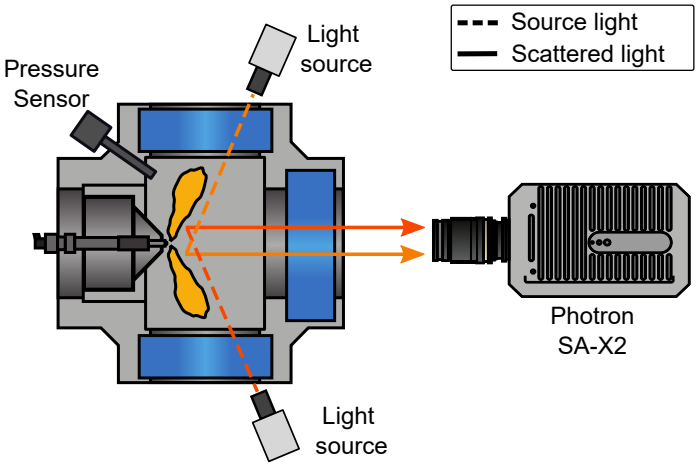


*Figure 3.14: MIE-scattering optical setup.*

to define other macroscopic parameters after the start of injection (ASOI) instead of after the start of energizing (ASOE). Lastly, Figure 3.15 illustrates a representative sequence of the images recorded through this this technique.

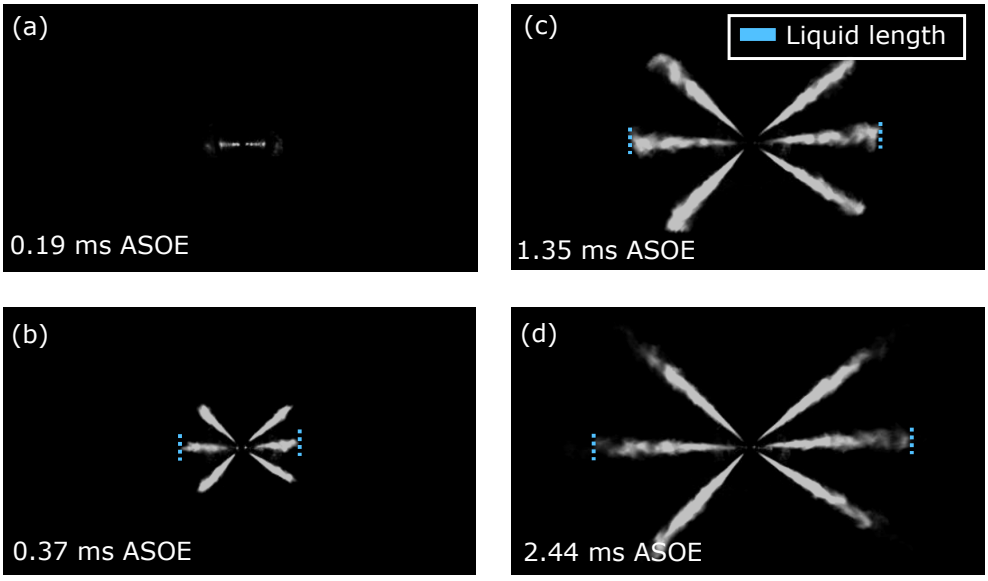


*Figure 3.15: Liquid length sequence after start of energizing.*

The algorithm employed to process the images is detailed in section 3.6.

### 3.5.2 Double-pass Schlieren

Schlieren imaging have been used in numerous works to obtain several macroscopic variables of the spray, such as liquid and vapor areas of the sprays [25–28] or ignition delay [29–33]. The working principle of this technique is depicted in Figure 3.16 and can be summarized in the following steps:

- Initially, a punctual light source is located at the focal distance of a curved lens (I), which is in charge of collimating the light beams of the light source.

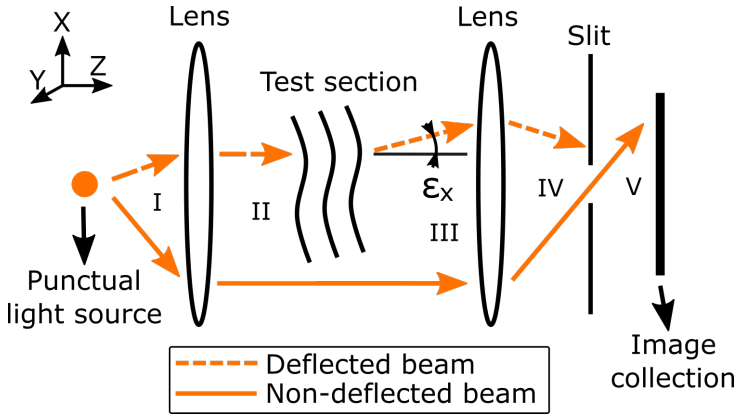


*Figure 3.16: Schlieren principle.*

- Then, the parallel beams go through the region of interest (II), in which the light beams facing any change in density (e.g., a liquid or concentrated gas) are deflected. Moreover, the stronger the refractive index ($n$) [34] of the medium they enter into, the greater the deviation of the light beams. On this area, Gladstone; and Dale [35] presented the following relationship between the refractive index and gas density ($\rho$):

$$n - 1 = k_{GD} \cdot \rho \tag{3.11}$$

  In which $k_{GD}$ represents the Gladstone-Dale coefficient. Moreover, the deflection angle $\varepsilon$ of a beam can be computed accounting for the refractive index of its surroundings ($n$) and the optical path length ($L$). For

instance, for a light beam traveling in direction Z, the angular deflection is calculated as depicted in Equation 3.12 [34]:

$$\varepsilon_x = \frac{L}{n}\frac{\partial n}{\partial x} \quad , \quad \varepsilon_y = \frac{L}{n}\frac{\partial n}{\partial y} \tag{3.12}$$

Thus, combining Equation 3.11 and Equation 3.12, a proportional relation between the deflection angle and the gas density can be obtained.

- Subsequently, the light beams travel through a second curved lens. At this point, the rays that did not encounter any change of density remain collimated (III), whereas those that collided with the matter of different density are not parallel anymore.
- After going through the second lens, the light beams that remained collimated converge at the focal distance of the lens (IV). On the other hand, diverged rays reach the outer area of this point, so it is possible to cut them with a slit so that only the collimated beams go through.
- Then, an image is formed (V) in which the object of interest is depicted as a dark shape, that is, the shape of the beams that did not go through the slit [36].

Regarding the optical setup, the two most common Schlieren imaging configurations are single-pass [37–43] and double-pass [28, 44–46]. The single-pass is frequently used for mono-orifice injectors as the line of sight is not blocked by neighbor jets, and there is no problem employing two optical access. On the other hand, double-pass Schlieren is usually applied to multi-orifices injectors, as this configuration only requires one optical access.

Nevertheless, a high-temperature resistant mirror is needed. For this purpose, a ceramic mirror with Silicon Carbide technology was fabricated by Mersen Boostec (Figure 3.17), which is capable of resisting higher temperatures than the mirrors previously employed in the test rig, while providing the following properties [47]:

- High mechanical strength and stiffness (420 GPa)
- High thermal conductivity (180 W/m/K)
- Exceptional resistance to corrosive and abrasive environments
- Insensitivity to mechanical fatigue

- Low Coefficient of Thermal Expansion (CTE)

As a drawback, the polished surface of the ceramic is less reflective than previously employed mirrors, so a higher intensity light-source was required.

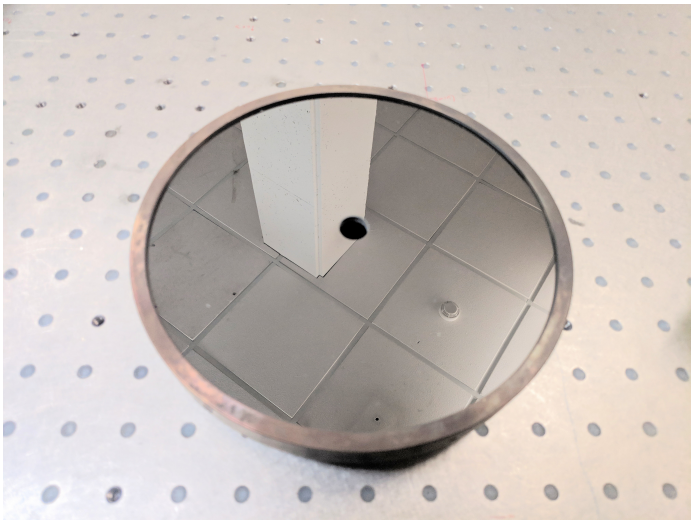

*Figure 3.17: Mersen Silicon Carbide mirror, capable of resisting up to 1000 K of temperature.*

Then, a double-pass Schlieren technique was employed in this campaign. These measurements were done with two purposes:

- To obtain another macroscopic metric to compare the sprays of interest of the injectors under inert conditions.
- To test the ceramic mirror inside the test rig. This mirror allowed Schlieren double-pass measurements of multi-orifices injectors at up to 1000 K chamber temperature, a new achievement under this technique and test rig at CMT-Motores Térmicos.

The setup depicted in Figure 3.18 was employed to apply the double-pass Schlieren methodology. In particular, a 150 W quartz-halogen continuous light source (Dolan-Jenner PL800) is connected to an optic fiber with a punctual output, obtaining a punctual light source. This light is redirected to the lens through a 50:50 beam splitter.

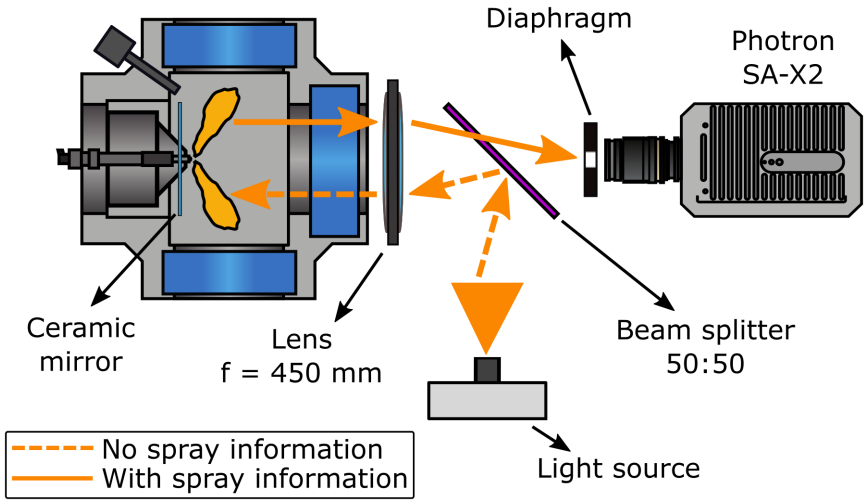


*Figure 3.18: Double-pass Schlieren optical setup. The light source is redirected to the test chamber by a beam splitter, then the ceramic mirror reflects it with the spray information, and it is finally collected by the high-speed camera.*

Moreover, the distance between the light source and the lens is equal to the focal length of the lens ($f = 450\ mm$). Thus, the light beams are collimated by the lens prior to the light entrance to the test chamber. Then, the light travels through the fuel sprays, reaches the ceramic mirror, and bounces back out of the test chamber, passing one more time through the jets (hence the "double-pass" tag). At this point, the light beams that collided with the sprays were deviated and are no longer collimated.

Afterward, the light goes through the lens again, and the beams converge to a point located at the focal distance of the lens (the Fourier plane). At this point, an iris diaphragm with a cut-off diameter of 3 mm is placed to block all but the beams that were not deviated by the sprays, that is, the beams that remained collimated in the test chamber.

Then, the light beams that go through the diaphragm are captured by the high-speed camera (Photron SA-X2). Images were recorded at a frequency of 25000 fps, with an image resolution of 1024 x 336 pixels, in which 6.12 pixels corresponded to 1 millimeter. Lastly, an image is formed in which the sprays are depicted as dark shapes, and the background is illuminated.

In Figure 3.19, a representative sequence of the images recorded through this setup is depicted, and the algorithm employed to compute the spray

penetration is detailed in section 3.6.

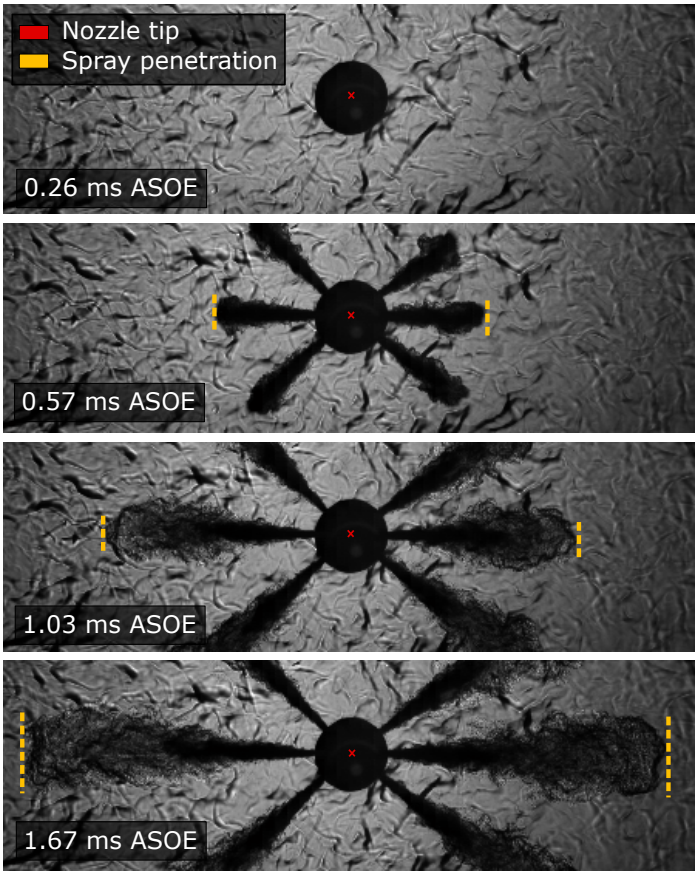


*Figure 3.19: Double pass Schlieren sequence after start of energizing. Chamber temperature: 800 K, chamber density:* 15.2 $kg/m^3$*, injection pressure 150 MPa, injector: 3v3.*

### 3.5.3 OH* chemiluminescence

During the combustion event, chemical reactions produce molecules in a transient high-energy state which then move to a lower energy level, emitting light during the process [48]. Formally, this process is known as chemiluminescence and can be used to track the ignition of the combustion.

Specifically, CH radicals are considered to be appropriate markers of the cool flames or combustion first phase, whereas the appearance of OH radicals

is used to characterize the second stage ignition (SSI), as they appear under high-temperature stoichiometric combustion [49]. Thus, the appearance of OH radicals can be used to measure the ignition delay [50], as the latter is typically defined as the time between the start of injection and the second stage ignition.

Moreover, OH radicals are found at the flame stabilization region on lifted and diffusive flames [51], and have the strongest light emittance band at 306 nm, which is distant from most soot incandescence. Therefore, OH* chemiluminescence is also considered as a reliable marker to measure lift-off length [52, 53].

Thus, it is possible to measure ignition delay and lift-off length through OH* chemiluminescence. To do so, the optical setup depicted in Figure 3.20 was employed.

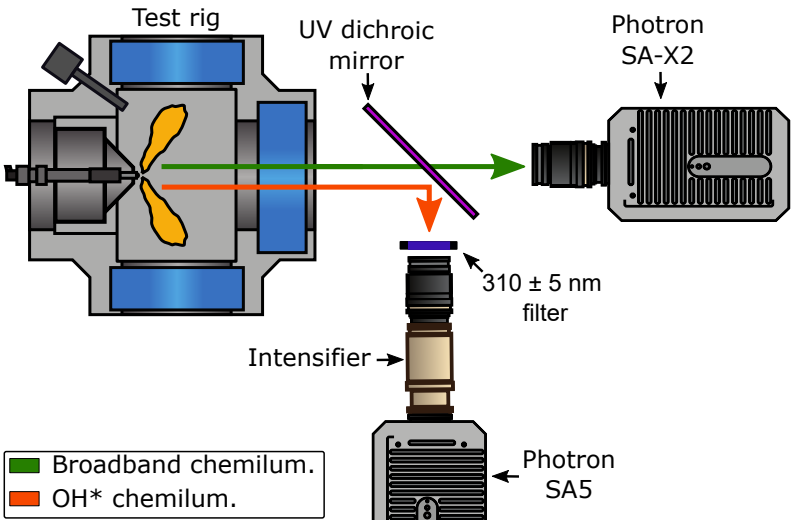


*Figure 3.20: OH* and broadband chemiluminescence optical setup.*

First, the light emitted from the combustion reaches a dichroic mirror which mostly reflects UV radiation. Then, the reflected light goes through a narrow band-pass filter of 310 ± 5 nm to capture the desired emittance, a configuration extensively reported in the literature [21, 29, 51]. Finally, the light goes into a UV f/4 100 mm focal length lens connected to a high-speed image intensifier (Hamamatsu C10880) coupled to the high-speed camera (Photron FastCam SA5) where the image is recorded. Images were obtained at a 25000 fps frequency and an image resolution of 736 x 320 pixels, where 4.39 pixels

corresponded to one millimeter. An example of the images recorded through this setup is presented on Figure 3.21.

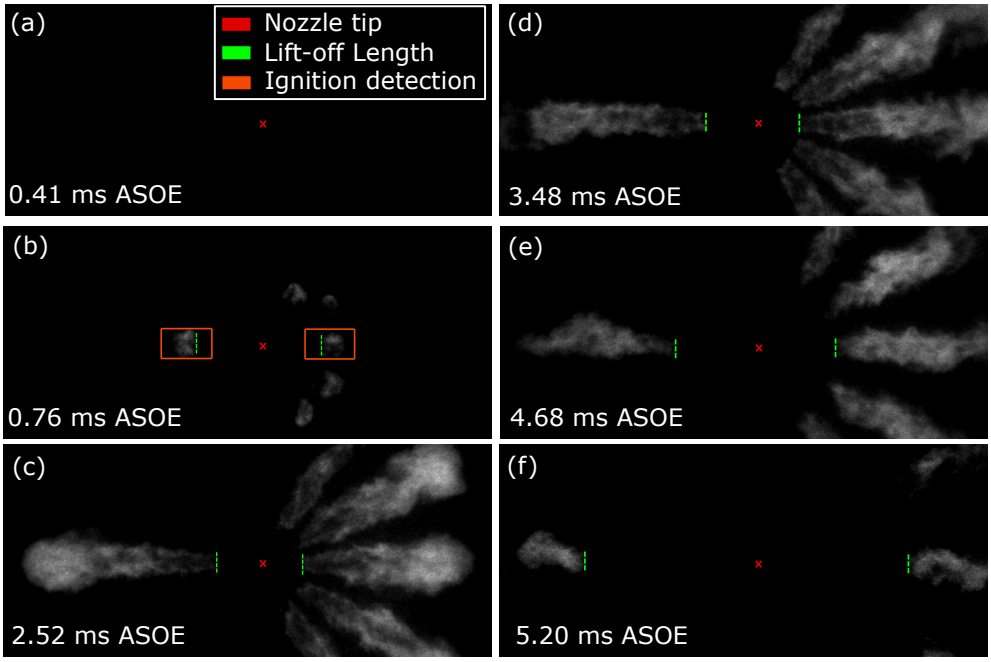


*Figure 3.21: OH* chemiluminescence sequence after start of energizing. Chamber temperature: 900 K, chamber density:* 30.4 $kg/m^3$*, injection pressure 150 MPa, injector: 1v5.*

The optical array depicted in Figure 3.20 also includes the broadband chemiluminescence setup (with the Photron SA-X2) and will be described in the following section.

### 3.5.4 Broadband chemiluminescence

Together with the OH* chemiluminescence recordings, broadband radiation of the flame was recorded with a high-speed camera (Photron FastCam SA-X2) equipped with a Zeiss 100 mm lens, as depicted in Figure 3.20. Images were taken with a 40000 fps frequency and an image resolution of 1024x312 pixels, where 5.9 pixels were equivalent to one millimeter.

Considering the spectral response of the camera, together with the dichroic mirror reflecting the UV radiation, the light collected would mainly be due

to the thermal radiation emitted from the soot particles [48, 54, 55]. Then, a qualitative evolution of the sooting flame can be obtained. This configuration was employed to detect any alteration, due to inter-jet spacing variations, of the moment of initial appearance of soot particles. An example of the images recorded is presented in Figure 3.22, in which the soot detection moment is depicted.

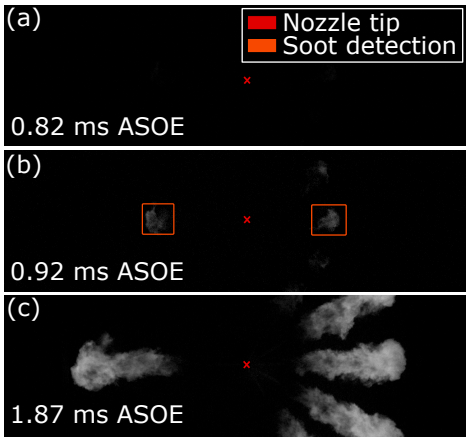


*Figure 3.22: Broadband chemiluminescence sequence after start of energizing. Chamber temperature: 1000 K, chamber density:* 22.8 $kg/m^3$*, injection pressure 100 MPa, injector: 1v5.*

### 3.5.5 Soot-DBI

In recent years, applying the Diffuse Back-Illumination (DBI) technique has become increasingly popular, specially with the appearance of fast light-emitting diodes (LEDs). In this sense, LEDs can be configured to emit strong light intensity for a brief period (nanoseconds), even smaller than the shorter exposure time per frame of a camera. Thus, the light exposure per frame can be governed by the LED pulse, and the images obtained with this technique can be of a much sharper resolution than with other continuous light source techniques [56–59].

Moreover, this technique can be applied to assess the soot formation on the injection event. On this matter, the Laser Extinction Method has been previously employed to evaluate soot development. Nevertheless, this technique can typically provide only a single image per injection event [60, 61], and the spatial distribution is also limited [62].

In contrast, the fast-response LED allows capturing the temporal evolution of soot in the DBI technique, although limited to the image's dynamic range. Moreover, a wider chamber area can be recorded, frequently obtaining the entire spray development. The methodology employed to compute this parameter is described in section 3.6.6.

Regarding the optical setup, a cleared line of sight is required both in the front and back of the spray to apply the Diffuse Back-Illumination technique, which is particularly complex for multi-orifice injectors. To fulfill this requirement, a novel window was designed and fabricated to use the DBI optical technique on multi-hole injectors. To this end, the injector holder and optical access for the illumination needed to be placed in the same piece, as seen in Figure 3.23 (left).

Additionally, various pieces of the injector holder had to be designed and fabricated (Figure 3.23 (right)) to allow the rotation of the injector mounted on the window. Then, it was possible to rotate the injector and align the spray of interest without having to dismount the injector and, consequently, the optical setup behind the window.

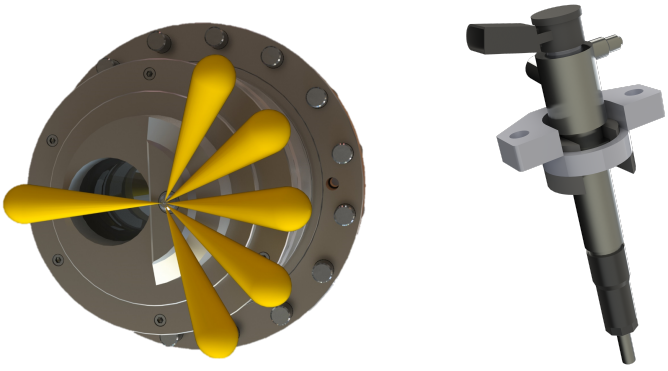

*Figure 3.23: Novel window for DBI measurements on multi-hole injectors (left), and fabricated pieces to allow the rotation of the injector (right).*

Thus, it was possible to illuminate the spray from the opposite side of the camera, as seen in Figure 3.24. Specifically, the light originating from the red LED (light wavelength = 660 nm) was properly directed with a Fresnel lens and then passed through an engineered diffuser (EDC-20 by RPC Photonics), which created a diffused Lambertian intensity profile [63]. Afterward, the light went through the soot cloud and into the camera, capturing the attenuation produced by the soot concentration. Images were obtained at a 36000

fps frequency and an image resolution of 768 x 304 pixels, where 6.45 pixels corresponded to one millimeter.

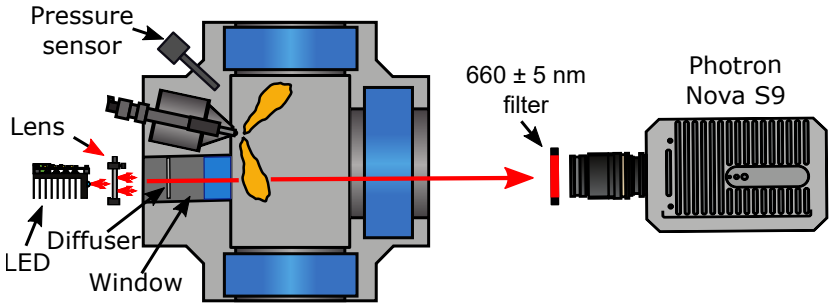


*Figure 3.24: Soot-DBI optical set up*

During the event, the high-speed camera records a frame with the LED-on ($I_{on}$), and the next one with the LED-off ($I_{off}$), then back on, and so on (Figure 3.25). The novel Photron Nova S9 camera was employed, with its sensor enhanced by the manufacturer to inhibit image ghosting [64]. Afterward, the soot formation can be analyzed and this process is explained in detail in section 3.6.7.

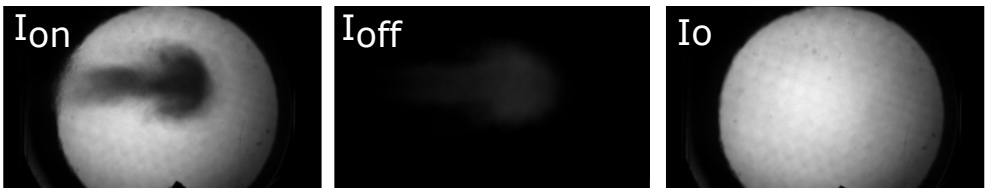


*Figure 3.25: Light intensity of frame with LED-on (left), LED-off (center), and background before the start of injection(right).*

## 3.6 Image processing methods

The optical setups described in the previous section serve to obtain the raw movies of the injection event. Then, different macroscopic parameters of the spray can be retrieved from each of the optical techniques employed.

To do so, image processing algorithms have been developed in MATLAB throughout the years by the members of the injection group at CMT-Motores

Térmicos. This work has contributed to analyzing multiple sprays and improving the algorithms to analyze the soot mass production in multi-orifices injectors.

The image processing methodology can be grouped in four stages for most optical techniques: mask construction, background subtraction, contour detection, and contour analysis. Thus, the procedure will be described in a generic way for the techniques that follow it: MIE-Scattering, Schlieren, and broadband chemiluminescence.

On the other hand, OH* chemiluminescence and soot-DBI images go through different or additional steps, so they will be detailed in supplementary sections.

### 3.6.1 Mask construction

The first step is isolating the sprays of interest from the surroundings to remove the neighbor jets that could influence the computation in the following steps. This phase is applied to every optical technique employed, removing any area not required for the spray analysis. In Figure 3.26, an example is shown in which a mask is applied to a particular frame of a sequence recorded with the Schlieren technique.

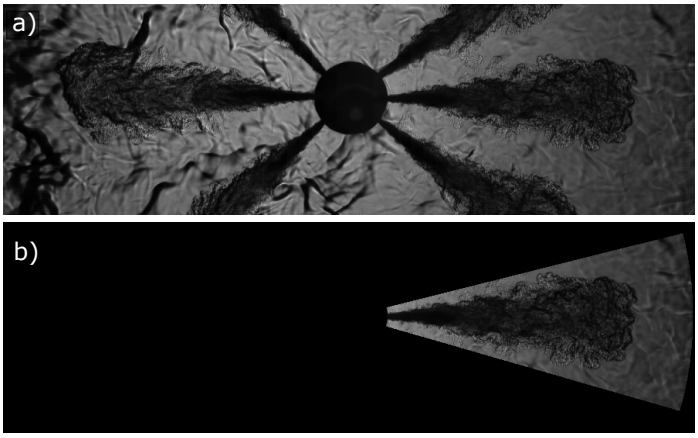


*Figure 3.26: Mask application to isolate the spray. Chamber temperature: 900 K, chamber density: 22.8 $kg/m^3$, injection pressure 150 MPa, Time ASOE: 1.64 ms, injector: 3v3.*

For illustrative purposes, the same time frame ($i$) image is used to describe most of the image processing methodology.

### 3.6.2 Background segmentation

The next step is to separate the spray from the background in the isolated area obtained through the mask application. For MIE and natural luminosity techniques, this is done by subtracting the current frame ($i$) to the background image acquired prior to the start of the injection, exposing the spray shape.

For the schlieren technique, additional steps are required since the background image is subject to alterations after the start of injection due to local changes in the chamber density. Thus, it might not be accurate to only compare the current frame to the background image obtained before the start of the injection.

Moreover, as the spray develops, the local density of the jet could be similar to that of its surroundings. Consequently, the spray and background could be optically similar in some areas, reducing the efficiency of the background subtraction technique. Therefore, additional analysis is required to attend these two issues.

Specifically, the dynamic background technique is applied [27, 28, 33, 65]. This process is done by updating the background image for each frame to obtain a more accurate segmentation from the spray. This methodology is graphically detailed in Figure 3.27.

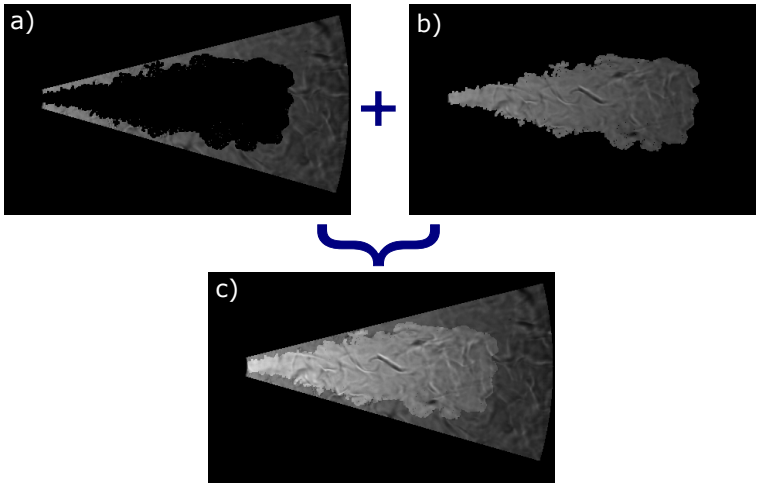


*Figure 3.27: Dynamic background preparation with the previous frame. Time ASOE: 1.61 ms.*

First, the background surrounding of the spray on the previous frame ($i-1$) is extracted (Figure 3.27.a)). Additionally, the spray shape of this previous

frame $(i-1)$ is filled with the pixel-wise background image obtained before the start of the injection (Figure 3.27.b). Lastly, image a) and b) are summed up to obtain the final background (Figure 3.27.c) to be subtracted to the current spray frame $(i)$. This process is done for each frame to constantly renew the background image, hence named the dynamic background methodology.

It is convenient to note that the spray shape has been highlighted in (Figure 3.27.c)) for illustration purposes. Nevertheless, the actual image obtained from the dynamic background methodology can be observed in (Figure 3.28.a).

Once the background image is defined, the spray is separated from the background, as seen on the Figure 3.28. To do so, the current frame is pixel-wise subtracted to the background image acquired on the previous frame (Figure 3.28.a), obtaining the spray shape seen in Figure 3.28.b.

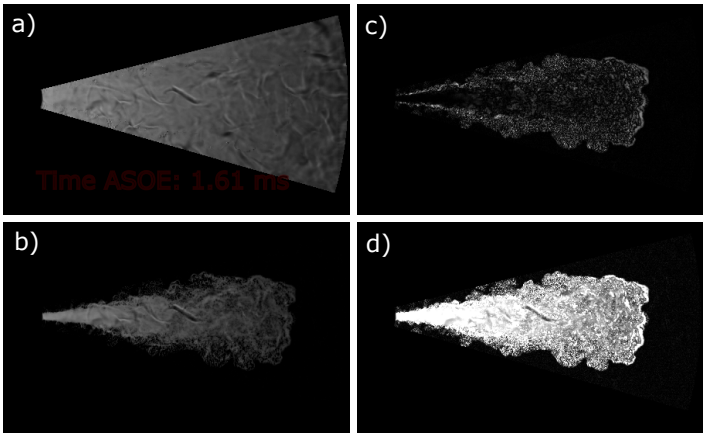


*Figure 3.28: Spray separation from the background. Time ASOE: 1.64 ms.*

This methodology does well when the local density of the spray is considerably different from that of its surroundings. Consequently, this technique is appropriate to obtain the core of the spray, but it is not the best suited to extract the boundary of the spray as it moves forward and the local density in that area is similar to that of the chamber gas.

To solve this issue, a second methodology is applied: the image-temporal-derivative approach [21, 28, 36, 66]. This technique works by comparing the pixel-wise change in intensity of the current frame to that of the previous two frames ($i-1$ and $i-2$ time steps). This methodology bodes very well to detect the contour of the spray, and an example is depicted in Figure 3.28.c. Nevertheless, the algorithm struggles to capture the spray area that does not have a considerable change in intensity, that is, the core of the spray.

Thus, the two methodologies complement each other, so both results are merged into the final shape spray image (Figure 3.28.d).

### 3.6.3 Contour detection

The background segmentation process served to separate the background from the spray (Figure 3.29.a). Nevertheless, this process is not perfect, and some pixels could mistakenly be taken as sprays.

Thus, a fine-tuning and filtering process of this image is done to improve the final contour of the spray. Initially, the image is binarized with a threshold level equal to 3% of the dynamic range (Figure 3.29.b). Then, the image is eroded to reduce the background noise (Figure 3.29.c). However, this step also reduces the spray dimensions on its periphery, so a dilation proceeding is made to neutralize this effect (Figure 3.29.d).

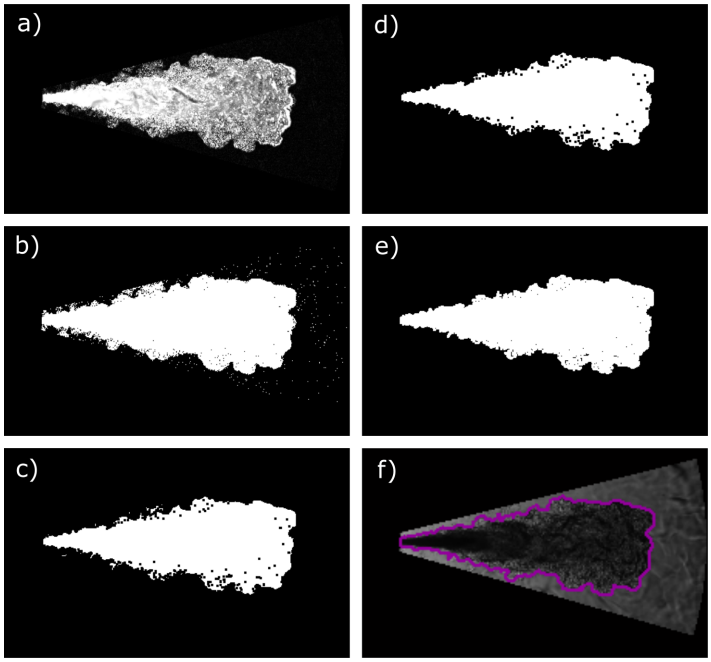


*Figure 3.29: Detection of the contour of the spray. Time ASOE: 1.64 ms.*

Lastly, a pixel-connectivity analysis is made to discard the remaining pixel islands that are not connected to the core of the spray(Figure 3.29.e), obtaining the final contour of the jet (Figure 3.29.f).

This process is repeated for every frame of the recording, obtaining the spray contour for the entire injection.

### 3.6.4 Contour analysis

Once the spray contour is computed, it is possible to obtain the parameters of interest: the liquid length through the MIE scattering and spray penetration by the schlieren technique (Figure 3.30).

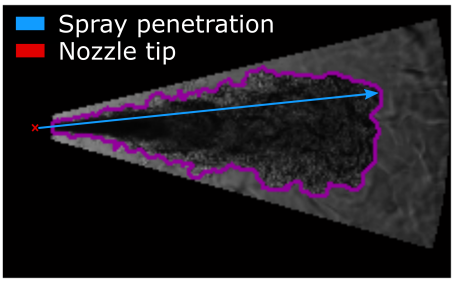


*Figure 3.30: Analysis of the contour of the spray. Time ASOE: 1.64 ms.*

### 3.6.5 OH* processing: Ignition delay and lift-off length

The section 3.5.3 detailed the methodology employed to acquire OH* chemiluminescence images of the injection event, which are then processed on MATLAB. At the beginning of the image processing, the previously detailed mask application (section 3.6.1) is also made to isolate the spray of interest from the others. Afterward, the spray analysis has various distinct steps to obtain the ignition delay and lift-off length.

Following ECN guidelines [3], the ignition delay is defined as the time at which the chemiluminescence intensity level is 50% of the high-temperature intensity level, measured from the background noise level (Figure 3.31). The same methodology was employed to obtain the initial soot appearance through broadband chemiluminescence.

This threshold is chosen to be sufficiently above the noise floor and cool-flame chemiluminescence of the camera and sufficiently under the high-temperature chemiluminescence that can vary with time.

Likewise, the lift-off length is also computed following the Engine Combustion Network guidelines [3]. Specifically, the lift-off length is calculated as the distance between the nozzle tip and the first pixel with a value above 50%

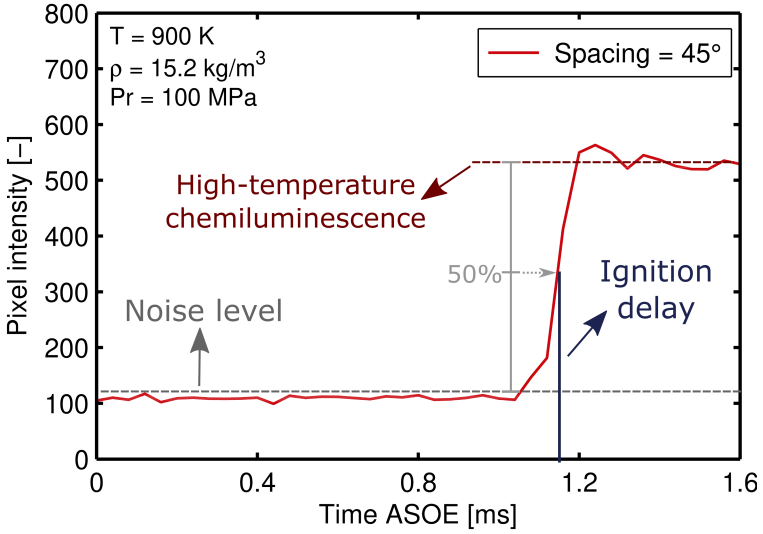


*Figure 3.31: Ignition delay computation.*

of the high-temperature chemiluminescence level. This process is done twice since the flame is divided through its axis into the top and bottom profiles, as seen in Figure 3.32. Then, the lift-off length of each sector is computed, and they are then averaged into a final lift-off length value.

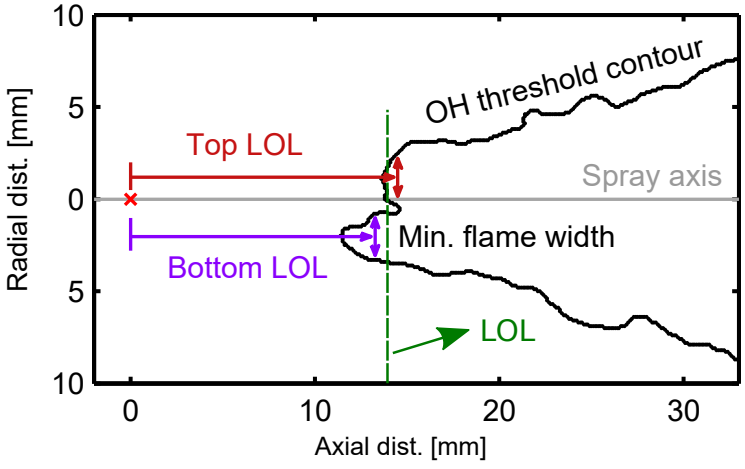


*Figure 3.32: Lift-off length computation [16].*

This process is done for every frame, and a time-dependent lift-off length is obtained as seen, for instance, in Figure 3.33.

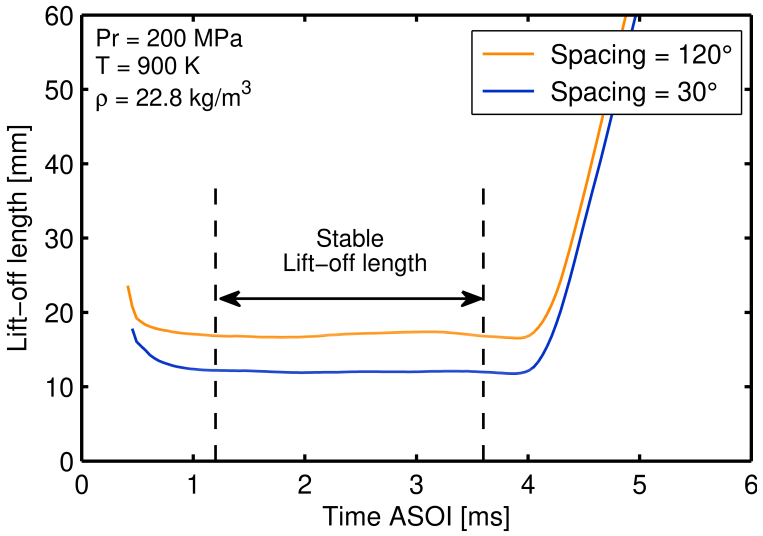


*Figure 3.33: Temporal evolution of the lift-off length after start of injection.*

The observed trend is representative of the general trend seen throughout the measurements: Initially, a transient behavior is depicted as the lift-off gets closer to the nozzle tip, followed by a stable lift-off phase during the injection period, and finalizing with the flame propagation after the end of injection (Figure 3.21 depicts these steps). Lastly, the lift-off length of the tested point is calculated as the mean of the lift-off length values contained in the steady region time frame.

### 3.6.6 Soot-DBI processing: KL profile

Recalling from section 3.5.5, the soot-DBI optical setup (Figure 3.24) allowed for the high-speed camera to obtain a frame with the LED-on ($I_{on}$), followed by a frame with the LED-off ($I_{off}$), and so on. The LED-on frame details the amount of light coming from the LED plus the natural luminosity of the spray. On the other hand, the LED-off frame only depicts the natural luminosity of the spray (Figure 3.25).

Nevertheless, this methodology implies that the frame with the LED-on is not obtained on the same time frame as the image with the LED-off, but one time step earlier or later. Therefore, a two-frame motion interpolation process

based on polynomial expansion was employed. In particular, it estimates the direction and speed of the optical flow from the previous video frame to the current one, using Gunnar Farneback's motion estimator algorithm [67].

Then, an intermediate frame can be recreated, as depicted in Figure 3.34, and the $I_{on}$ and $I_{off}$ frames can be compared on the same time step.

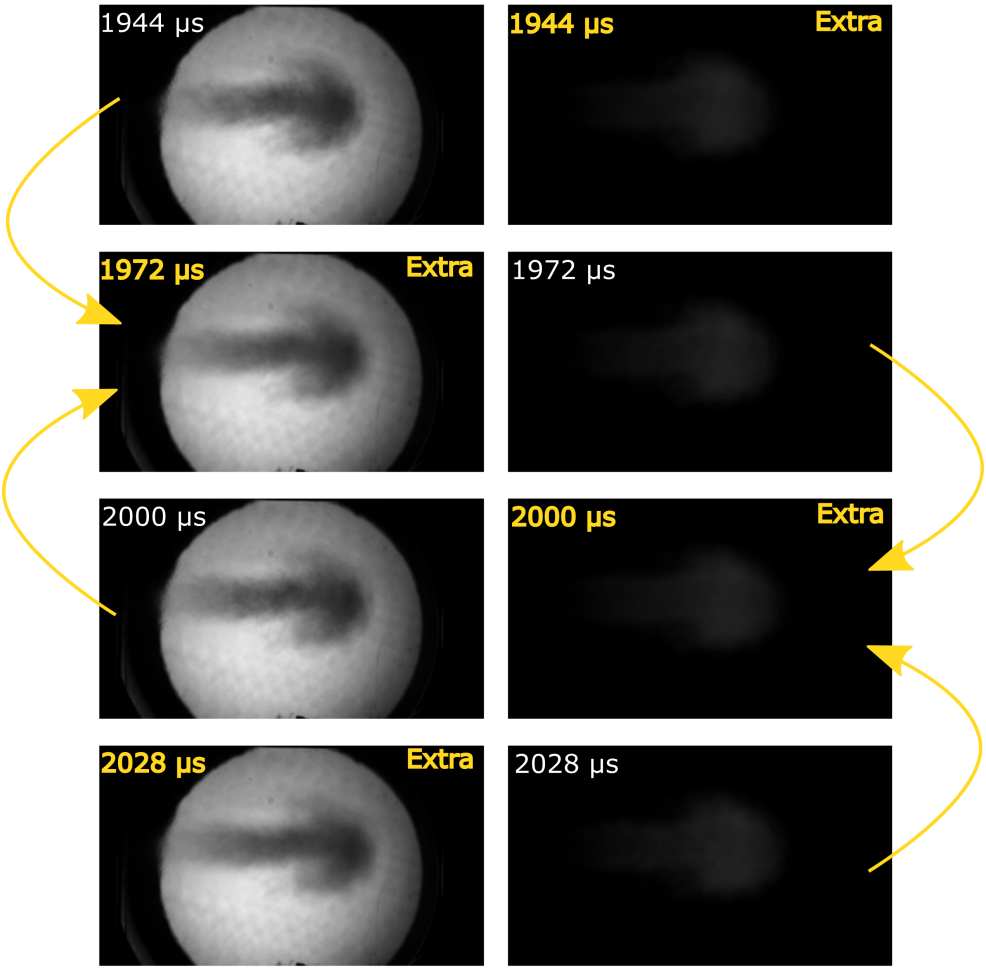


*Figure 3.34: Interpolation process, time ASOE. Chamber temperature: 1000 K, chamber density:* 15.2 $kg/m^3$*, injection pressure 200 MPa, oxygen concentration: 17%, inter-jet spacing: 120°.*

Specifically, the natural luminosity of the spray (LED-off frame) is subtracted to the frame with the LED-on frame for each time frame to obtain the real attenuation. Then, a qualitative measurement of the soot concentration [55] can be calculated through the Beer-Lambert equation:

$$\frac{I_{on} - I_{off}}{I_o} = e^{-KL} \tag{3.13}$$

Where $I_{on}$ represents the pixel intensity with the LED-on, $I_{off}$ the intensity with the LED-off, $I_o$ the intensity before the start of the injection, $K$ the soot dimensional extinction coefficient, and $L$ the light beam path length through the soot cloud. Thus, the product $KL$ represents the soot extinction coefficient across the soot cloud and is related to the soot produced. Then, Equation 3.13 can be applied to obtain the $KL$ profile for each frame of the injection. This process is graphically depicted in Figure 3.35.

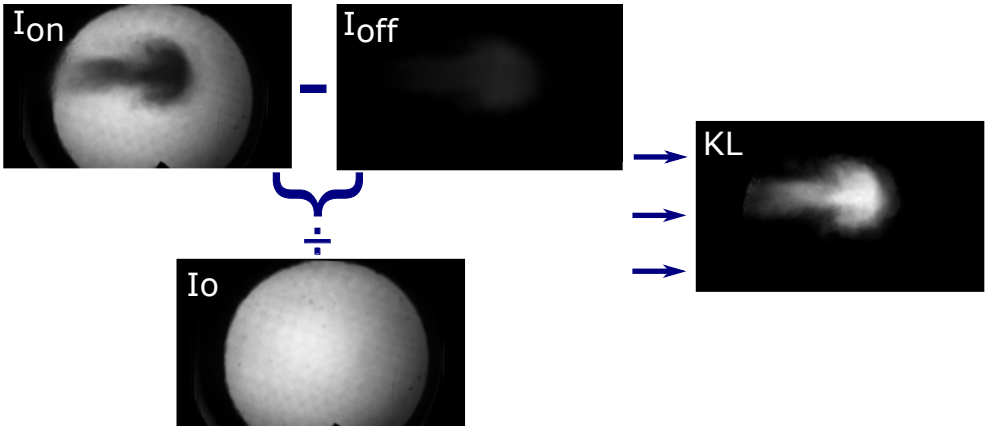


*Figure 3.35: KL profile calculation. Chamber temperature: 900 K, chamber density: 22.8 kg/m$^3$, injection pressure 150 MPa, Time ASOE: 2.7 ms, oxygen concentration:17%, inter-jet spacing: 36°.*

Afterward, the KL profile of every frame can be added up to obtain the cross-sectional KL for each axial distance from the nozzle, which gives a proper qualitative measurement of the amount of soot produced during the entire injection.

This process is depicted in Figure 3.36, and can be summarized on the following steps:

- Figure 3.36 (Left) depicts the KL profile intensity for a given time step (2.7 ms ASOE in this example). The pixel intensity along the Y-axis (cross-sectional axis) is added up for each axial distance from the nozzle. For instance, this addition is represented by the red dashed line on Figure 3.36 (Left), at 60 mm of axial distance from the nozzle tip.
- The resulting value is then plotted in the KL map (Figure 3.36 (right)). In this case, the red dot represents the sum of every KL intensity along the red dashed line on the left, which is why this dot is located at 60 mm and 2.7 ms ASOE.
- This process is done for every axial distance of the KL profile (left) and plotted on the KL map (right), resulting in the white dashed line. This line represents the KL produced by the spray at 2.7 ms ASOE.
- Lastly, this process is repeated for every time step of the injection, computing the KL map for the entire event (right plot of Figure 3.36).

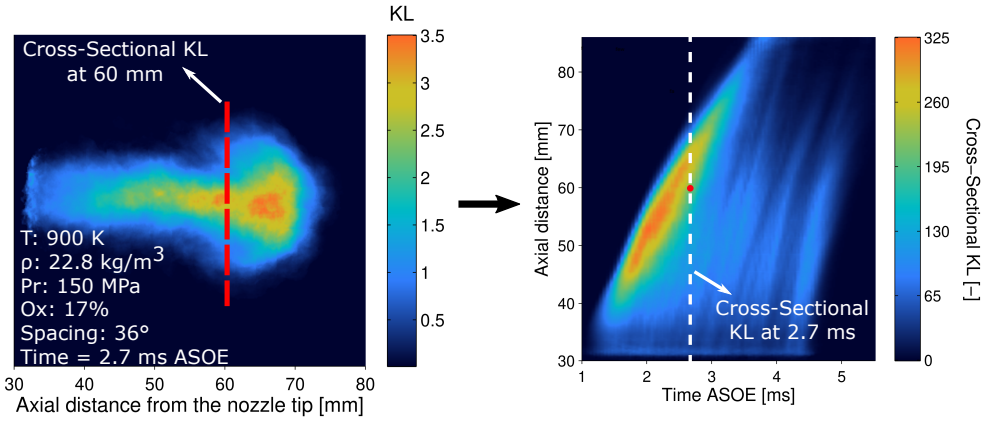


*Figure 3.36: Computation of the KL map.*

### Maximum measurable KL

KL values are dependent on the light attenuation produced by the soot cloud, and this attenuation is directly related to the density of the soot cloud. Specifically, the denser the soot cloud, the higher the attenuation and thus the KL value. In this sense, the maximum measurable KL occurs when the soot cloud

completely attenuates the LED light. Then, the light captured by the camera in the spray area only comes from the natural luminosity of the spray, both in the LED-on and LED-off frame.

Thus, the term $I_{on} - I_{off}$ from Equation 3.13 results in a black image in the spray region, as both images cancel out. Then, the maximum measurable KL ($KL_{max}$) can be computed through Equation 3.14:

$$\frac{I_{camzero}}{I_o} = e^{-KL_{max}} \tag{3.14}$$

Where $I_{camzero}$ represents the pixel-wise intensity of the digital black of the camera (slightly above zero), and it was computed by averaging the $I_{off}$ frames before the start of injection.

### 3.6.7 Soot-DBI processing: soot mass

Through the small particle Mie theory, the dimensional extinction coefficient ($K$) has been related to the soot volume fraction ($f_v$) along the line of sight of the extinction path [68]. Specifically, the relationship is reflected in the literature as [62, 68]:

$$f_v = \frac{K\lambda}{k_e} \tag{3.15}$$

Integrating along the soot path length ($L$), the average path-integrated soot volume fraction ($\bar{f}_v L$) can be related to the experimentally measured optical thickness ($KL$) [68–70]:

$$\int_0^L f_v dl = \frac{KL\lambda}{k_e} \tag{3.16}$$

In which $\lambda$ is the wavelength of the LED (660 nm) and $k_e$ is the dimensionless optical extinction coefficient. On the other hand, recalling the relationship between mass ($m$), density ($\rho$) and volume ($V$):

$$m_{soot} = \rho_{soot} \cdot V_{soot} = \rho_{soot} \cdot f_v \cdot V_{flame} \tag{3.17}$$

Merging Equation 3.16 and Equation 3.17, the soot mass along the line of sight of each pixel can be expressed as [62, 69, 71]:

$$m_{soot,\,pixel} = \rho_{soot} \int \frac{KL \cdot \lambda}{k_e} \cdot dA \tag{3.18}$$

Where $dA$ represents the differential area in the line of sight projected onto the camera. Thus, the soot mass projected to each pixel is defined as [69, 72]:

$$m_{soot,\,pixel} = \rho_{soot} \frac{KL \cdot \lambda}{k_e} \cdot A_{pixel} \tag{3.19}$$

In which the pixel area ($A_{pixel}$) is computed from the pixel-mm image ratio (6.45 px/mm), the soot density was assumed as 1.8 $g/cm^3$ from Choi et al. [68] work, and $k_e$ was computed with Equation 3.20, following the Rayleigh-Debye-Gans methodology (RDG) [61, 62, 73, 74]:

$$k_e = (1 \; + \; \alpha_{sa}) \cdot 6\pi \cdot E(n_s) \tag{3.20}$$

Where $\alpha_{sa}$ represents the scattering-to-absorption ratio, and $E(n_s)$ the imaginary part of $(n_s^2-1)/(n_s^2+2)$, in which $n_s$ refers to the complex refractive index of the soot particles. $\alpha_{sa}$ and $n_s$ were extracted from Manin et al. [74] and Köylü et al. [73], and $k_e$ was determined as $k_e = 7.27$ for the LED wavelength of 660 nm. A detailed explanation of the employed methodology is done by Manin et al. [74] and Yon et al. [75].

Then, the soot mass of the frame ($m_{soot}$) is the sum of all pixel specific $m_{soot,\,pixel}$ values over the entire spray in the image. That is, from Equation 3.19:

$$m_{soot} = \rho_{soot} \frac{\sum KL \cdot \lambda}{k_e} \cdot A_{pixel} \tag{3.21}$$

Lastly, Equation 3.21 is applied to every frame of the injection event, obtaining the soot mass produced for every time step of the injection within the optical range of the window (Figure 3.37).

Nonetheless, this methodology requires wariness in the soot computation due the considerable uncertainties associated with the soot optical properties (both $n_s$ and $\alpha_{sa}$) employed to relate the extinction coefficient to the soot volume fraction, documented in various works [76–79]. Moreover, the assumed uniform soot density can deteriorate the accuracy too.

These limitations were kept in mind to cautiously assess the results. Nevertheless, this methodology still provides useful information for CFD modeling [80], and have thus been employed in numerous works [62, 63, 71, 72, 81]. Regarding this thesis, the main objective of this section was to visually complement the KL maps results, as the soot mass line of every inter-jet spacing configuration can be drawn on the same plot. Therefore, a clearer assessment of the observed trends can be made.

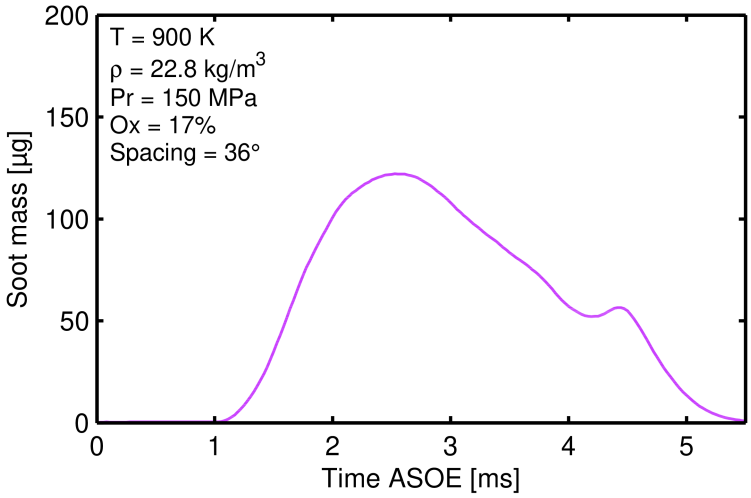


*Figure 3.37: Soot mass produced during the injection event, within the optical range of the window.*

## References

[1] Boehner, Wolfgang; and Hummel, Karsten. "Common Rail Injection System for Commercial Diesel Vehicles". In: *SAE Technical Paper 970345* (1997). DOI: 10.4271/970345.

[2] Payri, Raul; Tormos, Bernardo; Salvador, Francisco Javier; and Plazas, Alejandro Hernan. "Using one-dimensional modelling codes to analyse the influence of diesel nozzle geometry on injection rate characteristics". In: *International Journal of Vehicle Design* 38.1 (2005), pp. 58–78.

[3] ECN. *Online: https://ecn.sandia.gov/diesel-spray-combustion/target-condition/spray-ab/, accessed on 20-01-2022.*

[4] Payri, Raul; Martí-Aldavarí, Pedro; Montiel, Tomas; and Viera, Alberto. "Influence of aging of a diesel injector on multiple injection strategies". In: *Applied Thermal Engineering* 181.August (2020), p. 115891. DOI: 10.1016/j.applthermaleng.2020.115891.

[5] Payri, Raul; Hardy, Gilles; Gimeno, Jaime; and Bautista, Abian. "Analysis of counterbore effect in five diesel common rail injectors". In: *Experimental Thermal and Fluid Science* 107.February (2019), pp. 69–78. DOI: 10.1016/j.expthermflusci.2019.05.008.

[6] Payri, Raul; Garcia-Oliver, Jose Maria; Salvador, Francisco Javier; and Gimeno, Jaime. "Using spray momentum flux measurements to understand the influence of diesel nozzle geometry on spray characteristics". In: *Fuel* 84.5 (2005), pp. 551–561. DOI: 10.1016/j.fuel.2004.10.009.

[7] Som, Sibendu et al. "Effect of nozzle orifice geometry on spray, combustion, and emission characteristics under diesel engine conditions". In: *Fuel* 90.3 (2011), pp. 1267–1276. DOI: 10.1016/j.fuel.2010.10.048.

[8] Payri, Raul; Gimeno, Jaime; Mata, Carmen; and Viera, Alberto. "Rate of injection measurements of a direct-acting piezoelectric injector for different operating temperatures". In: *Energy Conversion and Management* 154 (2018), pp. 387–393. DOI: 10.1016/j.enconman.2017.11.029.

[9] Bosch, Wilhelm. "The Fuel Rate Indicator: A New Measuring Instrument for Display of the Characteristics of Individual Injection". In: *SAE Technical Paper 660749* (1966). DOI: 10.4271/660749.

[10] Salvador, Francisco Javier; Gimeno, Jaime; Carreres, Marcos; and Crialesi-Esposito, Marco. "Fuel temperature influence on the performance of a last generation common-rail diesel ballistic injector. Part I: Experimental mass flow rate measurements and discussion". In: *Energy Conversion and Management* 114 (2016), pp. 364–375. DOI: 10.1016/j.enconman.2016.02.042.

[11] Bardi, Michele. "Partial needle lift and injection rate shape effect on the formation and combustion of the Diesel spray". PhD thesis. Valencia (Spain): Universitat Politècnica de València, 2014. DOI: 10.4995/Thesis/10251/37374.

[12] Payri, Raul; Salvador, Francisco Javier; Gimeno, Jaime; and Bracho, Gabriela. "The effect of temperature and pressure on thermodynamic properties of diesel and biodiesel fuels". In: *Fuel* 90.3 (2011), pp. 1172–1180. DOI: 10.1016/j.fuel.2010.11.015.

[13] Payri, Raul; Salvador, Francisco Javier; Gimeno, Jaime; and Bracho, Gabriela. "A new methodology for correcting the signal cumulative phenomenon on injection rate measurements". In: *Experimental Techniques* 32.February (2008), pp. 46–49. DOI: 10.1111/j.1747-1567.2007.00188.x.

[14] Gimeno, Jaime. "Desarrollo y aplicación de la medida de flujo de cantidad de movimiento de un chorro Diesel". PhD thesis. E.T.S. Ingenieros Industriales, Universidad Politécnica de Valencia, 2008. DOI: 10.4995/Thesis/10251/8306.

[15] Venegas, Oscar. "Estudio del fenómeno de la cavitación en la inyección diesel mediante la visualización del flujo interno en orificios transparentes." PhD thesis. Universitat Politècnica de València, 2014. DOI: 10.4995/Thesis/10251/37375.

[16] Viera, Alberto. "Effect of multiple injection strategies on the diesel spray formation and combustion using optical diagnostics". PhD thesis. Universitat Politècnica de València, 2019. DOI: 10.4995/Thesis/10251/123954.

[17] Essien, S.; Archibong-Eso, A.; and Lao, L. "Discharge coefficient of high viscosity liquids through nozzles". In: *Experimental Thermal and Fluid Science* 103.January (2019), pp. 1–8. DOI: 10.1016/j.expthermflusci.2019.01.004.

[18] Fox, T A; and Stark, J. "Discharge coefficients for miniature fuel injectors". In: *Aerospace Engineering* 203.1 (1989), pp. 75–78. DOI: 10.1243/PIME_PROC_1989_203_056_01.

[19] Salvador, Francisco Javier. "Estudio teórico experimental de la influencia de la geometría de toberas de inyección Diésel sobre las características del flujo interno y del chorro". PhD thesis. Valencia: E.T.S. Ingenieros Industriales. Universidad Politécnica de Valencia, 2003.

[20] Meijer, Maarten et al. "Engine Combustion Network (ECN): Characterization and comparison of boundary conditions for different combustion vessels". In: *Atomization and Sprays* 22.9 (2012), pp. 777–806. DOI: 10.1615/AtomizSpr.2012006083.

[21] Bardi, Michele et al. "Engine Combustion Network: Comparison of Spray Development, Vaporization, and Combustion in Different Combustion Vessels". In: *Atomization and Sprays* 22.10 (2012), pp. 807–842. DOI: 10.1615/AtomizSpr.2013005837.

[22] Payri, Raul; Giraldo, Jhoan S.; Ayyapureddi, S.; and Versey, Z. "Experimental and analytical study on vapor phase and liquid penetration for a high pressure diesel injector". In: *Applied Thermal Engineering* 137.March (2018), pp. 721–728. DOI: 10.1016/j.applthermaleng.2018.03.097.

[23] Li, Feng; Lee, Chia Fon; Wang, Ziman; Pei, Yiqiang; and Lu, Guoxiang. "Impacts of duct inner diameter and standoff distance on macroscopic spray characteristics of ducted fuel injection under non-vaporizing conditions". In: *International Journal of Engine Research* (2020), pp. 1–12. DOI: 10.1177/1468087420914714.

[24] Giraldo, Jhoan S.; Payri, Raul; Marti-Aldaravi, Pedro; and Montiel, Tomas. "Effect of high injection pressures and ambient gas properties over the macroscopic characteristics of the diesel spray on multi-hole nozzles". In: *Atomization and Sprays* 28.12 (2018), pp. 1145–1160. DOI: 10.1615/AtomizSpr.2019029651.

[25] Naber, Jeffrey D; and Siebers, Dennis L. "Effects of Gas Density and Vaporization on Penetration and Dispersion of Diesel Sprays". In: *SAE Paper 960034*. Vol. 105. 412. Society of Automotive Engineers, Inc., Warrendale, Pennsylvania, USA, 1996, pp. 82–111. DOI: 10.4271/960034.

[26] Pastor, Jose Vicente; Lopez, Jose Javier; Garcia-Oliver, Jose Maria; and Pastor, Jose Manuel. "A 1D model for the description of mixing-controlled inert diesel sprays". In: *Fuel* 87.13-14 (2008), pp. 2871–2885. DOI: 10.1016/j.fuel.2008.04.017.

[27] Payri, Raul; Gimeno, Jaime; Bracho, Gabriela; and Vaquerizo, Daniel. "Study of liquid and vapor phase behavior on Diesel sprays for heavy duty engine nozzles". In: *Applied Thermal Engineering* 107 (2016), pp. 365–378. DOI: 10.1016/j.applthermaleng.2016.06.159.

[28] Payri, Raul; Salvador, Francisco Javier; Bracho, Gabriela; and Viera, Alberto. "Differences between single and double-pass schlieren imaging on diesel vapor spray characteristics". In: *Applied Thermal Engineering* 125 (2017), pp. 220–231. DOI: 10.1016/j.applthermaleng.2017.06.140.

[29] Benajes, Jesus; Payri, Raul; Bardi, Michele; and Martí-aldaraví, Pedro. "Experimental characterization of diesel ignition and lift-off length using a single-hole ECN injector". In: *Applied Thermal Engineering* 58.1-2 (2013), pp. 554–563. DOI: 10.1016/j.applthermaleng.2013.04.044.

[30] Payri, Raul; Salvador, Francisco Javier; Manin, Julien; and Viera, Alberto. "Diesel ignition delay and lift-off length through different methodologies using a multi-hole injector". In: *Applied Energy* 162 (2016), pp. 541–550. DOI: 10.1016/j.apenergy.2015.10.118.

[31] Payri, Raul; Viera, Juan Pablo; Gopalakrishnan, Venkatesh; and Szymkowicz, Patrick G. "The effect of nozzle geometry over ignition delay and flame lift-off of reacting direct-injection sprays for three different fuels". In: *Fuel* 199 (2017), pp. 76–90. DOI: 10.1016/j.fuel.2017.02.075.

[32] Lillo, Peter M; Pickett, Lyle M; Persson, Helena; Andersson, Oivind; and Kook, Sanghoon. "Diesel Spray Ignition Detection and Spatial/Temporal Correction". In: *SAE Paper 2012-01-1239* (2012), pp. 1–21. DOI: 10.4271/2012-01-1239.

[33] Payri, Raul; Viera, Juan Pablo; Pei, Yuanjiang; and Som, Sibendu. "Experimental and numerical study of lift-off length and ignition delay of a two-component diesel surrogate". In: *Fuel* 158 (2015), pp. 957–967. DOI: 10.1016/j.fuel.2014.11.072.

[34] Settles, G. S. *Schlieren and Shadowgraph Techniques*. Berlin, Heidelberg: Springer Berlin Heidelberg, 2001, p. 376. DOI: 10.1007/978-3-642-56640-0.

[35] Gladstone, J H; and Dale, T P. "Researches on the Refraction, Dispersion, and Sensitiveness of Liquids". In: *Philosophical Transactions of the Royal Society of London* 153 (1863), pp. 317–343. DOI: 10.2307/108799.

[36] Pastor, Jose Vicente; Payri, Raul; Garcia-Oliver, Jose Maria; and Nerva, Jean-Guillaume. "Schlieren Measurements of the ECN-Spray A Penetration under Inert and Reacting Conditions". In: *SAE Technical Paper 2012-01-0456* (2012). DOI: 10.4271/2012-01-0456.

[37] Pickett, Lyle M et al. "Relationship Between Diesel Fuel Spray Vapor Penetration/Dispersion and Local Fuel Mixture Fraction". In: *SAE International Journal of Engines* 4.1 (2011), pp. 764–799. DOI: 10.4271/2011-01-0686.

[38] Montanaro, Alessandro et al. "Schlieren and Mie Scattering Visualization for Single- Hole Diesel Injector under Vaporizing Conditions with Numerical Validation". In: *SAE Technical Paper 2014-01-1406* (2014). DOI: 10.4271/2014-01-1406.

[39] Kook, Sanghoon; and Pickett, Lyle M. "Liquid length and vapor penetration of conventional , Fischer - Tropsch , coal-derived , and surrogate fuel sprays at high-temperature and high-pressure ambient conditions". In: *Fuel* 93 (2012), pp. 539–548. DOI: 10.1016/j.fuel.2011.10.004.

[40] Payri, Raul; Salvador, Francisco Javier; Martí-Aldaraví, Pedro; and Vaquerizo, Daniel. "ECN Spray G external spray visualization and spray collapse description through penetration and morphology analysis". In: *Applied Thermal Engineering* 112 (2017), pp. 304–316. DOI: 10.1016/j.applthermaleng.2016.10.023.

[41] Knox, Benjamin; and Genzale, Caroline L. "Effects of End-of-Injection Transients on Combustion Recession in Diesel Sprays". In: *SAE International Journal of Engines* 9.2 (2016), pp. 1–18. DOI: 10.4271/2016-01-0745.

[42] Allocca, Luigi; Lazzaro, Maurizio; Meccariello, Giovanni; and Montanaro, Alessandro. "Schlieren visualization of a GDI spray impacting on a heated wall: Non-vaporizing and vaporizing evolutions". In: *Energy* 108 (2016), pp. 93–98. DOI: 10.1016/j.energy.2015.09.107.

[43] Nerva, Jean-Guillaume; Genzale, Caroline L; Kook, Sanghoon; Garcia-Oliver, Jose Maria; and Pickett, Lyle M. "Fundamental Spray and Combustion Measurements of Soy Methyl-Ester Biodiesel". In: *International Journal of Engine Research* 14.4 (2013), pp. 373–390. DOI: doi:10.1177/1468087412456688.

[44] Payri, Raul; Gimeno, Jaime; Viera, Juan Pablo; and Plazas, Alejandro Hernan. "Needle lift profile influence on the vapor phase penetration for a prototype diesel direct acting piezoelectric injector". In: *Fuel* 113 (2013), pp. 257–265. DOI: 10.1016/j.fuel.2013.05.057.

[45] Payri, Raul; Salvador, Francisco Javier; Garcia, Antonio; and Gil, Antonio. "Combination of visualization techniques for the analysis of evaporating diesel sprays". In: *Energy and Fuels* 26 (2012), pp. 5481–5490. DOI: 10.1021/ef3008823.

[46] Pastor, Jose Vicente; Garcia-Oliver, Jose Maria; Pastor, Jose Manuel; and Zapata, Luis Daniel. "Evaporating Diesel Spray Visualization using a Double-pass Shadowgraphy / Schlieren Imaging". In: *SAE technical Paper 2007-24-0026* (2007). DOI: 10.4271/2007-24-0026.

[47] Mersen-Boostec. *Online: https://www.mersen.com/products/graphite-specialties/boostec-silicon-carbide-sic, accessed on 21-01-2022.*

[48] Gaydon, A G. *The Spectroscopy of Flames*. Springer Netherlands, 1974. DOI: 10.1007/978-94-009-5720-6.

[49] Dec, John E; and Espey, Christoph. "Chemiluminescence Imaging of Autoignition in a DI Diesel Engine". In: *SAE Technical Paper 982685* 724 (1998). DOI: 10.4271/982685.

[50] Jakob, Markus et al. "Simultaneous high-speed visualization of soot luminosity and OH * chemiluminescence of alternative-fuel combustion in a HSDI diesel engine under realistic operating conditions". In: *Combustion and Flame* 159.7 (2012), pp. 2516–2529. DOI: 10.1016/j.combustflame.2012.03.004.

[51] Higgins, Brian; and Siebers, Dennis L. "Measurement of the Flame Lift-Off Location on DI Diesel Sprays Using OH Chemiluminescence". In: *SAE Technical Paper 2001-01-0918* (2001).

[52] Persson, Helena; Andersson, Öivind; and Egnell, Rolf. "Fuel effects on flame lift-off under diesel conditions". In: *Combustion and Flame* 158.1 (2011), pp. 91–97. DOI: 10.1016/j.combustflame.2010.07.020.

[53] Donkerbroek, A. J.; Boot, M. D.; Luijten, C. C.M.; Dam, N. J.; and Meulen, J. J. ter. "Flame lift-off length and soot production of oxygenated fuels in relation with ignition delay in a DI heavy-duty diesel engine". In: *Combustion and Flame* 158.3 (2011), pp. 525–538. DOI: 10.1016/j.combustflame.2010.10.003.

[54] Pastor, Jose Vicente; Garcia-Oliver, Jose Maria; Garcia, Antonio; and Pinotti, Mattia. "Soot Characterization of Diesel/Gasoline Blends Injected through a Single Injection System in CI engines". In: *SAE Technical Papers* 2017-Septe (2017). DOI: 10.4271/2017-24-0048.

[55] Pastor, José V.; García, A.; Micó, C.; and García-Carrero, Alba A. "Experimental study of influence of Liquefied Petroleum Gas addition in Hydrotreated Vegetable Oil fuel on ignition delay, flame lift off length and soot emission under diesel-like conditions". In: *Fuel* 260.July 2019 (2020), p. 116377. DOI: 10.1016/j.fuel.2019.116377.

[56] Jung, Yongjin; Manin, Julien; Skeen, Scott A; and Pickett, Lyle M. "Measurement of Liquid and Vapor Penetration of Diesel Sprays with a Variation in Spreading Angle". In: *SAE Technical Paper 2015-01-0946* (2015). DOI: 10.4271/2015-01-0946.

[57] Payri, Raul; Bracho, Gabriela; Marti-Aldaravi, Pedro; and Viera, Alberto. "Near field visualization of diesel spray for different nozzle inclination angles in non-vaporizing conditions". In: *Atomization and Sprays* 27.3 (2017), pp. 251–267. DOI: 10.1615/AtomizSpr.2017017949.

[58] Manin, Julien; Bardi, Michele; and Pickett, Lyle M. "Evaluation of the liquid length via diffused back-illumination imaging in vaporizing diesel sprays". In: *Comodia*. Fukuoka, 2012.

[59] Manin, Julien; Bardi, Michele; Pickett, Lyle M; Dahms, R. N.; and Oefelein, J. C. "Microscopic investigation of the atomization and mixing processes of diesel sprays injected into high pressure and temperature environments". In: *Fuel* 134 (2014), pp. 531–543. DOI: 10.1016/j.fuel.2014.05.060.

[60] Manin, Julien; Pickett, Lyle M.; and Skeen, Scott A. "Two-Color Diffused Back-Illumination Imaging as a Diagnostic for Time-Resolved Soot Measurements in Reacting Sprays". In: *SAE International Journal of Engines* 6.4 (2013), pp. 1908–1921. DOI: 10.4271/2013-01-2548.

[61] Payri, Raul; Gimeno, Jaime; Cardona, Santiago; and Ayyapureddi, Sridhar. "Experimental study of the influence of the fuel and boundary conditions over the soot formation in multi-hole diesel injectors using high-speed color diffused back-illumination technique". In: *Applied Thermal Engineering* 158 (2019), p. 113746. DOI: 10.1016/J.APPLTHERMALENG.2019.113746.

[62] Xuan, Tiemin. "Optical investigations on diesel spray dynamics and inflame soot formation". PhD thesis. Universitat Politècnica de València, 2017. DOI: 10.4995/Thesis/10251/94626.

[63] Pastor, José V.; García-Oliver, José M.; Micó, Carlos; García-Carrero, Alba A.; and Gómez, Arantzazu. "Experimental study of the effect of hydrotreated vegetable oil and oxymethylene ethers on main spray and combustion characteristics under engine combustion network spray A conditions". In: *Applied Sciences (Switzerland)* 10.16 (2020). DOI: 10.3390/APP10165460.

[64] Manin, Julien; Pickett, Lyle M; and Skeen, Scott A. "Toward quantitative spray measurements using high-performance high-speed video cameras". In: *ILASS Americas 2016* (2016), pp. 511–518.

[65] Payri, Raul; Salvador, Francisco Javier; Gimeno, Jaime; and Viera, Alberto. "Effect of Injection Rate Shaping over Diesel Spray Development in Non-Reacting Evaporative Conditions". In: *10. Tagung Diesel- und Benzindirekteinspritzung 2016*. Ed. by Helmut Tschöke; and Ralf Marohn. 1. Springer Vieweg, 2016, pp. 133–152. DOI: 10.1007/978-3-658-15327-4.

[66] Payri, Raul; Viera, Juan Pablo; Gopalakrishnan, Venkatesh; and Szymkowicz, Patrick G. "The effect of nozzle geometry over the evaporative spray formation for three different fuels". In: *Fuel* 188 (2017), pp. 645–660. DOI: 10.1016/j.fuel.2016.06.041.

[67] Farnebäck, Gunnar. "Two-frame motion estimation based on polynomial expansion". In: *Lecture Notes in Computer Science (including subseries Lecture Notes in Artificial Intelligence and Lecture Notes in Bioinformatics)* 2749.May (2003), pp. 363–370. DOI: 10.1007/3-540-45103-x_50.

[68] Choi, M.Y. Y; Mulholland, G.W. W; Hamins, A.; and Kashiwagi, T. "Comparisons of the soot volume fraction using gravimetric and light extinction techniques". In: *Combustion and Flame* 102.1-2 (1995), pp. 161–169. DOI: 10.1016/0010-2180(94)00282-W.

[69] Yasutomi, Koji; and Skeen, Scott A. "Observations of soot optical property characteristics using high-speed, multiple wavelength, extinction imaging in heavy-duty diesel sprays". In: *10th U.S. National Combustion Meeting* 2017-April (2017), pp. 1–11. DOI: 10.4271/2018-01-0233.Abstract.

[70] Williams, T.C.; Shaddix, C.R.; Jensen, K.A.; and Suo-Anttila, J.M. "Measurement of the dimensionless extinction coefficient of soot within laminar diffusion flames". In: *International Journal of Heat and Mass Transfer* 50.7 (2007), pp. 1616–1630. DOI: 10.1016/j.ijheatmasstransfer.2006.08.024.

[71] Skeen, Scott A; Manin, Julien; Dalen, Kristine; and Pickett, Lyle M. "Extinction-based Imaging of Soot Processes over a Range of Diesel Operating Conditions". In: *8th US National Combustion Meeting*. Utah, USA, 2013, pp. 1–13.

[72] Xuan, Tiemin et al. "In-flame soot quantification of diesel sprays under sooting/non-sooting critical conditions in an optical engine". In: *Applied Thermal Engineering* 149.301 (2019), pp. 1–10. DOI: 10.1016/j.applthermaleng.2018.11.112.

[73] Köylü, Ü Ö; Mcenally, C. S.; Rosner, D. E.; and Pfefferle, L. D. "Simultaneous measurements of soot volume fraction and particle size / microstructure in flames using a thermophoretic sampling technique". In: *Combustion and Flame* 110.4 (1997), pp. 494–507. DOI: 10.1016/S0010-2180(97)00089-8.

[74] Manin, Julien; Skeen, Scott A; and Pickett, Lyle M. "Two-color diffused back-illumination imaging as a diagnostic for time-resolved soot measurements in reacting sprays". In: *SAE Int. J. Engines* 6.4 (2013), pp. 1908–1921. DOI: 10.4271/2013-01-2548.

[75] Yon, J. et al. "Examination of wavelength dependent soot optical properties of diesel and diesel/rapeseed methyl ester mixture by extinction spectra analysis and LII measurements". In: *Applied Physics B: Lasers and Optics* 104.2 (2011), pp. 253–271. DOI: 10.1007/s00340-011-4416-4.

[76] Smyth, Kermit C.; and Shaddix, Christopher R. "The elusive history of m = 1.57 - 0.56i for the refractive index of soot". In: *Combustion and Flame* 107.3 (1996), pp. 314–320. DOI: 10.1016/S0010-2180(96)00170-8.

[77] Wu, J. S.; Krishnan, S. S.; and Faeth, G. M. "Refractive indices at visible wavelengths of soot emitted from buoyant turbulent diffusion flames". In: *Journal of Heat Transfer* 119.2 (1997), pp. 230–237. DOI: 10.1115/1.2824213.

[78] Chang, H; and Charalampopoulos, T T. "Determination of the wavelength dependence of refractive indices of flame soot". In: *Proceedings of the Royal Society of London. Series A: Mathematical and Physical Sciences* 430.1880 (1990), pp. 577–591. DOI: 10.1098/rspa.1990.0107.

[79] Sorensen, Christopher M. "Light Scattering by Fractal Aggregates: A Review". In: *Aerosol Science and Technology* 35.2 (2001), pp. 648–687. DOI: 10.1080/02786820117868.

[80] Pachano, Leonardo. "CFD Modeling of Combustion and Soot Production in Diesel Sprays". PhD thesis. Universitat Politècnica de València, 2020, pp. 1–157.

[81] Desantes, Jose Maria; García-Oliver, José Maria; García, Antonio; and Xuan, Tiemin. "Optical study on characteristics of non-reacting and reacting diesel spray with different strategies of split injection". In: *International Journal of Engine Research* 301 (2018). DOI: 10.1177/1468087418773012.

# Chapter 4

# Non-reactive spray development

## 4.1 Introduction

The following three chapters detail the results obtained throughout this thesis.

In particular, the present chapter contains the analysis of the development of the sprays in a non-reactive environment. Initially, the results regarding the rate of injection (ROI) experiments are presented, assessing the internal behavior of each injector. Then, the momentum flux measurements are analyzed to study the hydraulic performance of each orifice of interest. These results are followed by the analysis under an inert environment of the liquid length and vapor spray penetration of each spray, obtained with the MIE scattering and double-pass Schlieren optical techniques, respectively.

The main objective of these measurements is to assess and compare the behavior of each injector and each orifice of interest under non-reactive conditions to quantify the similarity or variance in performance due to fabrication differences. Then, it would be possible to distinguish these inherent differences from those observed on the following combustion experiments campaign in a reactive environment.

## 4.2 Test plan

The boundary conditions employed throughout the momentum flux, ROI, and non-reactive visualization experiments are depicted in Table 4.1 and Table 5.1, respectively.

*Table 4.1: Conditions matrix for the momentum flux and ROI experiments.*

| **Parameter** | **Momentum flux** | **Rate of injection** |
|---|---|---|
| Rail pressure [MPa] | 100 - 150 - 200 | 100 - 150 - 200 |
| Chamber Temperature [K] | 298 | 298 |
| Back pressure [MPa] | 2 - 5 - 8 | 2 - 5 - 8 |
| Chamber gas or liquid* [-] | Nitrogen | Diesel |
| Injection frequency [Hz] | 1 | 1 |
| Energizing time [ms] | 1.5 | 1.5 |
| Cycles per test point [-] | 50 | 50 |

* The momentum chamber is filled and pressurized with nitrogen gas, whereas the IRDCI long-tube is filled with diesel fuel, as detailed in section 3.3.

*Table 4.2: Conditions matrix for the non-reactive spray visualization experiments.*

| **Parameter** | **Value** |
|---|---|
| Rail pressure [MPa] | 100 - 150 - 200 |
| Chamber Temperature [K] | 800 - 900 - 1000 |
| Chamber density [kg/m$^3$] | 15.2 - 22.8 - 30.4 |
| Injection frequency [Hz] | 0.25 |
| Energizing time [ms] | 1.5 |
| Cycles per test point [-] | 10 |

On the hydraulic characterization, 50 cycles were made for every test point. These cycles were averaged into a final curve from which the steady-state mass flow and momentum flux were extracted, as detailed in subsection 3.3.2. A similar process was made on the spray visualization campaign.

The relative standard deviation (RSD) of the stationary injection rate and momentum flux was computed to account for the cycle-to-cycle variations and assess the repeatability of the results. This statistical parameter also serves to analyze whether the standard deviation (std) of the test point is a small or large quantity when compared to its mean ($\overline{X}$) [1]:

$$RSD_X = 100 \cdot \frac{std([X_1\ X_2\ X_3\ ...\ X_{50}])}{\overline{X}} \qquad [\%] \qquad (4.1)$$

## 4.3 Hydraulic characterization

### 4.3.1 Rate of injection

The current section details the outcomes of the injection rate campaign. This test rig captures the injection rate of the nozzle orifices as a whole, so it served to compare the hydraulic performance of one injector against the other.

#### Temporal development of the rate of injection

In Figure 4.1, the rate of injection signal for various conditions is plotted against the time after the start of energizing (ASOE). Additionally, the electric signal sent to the injector is also shown above each corresponding rate of injection curve.

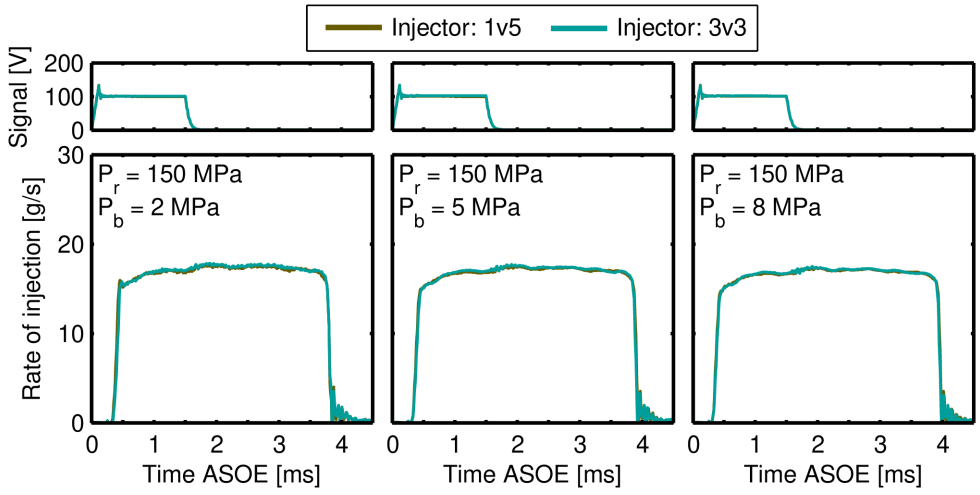


*Figure 4.1: Electric (Top) and rate of injection (bottom) signals after start of energizing.*

The ET remained at 1.5 ms for every condition tested, whereas higher rail pressures required a larger voltage to lift the needle. The manufacturer facilitated the adequate voltage values for each rail pressure.

Moreover, Figure 4.2 depicts the ROI signal for the remaining boundary conditions tested.

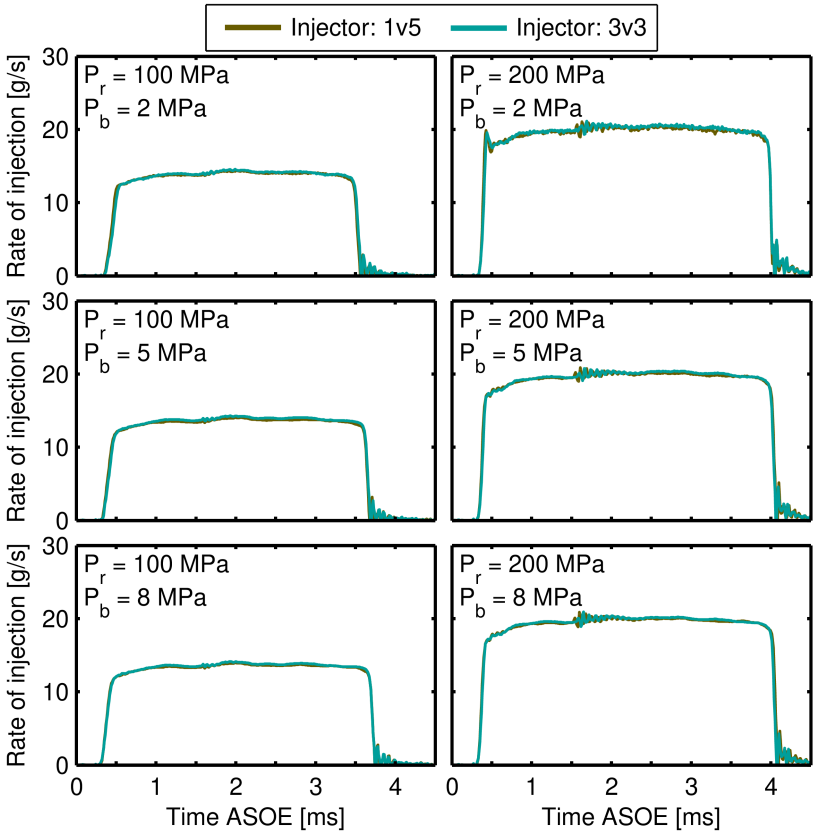


*Figure 4.2: Rate of injection signal after start of energizing.*

In particular, the following trends can be depicted:

- Start of injection. Once the electric pulse is sent to the injectors, both of them required very similar times to overcome the hydraulic forces, lift the needle, start the injection, and reach the steady-state.

  Regarding the boundary conditions, the start of injection (SOI) delay generally decreases with larger chamber pressure values, as this pressure helps in overcoming the hydraulic resistance and push the needle of the injector upwards.

On the other hand, the effect of the rail pressure was smaller, especially for larger chamber pressures. These trends are also depicted with more clarity in Figure 4.3.

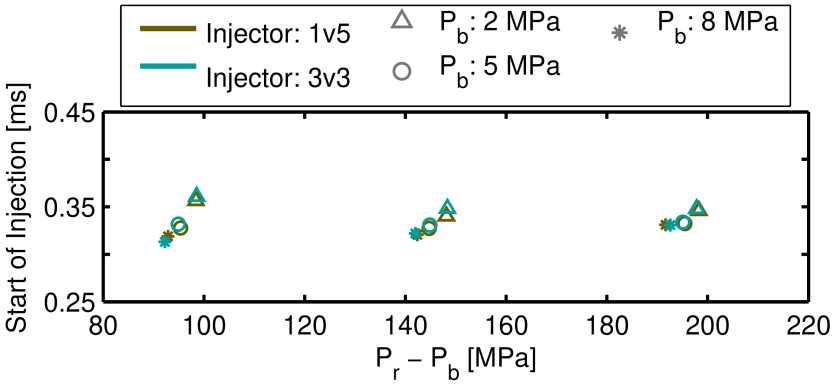


*Figure 4.3: Start of injection for every condition tested.*

- End of injection. Likewise, similar hydraulic delay after the end of energizing is seen for both injectors in every boundary condition. This phenomenon can also be quantitatively observed in Figure 4.4.

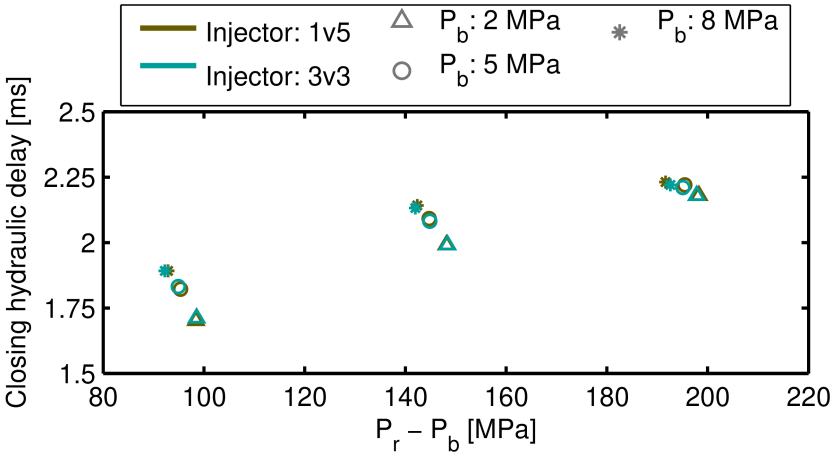


*Figure 4.4: Closing hydraulic delay for every condition tested.*

Furthermore, the injection duration gradually enlarges as the difference between the rail and chamber pressure ($\Delta P$) increases, for the same

energizing time. In this sense, as $\Delta P$ enlarges, so does the difference in pressure between the control volume and the injector nozzle [2].

Thus, the closing hydraulic delay or time required for the injector to compensate for this difference is longer, given that the volume control has to reach a bigger pressure to overcome the hydraulic forces facing the needle on its downwards movement to seal the fuel outlet.

- Steady-state rate of injection ($\dot{m}$). As the injection stabilizes, both injectors settle at a very similar steady-state rate of injection values (Figure 4.5). It can also be detailed that increasing $\Delta P$ enlarges the steady-state injection rate. Moreover, this increase is linearly proportional to the square root of $\Delta P$.

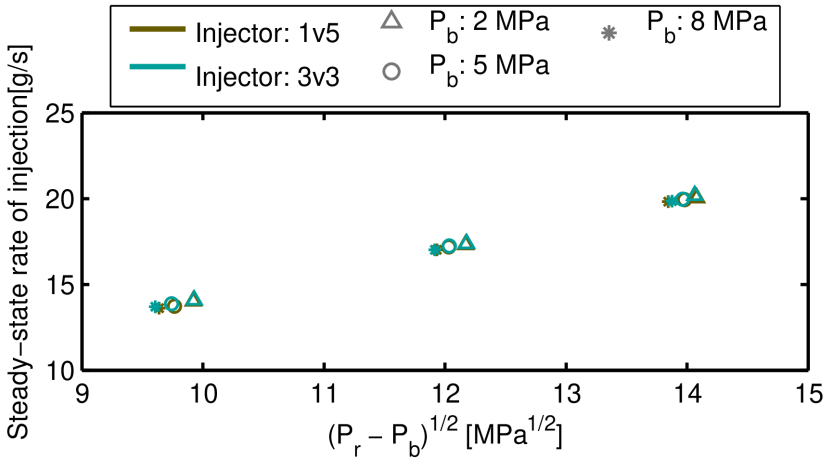


*Figure 4.5: Steady-state rate of injection for every condition tested.*

Several authors have found these trends [3–7], and serve to contrast the consistency of these experiments with well-known spray behavior.

### Shot-to-shot dispersion of the rate of injection

The results presented in the previous section come from averaging 50 repetitions for each test point. The shot-to-shot dispersion of the steady-state injection rate was computed to account for the reliability of these results. In Figure 4.6, the relative standard deviation of the steady-state rate of injection measurements is shown for every condition tested.

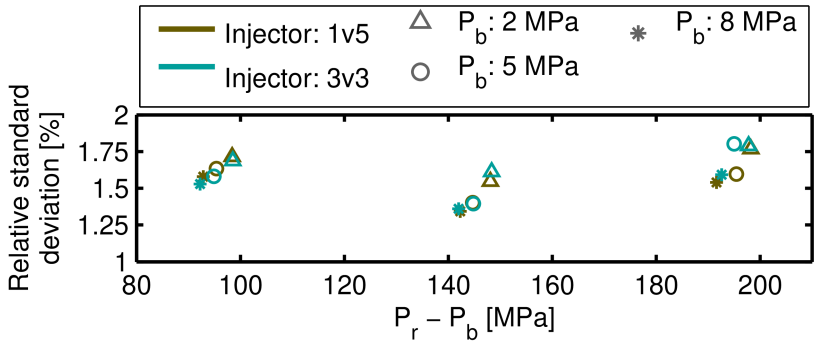


*Figure 4.6: RSD of the stabilized injection rate values.*

It can be observed that the relative standard deviation remained under 2% for every condition tested, accounting for the repeatability of the results found for both injectors.

### 4.3.2 Momentum Flux

This section details the outcomes from the momentum flux experiments.

#### Temporal development of the momentum flux

Figure 4.7 shows the temporal evolution of the momentum flux of each spray.

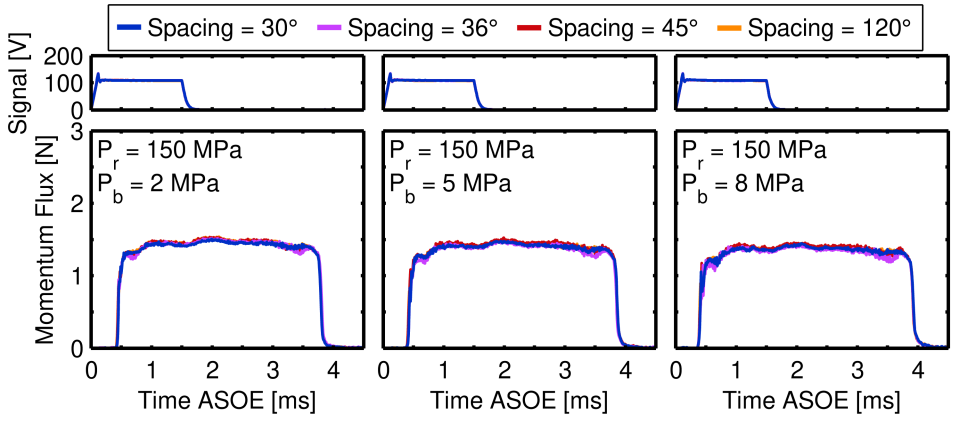


*Figure 4.7: Temporal evolution of the momentum flux.*

Moreover, Figure 4.8 depicts the temporal evolution of the momentum flux for the rest of the boundaries conditions employed. Contrary to the IRDCI, the momentum flux test rig can capture the development of each orifice separately, enabling the comparison in performance between them. Thus, both experiments complement each other.

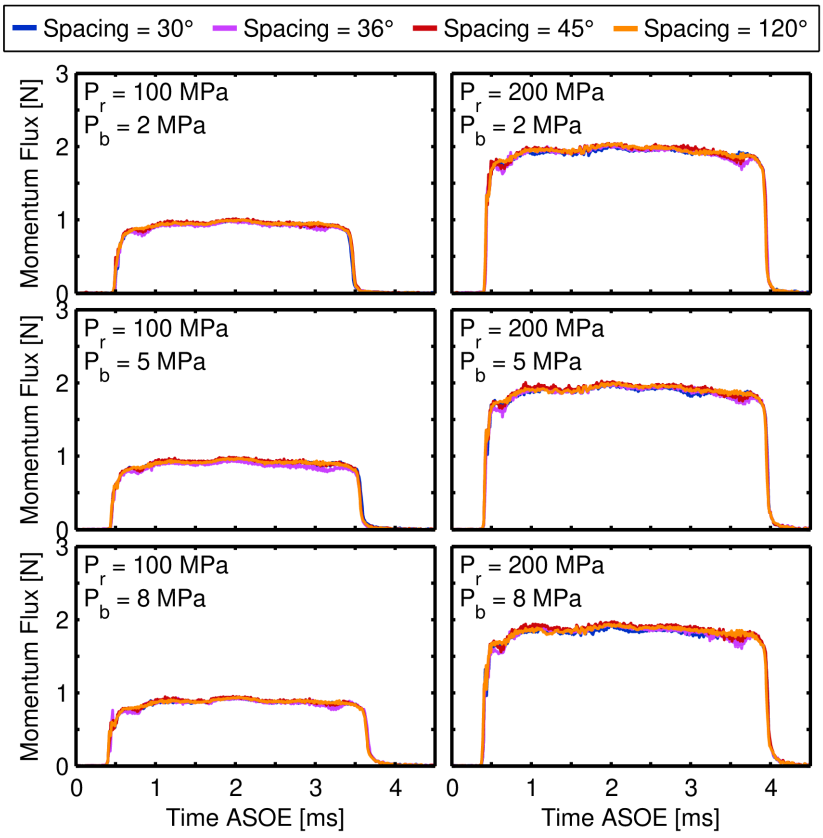


*Figure 4.8: Temporal evolution of the momentum flux for every inter-jet spacing configuration.*

Detailing both figures, similar conclusions to those obtained with the injection rate analysis can be extracted. In particular, it is observed that the momentum flux development through every spray of interest mainly remained constant for a given boundary condition, despite the geometric distribution of the holes.

Regarding the opening hydraulic delay, increasing the chamber pressure reduces the start of injection, although this phenomenon is less noticeable as

the injection pressure increases.

This trend can be observed with more clarity in Figure 4.9, which also reflects that the hydraulic delay generally decreases as the injection pressure enlarges. Concerning the orifices of interest, it can be observed that the start of injection remained highly similar between each orifice regardless of the inter-jet spacing configuration.

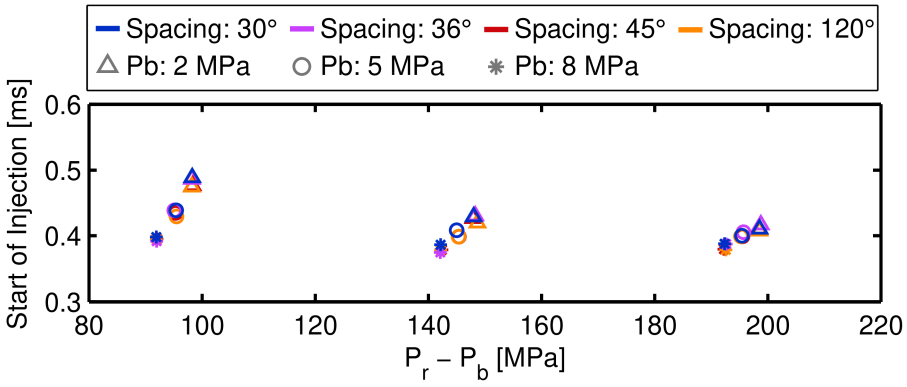


*Figure 4.9: Opening hydraulic delay against the difference between between the rail and back pressure for every condition tested.*

Respecting the closing hydraulic delay, Figure 4.10 depicts the values obtained for every condition tested. It can be seen that the delay was not affected by the geometric distribution of the outlet holes, remaining mostly constant throughout the orifices of interest.

Lastly, steady-state momentum flux values for every inter-jet spacing configuration are presented in Figure 4.11. It is reflected that enlarging the difference between the rail and chamber pressure ($\Delta P$) increases this parameter.

On the hand, altering the inter-jet spacing did not influence the momentum flux, with this value maintaining relatively constant despite the large variations of geometric configurations.

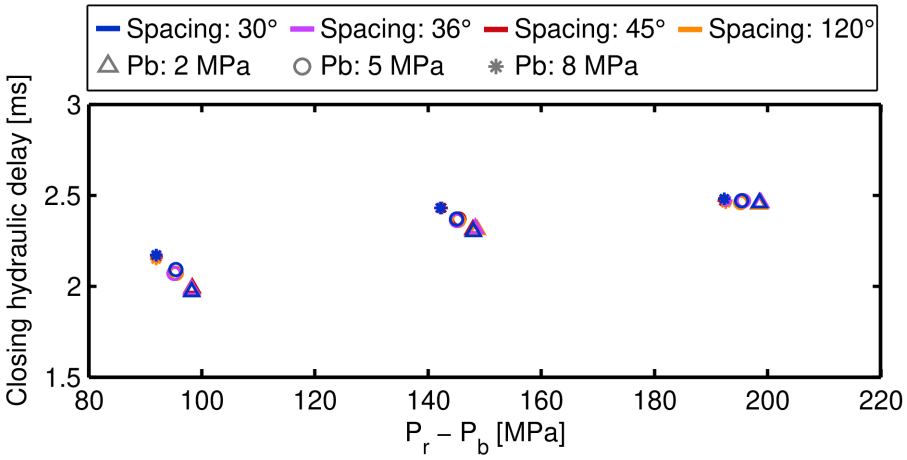


*Figure 4.10: Closing hydraulic delay against the difference between between the rail and back pressure for every condition tested.*

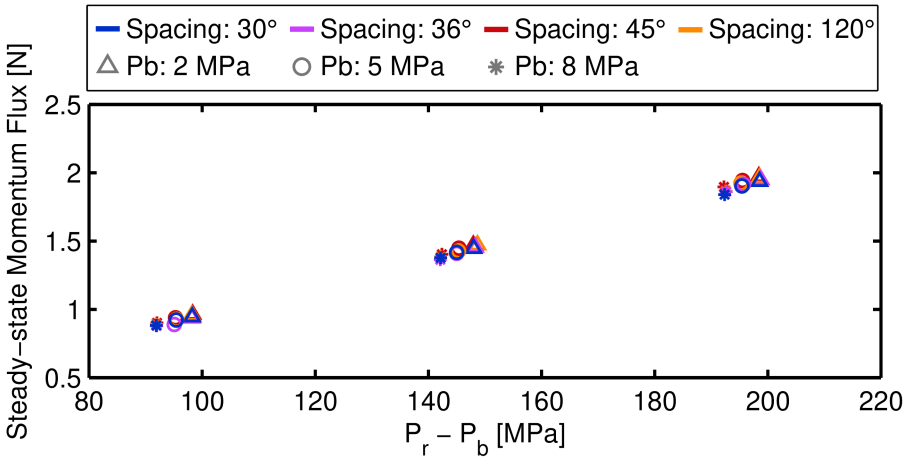


*Figure 4.11: Steady-state momentum flux against the difference between between the rail and back pressure for every condition tested.*

### Shot-to-shot dispersion of the momentum flux

Likewise, the shot-to-shot dispersion of the steady-state momentum flux was computed for each test point, and the results are detailed in Figure 4.12.

It is reflected that the relative standard deviation remained under 3% for every condition tested, accounting for the repeatability of the results found for each orifice of interest.

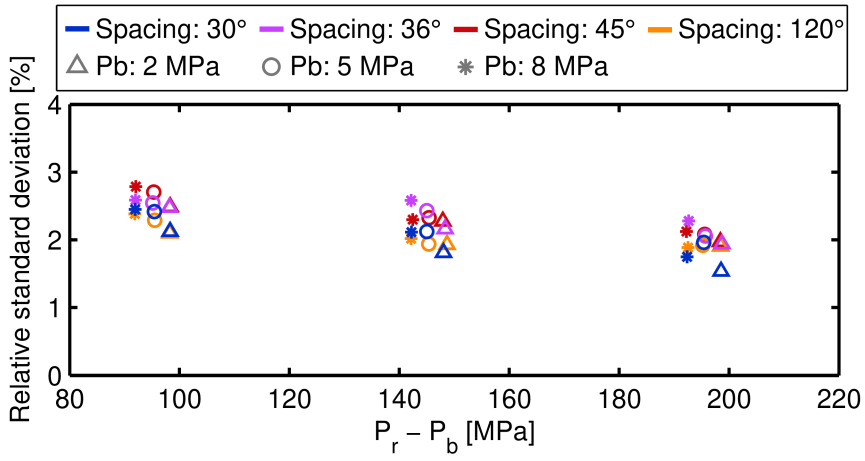


*Figure 4.12: Relative standard deviation of the steady-state momentum flux measurements for every condition tested.*

### 4.3.3 Hydraulic adimensional analysis

Figure 4.13 to Figure 4.15 detail the discharge, momentum, and velocity coefficient for every condition tested, respectively. The dashed line represents the mean coefficient of every condition tested for each geometric configuration. These values are also specified on the bottom-right corner of each figure.

The normalized evaluation is helpful to summarize the high similarity in hydraulic behavior between the orifices of interest.

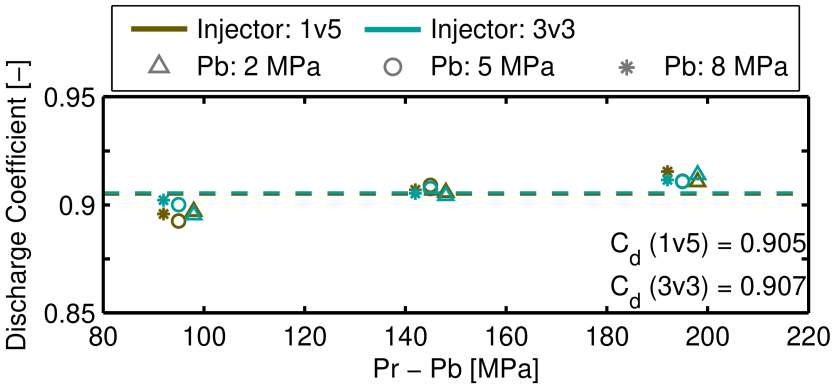


*Figure 4.13: Discharge coefficient of each injector for every condition tested. The average value is presented at the bottom right corner.*

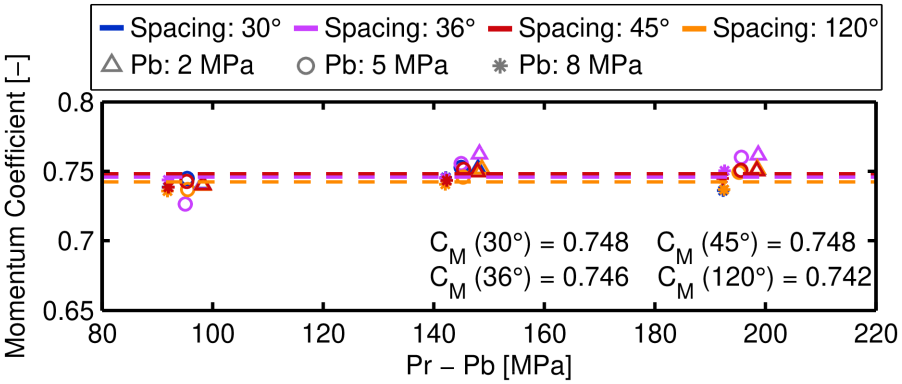


*Figure 4.14: Momentum coefficient of each orifice of interest.*

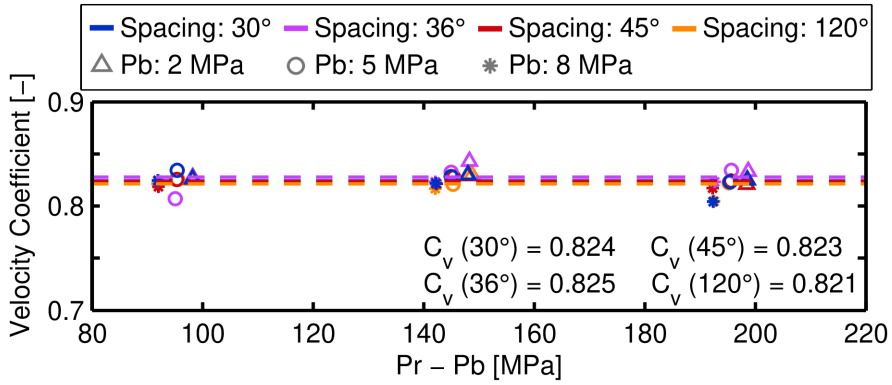


*Figure 4.15: Velocity coefficient of each orifice of interest.*

## 4.4 Spray visualization under inert conditions

The current subsection marks the beginning of the presentation of the visualization results. Representative footage of the images obtained with every optical technique are shown in section 3.5, and the methodology employed to analyze the recordings and obtain every macroscopic parameter is detailed in section 3.6.

### 4.4.1 Start of injection

Figure 4.16 shows the start of injection computed through the MIE scattering technique for every condition tested. Markers of each inter-jet spacing value have been horizontally displaced for better readability.

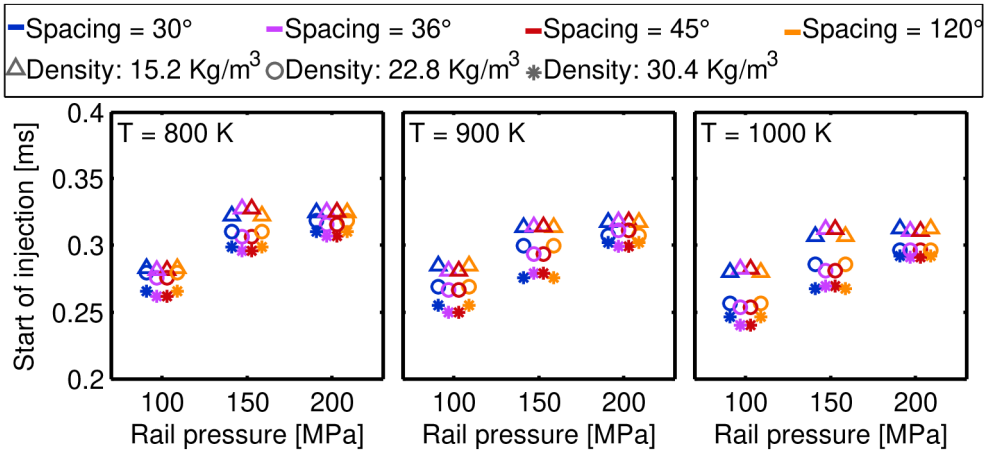


*Figure 4.16: Start of injection (MIE) for every condition tested.*

These experiments were done under high-pressure and high-temperature conditions, complementing the SOI analysis made on subsection 4.3.1 and subsection 4.3.2. Accordingly, similar influences of rail and chamber pressure were found. Moreover, it is observed that increasing the chamber temperature decreases the SOI slightly. Likewise, similar SOI values were found for every inter-jet configuration, with variations under 3% for every condition tested.

### 4.4.2 Liquid length

Figure 4.17 and Figure 4.18 depict liquid length values for most conditions tested.

It is depicted that the liquid length of the spray considerably decreases when the chamber temperature increases, as the larger enthalpy provided to the fuel droplets allows for a shorter evaporation distance. Furthermore, an increment of the chamber density reduces the liquid length as the rate of air entrainment increases, reducing the distance required to evaporate entirely.

Additionally, it is observed on Figure 4.18 that the rail pressure does not have a significant influence on the liquid length: enlarging the rail pressure increases the fuel velocity but also decreases the fuel droplet size, which enhances the air entrainment. Thus, a balance is created in which the final evaporation distance is not greatly affected. The effects produced by the chamber temperature, chamber density, and rail pressure have previously been observed [8–11].

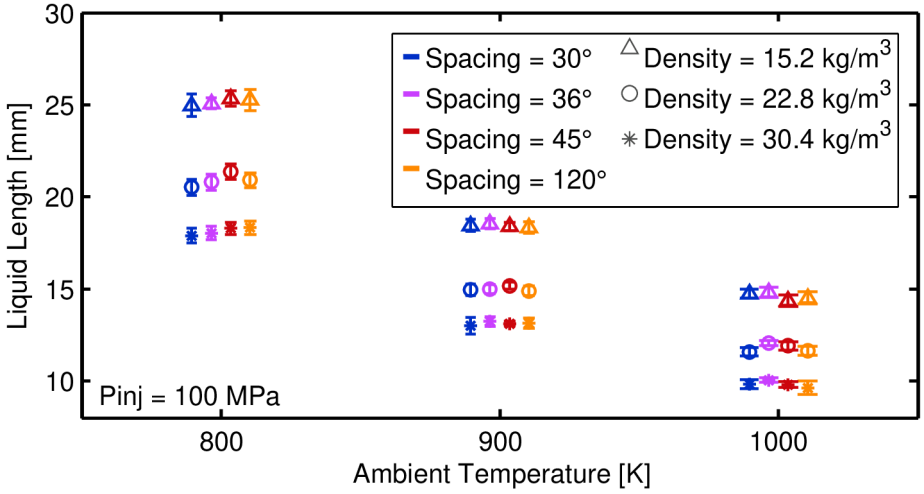


*Figure 4.17: Liquid length variation for several values of inter-jet spacing, chamber temperature and chamber density.*

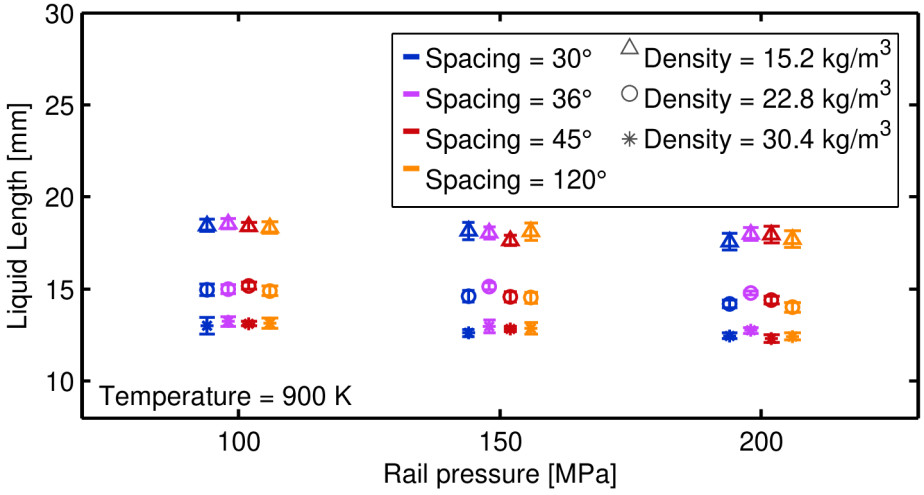


*Figure 4.18: Liquid length variation for several values of inter-jet spacing, injection pressure and chamber density.*

On the other hand, the results showed that altering the inter-jet spacing did not notably affect the liquid length values.

### 4.4.3 Vapor spray penetration

Figure 4.19 details the temporal development of the spray tip penetration for several boundary conditions. The optical access was limited to 45 mm from the nozzle tip.

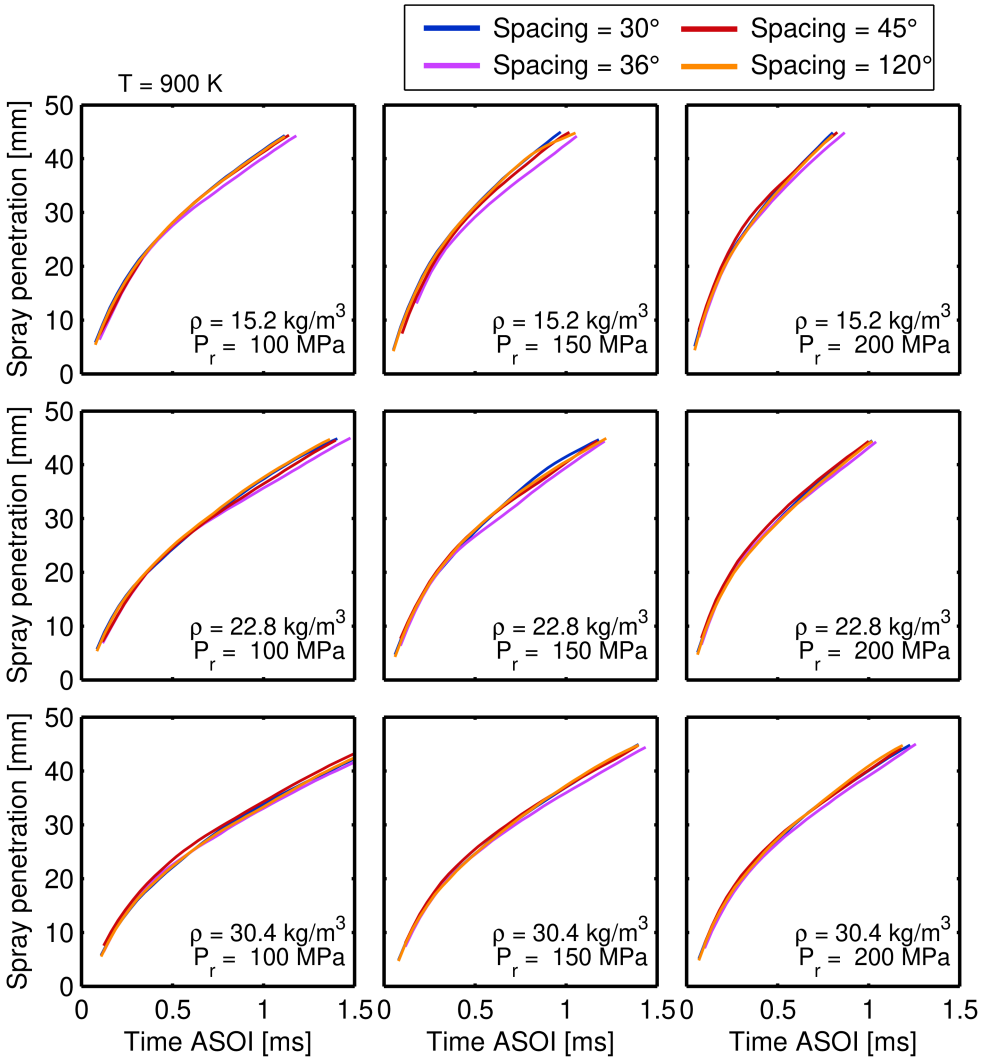


*Figure 4.19: Vapor spray penetration variation for several values of inter-jet spacing, rail pressure, and chamber density. chamber temperature = 900 K*

As denoted in subsection 2.4.4, the spray penetration is initially linearly proportional to time ($t$) until the breakup time. Afterward, it is proportional to the square root of time ($t^{1/2}$).

Additionally, it is depicted that augmenting the rail pressure accelerates the penetration rate, with the sprays reaching the border of the window in a shorter amount of time. On the other hand, increasing the chamber density results in a slower penetration rate, as the sprays are subject to a greater momentum exchange. These phenomena are reflected on Equation 2.11 and have been observed by numerous researchers [12–15], validating the reliability of the observed results.

Regarding the inter-jet spacing, altering the geometric distribution of the outlet holes did not have a notable influence on the penetration development, as the penetration development remained without considerable nor persistent variations throughout the tested conditions.

## 4.5 Summary and conclusions

The present chapter detailed the results obtained under non-reactive conditions. From the results, the following conclusions are drawn:

- The injection rate and momentum flux experiments revealed a high resemblance in hydraulic behavior between the orifices of interest, regardless of the inter-jet spacing configuration.
- The influence of the chamber density, temperature, and rail pressure on the liquid length and vapor spray penetration of the spray followed the trends found in the literature. On the other hand, these parameters were not notably affected by the geometric distribution of the outlet orifices.
- The start of injection remained generally unaltered for the range of inter-jet spacing configurations studied.

Overall, the injection event under non-reactive conditions was not affected by the inter-jet spacing. Moreover, the performance was similar between each orifice of interest for every parameter tested. Thus, any difference observed in a reactive environment could be attributed to phenomena occurring during the combustion.

# References

[1] Viera, Alberto. "Effect of multiple injection strategies on the diesel spray formation and combustion using optical diagnostics". PhD thesis. Universitat Politècnica de València, 2019. DOI: 10.4995/Thesis/10251/123954.

[2] Plamondon, E.; and Seers, P. "Development of a simplified dynamic model for a piezoelectric injector using multiple injection strategies with biodiesel/diesel-fuel blends". In: *Applied Energy* 131 (2014), pp. 411–424. DOI: 10.1016/j.apenergy.2014.06.039.

[3] Payri, Raul; Bracho, Gabriela; Gimeno, Jaime; and Bautista, Abian. "Rate of injection modelling for gasoline direct injectors". In: *Energy Conversion and Management* 166.February (2018), pp. 424–432. DOI: 10.1016/j.enconman.2018.04.041.

[4] Giraldo Valderrama, Jhoan Sebastián. "Macroscopic and microscopic characterization of non-reacting diesel sprays at low and very high injection pressures". PhD thesis. Universitat Politècnica de València, 2018.

[5] Viera, Juan Pablo. "Experimental study of the effect of nozzle geometry on the performance of direct-injection diesel sprays for three different fuels". PhD thesis. 2017. DOI: 10.4995/Thesis/10251/81857.

[6] Payri, Raul; Climent, Hector; Salvador, Francisco Javier; and Favennec, A.-G. "Diesel Injection System Modelling. Methodology and Application for a First-generation Common Rail System". In: *Proceedings of the Institution of Mechanical Engineers, Part D: Journal of Automobile Engineering* 218.1 (2004), pp. 81–91. DOI: 10.1243/095440704322829191.

[7] Benajes, Jesus; Pastor, Jose Vicente; Payri, Raul; and Plazas, Alejandro Hernan. "Analysis of the influence of Diesel nozzle geometry in the Injection Rate characteristic". In: *Journal of Fluids Engineering* 126.1 (2004), pp. 63–71. DOI: 10.1115/1.1637636.

[8] Siebers, Dennis L. "Scaling liquid-phase fuel penetration in diesel sprays based on mixing-limited vaporization". In: *SAE Technical Paper 1999-01-0528* (1999). DOI: 10.4271/1999-01-0528.

[9] Manin, Julien; Bardi, Michele; and Pickett, Lyle M. "Evaluation of the liquid length via diffused back-illumination imaging in vaporizing diesel sprays". In: *Comodia*. Fukuoka, 2012.

[10] Payri, Raul; Gimeno, Jaime; Bardi, Michele; and Plazas, Alejandro Hernan. "Study liquid length penetration results obtained with a direct acting piezo electric injector". In: *Applied Energy* 106.JUNE (2013), pp. 152–162. DOI: 10.1016/j.apenergy.2013.01.027.

[11] Payri, Raul; Gimeno, Jaime; Bracho, Gabriela; and Vaquerizo, Daniel. "Study of liquid and vapor phase behavior on Diesel sprays for heavy duty engine nozzles". In: *Applied Thermal Engineering* 107 (2016), pp. 365–378. DOI: 10.1016/j.applthermaleng.2016.06.159.

[12] Hiroyasu, Hiroyuki; and Arai, Masataka. "Structures of Fuel Sprays in Diesel Engines". In: *SAE Technical Paper 900475*. 1990. DOI: 10.4271/900475.

[13] Naber, Jeffrey D; and Siebers, Dennis L. "Effects of Gas Density and Vaporization on Penetration and Dispersion of Diesel Sprays". In: *SAE Paper 960034*. Vol. 105. 412. Society of Automotive Engineers, Inc., Warrendale, Pennsylvania, USA, 1996, pp. 82–111. DOI: 10.4271/960034.

[14] Payri, Francisco; Bermúdez, Vicente; Payri, Raul; and Salvador, Francisco Javier. "The influence of cavitation on the internal flow and the spray characteristics in diesel injection nozzles". In: *Fuel* 83.4-5 (2004), pp. 419–431. DOI: 10.1016/j.fuel.2003.09.010.

[15] Wan, Yuepeng; and Peters, Norbert. "Scaling of spray penetration with evaporation". In: *Atomization and Sprays* 9.2 (1999), pp. 111–132. DOI: 10.1615/AtomizSpr.v9.i2.10.

# Chapter 5

# Spray ignition and lift-off length

## 5.1 Introduction

The following results were obtained under a reacting environment, which is the main focus of this work as it is where the interactions between sprays could have a larger influence.

Specifically, the current section details the results from the OH* and broad-band chemiluminescence experiments, detailing any variation in ignition delay, initial soot appearance, and lift-off length due to inter-jet spacing variations. Lastly, a statistical analysis is done on the lift-off length results.

## 5.2 Test plan

Boundary conditions such as rail pressure, chamber density, and temperature were selected using guidelines from the Engine Combustion Network (ECN) [1] and are depicted in Table 5.1, in which every possible combination was employed. Moreover, the optical setup (Figure 3.20) allowed to obtain these parameters simultaneously for the same injection event.

Ten cycles of each tested condition were measured to reduce measuring errors and uncertainties. Afterward, all the repetitions were averaged into a final value, and the standard deviation was obtained for each parameter. The shot-to-shot dispersion is represented as error bars in each plot.

*Table 5.1: Test plan for each injector.*

| Parameter | Value | Units |
|---|---|---|
| Injection pressure | 100 - 150 - 200 | MPa |
| Chamber Temperature | 800 - 900 - 1000 | K |
| Chamber density | 15.2 - 22.8 - 30.4 | kg/m$^3$ |
| Fuel temperature | 363 | K |
| Injection frequency | 0.25 | Hz |
| Energizing time | 1.5 | ms |
| Cycles per test point | 10 | - |

## 5.3 Ignition delay

Ignition delay values for various boundary conditions are depicted in Figure 5.1 and Figure 5.2.

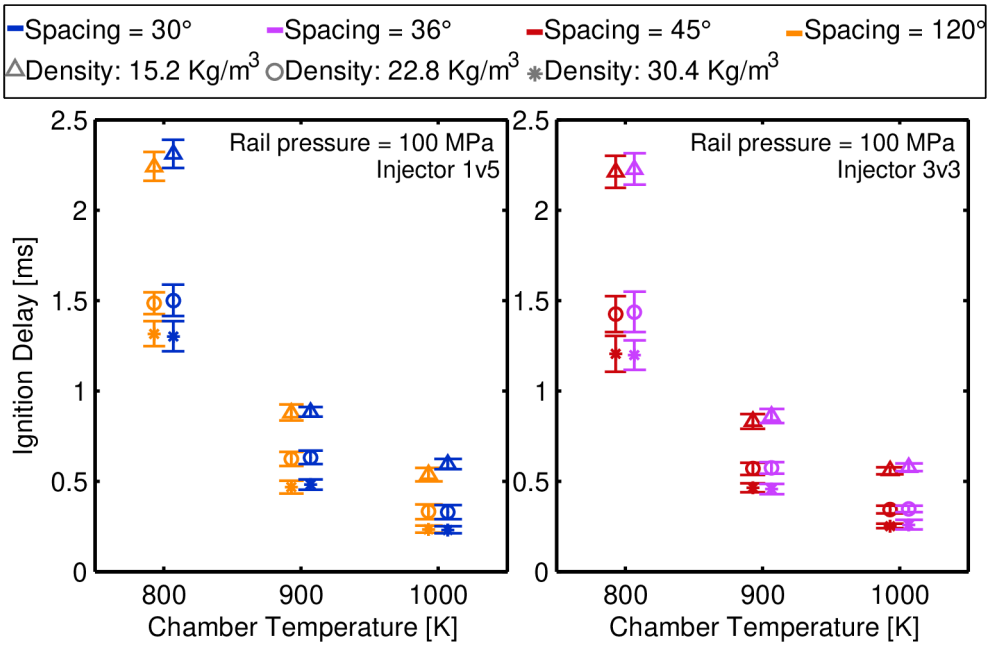


*Figure 5.1: Ignition delay variation for several values of inter-jet spacing, chamber temperature and chamber density (left plot: 1v5 injector; right plot: 3v3 injector).*

The results are initially separated by injector to improve their readability. On the left, the results of the injector 1v5 are depicted, whereas the right plot shows the ignition delay values of the injector 3v3 for the same boundary conditions. It is detailed that the ignition delay shortens with an increase of the chamber temperature, chamber density, and rail pressure, as these phenomena enhance the air-fuel mixing process, accelerating the reactions and start of combustion. This behavior has also been observed in previous works [2, 3].

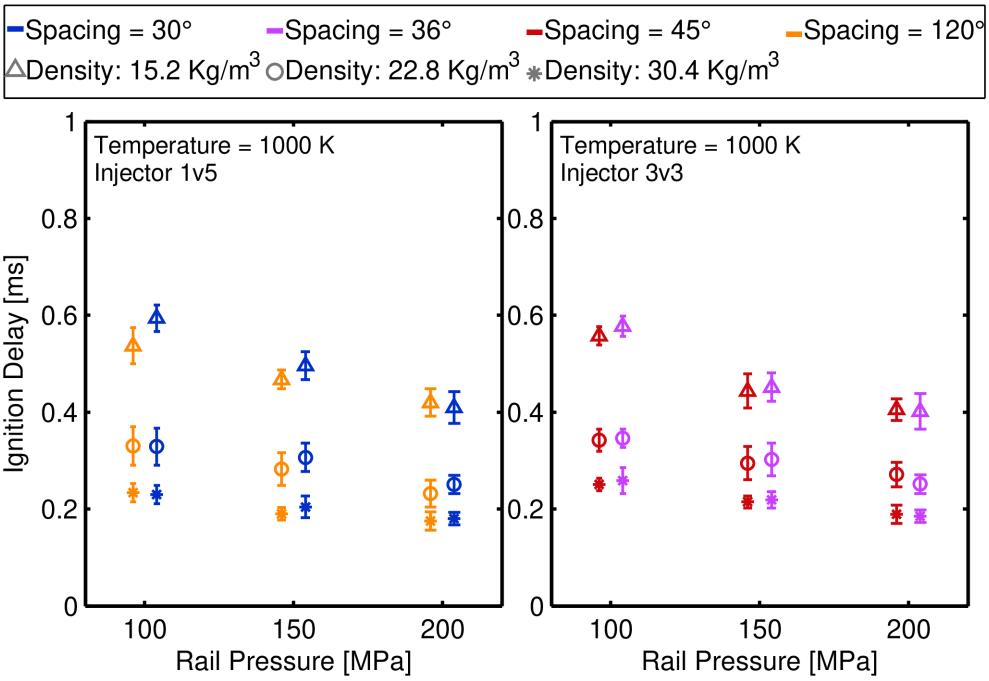


*Figure 5.2: Ignition delay variation for several values of inter-jet spacing, injection pressure and chamber density (left plot: 1v5 injector; right plot: 3v3 injector).*

On the other hand, the results showed that the inter-jet spacing had a limited impact overall. For most tested conditions, the ignition delay was only slightly altered throughout the geometric configurations analyzed, and these variations were frequently within the error interval of the isolated spray result.

This trend is also observed in figure Figure 5.3, which illustrates the relative ignition delay for every condition tested, a normalized value computed to

assess the influence of inter-jet spacing more clearly. To do so, each ignition delay value was divided by the ignition delay obtained with the isolated spray (spacing = 120°) at the same boundary condition, as depicted in Equation 5.1.

$$Relative\ ID_i = \frac{ID_i}{ID_{120}} \tag{5.1}$$

Nevertheless, differences were still observed as boundary conditions evolved. Specifically, sprays with neighbor jets tended to have equal or slightly smaller ignition delay values under poor mixing and ignition conditions, that is, low rail pressure, chamber temperature, or chamber density conditions. In these conditions, interactions between sprays could be accelerating the ignition event, such as a local increase in temperature due to radiative heat exchange between neighboring jets [4].

Interestingly, the opposite effect was generally observed as the boundary conditions were overall increased. In particular, higher chamber temperatures, densities, and rail pressures typically led to equal or higher ignition delay values for the sprays with neighbor jets, compared to that of the isolated spray.

Plausibly, the proximity between sprays could become counterproductive in accelerating the ignition as ignition-promoting boundary conditions increase. For instance, increasing the chamber density widens the spray spreading angle [5–7], further reducing the space and air available around each neighbor spray. This phenomenon could inhibit the mixing process and further delay the ignition event. Nonetheless, no clear trend was defined, with complex interactions and multiple factors simultaneously affecting the ignition event.

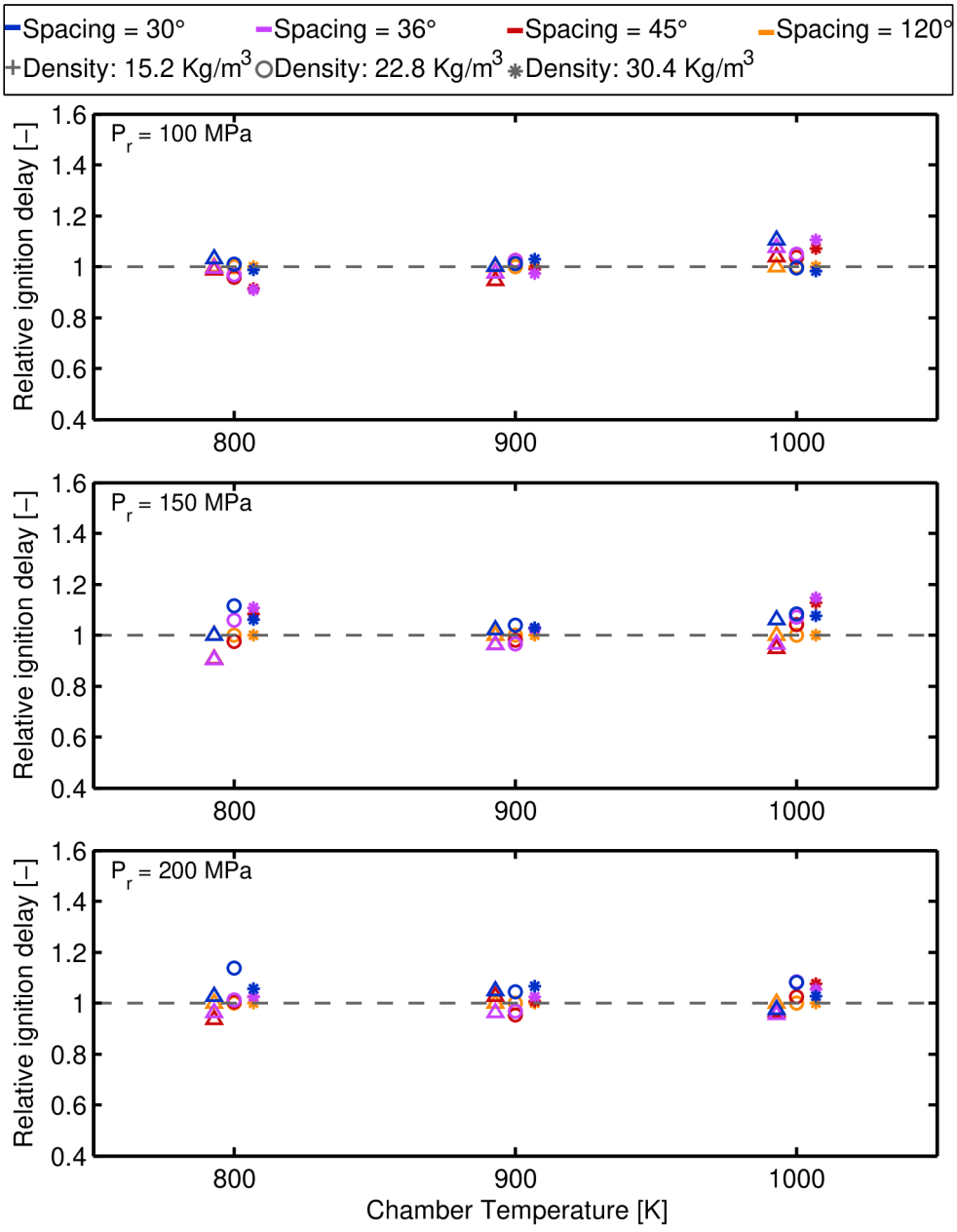


*Figure 5.3: Ignition delay variation for several values of inter-jet spacing, relative to the ignition delay value of the isolated spray (spacing = 120°).*

## 5.4 Initial soot appearance

To further analyze the effect of inter-jet spacing on the combustion development after ignition, the initial soot appearance was obtained through broadband chemiluminescence and compared to the ignition delay captured with OH* chemiluminescence on the same injection event (Figure 5.4).

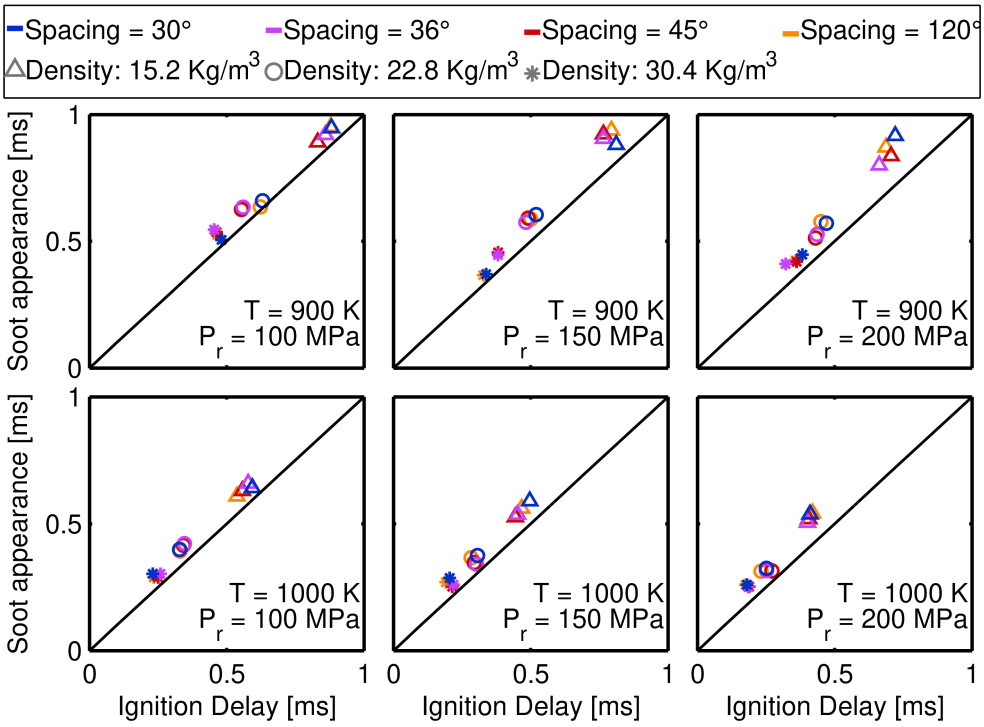


*Figure 5.4: Initial soot appearance against ignition delay for every inter-jet spacing configuration. Broadband chemiluminescence was non-existent or low (and unstable) for most of the test points at 800 K of chamber temperature.*

It is detailed that the initial soot appearance followed the same trends as the ignition delay. Specifically, the soot appearance delay shortens as the chamber temperature, chamber density, or rail pressure increases, serving as a qualitative measurement of the combustion timing.

On the other hand, it can be seen that, for a given condition, the results obtained with OH* chemiluminescence are constantly lower as OH radicals appear in the initial stages of the ignition process. Therefore, OH* chemiluminescence is preferred to obtain a quantitative ignition delay value [8, 9].

Regarding the proximity between orifices, it can be observed that for a given boundary condition, the inter-jet spacing did not considerably delay or advance the initial soot appearance, as this parameter remained almost unaltered within the range of geometric configurations studied.

## 5.5 Lift-off length

The values of lift-off length for several boundary conditions are depicted in Figure 5.5. Again, the results of both injectors are separated to improve readability and compare the same injection event. The same methodology is also applied for Figure 5.6, which accounts for the influence of the rail pressure on the lift-off length.

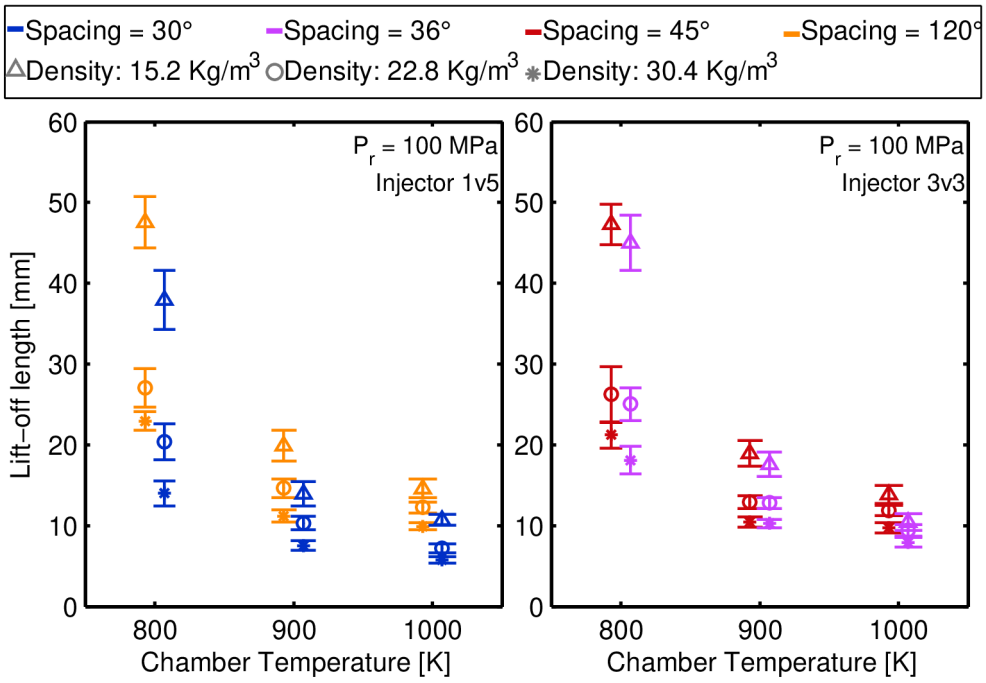


*Figure 5.5: Lift-off length variation for several values of inter-jet spacing, chamber temperature and chamber density (left plot: 1v5 injector; right plot: 3v3 injector).*

It can be observed that the lift-off length is highly dependent on the chamber temperature and density. Specifically, an increase of the temperature or

the density inside the chamber resulted in a reduction of the steady lift-off length, as the spay mixing process is enhanced. Additionally, Figure 5.6 depicts that an increase of the rail pressure generally produces a slightly larger lift-off length. Several authors have found these trends [10–12], which serve to validate the consistency of the experiments of this work with well-known spray behavior.

Regarding the influence of the inter-jet spacing, considerable variations were found when altering the jet-to-jet proximity. On the left plot of Figure 5.5 and Figure 5.6, it can be seen that, for every condition tested, the spray with inter-jet spacing of 30° had considerably lower lift-off length values than the isolated spray (Spacing = 120°).

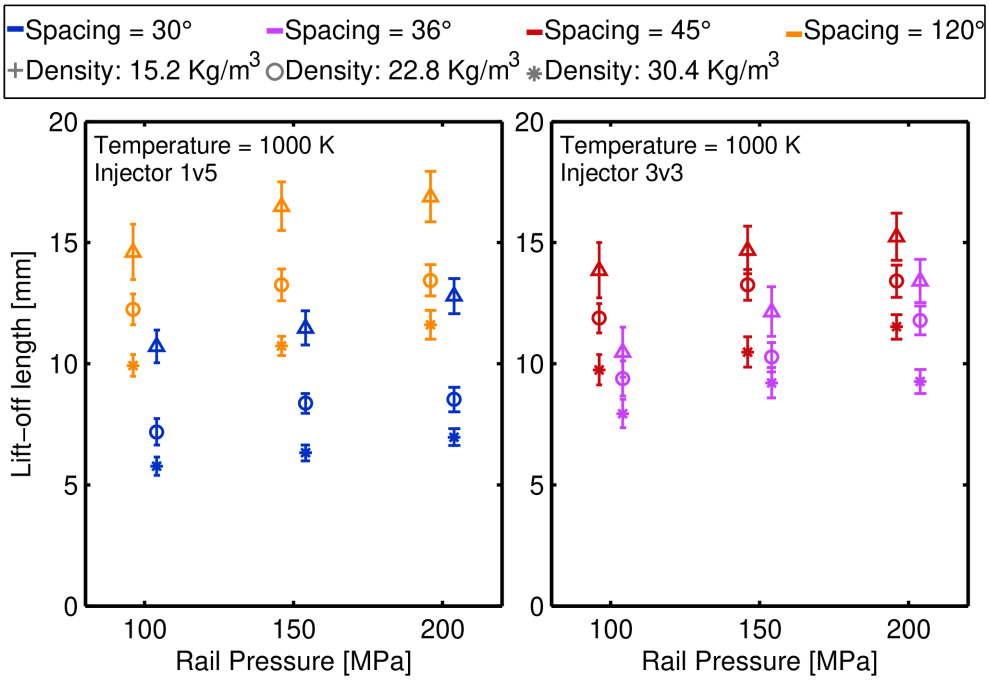


*Figure 5.6: Lift-off length variation for several values of inter-jet spacing, injection pressure and chamber density (left plot: 1v5 injector; right plot: 3v3 injector).*

This trend was generally observed in the injector 3v3 as well, although smaller differences were found between the sprays of study, in accordance with their more similar values of inter-jet spacing. Nevertheless, the spray

with 36° of inter-jet spacing tended to have a slightly smaller lift-off length value than the spray with 45° of inter-jet spacing.

This behavior change was found throughout every boundary point, as depicted in Figure 5.7. As with ignition delay results, this figure illustrates the normalized lift-off length values relative to the value of the isolated spray for every condition tested.

It is detailed with more clarity that the spray with 30° of inter-jet spacing had lower lift-off length values than any of the other inter-jet spacing configurations for every condition tested. Moreover, the spray with 36° of inter-jet spacing tended to have a slightly smaller lift-off length (LOL) value than the spray with 45° of inter-jet spacing, which had lift-off length values closer to those of the isolated spray. Lastly, the results show that this contrast was larger as the chamber density and temperature increased.

Overall, the results detailed that the LOL is notably reduced after certain proximity between sprays is reached (between 30° or 36° of inter-jet spacing, depending on the boundary conditions). On the other hand, when the inter-jet spacing is greater than this threshold value, the results are less distant to those obtained from the isolated spray (Spacing = 120°).

Similarly, Bazyn; and Koci [4] studied the lift-off length for a range of 6 to 18 orifices nozzles and noted a similar behavior to the results observed in this work. In particular, no significant variations were found up until the nozzle with 10 orifices (36° of inter-jet spacing), in which the sprays began to be considerably affected by the neighboring plumes, shortening the lift-off length.

The main plausible explanation for the observed change in behavior could be the interaction between combustion products of closely spaced jets. On this matter, Pickett et al. [13] conducted shadowgraphy imaging of reacting jet, revealing the presence of high-temperature reservoirs of combustion products and fresh ambient gas along the periphery of the spray.

Moreover, Pickett et al. [13] and Persson et al. [14] proposed that the gas entrained by the jet is previously mixed with these high-temperature products, creating autoignition events near the nozzle that influence the lift-off length. Additionally, the proportion of entrained hot combustion products and radicals could increase in closely spaced sprays [15]. Then, entrained gas at a higher temperature could trigger auto-ignition near the nozzle, reducing the lift-off length.

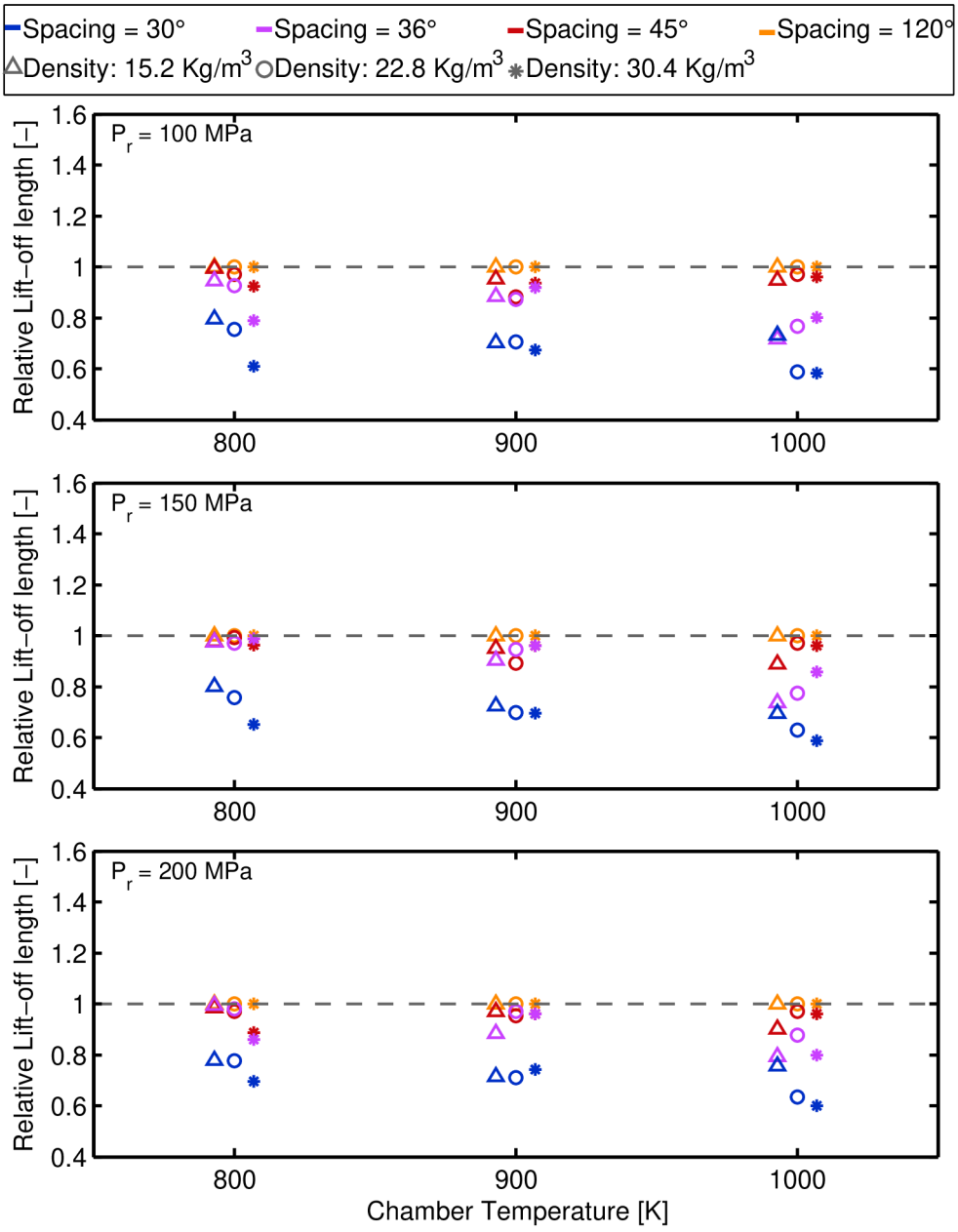


*Figure 5.7: Lift-off length variation for several values of inter-jet spacing, relative to the lift-off length value of the isolated spray (spacing = 120°).*

Other factors contributing to the observed results could be the radiative heat exchange occurring between the neighbor jets, which would be more intense as the sprays get closer to each other. Thus, the local temperature of the mixture could increase, accelerating the reactions and shortening the lift-off length, as seen in Figure 5.7. Lastly, the fluid dynamics around the spray could be affected by the presence of neighbor sprays, ultimately altering the lift-off length [16].

As the reduction in lift-off length was seen throughout the measurements campaign, and an extensive test matrix was employed, a statistical analysis of the observed results was done.

### 5.5.1 Statistical Analysis

Based on the large test matrix employed throughout the measurements, the results observed were used to obtain a regression for the lift-off length. On this matter, the same approach used by Benajes et al. [10] is applied to characterize the lift-off length, so an exponential equation is employed:

$$LOL \propto T^a \cdot \rho^b \cdot {U_{th}}^c \cdot \theta^d \tag{5.2}$$

In which $T$ refers to the chamber temperature, $\rho$ to the chamber density, $\theta$ to the inter-jet spacing in degrees, and $U_{th}$ to the theoretical velocity of the fuel at the nozzle exit, calculated by the equation [10]:

$$U_{th} = \sqrt{2\frac{\Delta P}{\rho_f}} \tag{5.3}$$

In which $\Delta P$ represents the difference between the rail pressure and the chamber pressure, and $\rho_f$ the fuel density.

In Table 5.2, the coefficients obtained for the Equation 5.2 are presented. Additionally, the table contains the results obtained by Benajes et al. [10] and Siebers; and Higgins [17], for reference purposes.

It can be observed that the coefficients obtained with the experimental data have a general agreement with the values presented by Benajes et al. [10] and Siebers; and Higgins [17] in terms of chamber density, fuel velocity, and chamber temperature, with the latter having the most significant impact on the lift-off length. Additionally, the high value of $R^2$ obtained confirms the repeatability and reliability of the results gathered.

Moreover, the experimental data regression introduced a new variable that takes into account the effect of the spacing between sprays on the lift-off length.

*Table 5.2: Coefficients obtained for the lift-off length correlation.*

| | $a$ | $b$ | $c$ | $d$ | $e^*$ | $R^2$ [%] |
|---|---|---|---|---|---|---|
| Experimental data | -4.79 | -0.83 | 0.71 | 0.81 | - | 94.1 |
| Benajes et al. [10] | -3.89 | -1 | 0.54 | - | -1 | 99.5 |
| Siebers; and Higgins [17] | -3.74 | -0.85 | 1 | - | -1 | - |

* Influence of the oxygen concentration (not within the scope of this study).

As seen in previously presented results, the inter-jet spacing considerably impacts the lift-off length value. The main physical mechanism producing this behavior could be the entrainment of hot combustion products near the nozzle, as detailed in the section of results and discussion of the lift-off length.

Finally, Figure 5.8 compares the experimental lift-off length values against the lift-off length obtained with the regression for each boundary condition.

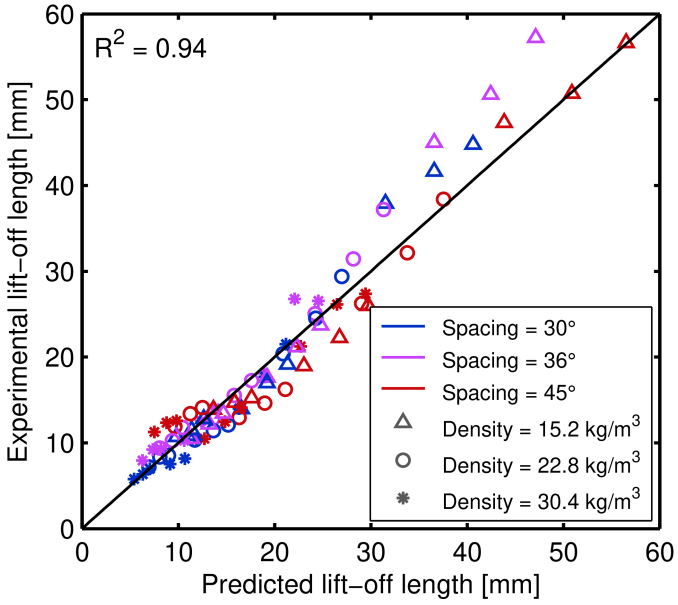


*Figure 5.8: Experimental vs predicted lift-off length values.*

Overall, the correlation can reproduce the general behavior of the spray for the wide range of boundary conditions tested. However, some points at the lowest value of chamber temperature and density were under-estimated. This trend aligns with the higher instability noted at those test points due to

poor boundary conditions for stable combustion, increasing the complexity in predicting its behavior.

Nevertheless, the general trend is represented with high accuracy for most operating conditions.

## 5.6 Summary and conclusions

This chapter studies the variation of the inter-jet spacing of a diesel injector and its effect on the ignition delay and lift-off length of the spray. This study was done employing a multi-hole injector with an outlet holes distribution that allowed to compare an isolated spray to another with an inter-jet spacing of 30°, during the same injection event. Additionally, the results were compared to the development of sprays of the other injector, containing jets with an inter-jet spacing of 36° and 45°.

From the results obtained, the following main conclusions are drawn:

- The measurements in reactive environment showed that after certain proximity between sprays is reached, the interaction between the sprays becomes a predominant factor in their behavior, and the lift-off length is considerably reduced. Moreover, as the inter-jet spacing increases, the performance gradually approaches to that obtained from the isolated spray.

- Plausibly, closely spaced sprays entrain a higher amount of hot combustion products and radicals. Then, the entrained gas with a higher temperature could trigger autoignition near the nozzle, reducing the lift-off length.

- The results obtained in the lift-off length were subject to statistical analysis. A novel regression for the lift-off length was developed, which accounted for the effect of the proximity between sprays.

- Regarding the ignition delay, the presence of neighbor jets had limited impact, as many test points had similar ignition delay for every inter-jet spacing configuration. Nevertheless, some variations were observed as boundary conditions evolved, although no clear trend was defined.

- On the one hand, sprays with neighbor jets tended to have equal or slightly smaller ignition delay values under poor mixing and ignition conditions (low rail pressure, chamber temperature, or chamber density

conditions). On the other hand, the opposite effect was generally observed as the boundary conditions were overall increased, with equal or higher ignition delay values within sprays with neighbor jets, compared to that of the isolated spray.

- An increase of the chamber temperature or density considerably reduced the lift-off length and ignition delay. Moreover, enlarging the rail pressure slightly reduced the ignition delay and increased the lift-off length. These are well-known spray behavior and served to validate the consistency of the experiments of this experimental campaign.

- The initial soot appearance obtained with broadband chemiluminescence followed the same trends as the ignition delay, serving as a qualitative measurement of the combustion timing. Nevertheless, OH* chemiluminescence captures the initial stages of the ignition process, thus being the preferred technique to obtain a quantitative ignition delay value.

# References

[1] ECN. *Online: https://ecn.sandia.gov/diesel-spray-combustion/target-condition/spray-ab/, accessed on 20-01-2022.*

[2] Pickett, Lyle M.; Siebers, Dennis L.; and Idicheria, Cherian A. "Relationship Between Ignition Processes and the Lift-Off Length of Diesel Fuel Jets". In: *SAE Paper 2005-01-3843* 724 (2005). DOI: 10.4271/2005-01-3843.

[3] Payri, Raul; Salvador, Francisco Javier; Manin, Julien; and Viera, Alberto. "Diesel ignition delay and lift-off length through different methodologies using a multi-hole injector". In: *Applied Energy* 162 (2016), pp. 541–550. DOI: 10.1016/j.apenergy.2015.10.118.

[4] Bazyn, Tim; and Koci, Chad. "The Effect of Jet Spacing on the Combustion Characteristics of Diesel Sprays". In: *THIESEL 2014 Conference on Thermo- and Fluid Dynamic Processes in Direct Injection Engines*. 2014, pp. 1–19.

[5] Payri, Francisco; Payri, Raul; Bardi, Michele; and Carreres, Marcos. "Engine combustion network: Influence of the gas properties on the spray penetration and spreading angle". In: *Experimental Thermal and Fluid Science* 53.September 2015 (2014), pp. 236–243. DOI: 10.1016/j.expthermflusci.2013.12.014.

[6] Giraldo, Jhoan S.; Payri, Raul; Marti-Aldaravi, Pedro; and Montiel, Tomas. "Effect of high injection pressures and ambient gas properties over the macroscopic characteristics of the diesel spray on multi-hole nozzles". In: *Atomization and Sprays* 28.12 (2018), pp. 1145–1160. DOI: 10.1615/AtomizSpr.2019029651.

[7] Manin, Julien; Pickett, Lyle M.; and Skeen, Scott A. "Two-Color Diffused Back-Illumination Imaging as a Diagnostic for Time-Resolved Soot Measurements in Reacting Sprays". In: *SAE International Journal of Engines* 6.4 (2013), pp. 1908–1921. DOI: 10.4271/2013-01-2548.

[8] Pastor, José V.; García, A.; Micó, C.; and García-Carrero, Alba A. "Experimental study of influence of Liquefied Petroleum Gas addition in Hydrotreated Vegetable Oil fuel on ignition delay, flame lift off length and soot emission under diesel-like conditions". In: *Fuel* 260.July 2019 (2020), p. 116377. DOI: 10.1016/j.fuel.2019.116377.

[9] Pastor, José V.; García-Oliver, José M.; Micó, Carlos; García-Carrero, Alba A.; and Gómez, Arantzazu. "Experimental study of the effect of hydrotreated vegetable oil and oxymethylene ethers on main spray and combustion characteristics under engine combustion network spray A conditions". In: *Applied Sciences (Switzerland)* 10.16 (2020). DOI: 10.3390/APP10165460.

[10] Benajes, Jesus; Payri, Raul; Bardi, Michele; and Martí-aldaraví, Pedro. "Experimental characterization of diesel ignition and lift-off length using a single-hole ECN injector". In: *Applied Thermal Engineering* 58.1-2 (2013), pp. 554–563. DOI: 10.1016/j.applthermaleng.2013.04.044.

[11] Higgins, Brian; and Siebers, Dennis L. "Measurement of the Flame Lift-Off Location on DI Diesel Sprays Using OH Chemiluminescence". In: *SAE Technical Paper 2001-01-0918* (2001).

[12] Lequien, Guillaume; Li, Zheming; Andersson, Oivind; and Richter, Mattias. "Lift-Off Length in an Optical Heavy-Duty Diesel Engine". In: *SAE International Journal of Engines* 8.5 (2015), pp. 2015–24–2442. DOI: 10.4271/2015-24-2442.

[13] Pickett, Lyle M; Kook, Sanghoon; Persson, Helena; and Andersson, Öivind. "Diesel fuel jet lift-off stabilization in the presence of laser-induced plasma ignition". In: *Proceedings of the Combustion Institute* 32 (2009), pp. 2793–2800. DOI: 10.1016/j.proci.2008.06.082.

[14] Persson, Helena; Andersson, Öivind; and Egnell, Rolf. "Fuel effects on flame lift-off under diesel conditions". In: *Combustion and Flame* 158.1 (2011), pp. 91–97. DOI: 10.1016/j.combustflame.2010.07.020.

[15] Chartier, Clément; Aronsson, Ulf; Andersson, Öivind; Egnell, Rolf; and Johansson, Bengt. "Influence of jet-jet interactions on the lift-off length in an optical heavy-duty di diesel engine". In: *Fuel* 112 (2013), pp. 311–318. DOI: 10.1016/j.fuel.2013.05.021.

[16] Musculus, Mark P.B. "Effects of the in-cylinder environment on diffusion flame lift-off in a di diesel engine". In: *SAE Technical Papers* 724 (2003). DOI: 10.4271/2003-01-0074.

[17] Siebers, Dennis L; and Higgins, Brian. "Flame Lift-Off on Direct-Injection Diesel Sprays Under Quiescent Conditions". In: *SAE Technical Paper 2001-01-0530* 724 (2001).

# Chapter 6

# Spray combustion and soot formation

## 6.1 Introduction

The following chapter contains the outcomes from the soot measurement campaign. These results represent the second and final experimental campaign under a reactive environment. The experiments were done in the optically accessible test rig and applying the Diffuse back-illumination (DBI) technique, as previously detailed in section 3.5.

First, the motivation behind extending the test matrix is detailed. Then, the optical thickness KL maps results are analyzed. Afterward, a comparison of the soot formation for all the inter-jet spacing configurations is made. Lastly, the main conclusions of the results are drawn.

## 6.2 Test plan

### 6.2.1 Optical setup considerations

As detailed in section 3.5, a novel window was fabricated to perform the diffuse back-illumination measurements. This window contained both the injector holder and the optical access, allowing the implementation of the DBI technique on multi-holes injectors.

Nevertheless, some considerations or limitations appeared as a trade-off to the complexity of the setup. In particular, the following restraints should be considered throughout the analysis of the results:

- **Field of view of the spray**. The injector and the optical window had to be mounted in the same piece, complying with the space available on the test rig. On the one hand, the injector holder needed a minimum spatial distance from the optical window. On the other hand, the optical access had to be small enough to fit in the test rig space available for the fabricated piece. These considerations resulted in the field of view of the spray starting at 30 mm and ending at 85 mm from the nozzle of the injector (Figure 6.1).

  Consequently, the influence of the boundary conditions on the soot formation could not be properly addressed on surroundings that promote faster premixed combustion near the nozzle (Figure 6.1), that is, the highest chamber temperature, density, and oxygen concentration conditions. Nevertheless, the field of view was large enough to capture most of the combustion event for the majority of the test points.

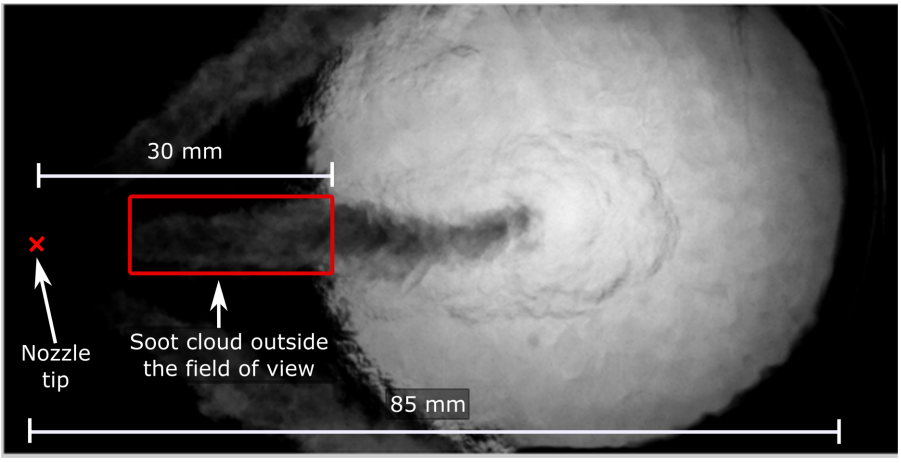


*Figure 6.1: Field of view of the spray*

- **Fixed optical setup**. It was necessary to maintain a constant optical setup to compare the KL results throughout the numerous boundary conditions. Thus, the LED intensity and the aperture of the camera diaphragm remained unaltered for the entire measurement campaign.

  Therefore, the illumination was set to properly cover as many boundary conditions as possible, accounting for the LED power trade-off. Specifically, the higher the LED light intensity, the greater the ability to

compute the soot in high-soot boundary conditions, but reducing the sensibility to capture the soot cloud in low-soot surroundings. On the other hand, the LED power capacity and the widest dynamic range the high-speed camera can capture limited the maximum light intensity that could be employed.

Additionally, the outlet orifices had small diameters ($<100\mu m$), which tend to produce less soot [1]. Then, for most cases the LED beams were strong enough to go through the soot cloud and to the camera, measuring the attenuation produced by the soot. From the attenuation and flame chemiluminescence, it was possible to compute the optical thickness KL of the spray through the Equation 3.13.

Figure 6.2 depicts the KL throughout the axis of one of the test points. It can be observed that the KL profile of the spray was always smaller than the maximum measurable KL (saturation KL).

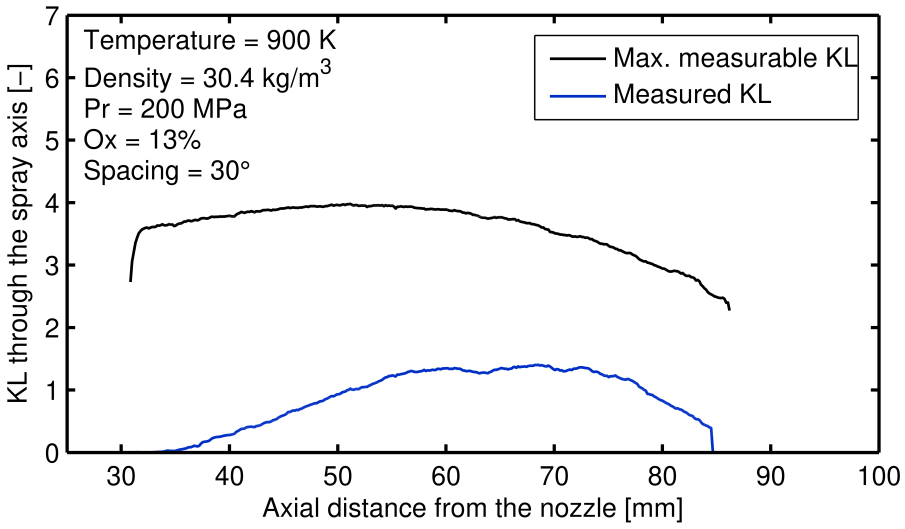


*Figure 6.2: KL without saturation*

Nevertheless, the available LED power was not always enough to work with the boundary conditions that had the highest-density soot clouds due to the phenomenon defined as KL saturation. This phenomenon occurs when the LED beams are not able to go through the soot cloud and to the camera [2]. Consequently, the only light that the camera captures comes from the natural luminosity of the spray, resulting in a constant light intensity both in the LED-on and LED-off frame.

In those cases, the LED light is completely attenuated, and it is not possible to compute the real KL of the spray. A KL saturation example is shown in Figure 6.3, and it is also diagnosed when the KL of the spray is equal to and capped by the maximum measurable KL (computed with Equation 3.14) during the combustion event, resulting in a distorted measured KL, which in reality would be higher.

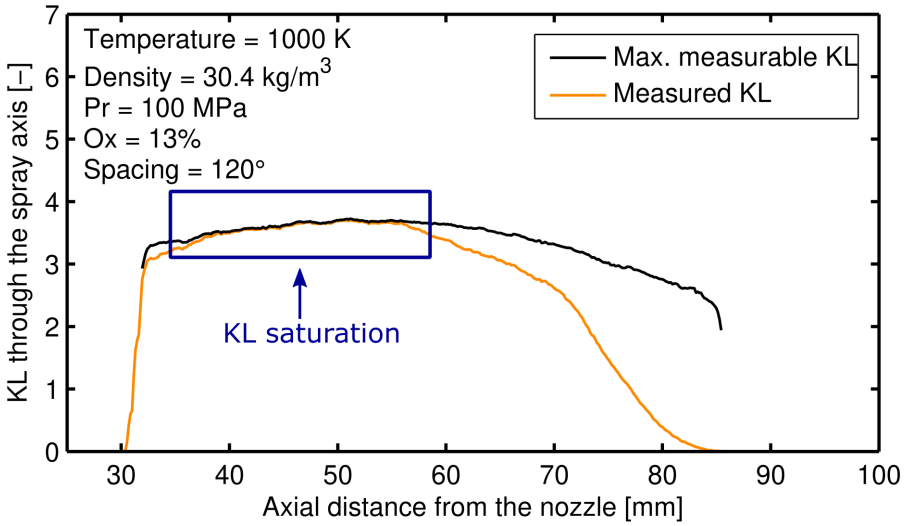


*Figure 6.3: KL with saturation*

### 6.2.2 Test matrix

As detailed in the previous section, the optical setup was appropriate for measuring KL and soot formation in most test points. Nevertheless, the physical constraint of the window, as well as the limited LED power capacity, were obstacles when analyzing all of the test points of the original test matrix. Therefore, the test matrix was extended to have enough data to assess the influence of the inter-jet spacing on soot formation properly.

In particular, an additional boundary condition was introduced: the oxygen concentration of the chamber air. This parameter is known to alter both the soot distribution and the amount of soot produced [3–6]. Moreover, this parameter will serve to simulate EGR conditions on the engine [7–9].

Specifically, the measurements were done at 13%, 17%, and 21% of oxygen concentration for each test point of the original test matrix, thus going from

27 to 81 boundary conditions tested. The test plan for this experimental campaign is presented in Table 6.1. A detailed explanation of the image processing methodology employed is available in subsection 3.6.6 and subsection 3.6.7.

*Table 6.1: Boundary conditions for the soot-DBI experiments.*

| **Parameter** | **Value** | **Units** |
|---|---|---|
| chamber temperature ($T$) | 800 - 900 - 1000 | K |
| chamber density ($\rho$) | 15.2 - 22.8 - 30.4 | $\mathrm{kg\,m^{-3}}$ |
| Rail pressure ($P_r$) | 100 - 150 - 200 | MPa |
| Oxygen concentration | 13 - 17 -21 | $\%_{\mathrm{vol}}$ |
| Fuel temperature | 363 | K |
| Injection frequency | 0.25 | Hz |
| Repetitions | 15 | - |

## 6.3 KL computation through diffused back-illumination

The following section depicts the optical thickness KL maps computed from the diffuse back-illumination measurements.

Regarding the soot formation, the chamber temperature is one of the parameters with the most significant influence on the soot produced [3, 10, 11]. Therefore, the KL results will be grouped in three sections: low temperature (800 K), intermediate temperature (900 K), and high temperature (1000 K). Within each temperature group, results are presented by increasing chamber density, constantly analyzing the influence of every boundary condition. The methodology employed to compute the flame soot in terms of the optical thickness KL was described in section 3.6.

On the other hand, throughout the measurements, the soot cloud location got closer to the nozzle as the oxygen concentration increased, altering the amount of soot inside the field of view. Consequently, no definite quantitative or qualitative assessment could be made on this parameter.

Nevertheless, altering the oxygen concentration served to obtain more test points inside the field of view. Specifically, the chamber density and temperature affected the ignition location as well, so changing the oxygen concentration worked to compensate for these effects and have more test points inside the field of view at every temperature and density.

Thus, each original test point will be presented at the oxygen concentration on which the ignition and soot had the greater development within the field of view, to improve readability. The KL maps for the remaining boundary conditions are available in Appendix A.

### 6.3.1 KL maps under low temperatures

The current section depicts the soot-DBI results under low temperatures. For low chamber density conditions (15.2 $kg/m^3$), none or negligible soot amounts (KL $< 20$) were observed, as depicted in Figure 6.4. However, a better assessment could be made once the chamber density is increased.

In this sense, Figure 6.5 depict the KL maps for the intermediate chamber density of 22.8 $kg/m^3$. Soot particles appeared on the field of view at these conditions, although these appearances were unstable due to the still poor combustion boundary conditions.

Nevertheless, it can be observed that no soot was observed with the isolated jet (Spacing = 120°). In contrast, some soot (although in small quantities) appeared on sprays with neighbor jets, especially under the 30° inter-jet spacing configuration.

Lastly, the results at the highest chamber density studied (30.4 $kg/m^3$) are presented in Figure 6.6. At this chamber density, the appearance of soot became more stable and noticeable.

Regarding the influence of the inter-jet spacing, it was observed that the sprays with the closest distance to their neighbor jets ((30° and 36°)) generally had a denser soot-cloud in terms of the optical thickness KL. However, this trend was not always noticeable since the combustion conditions were overall poor and unstable under the low temperature of 800 K. Therefore, broader conclusions will be made once the development under higher temperatures is analyzed.

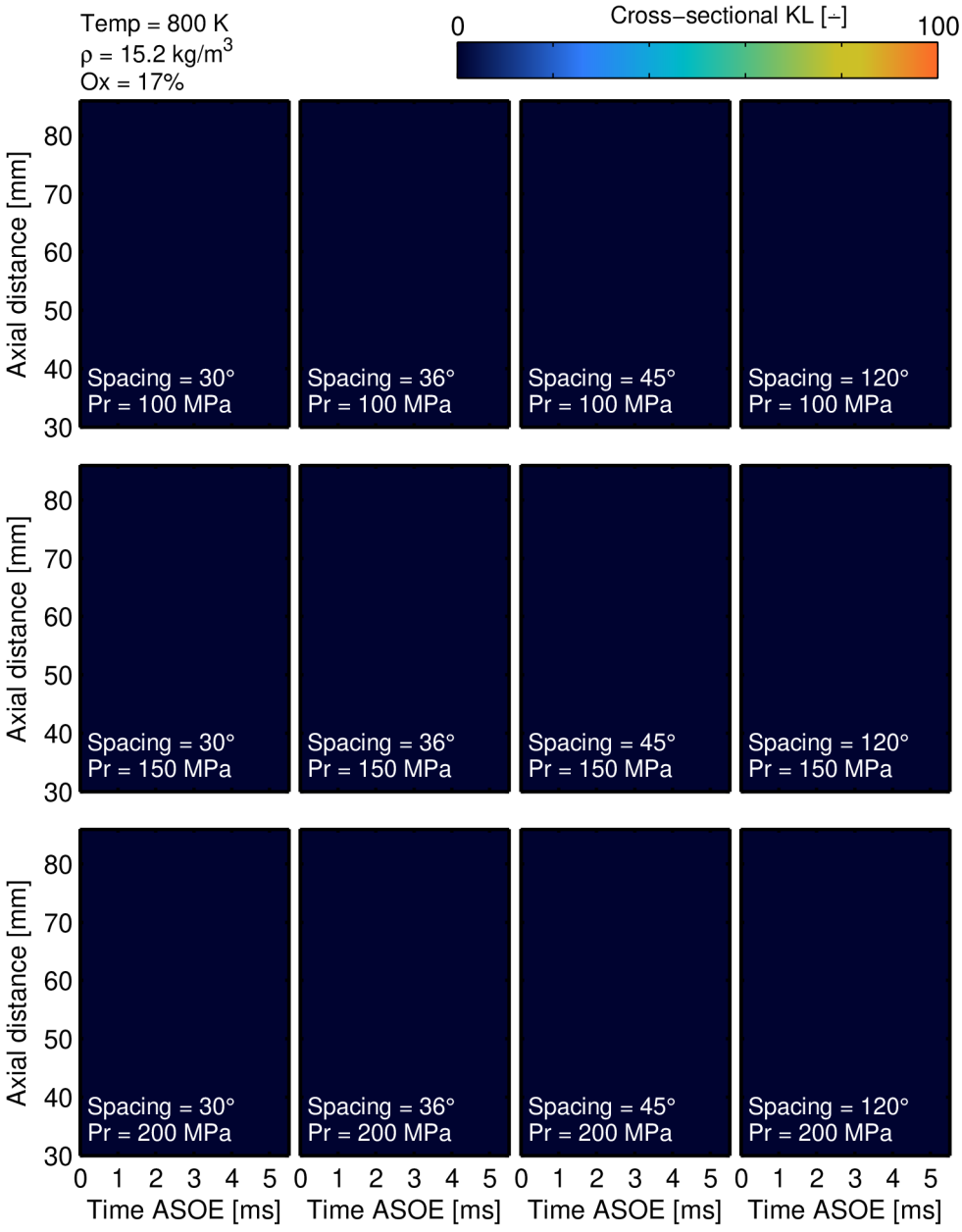


*Figure 6.4: KL maps for every inter-jet spacing configuration and injection pressure. chamber temperature = 800 K, chamber density = 15.2 kg/m$^3$, oxygen concentration = 17%.*

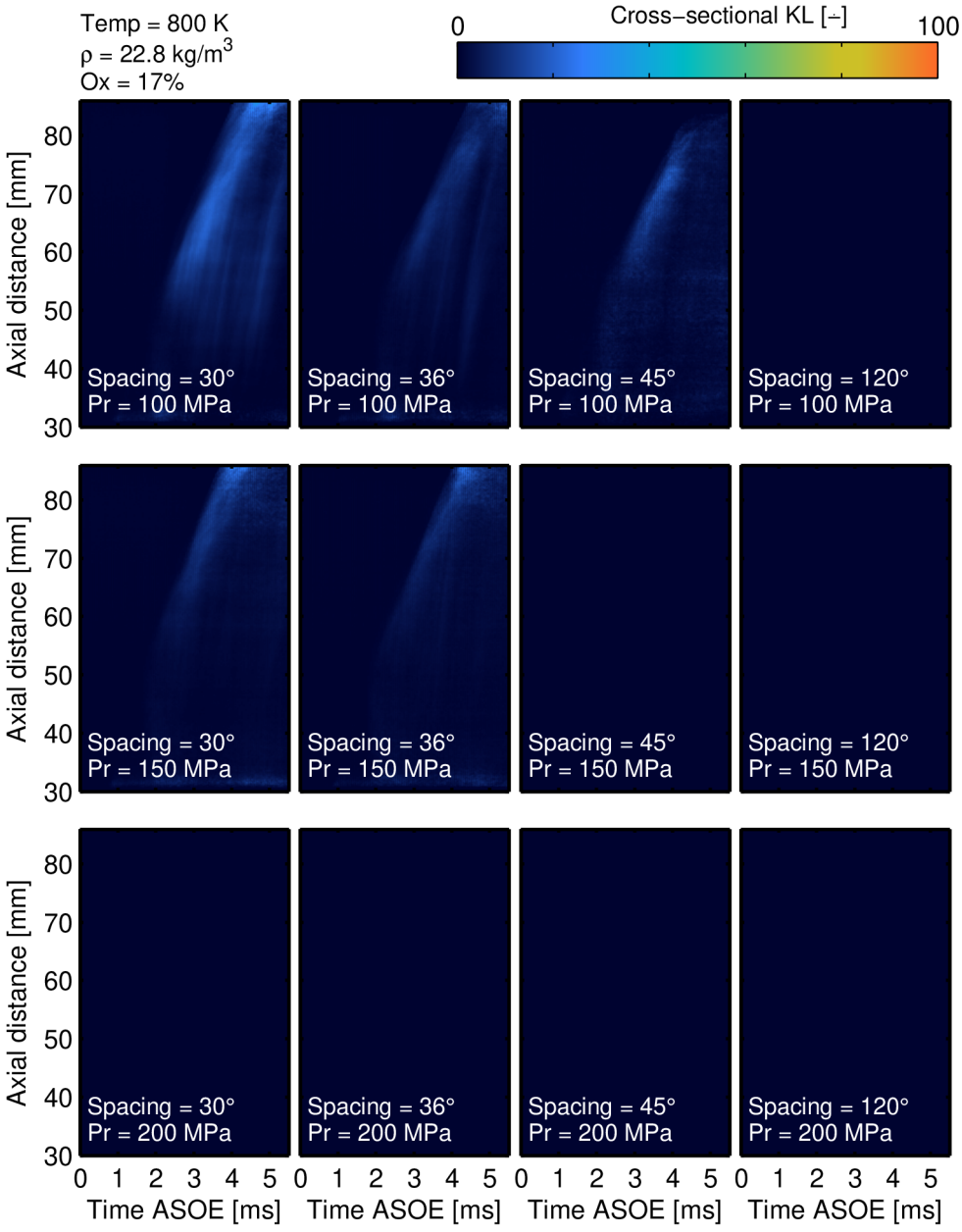


*Figure 6.5: KL maps for every inter-jet spacing configuration and injection pressure. chamber temperature = 800 K, chamber density = 22.8 kg/m$^3$, oxygen concentration = 17%.*

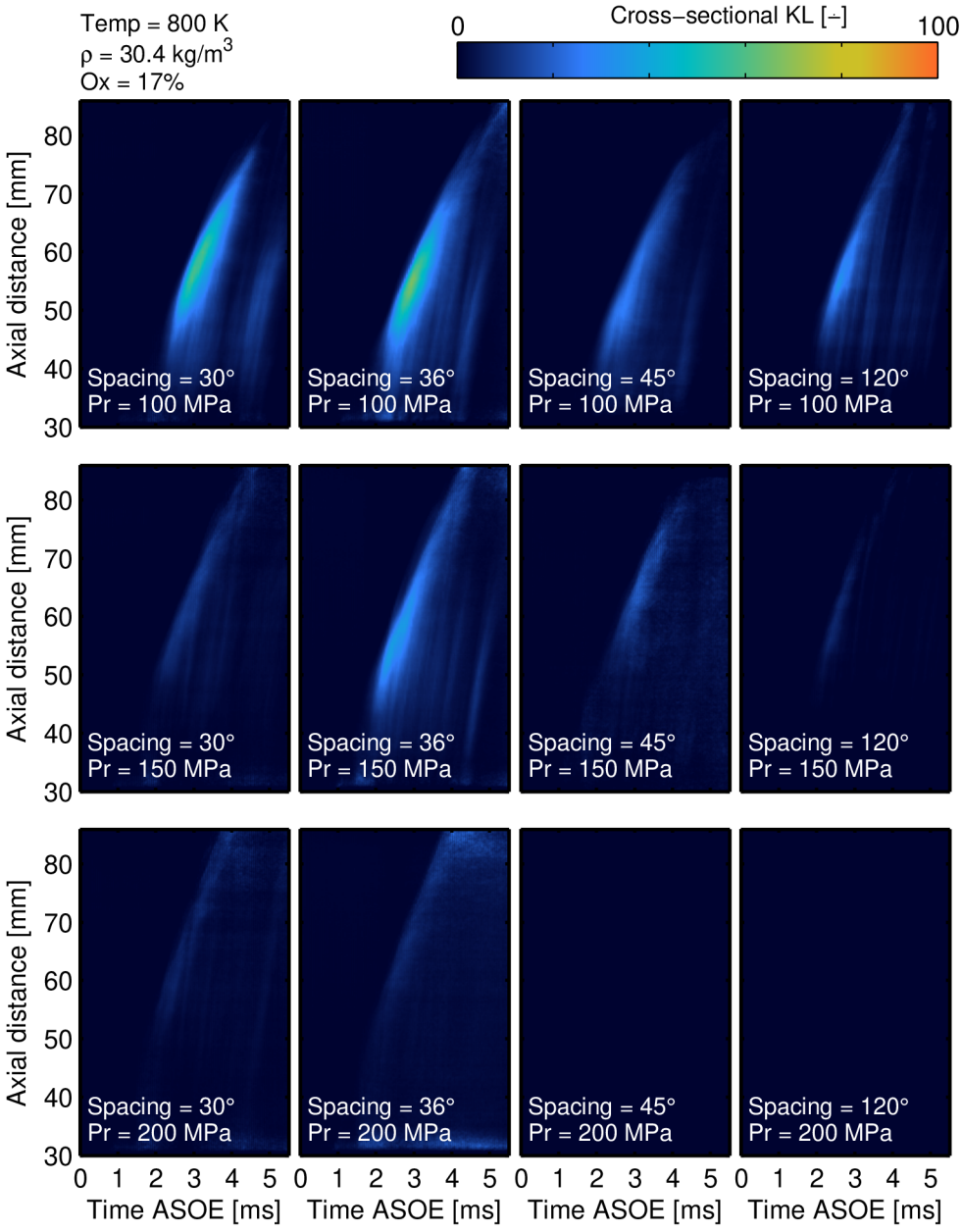


*Figure 6.6: KL maps for every inter-jet spacing configuration and injection pressure. chamber temperature = 800 K, chamber density = 30.4 kg/m$^3$, oxygen concentration = 17%.*

### 6.3.2 KL maps under intermediate temperatures

Once the chamber temperature was increased to 900 K, the considerable influence of this parameter on the soot formation readily appeared. Specifically, soot clouds were more stable and prominent with cross-sectional KL values in the range of 200-400, in contrast with the maximum 50-60 found at 800 K of chamber temperature. In this sense, increasing the chamber temperature shortens both ignition delay and lift-off length [12–16], as observed in section 5.3 and section 5.5, resulting in richer air-fuel mixture ratios near the lift-off area, which promotes the soot production [17–22].

Regarding the rail pressure, enlarging this parameter reduced the soot formation given that the fuel-air mixing rate [23, 24] is enhanced and the lift-off length enlarged [25], as observed in section 5.5. Thus, the combustion happens under leaner equivalence ratio conditions, partially inhibiting the soot formation.

On the chamber density, Figure 6.8 shows the optical thickness development for the intermediate chamber density (22.8 $kg/m^3$). Enlarging the chamber density resulted in cross-sectional KL values reaching magnitudes near 400, which reflects the direct influence of enlarging the chamber density on boosting the soot formation, following trends found in the literature [3, 11].

Regarding the inter-jet spacing, it is depicted that the configurations with the closest spacing between sprays generally had denser soot clouds, a pattern continuously observed to some extent throughout the measurements campaign. This trend is in line with the lift-off length results observed in chapter 5, in which the closely spaced jets had a shorter lift-off length. This shortening would lead to the combustion occurring under richer mixture conditions, suitable for soot formation.

Moreover, this contrast increased when lowering the rail pressure. Thus, the impact of the inter-jet spacing could be more significant under the poor atomization and mixing development inherent to low rail pressures.

Lastly, Figure 6.9 depicts the development of the spray under the highest chamber density condition employed and the oxygen concentration of 13% (Figure 6.9), in which the influence of the inter-jet spacing is depicted again. On the other hand, the combustion under 17% and 21% of oxygen concentration (Figure A.7 and Figure A.8 of Appendix A) typically started closer to the nozzle of the injector and outside the field of view. Consequently, the influence (if any) of the inter-jet spacing at the highest density could not be adequately addressed under these concentrations.

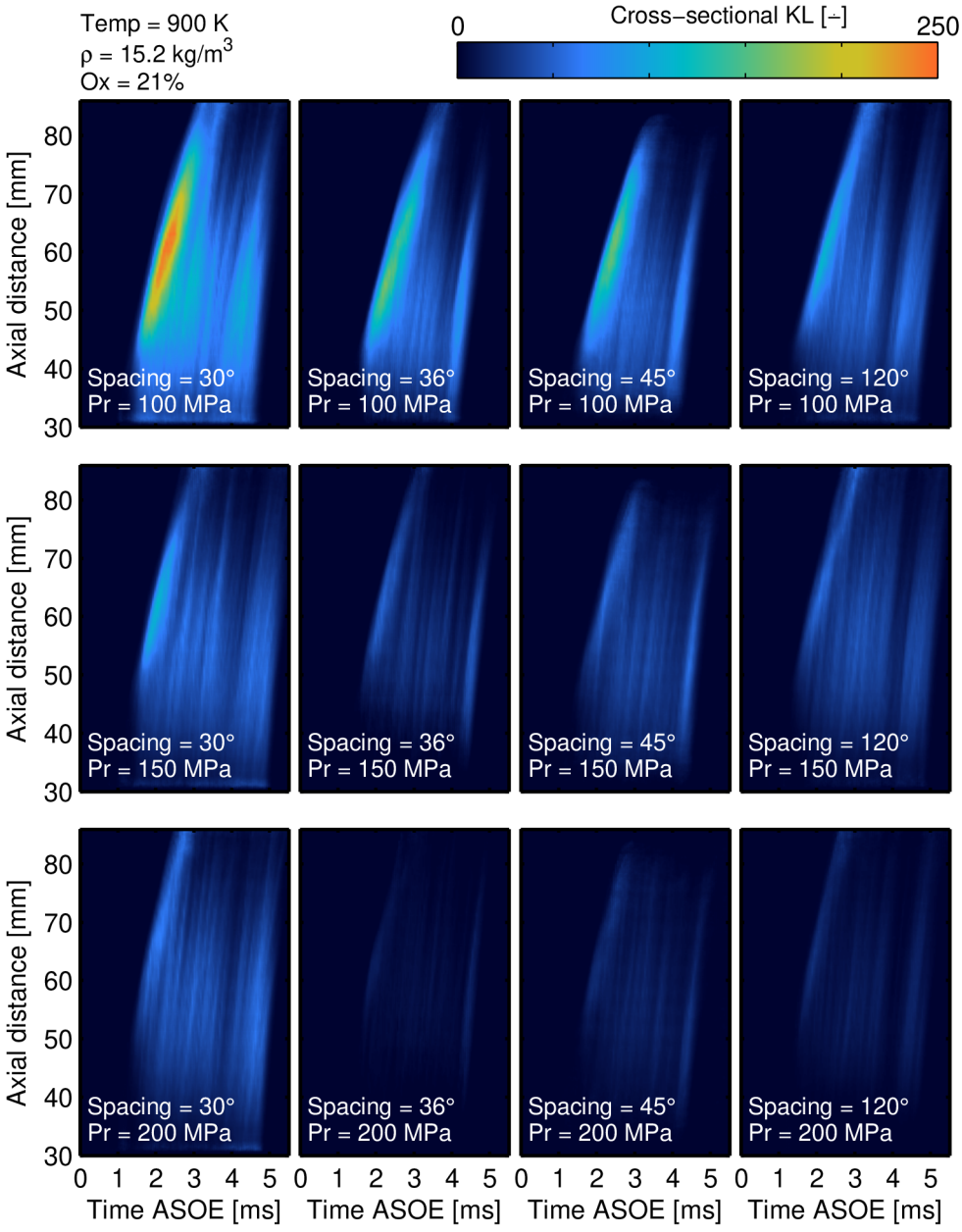


*Figure 6.7: KL maps for every inter-jet spacing configuration and injection pressure. chamber temperature = 900 K, chamber density = 15.2 kg/m$^3$, oxygen concentration = 21%.*

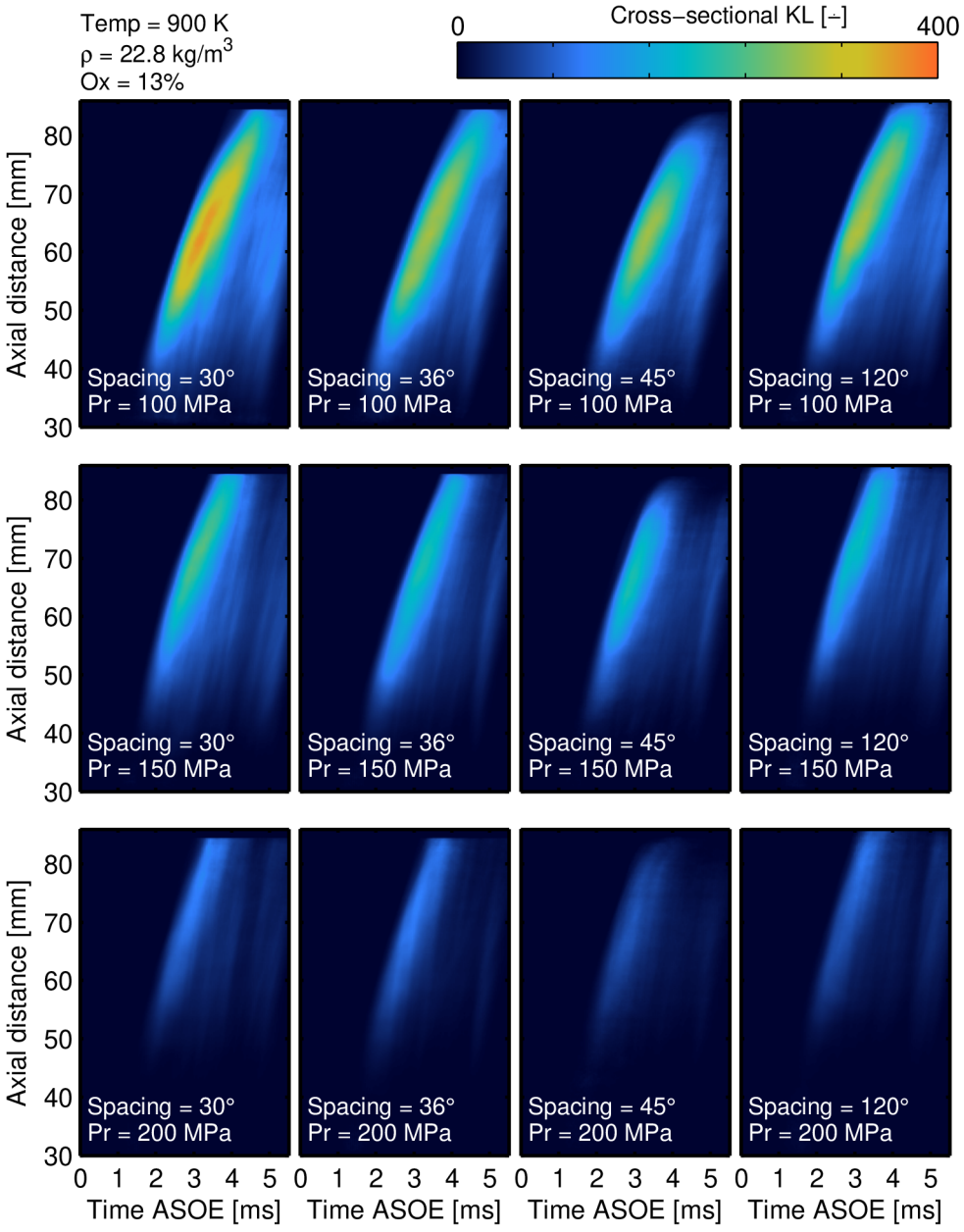


*Figure 6.8: KL maps for every inter-jet spacing configuration and injection pressure. chamber temperature = 900 K, chamber density = 22.8 kg/m$^3$, oxygen concentration = 13%.*

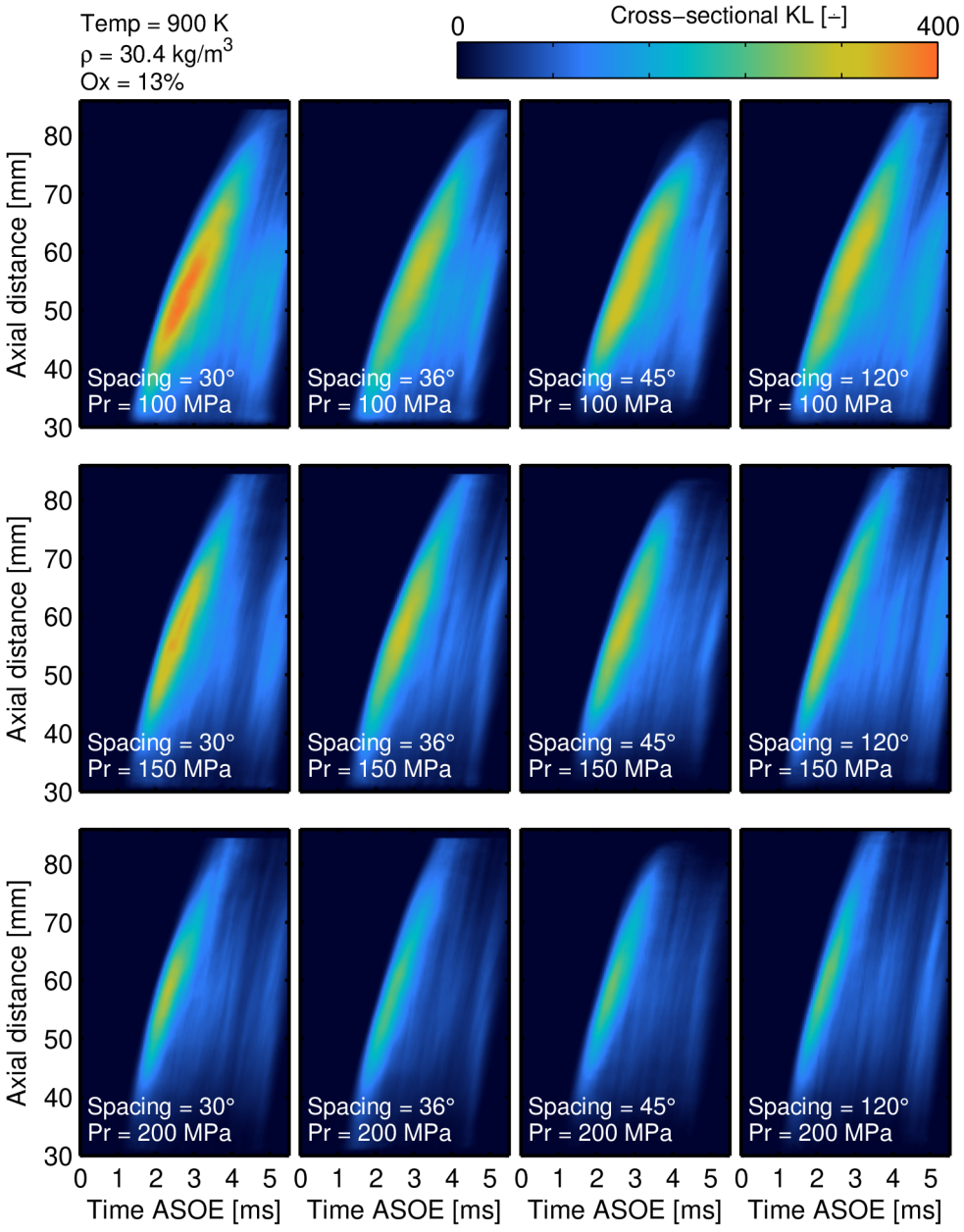


*Figure 6.9: KL maps for every inter-jet spacing configuration and injection pressure. chamber temperature = 900 K, chamber density = 30.4 kg/m$^3$, oxygen concentration = 13%.*

### 6.3.3 KL maps under high temperatures

The current section depicts the soot-DBI results under the high temperature of 1000 K.

Accordingly, the direct influence of the chamber temperature on the soot formation emerged again with the appearance of the densest soot clouds of the test campaign. Moreover, various test points could not be analyzed due to KL saturation, the previously detailed phenomenon.

In particular, most of the saturated test points appeared under the oxygen concentration of 13% as more spray appeared within the field of view. Additionally, the reduction of oxygen availability could result in denser soot clouds, as the oxidation process is inhibited [3, 10]. Due to the KL saturation occurring at 13%, KL maps at 17% are also presented.

Specifically, these phenomena can be observed under the low chamber density conditions depicted in Figure 6.10 and Figure 6.11. In Figure 6.10, it is seen that KL saturation appeared on the sprays with neighbor jets, whereas the soot map of the isolated spray could be measured, which could indicate that less soot was produced under these conditions. Nevertheless, Figure 6.11 depicts that the influence of inter-jet spacing on soot formation was less predominant under 1000 K of chamber temperature, in comparison with the previous values studied.

Plausibly, the influence of the high chamber temperature could overall be overcoming the local effect that the interaction between the sprays can have. Nonetheless, the sprays with closely spaced neighbor jets still showed slightly higher soot formation in numerous cases.

Similar trends were observed for the intermediate chamber density, as seen in Figure 6.12 and Figure 6.13.

Under the highest chamber density (30.4 $kg/m^3$), at 13% of oxygen concentration, every test point suffered from KL saturation. On the other hand, at 17% and 21%, the sprays mostly ignited and developed before entering the field of view, as seen, for instance, in Figure 6.14. As detailed in subsection 6.3.2, the limited optical access prevented from depicting any differences near the nozzle of the injector.

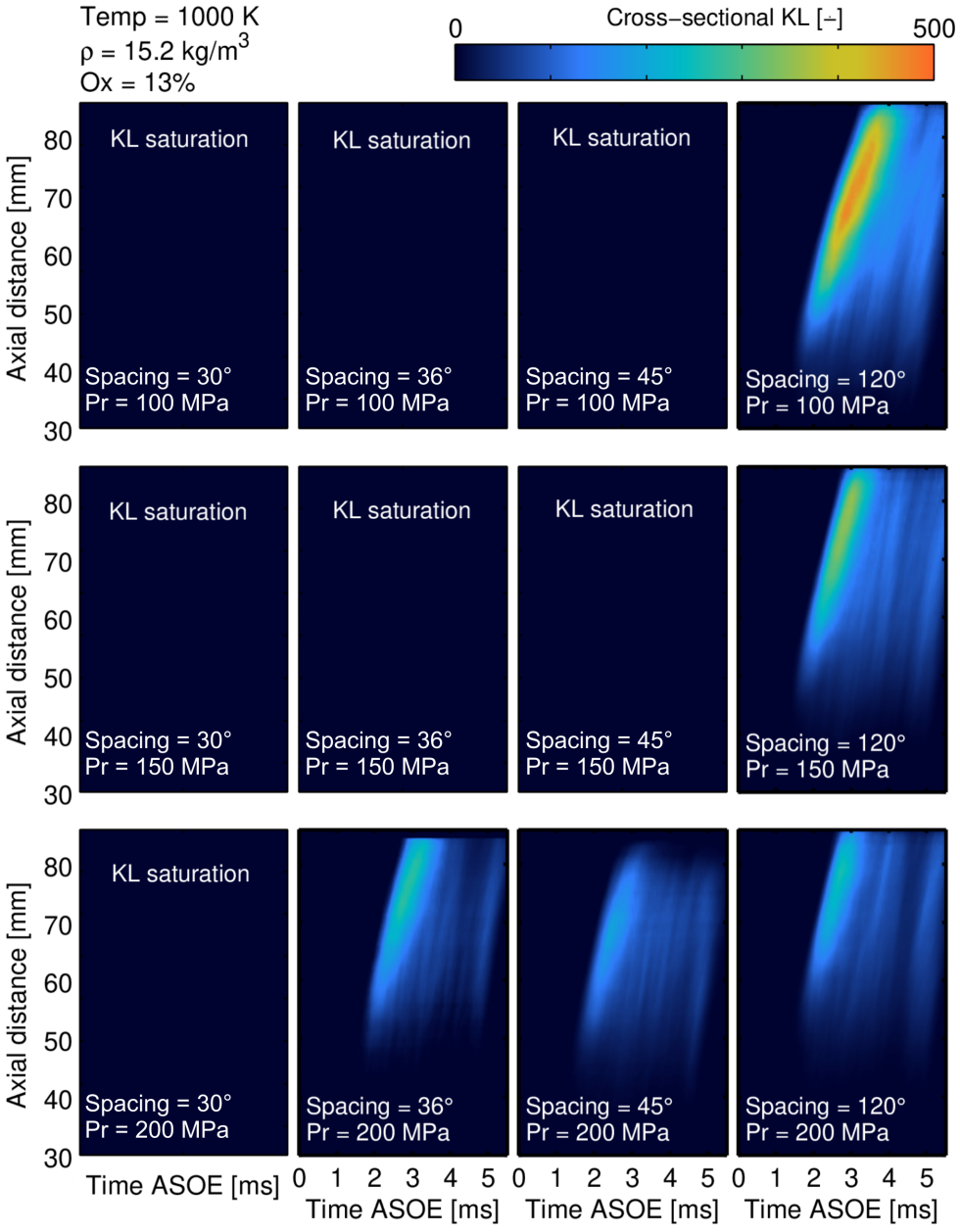


*Figure 6.10: KL maps for every inter-jet spacing configuration and injection pressure. chamber temperature = 1000 K, chamber density = 15.2 kg/m$^3$, oxygen concentration = 13%.*

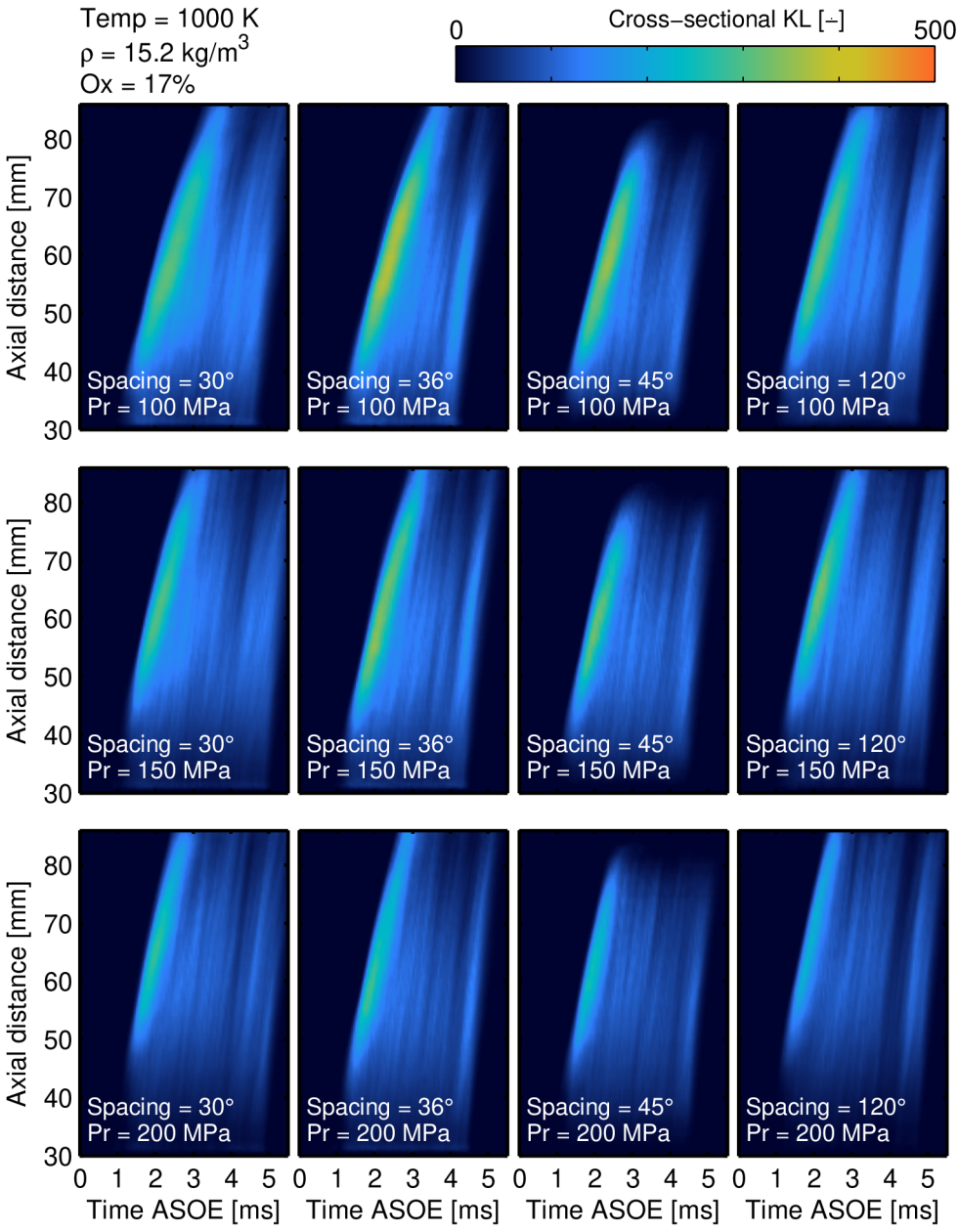


*Figure 6.11: KL maps for every inter-jet spacing configuration and injection pressure. chamber temperature = 1000 K, chamber density = 15.2 kg/m$^3$, oxygen concentration = 17%.*

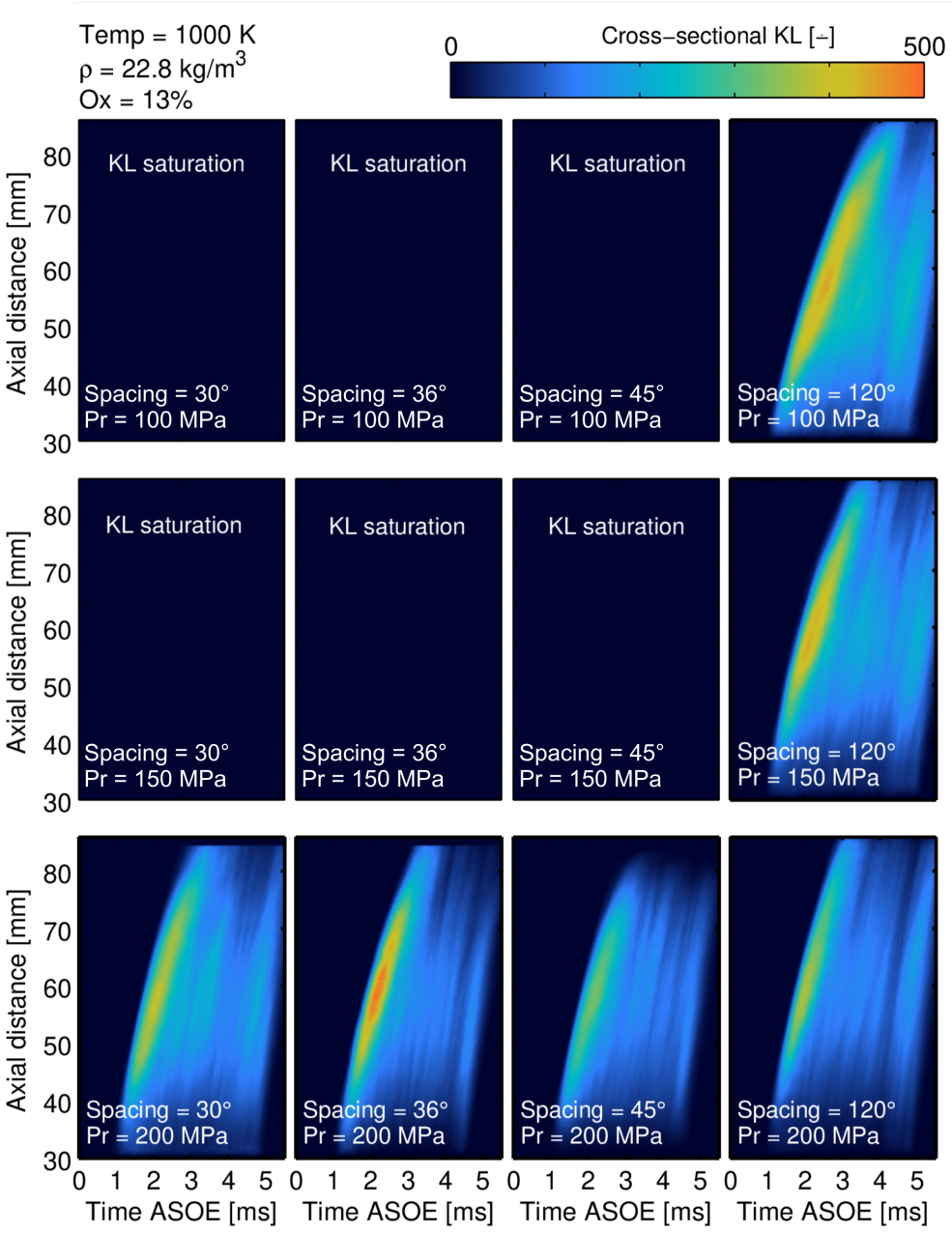


*Figure 6.12: KL maps for every inter-jet spacing configuration and injection pressure. chamber temperature = 1000 K, chamber density = 22.8 kg/m$^3$, oxygen concentration = 13%.*

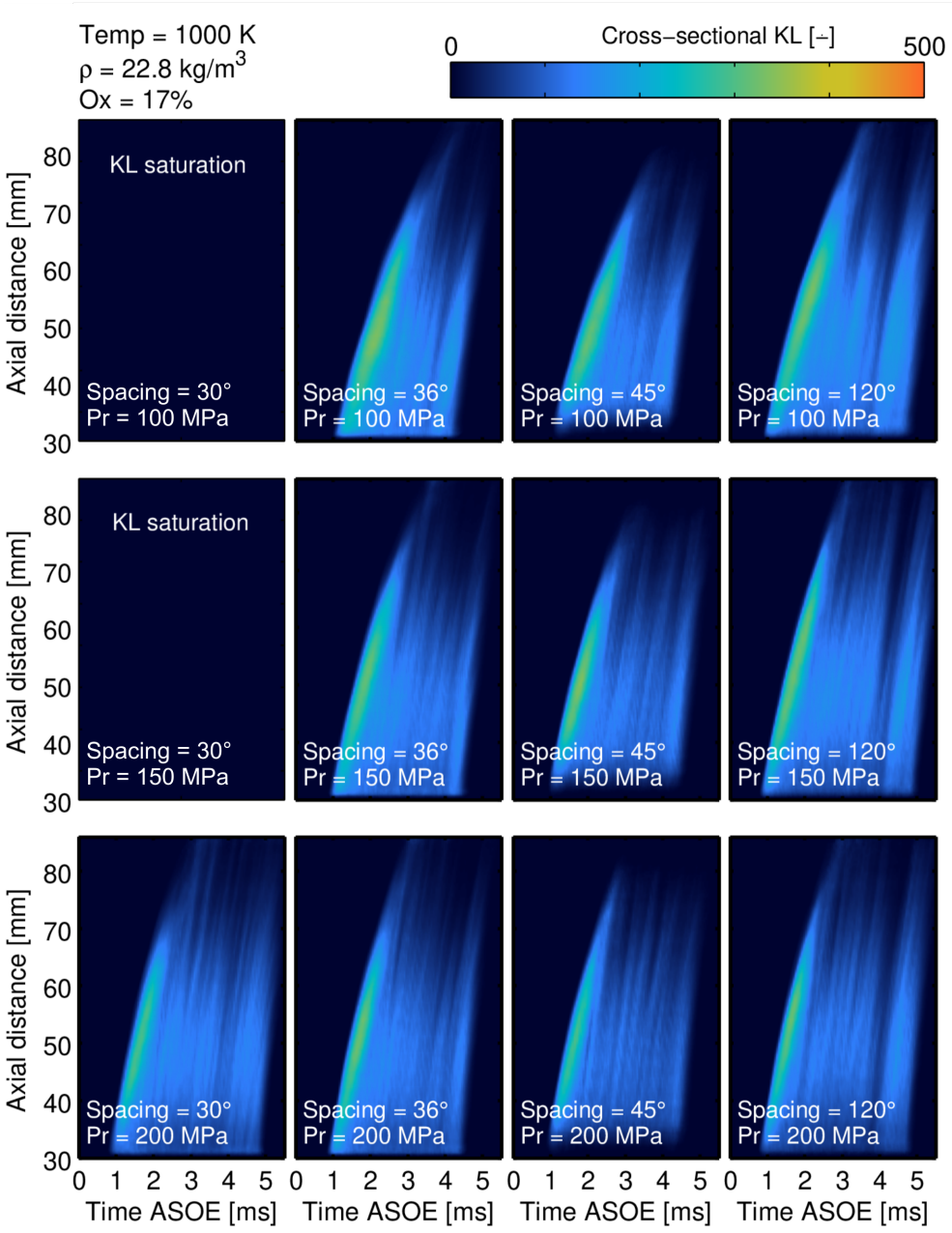


*Figure 6.13: KL maps for every inter-jet spacing configuration and injection pressure. chamber temperature = 1000 K, chamber density = 22.8 kg/m$^3$, oxygen concentration = 17%.*

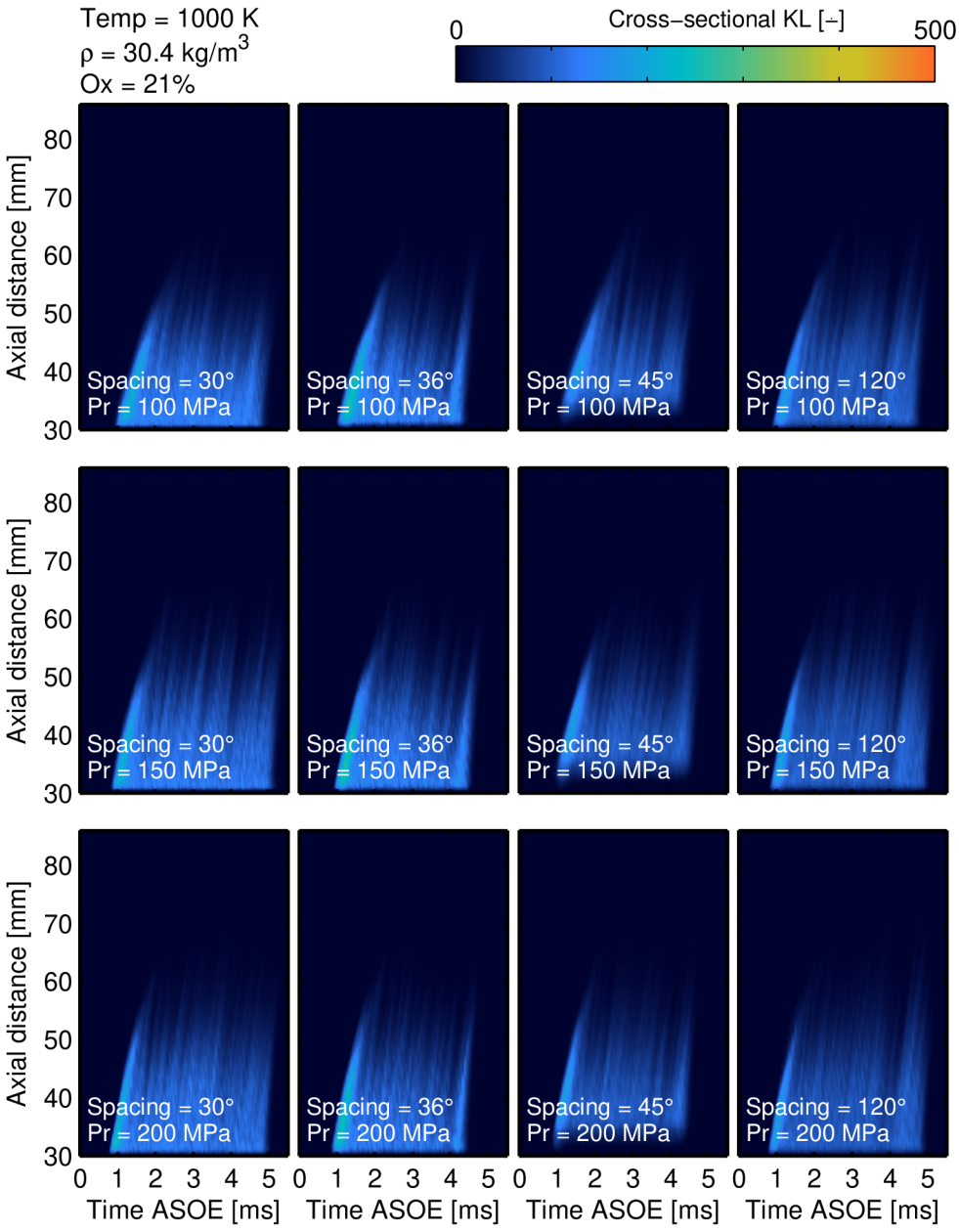


*Figure 6.14: KL maps for every inter-jet spacing configuration and injection pressure. chamber temperature = 1000 K, chamber density = 30.4 kg/m$^3$, oxygen concentration = 21%.*

## 6.4 Soot formation

The following section explores the soot mass computed from the optical thickness KL of the spray within the field of view of the window. As detailed in section section 3.6, each curve was computed from its corresponding KL map, aggregating the KL at each time-step and applying equation Equation 3.19.

In this sense, Figure 6.15 to Figure 6.21 depict the soot mass obtained within the optical access for every boundary condition except those in which KL saturation occurred. Additionally, the shade throughout each curve represents the 95% confidence interval of that test point.

Although the computation methodology presents some constraints (detailed in subsection 3.6.7), these figures serve as a complement to the results observed in section 6.3, as they provide a comparison for every inter-jet spacing on a given boundary condition, but in the same plot. Then, a clearer assessment of the observed trends can be made.

At 800 K of chamber temperature (Figure 6.15 to Figure 6.17), the sprays with closest neighbor jets typically formed more soot than the isolated spray. Moreover, the soot only appeared within sprays with neighbor jets in some boundary conditions. Nevertheless, the soot formation was unstable from cycle to cycle, reflected on the wider confidence interval compared to higher-temperature test points. Lastly, the temporal soot formation was low, with values consistently below 30 $\mu$g and many test points without any soot observance.

On the other hand, parametric variations of the boundary conditions depicted similar influences on the soot formation to those observed during the KL maps analysis (section 6.3) and in the literature [3–5, 10, 11]. When the temperature was set to 900 K (Figure 6.18 to Figure 6.20), the soot formation notably increased (y-axis limit expanded from 100 to 250). Furthermore, increasing the rail pressure reduced the soot formation. Also, higher chamber densities increased the soot appearance, although this trend was not always noticeable at 30.4 $kg/m^3$ since the sprays typically ignited before entering the field of view. A similar limitation appeared when increasing the oxygen concentration.

Regarding the inter-jet spacing, the sprays with an inter-jet spacing of 30° and 36° frequently produced more soot than the others. Furthermore, the jet with a spacing of 45° reported an intermediate behavior, with its soot production typically more similar to that of the isolated spray. On the other hand, it can also be observed that the influence of the inter-jet spacing generally

decreased as the air/fuel mixing conditions were enhanced, that is, as the chamber density and injection pressure increased.

Lastly, Figure 6.21 presents the soot formation at 1000 K of chamber temperature on the test points on which, for every inter-jet spacing configuration, no KL saturation occurred and had the soot formation mostly happening within the field of view. It is noted again that sprays with an inter-jet spacing of 30° and 36° still generally had higher peak values of soot produced.

On the other hand, the impact of the inter-jet spacing was smaller as the boundary conditions promoting soot appearance were enhanced, that is, increasing the chamber density, temperature, or decreasing the rail pressure. Plausibly, the influence of these parameters on the soot formation could be overcoming the local effects of the interaction between the sprays.

Nevertheless, the plots presented in this section showed a trend also depicted on the optical thickness KL maps. Overall, the sprays with neighbor jets tended to produce more soot for a given boundary condition when compared to the development of the isolated spray (spacing = 120°). Specifically, the sprays with an inter-jet spacing of 30° and 36° frequently produced the denser optical thickness and, consequently, the highest peak in soot production.

These trends align with the shorter lift-off length observed in closely spaced jets (section 5.5). Specifically, the shortening of the LOL reduces the space available for the air/fuel mixing process to develop. Consequently, the combustion could occur under higher equivalence ratio conditions, increasing the soot formation [17–22].

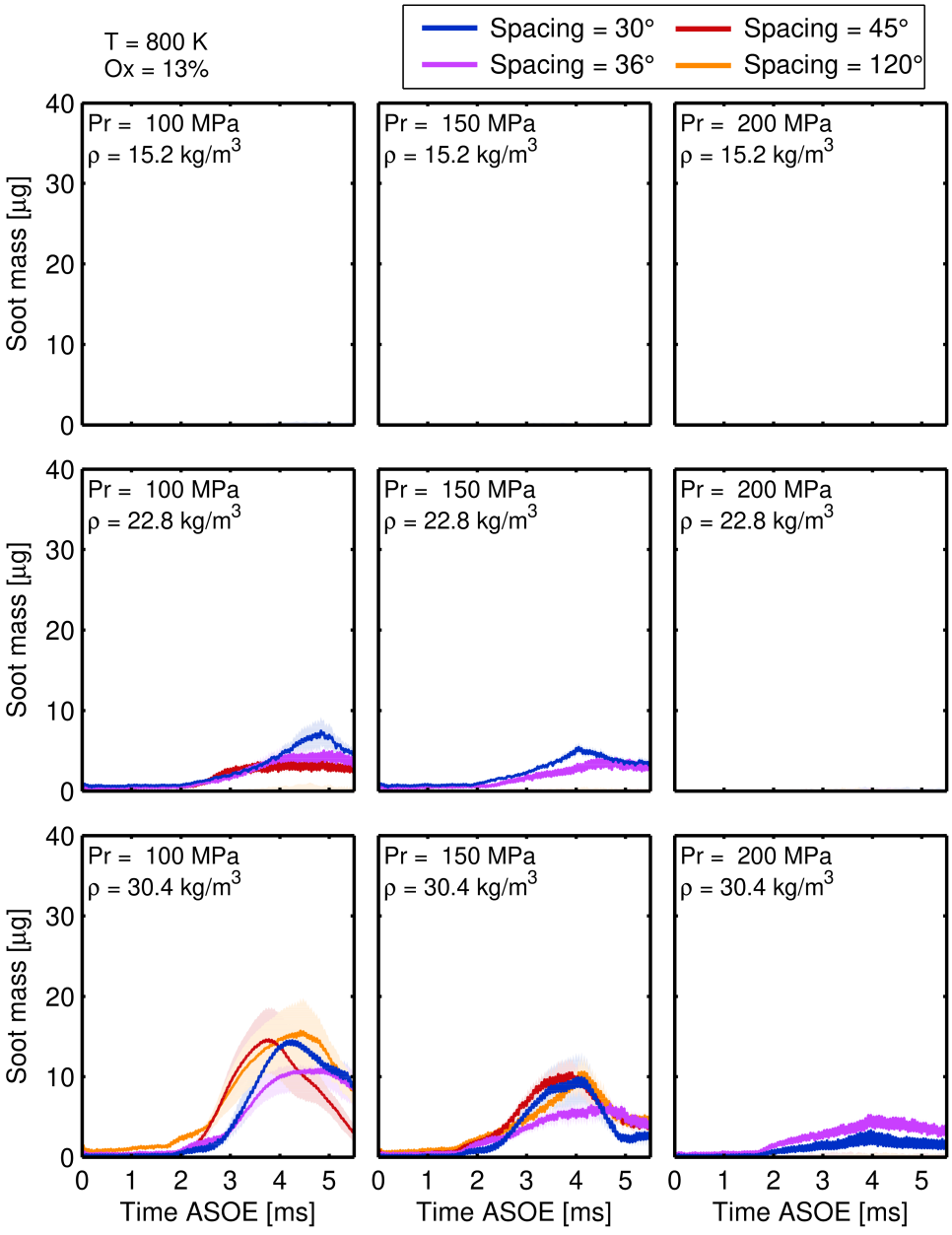


*Figure 6.15: Temporal evolution of the soot mass captured through the optical access for every inter-jet spacing configuration, injection pressure, and chamber density. chamber temperature = 800 K, oxygen concentration = 13%.*

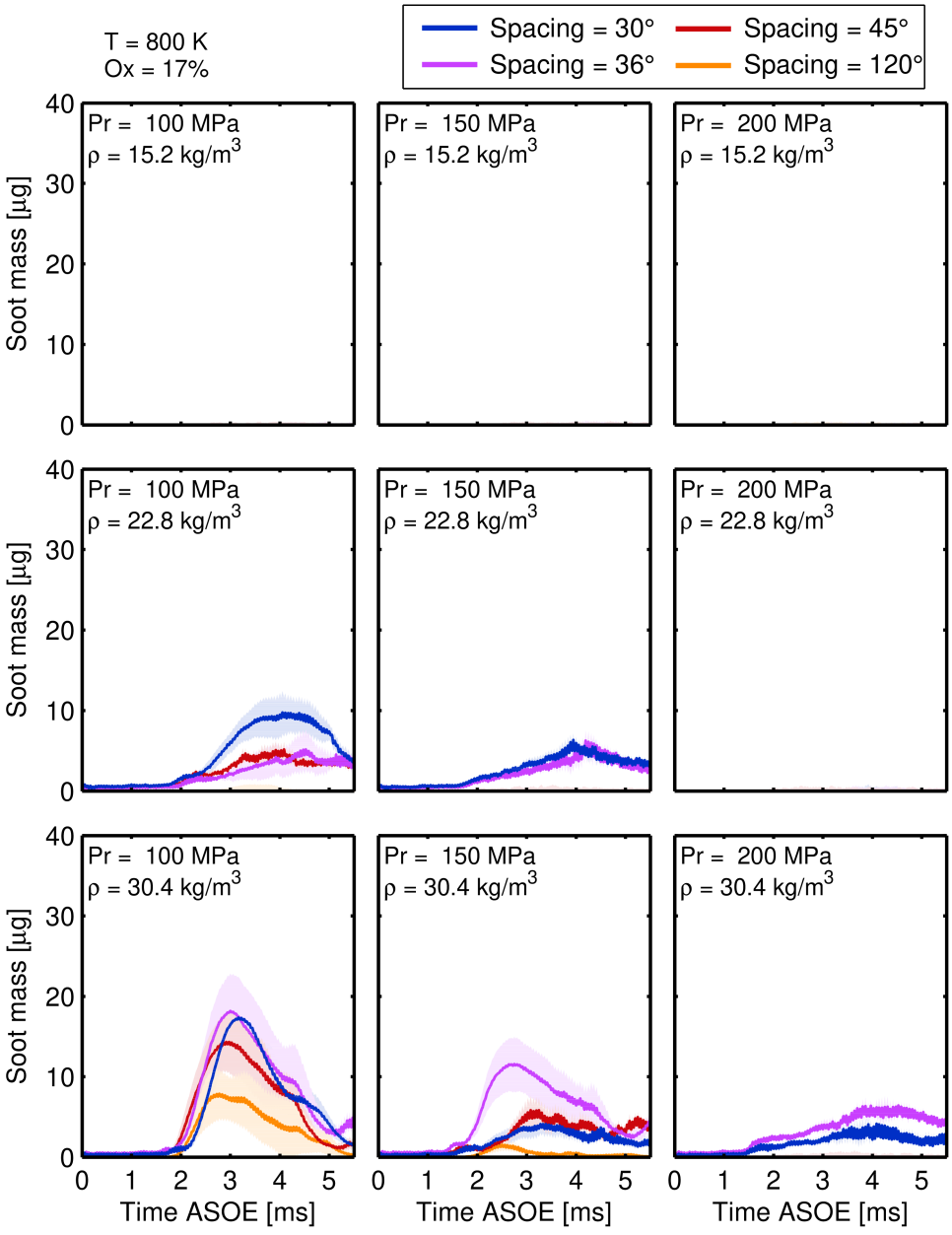


*Figure 6.16: Temporal evolution of the soot mass captured through the optical access for every inter-jet spacing configuration, injection pressure, and chamber density. chamber temperature = 800 K, oxygen concentration = 17%.*

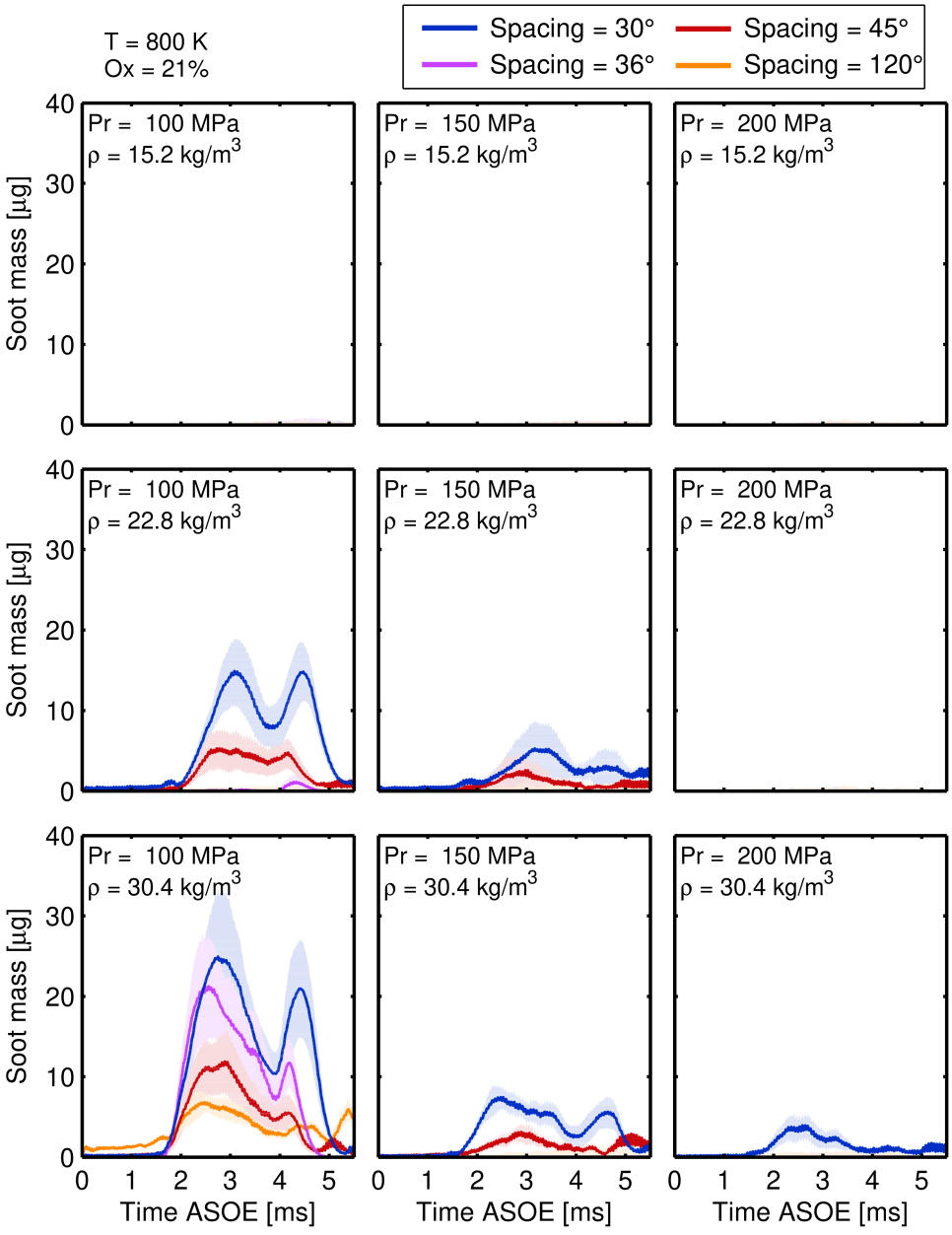


*Figure 6.17: Temporal evolution of the soot mass captured through the optical access for every inter-jet spacing configuration, injection pressure, and chamber density. chamber temperature = 800 K, oxygen concentration = 21%.*

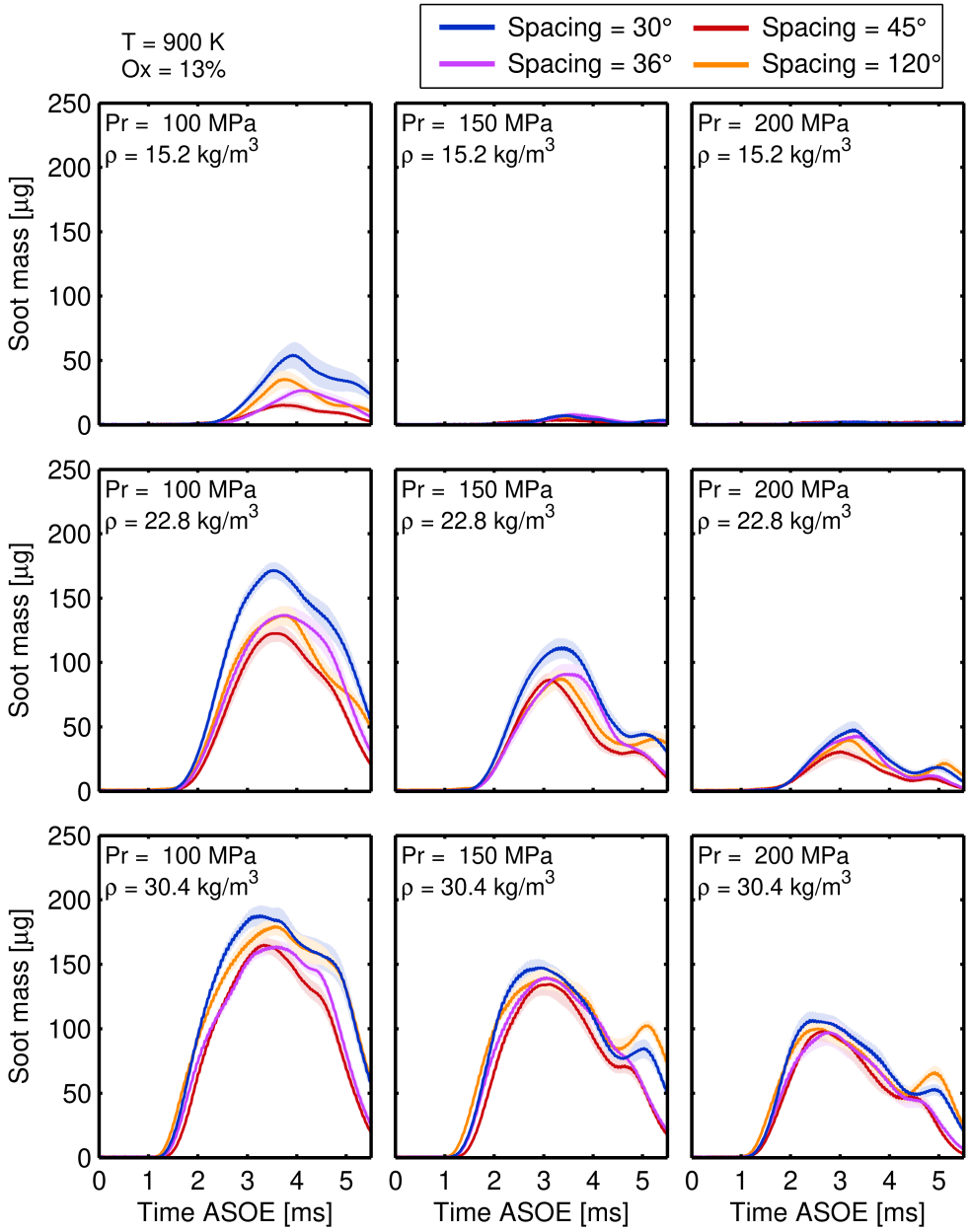


*Figure 6.18: Temporal evolution of the soot mass captured through the optical access for every inter-jet spacing configuration, injection pressure, and chamber density. chamber temperature = 900 K, oxygen concentration = 13%.*

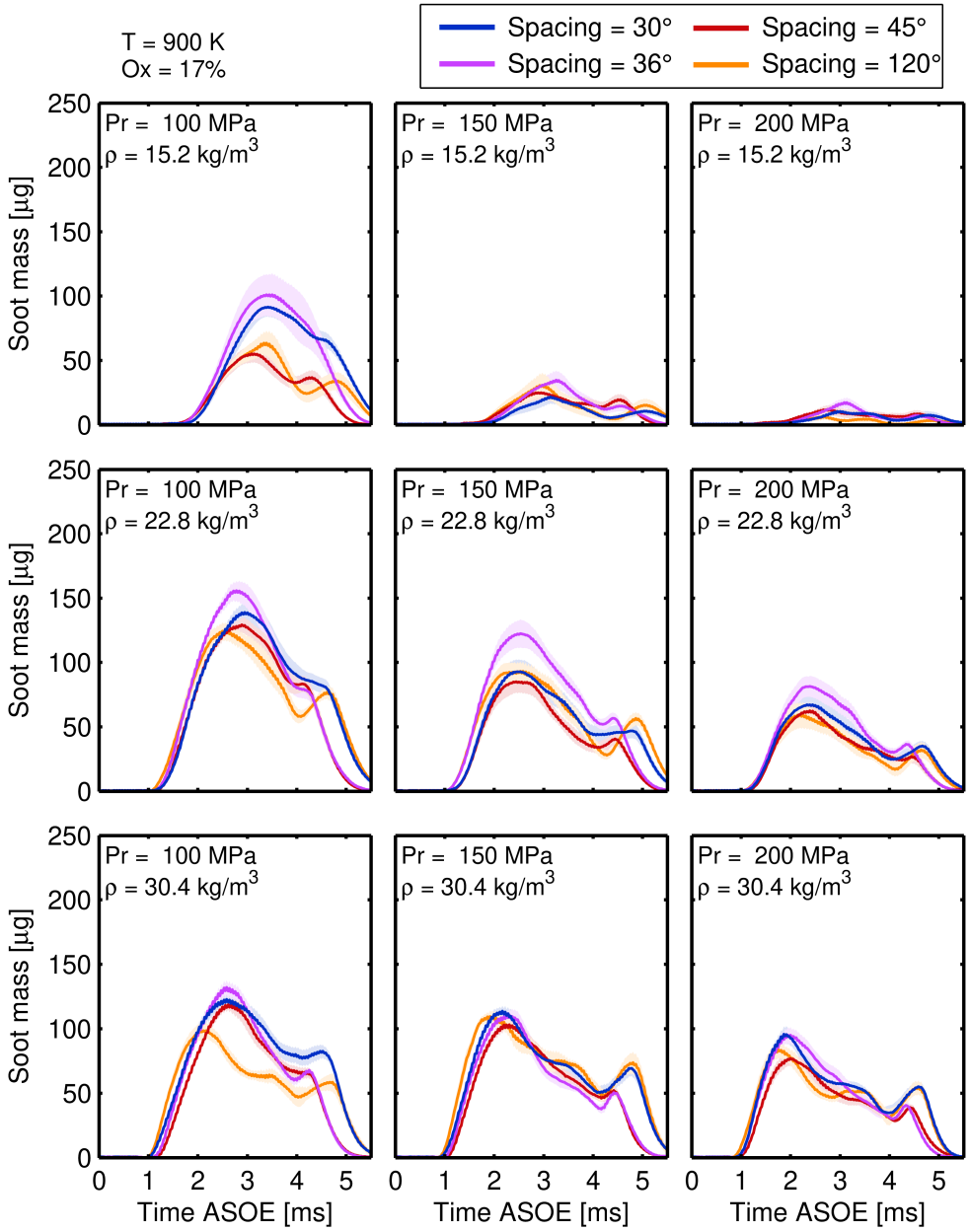


*Figure 6.19: Temporal evolution of the soot mass captured through the optical access for every inter-jet spacing configuration, injection pressure, and chamber density. chamber temperature = 900 K, oxygen concentration = 17%.*

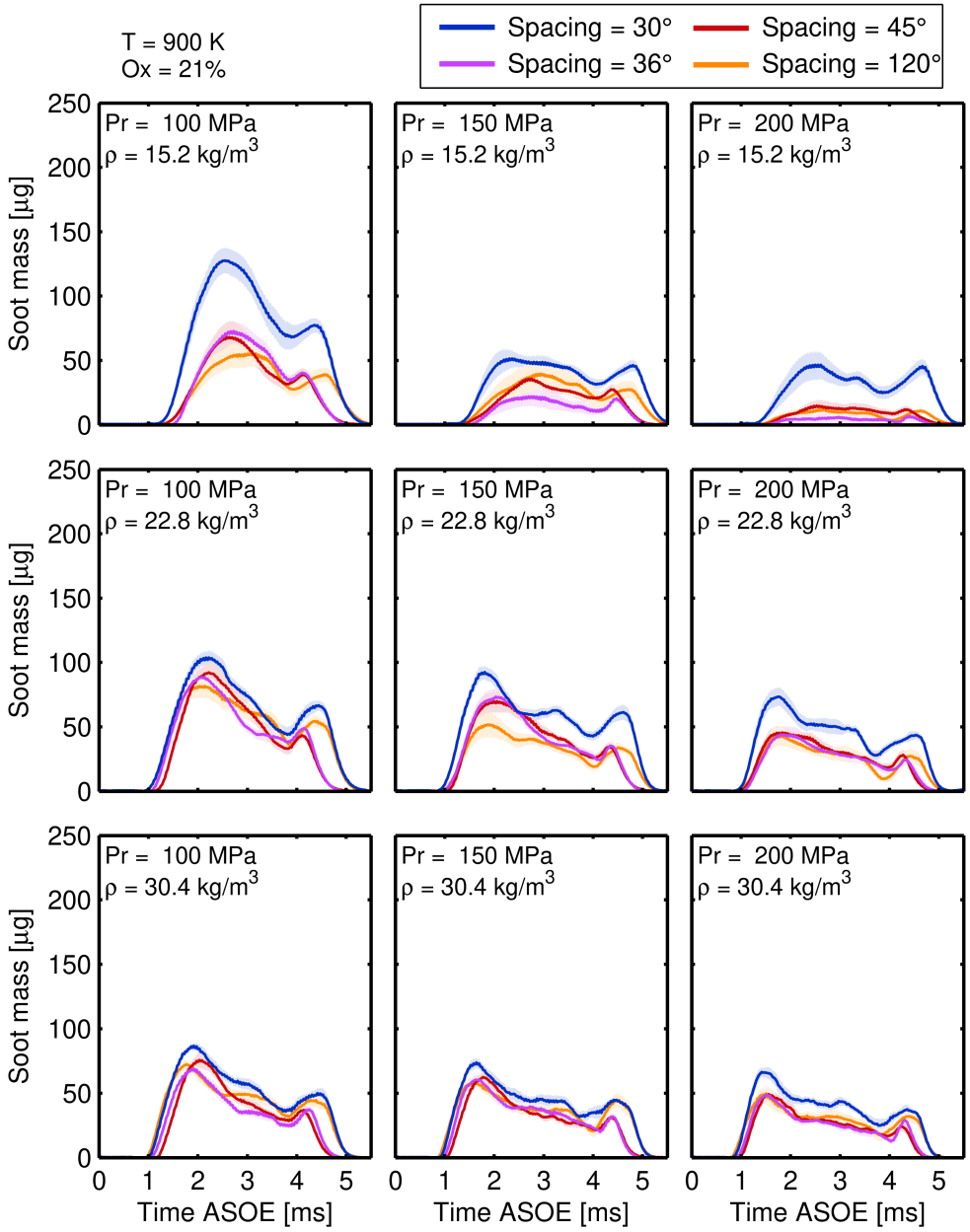


*Figure 6.20: Temporal evolution of the soot mass captured through the optical access for every inter-jet spacing configuration, injection pressure, and chamber density. chamber temperature = 900 K, oxygen concentration = 21%.*

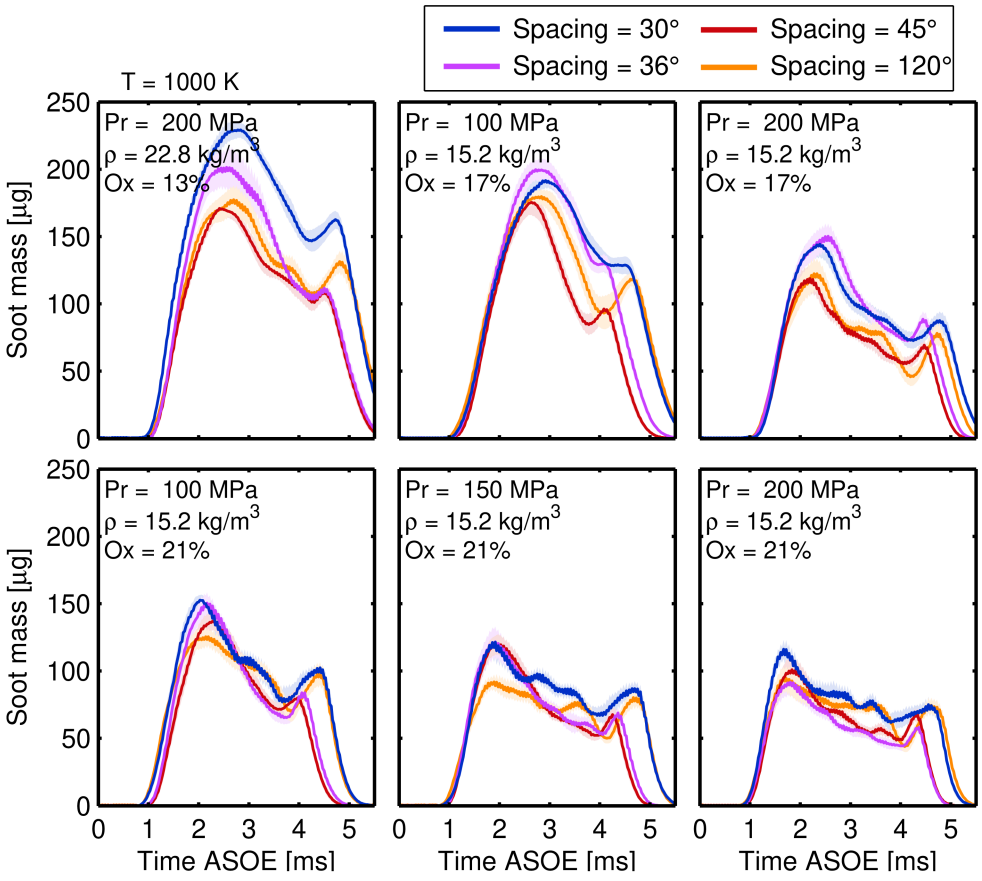


*Figure 6.21: Temporal evolution of the soot mass for the test points on which every inter-jet spacing configuration could be properly measured at an chamber temperature of 1000 K.*

## 6.5 Summary and conclusions

The present chapter discusses the results of the spray performance and soot formation for multiple inter-jet spacing configurations in reactive conditions. The experiments were done in a high-pressure and high-temperature test rig with optical access. The optical alignment consisted of a diffused back-illumination to compute the optical thickness KL of the spray, a direct indicator of the soot production.

To do so, a novel optical window was fabricated to apply the diffused back-illumination technique (DBI) on multi-hole injectors. Nevertheless, the field of view was restrained and started at 30 mm from the nozzle of the injector and ended at 85 mm from it. Lastly, the soot mass observed within the field of view was computed by aggregating the KL at each time-step and applying Equation 3.19. Therefore, the oxygen concentration parameter was added to the test matrix to increase the test points and spray information obtained through the optical access.

From the results, the following conclusions were drawn:

- In general terms, the sprays with closely spaced neighbor jets (30° and 36°) had higher optical thickness KL and peak soot mass values for a given boundary condition when compared to the development of the isolated spray (spacing = 120°).
- These trends are in line with the lift-off length results observed in the previous chapter, in which the closely spaced jets had a shorter lift-off length due to (plausibly) hot gases re-entrainment. This shortening would deteriorate the air/fuel mixing before the onset combustion and, consequently, a richer mixture is ignited, suitable for soot appearance.
- On the other hand, the impact of the inter-jet spacing was smaller as the boundary conditions promoting soot formation were enhanced, that is, increasing the ambient density, ambient temperature, or reducing the rail pressure. Plausibly, the influence of these parameters on the soot formation could be overcoming the local effects occurring between the sprays.
- The novel optical window served to analyze the soot development for multi-hole injectors. Nevertheless, the field of view limitations prevented from observing the spray development near the nozzle. Consequently, the influence of the inter-jet spacing could not be properly addressed when the ignition occurred before the spray entered the field of view.
- Nonetheless, a wide test matrix was employed, collecting data on the boundary conditions at which the spray develops within the field of view. This information could help select an efficient test matrix in future works, saving time and additional expenses from experimental measurements.

- Additionally, the influence of the remaining boundary conditions on the soot formation was assessed. Firstly, increasing the rail pressure inhibited the soot formation, as combustion occurred with a leaner air/fuel mixture. On the other hand, enlarging the chamber density or the chamber temperature increased the soot formation, as the combustion developed under a higher equivalence ratio around the lift-off area. These trends follow previous analyses found in the literature and serve to validate the consistency of the work done.

# References

[1] Nishida, Keiya; Jingyu, Zhu; Xianyin, Leng; and He, Zhixia. "Effects of micro-hole nozzle and ultra-high injection pressure on air entrainment, liquid penetration, flame lift-off and soot formation of diesel spray flame". In: *International Journal of Engine Research* 18.1-2 (2017), pp. 51–65.

[2] Pastor, Jose Vicente; Garcia-Oliver, Jose Maria; Novella, Ricardo; and Xuan, Tiemin. "Soot Quantification of Single-Hole Diesel Sprays by Means of Extinction Imaging". In: *SAE International Journal of Engines* 8.5 (2015), pp. 2068–2077. DOI: 10.4271/2015-24-2417.

[3] Xuan, Tiemin. "Optical investigations on diesel spray dynamics and inflame soot formation". PhD thesis. Universitat Politècnica de València, 2017. DOI: 10.4995/Thesis/10251/94626.

[4] Pandurangi, Sushant S et al. "Onset and progression of soot in high-pressure n - Dodecane sprays under diesel engine conditions". In: *International Journal of Engine Research* 18.5-6 (2017), pp. 436–452. DOI: 10.1177/1468087416661041.

[5] Skeen, Scott A; Manin, Julien; Dalen, Kristine; and Pickett, Lyle M. "Extinction-based Imaging of Soot Processes over a Range of Diesel Operating Conditions". In: *8th US National Combustion Meeting*. Utah, USA, 2013, pp. 1–13.

[6] Dronniou, Nicolas; Lejeune, Marc; Balloul, Iyad; and Higelin, Pascal. "Combination of High EGR Rates and Multiple Injection Strategies to Reduce Pollutant Emissions". In: *SAE Technical Paper 2005-01-3726* (2005). DOI: 10.4271/2005-01-3726.

[7] Payri, Raul; Salvador, Francisco Javier; Gimeno, Jaime; and Viera, Alberto. "Effect of Injection Rate Shaping over Diesel Spray Development in Non-Reacting Evaporative Conditions". In: *10. Tagung Diesel- und Benzindirekteinspritzung 2016*. Ed. by Helmut Tschöke; and Ralf Marohn. 1. Springer Vieweg, 2016, pp. 133–152. DOI: 10.1007/978-3-658-15327-4.

[8] Pastor, Jose Vicente; Payri, Raul; Garcia-Oliver, Jose Maria; and Nerva, Jean-Guillaume. "Schlieren Measurements of the ECN-Spray A Penetration under Inert and Reacting Conditions". In: *SAE Technical Paper 2012-01-0456* (2012). DOI: 10.4271/2012-01-0456.

[9] Manin, Julien; Skeen, Scott A; and Pickett, Lyle M. "Two-color diffused back-illumination imaging as a diagnostic for time-resolved soot measurements in reacting sprays". In: *SAE Int. J. Engines* 6.4 (2013), pp. 1908–1921. DOI: 10.4271/2013-01-2548.

[10] Pastor, José V.; García-Oliver, José M.; Micó, Carlos; García-Carrero, Alba A.; and Gómez, Arantzazu. "Experimental study of the effect of hydrotreated vegetable oil and oxymethylene ethers on main spray and combustion characteristics under engine combustion network spray A conditions". In: *Applied Sciences (Switzerland)* 10.16 (2020). DOI: 10.3390/APP10165460.

[11] Payri, Raul; Gimeno, Jaime; Cardona, Santiago; and Ayyapureddi, Sridhar. "Measurement of Soot Concentration in a Prototype Multi-Hole Diesel Injector by High-Speed Color Diffused Back Illumination Technique". In: *SAE Technical Paper 2017-01-2255*. 2017, p. 11. DOI: 10.4271/2017-01-2255.

[12] Pickett, Lyle M.; Siebers, Dennis L.; and Idicheria, Cherian A. "Relationship Between Ignition Processes and the Lift-Off Length of Diesel Fuel Jets". In: *SAE Paper 2005-01-3843* 724 (2005). DOI: 10.4271/2005-01-3843.

[13] Payri, Raul; Salvador, Francisco Javier; Manin, Julien; and Viera, Alberto. "Diesel ignition delay and lift-off length through different methodologies using a multi-hole injector". In: *Applied Energy* 162 (2016), pp. 541–550. DOI: 10.1016/j.apenergy.2015.10.118.

[14] Benajes, Jesus; Payri, Raul; Bardi, Michele; and Martí-aldaraví, Pedro. "Experimental characterization of diesel ignition and lift-off length using a single-hole ECN injector". In: *Applied Thermal Engineering* 58.1-2 (2013), pp. 554–563. DOI: 10.1016/j.applthermaleng.2013.04.044.

[15] Higgins, Brian; and Siebers, Dennis L. "Measurement of the Flame Lift-Off Location on DI Diesel Sprays Using OH Chemiluminescence". In: *SAE Technical Paper 2001-01-0918* (2001).

[16] Lequien, Guillaume; Li, Zheming; Andersson, Oivind; and Richter, Mattias. "Lift-Off Length in an Optical Heavy-Duty Diesel Engine". In: *SAE International Journal of Engines* 8.5 (2015), pp. 2015–24–2442. DOI: 10.4271/2015-24-2442.

[17] Li, Tie; and Ogawa, Hideyuki. "Analysis of the Trade-off between Soot and Nitrogen Oxides in Diesel-Like Combustion by Chemical Kinetic Calculation". In: *SAE International Journal of Engines* 5.2 (2011), pp. 2011–01. DOI: 10.4271/2011-01-1847.

[18] Potter, Mike; and Durrett, Russell P. "High-Efficiency Clean Combustion Design for Compression Ignition Engines". In: *Diesel Engine-Efficiency and Emissions Research (DEER)*. Detroit, 2006.

[19] De Lima Moradell, Daniela. "Analysis of combustion concepts in a poppet valve two-stroke downsized compression ignition engine designed for passenger car applications". PhD thesis. Universitat Politècnica de València, 2016. DOI: 10.4995/Thesis/10251/68502..

[20] Neely, Gary D; Sasaki, Shizuo; Huang, Yiqun; Leet, Jeffrey A; and Stewart, Daniel W. "New Diesel Emission Control Strategy to Meet US Tier 2 Emissions Regulations". In: *SAE Technical Paper 2005-01-1091* (2005). DOI: 10.4271/2005-01-1091.

[21] Li, Tie; Suzuki, Masaru; and Ogawa, Hideyuki. "Characteristics of Smokeless Low Temperature Diesel Combustion in Various Fuel-Air Mixing and Expansion of Operating Load Range". In: *SAE Technical Paper 2009-01-1449* (2009). DOI: 10.4271/2009-01-1449.

[22] Kamimoto, Takeyuki; and Bae, Myurng-hoan. "High Combustion Temperature for the Reduction of Particulate in Diesel Engines". In: *SAE Technical Paper 880423* (1988). DOI: 10.4271/880423.

[23] Siebers, Dennis L. "Liquid-Phase Fuel Penetration in Diesel Sprays". In: *SAE Technical Paper 980809* (1998), pp. 1–23. DOI: 10.4271/980809.

[24] Siebers, Dennis L. "Scaling liquid-phase fuel penetration in diesel sprays based on mixing-limited vaporization". In: *SAE Technical Paper 1999-01-0528* (1999). DOI: 10.4271/1999-01-0528.

[25] Siebers, Dennis L; and Higgins, Brian. "Flame Lift-Off on Direct-Injection Diesel Sprays Under Quiescent Conditions". In: *SAE Technical Paper 2001-01-0530* 724 (2001).

# Chapter 7

# Summary and future works

The present chapter summarizes the studies and main findings achieved throughout the research done. Additionally, future works are suggested.

## 7.1 Summary

The current thesis aimed to analyze the influence of inter-jet spacing on the injection development and enhance the methodology employed to study injection events of multi-holes injectors, accounting for the interactions between jets in the combustion event.

To this end, two diesel injectors with six outlet orifices were manufactured by Continental with identical design, except for the geometric distribution of the outlet holes of each nozzle, as they were specifically allocated to study the influence of inter-jet spacing on the injection event. Concretely, the first injector allowed the study of the development of an isolated spray on one side and a spray with an inter-jet spacing of 30° on the other side during the same injection event. Moreover, the second injector has two additional orifices distributions, so a total of three inter-jet spacing configurations (30° - 36° - 45°) were compared to the performance of the isolated spray.

The results were grouped into analyses under non-reactive and reactive environments. The analysis under a non-reactive environment was mainly done to assess the similarity or variance in performance due to fabrication differences between the injectors. Then, it would be possible to distinguish any

inherent variations from those observed in the following experiments under a reactive environment. The experiments under a non-reactive environment included the hydraulic characterization of the injectors through injection rate and momentum flux measurements, and the visual analysis of the liquid length and vapor spray penetration of each jet, obtained with the MIE scattering and double-pass Schlieren optical technique, respectively. Overall, the inter-jet spacing did not affect the injection event under non-reactive conditions. Moreover, the performance was similar between each orifice of interest for every parameter tested. Thus, any difference observed in a reactive environment could be attributed to phenomena occurring during the combustion event.

Then, the studies focused on the spray development under a reactive environment, where the interactions between sprays could have a larger influence. Specifically, the influence of inter-jet spacing on the ignition delay, lift-off length, initial soot appearance, and soot formation were investigated.

Regarding the ignition delay, sprays with neighbor jets tended to have equal or slightly smaller ignition delay values under poor mixing and ignition conditions (low rail pressure, chamber temperature, or chamber density conditions). On the other hand, the opposite effect was generally observed as the boundary conditions were overall increased, with equal or higher ignition delay values within sprays with neighbor jets, compared to that of the isolated spray. Nonetheless, no clear trend was defined, with complex interactions and multiple factors simultaneously affecting the ignition event.

On the other hand, the initial soot appearance obtained with broadband chemiluminescence followed the same trends as the ignition delay, serving as a qualitative measurement of the combustion timing. Nevertheless, OH* chemiluminescence captures the initial stages of the ignition process, thus being the appropriate technique to obtain a quantitative ignition delay value.

On the lift-off length, the results showed that after certain proximity between sprays is reached, the interaction between the jets becomes a predominant factor in their behavior, and the lift-off length is considerably reduced. Moreover, as the inter-jet spacing increases, the performance gradually approaches that obtained from the isolated spray. Plausibly, closely spaced sprays entrain a higher amount of hot combustion products and radicals. Then, the entrained gas with a higher temperature could trigger autoignition near the nozzle, reducing the lift-off length. Lastly, a novel regression for the lift-off length was developed, which accounted for the effect of the proximity between sprays.

Respecting the soot formation, the sprays with closely spaced neighbor jets (30° and 36°) generally had higher optical thickness KL and peak soot

mass values for a given boundary condition when compared to the development of the isolated spray (spacing = 120°). These trends are in line with the lift-off length results observed, in which the closely spaced jets had a shorter lift-off length due to (plausibly) hot gases re-entrainment. This shortening would deteriorate the air/fuel mixing before the onset combustion and, consequently, a richer mixture is ignited, suitable for soot appearance. On the other hand, the impact of the inter-jet spacing was smaller as the boundary conditions promoting soot formation were enhanced, that is, increasing the ambient density, ambient temperature, or reducing the rail pressure.

Moreover, the field of view limitations on the soot analysis campaign prevented observing the spray development near the nozzle. Consequently, the influence of the inter-jet spacing could not be properly addressed when the ignition occurred before the spray entered the field of view. Nonetheless, a wide test matrix was employed, collecting data on the boundary conditions at which the spray develops within the field of view. This information could help select an efficient test matrix in future works, saving time and additional expenses from experimental measurements.

Additionally, the influence of the chamber temperature, chamber density, and rail pressure on the spray behavior was assessed. The observed impact of these parameters on the spray followed the trends found in the literature and served to validate the consistency of the work done.

Lastly, various objectives were achieved as the measurements were made. Among them:

- A variety of optical diagnostic techniques were successfully applied to analyze the spray development on multi-holes injectors: MIE scattering for the liquid length, double-pass Schlieren for the vapor spray penetration, OH* chemiluminescence for the ignition delay and lift-off length, broadband chemiluminescence for the initial soot appearance, and diffuse back-illumination (DBI) for the soot formation.

- A novel window was implemented to perform the diffuse back-illumination measurements. This window contained both the injector holder and the optical access, allowing the implementation of the DBI technique on multi-holes injectors.

- Moreover, a high-temperature ceramic mirror was successfully tested on the double-pass Schlieren experiments. Specifically, the mirror allowed to measure test points reaching 1000 K of chamber temperature, a new

achievement on this test rig and optical technique at CMT-Motores Térmicos.

## 7.2 Future works

Even though the main objectives of the thesis were achieved, several proposals appeared during and after the research. In particular:

- Analyze the influence of inter-jet spacing on $NOx$ formation through laser-induced fluoresce to assess further the impact of the geometric distribution of the outlet-holes on the soot-$NOx$ trade-off.
- Perform the soot-DBI measurements with more powerful LEDs to avoid KL saturation and fluently assess the influence of the inter-jet spacing on the soot formation under a wider matrix of boundary conditions.
- Carry out the experiments in an optically accessible engine to study the effect of jet-wall interactions and air movement in closely-spaced sprays.
- Employ the experimental data gathered in this work to develop and validate models that account for the influence of the inter-jet spacing on the spray development.

# Global Bibliography


Alkidas, A C. "On the Premixed Combustion in a Direct-Injection Diesel Engine". In: *Journal of Engineering for Gas Turbines and Power* 109.2 (1987), pp. 187–192. DOI: 10.1115/1.3240023 (cited on page 23).

Allocca, Luigi; Lazzaro, Maurizio; Meccariello, Giovanni; and Montanaro, Alessandro. "Schlieren visualization of a GDI spray impacting on a heated wall: Non-vaporizing and vaporizing evolutions". In: *Energy* 108 (2016), pp. 93–98. DOI: 10.1016/j.energy.2015.09.107 (cited on page 64).

Altenschmidt, Frank; Banzhaf, Gerald; Kraus, Eberhard; and Loll, Steffen. "The SI-engine - at the end of its development?" In: *16th Conference The Working Process of the Internal Combustion Engine*. Ed. by Helmut Eichlseder; and Andreas Wimmer. Graz: Verlag der Technischen Universität Graz, 2017, pp. 35–49 (cited on page 1).

Aori, Gele; Hung, David L S; and Zhang, Ming. "Effect of Nozzle Configuration on Macroscopic Spray Characteristics of Multi-Hole Fuel Injectors Under Superheated Conditions". In: *Atomization and Sprays* 26.5 (2016), pp. 439–462. DOI: 10.1615/AtomizSpr.2015011990 (cited on pages 4, 31).

Armas, Octavio. "Diagnóstico experimental del proceso de combustión en motores Diesel de inyección directa". PhD thesis. Valencia: E.T.S. Ingenieros Industriales. Universidad Politécnica de Valencia, 1998 (cited on page 15).

Badami, M; Millo, Federico; and D'Amato, D D. "Experimental investigation on soot and NOx formation in a DI common rail diesel engine with pilot injection". In: *SAE Technical Paper 2001-01-0657* (2001). DOI: 10.4271/2001-01-0657 (cited on page 23).

Baert, Rik S G et al. “Design and operation of a high pressure, high temperature cell for HD diesel spray diagnostics: guidelines and results”. In: *SAE paper 2009-01-0649* 4970 (2009). DOI: 10.4271/2009-01-0649 (cited on page 5).

Balmer, Robert T. *Vapor and Gas Power Cycles*. 2011, pp. 447–534. DOI: 10.1016/b978-0-12-374996-3.00013-0 (cited on pages 16, 17).

Bardi, Michele. “Partial needle lift and injection rate shape effect on the formation and combustion of the Diesel spray”. PhD thesis. Valencia (Spain): Universitat Politècnica de València, 2014. DOI: 10.4995/Thesis/10251/37374 (cited on pages 5, 19, 50).

Bardi, Michele et al. “Engine Combustion Network: Comparison of Spray Development, Vaporization, and Combustion in Different Combustion Vessels”. In: *Atomization and Sprays* 22.10 (2012), pp. 807–842. DOI: 10.1615/AtomizSpr.2013005837 (cited on pages 59, 68, 75).

Bazyn, Tim; and Koci, Chad. “The Effect of Jet Spacing on the Combustion Characteristics of Diesel Sprays”. In: *THIESEL 2014 Conference on Thermo- and Fluid Dynamic Processes in Direct Injection Engines*. 2014, pp. 1–19 (cited on pages 33, 116, 121).

Benajes, Jesus; Pastor, Jose Vicente; Payri, Raul; and Plazas, Alejandro Hernan. “Analysis of the influence of Diesel nozzle geometry in the Injection Rate characteristic”. In: *Journal of Fluids Engineering* 126.1 (2004), pp. 63–71. DOI: 10.1115/1.1637636 (cited on pages 19, 100).

Benajes, Jesus; Payri, Raul; Bardi, Michele; and Martí-aldaraví, Pedro. “Experimental characterization of diesel ignition and lift-off length using a single-hole ECN injector”. In: *Applied Thermal Engineering* 58.1-2 (2013), pp. 554–563. DOI: 10.1016/j.applthermaleng.2013.04.044 (cited on pages 5, 28–31, 63, 68, 120, 123, 124, 138).

Bermúdez, Vicente; Payri, Raul; Salvador, Francisco Javier; and Plazas, Alejandro Hernan. “Study of the influence of nozzle seat type on injection rate and spray behavior”. In: *ImechE. Journal of automobile engineering* 219.5 (2005), pp. 677–689. DOI: 10.1243/095440705X28303 (cited on page 19).

Binde, Andreas; Busch, Stephen; Velji, Amin; and Wagner, Uwe. “Soot and NO x Reduction by Spatially Separated Pilot Injection”. In: *SAE International Journal of Engines* 5.3 (2012), pp. 1242–1259. DOI: 10.4271/2012-01-1159 (cited on page 23).

Boehner, Wolfgang; and Hummel, Karsten. “Common Rail Injection System for Commercial Diesel Vehicles”. In: *SAE Technical Paper 970345* (1997). DOI: 10.4271/970345 (cited on page 45).

Bosch, Wilhelm. "The Fuel Rate Indicator: A New Measuring Instrument for Display of the Characteristics of Individual Injection". In: *SAE Technical Paper 660749* (1966). DOI: 10.4271/660749 (cited on pages 20, 50).

BP. *Statistical Review of World Energy*. 2020 (cited on pages 2, 4).

Bruneaux, Gilles. "Development of optical diagnostics techniques to correlate mixing and auto-ignition processes in high pressure diesel jets". In: *Oil and Gas Science and Technology* 63.4 (2008), pp. 461–477. DOI: 10.2516/ogst:2008031 (cited on page 29).

Carlucci, Paolo; Ficarella, Antonio; and Laforgia, Domenico. "Effects on combustion and emissions of early and pilot fuel injections in diesel engines". In: *International Journal of Engine Research* 6.1 (2005), pp. 43–60. DOI: 10.1243/146808705X7301 (cited on page 23).

Carreres, Marcos. "Thermal Effects Influence on the Diesel Injector Perfomance through a Combined 1D Modelling and Experimental Approach". PhD thesis. Universitat Politècnica de València, 2016. DOI: 10.4995/Thesis/10251/73066 (cited on pages 19, 20).

Chang, H; and Charalampopoulos, T T. "Determination of the wavelength dependence of refractive indices of flame soot". In: *Proceedings of the Royal Society of London. Series A: Mathematical and Physical Sciences* 430.1880 (1990), pp. 577–591. DOI: 10.1098/rspa.1990.0107 (cited on page 84).

Chaplya, Pavel M; Mitrovic, Milan; Carman, Gregory P; and Straub, Friedrich K. "Durability properties of piezoelectric stack actuators under combined electromechanical loading". In: *Journal of Applied Physics* 100.12 (2006), p. 124111. DOI: 10.1063/1.2407269 (cited on page 19).

Chartier, Clément; Aronsson, Ulf; Andersson, Öivind; Egnell, Rolf; and Johansson, Bengt. "Influence of jet-jet interactions on the lift-off length in an optical heavy-duty di diesel engine". In: *Fuel* 112 (2013), pp. 311–318. DOI: 10.1016/j.fuel.2013.05.021 (cited on pages 4, 32, 121).

Choi, M.Y. Y; Mulholland, G.W. W; Hamins, A.; and Kashiwagi, T. "Comparisons of the soot volume fraction using gravimetric and light extinction techniques". In: *Combustion and Flame* 102.1-2 (1995), pp. 161–169. DOI: 10.1016/0010-2180(94)00282-W (cited on pages 83, 84).

Claßen, Johannes et al. "Statistically supported real driving emission calibration: Using cycle generation to provide vehicle-specific and statistically representative test scenarios for Euro 7". In: *International Journal of Engine Research* 21.10 (2020), pp. 1783–1799. DOI: 10.1177/1468087420935221 (cited on page 1).

CMT. *Official website: https://www.cmt.upv.es, accessed on 15-12-2021* (cited on page 5).

Correas, David. "Estudio teórico-experimental del chorro libre Diesel isotermo". PhD thesis. Valencia: E.T.S. Ingenieros Industriales. Universidad Politécnica de Valencia, 1998 (cited on page 26).

De Lima Moradell, Daniela. "Analysis of combustion concepts in a poppet valve two-stroke downsized compression ignition engine designed for passenger car applications". PhD thesis. Universitat Politècnica de València, 2016. DOI: 10.4995/Thesis/10251/68502. (cited on pages 138, 149).

Dec, John E. "A Conceptual Model of DI Diesel Combustion Based on Laser-Sheet Imaging". In: *SAE Technical Paper 970873* (1997). DOI: 10.4271/970873 (cited on page 29).

Dec, John E; and Canaan, Robert E. "PLIF Imaging of NO Formation in a DI Diesel Engine". In: *SAE Technical Paper 980147* (1998). DOI: 10.4271/980147 (cited on page 29).

Dec, John E; and Coy, Edward B. "OH Radical Imaging in a DI Diesel Engine and the Structure of the Early Diffusion Flame". In: 412 (1996). DOI: 10.4271/960831 (cited on page 29).

Dec, John E; and Espey, Christoph. "Chemiluminescence Imaging of Autoignition in a DI Diesel Engine". In: *SAE Technical Paper 982685* 724 (1998). DOI: 10.4271/982685 (cited on pages 27, 68).

Delacourt, E; Desmet, B; and Besson, B. "Characterisation of very high pressure Diesel sprays using digital imaging techniques". In: *Fuel* 84.7-8 (2005), pp. 859–867. DOI: 10.1016/j.fuel.2004.12.003 (cited on page 26).

Desantes, Jose Maria; García-Oliver, José Maria; García, Antonio; and Xuan, Tiemin. "Optical study on characteristics of non-reacting and reacting diesel spray with different strategies of split injection". In: *International Journal of Engine Research* 301 (2018). DOI: 10.1177/1468087418773012 (cited on pages 5, 84).

Desantes, Jose Maria; Pastor, Jose Vicente; Garcia-Oliver, Jose Maria; and Pastor, Jose Manuel. "A 1D model for the description of mixing-controlled reacting diesel sprays". In: *Combustion and Flame* 156.1 (2009), pp. 234–249. DOI: 10.1016/j.combustflame.2008.10.008 (cited on pages 5, 22).

Desantes, Jose Maria; Salvador, Francisco Javier; Carreres, Marcos; and Martínez-López, Jorge. "Large-eddy simulation analysis of the influence of the needle lift on the cavitation in diesel injector nozzles". In: *Proceedings of the Institution of Mechanical Engineers, Part D: Journal of Automobile Engineering* 229.4 (2014), pp. 407–423. DOI: 10.1177/0954407014542627 (cited on page 22).

Donkerbroek, A. J.; Boot, M. D.; Luijten, C. C.M.; Dam, N. J.; and Meulen, J. J. ter. "Flame lift-off length and soot production of oxygenated fuels in relation with ignition delay in a DI heavy-duty diesel engine". In: *Combustion and Flame* 158.3 (2011), pp. 525–538. DOI: 10.1016/j.combustflame.2010.10.003 (cited on page 68).

Dronniou, Nicolas; Lejeune, Marc; Balloul, Iyad; and Higelin, Pascal. "Combination of High EGR Rates and Multiple Injection Strategies to Reduce Pollutant Emissions". In: *SAE Technical Paper 2005-01-3726* (2005). DOI: 10.4271/2005-01-3726 (cited on page 132).

ECN. *Online: https://ecn.sandia.gov/diesel-spray-combustion/target-condition/spray-ab/, accessed on 20-01-2022* (cited on pages 45, 77, 113).

Essien, S.; Archibong-Eso, A.; and Lao, L. "Discharge coefficient of high viscosity liquids through nozzles". In: *Experimental Thermal and Fluid Science* 103.January (2019), pp. 1–8. DOI: 10.1016/j.expthermflusci.2019.01.004 (cited on pages 20, 58).

European Comittee for Standardization. *Regulation EC No 595/2009.* 2009 (cited on page 1).

Farnebäck, Gunnar. "Two-frame motion estimation based on polynomial expansion". In: *Lecture Notes in Computer Science (including subseries Lecture Notes in Artificial Intelligence and Lecture Notes in Bioinformatics)* 2749.May (2003), pp. 363–370. DOI: 10.1007/3-540-45103-x_50 (cited on page 80).

Flynn, P et al. "Diesel combustion: an integrated view combining laser diagnostics, chemical kinetics, and empirical validation". In: *SAE Paper 1999-01-0509* 724 (1999) (cited on page 29).

Fox, T A; and Stark, J. "Discharge coefficients for miniature fuel injectors". In: *Aerospace Engineering* 203.1 (1989), pp. 75–78. DOI: 10.1243/PIME_PROC_1989_203_056_01 (cited on pages 20, 58).

Garcia-Oliver, Jose Maria. "Aportaciones al estudio del proceso de combustión turbulenta de chorros en motores Diesel de inyección directa". PhD thesis. Valencia: E.T.S. Ingenieros Industriales. Universidad Politécnica de Valencia, 2004 (cited on pages 15, 22).

Gaydon, A G. *The Spectroscopy of Flames*. Springer Netherlands, 1974. DOI: 10.1007/978-94-009-5720-6 (cited on pages 27, 67, 70).

Gimeno, Jaime. "Desarrollo y aplicación de la medida de flujo de cantidad de movimiento de un chorro Diesel". PhD thesis. E.T.S. Ingenieros Industriales, Universidad Politécnica de Valencia, 2008. DOI: 10.4995/Thesis/10251/8306 (cited on pages 18, 20–22, 26, 52, 54, 58).

Giraldo, Jhoan S.; Payri, Raul; Marti-Aldaravi, Pedro; and Montiel, Tomas. "Effect of high injection pressures and ambient gas properties over the macroscopic characteristics of the diesel spray on multi-hole nozzles". In: *Atomization and Sprays* 28.12 (2018), pp. 1145–1160. DOI: 10.1615/AtomizSpr.2019029651 (cited on pages 5, 61, 116).

Giraldo Valderrama, Jhoan Sebastián. "Macroscopic and microscopic characterization of non-reacting diesel sprays at low and very high injection pressures". PhD thesis. Universitat Politècnica de València, 2018 (cited on pages 26, 100).

Gladstone, J H; and Dale, T P. "Researches on the Refraction, Dispersion, and Sensitiveness of Liquids". In: *Philosophical Transactions of the Royal Society of London* 153 (1863), pp. 317–343. DOI: 10.2307/108799 (cited on page 63).

Grigoratos, Theodoros; Gustafsson, Mats; Eriksson, Olle; and Martini, Giorgio. "Experimental investigation of tread wear and particle emission from tyres with different treadwear marking". In: *Atmospheric Environment* 182.March (2018), pp. 200–212. DOI: 10.1016/j.atmosenv.2018.03.049 (cited on page 2).

Han, Sangwook; Kim, Jaeheun; and Bae, Choongsik. "Effect of air-fuel mixing quality on characteristics of conventional and low temperature diesel combustion". In: *Applied Energy* 119 (2014), pp. 454–466. DOI: 10.1016/j.apenergy.2013.12.045 (cited on pages 3, 31).

Heywood, John B. *Internal Combustion Engine Fundamentals*. Vol. 21. 1988, p. 930 (cited on pages 15, 22, 27).

Higgins, Brian; and Siebers, Dennis L. "Measurement of the Flame Lift-Off Location on DI Diesel Sprays Using OH Chemiluminescence". In: *SAE Technical Paper 2001-01-0918* (2001) (cited on pages 29, 30, 68, 120, 138).

Higgins, Brian; Siebers, Dennis L; and Aradi, Allen. "Diesel-Spray Ignition and Premixed-Burn Behavior". In: *SAE Technical Paper 2000-01-0940* (2000). DOI: 10.4271/2000-01-0940 (cited on page 27).

Hiroyasu, Hiroyuki; and Arai, Masataka. "Structures of Fuel Sprays in Diesel Engines". In: *SAE Technical Paper 900475*. 1990. DOI: 10.4271/900475 (cited on pages 26, 110).

Hulkkonen, Tuomo; Sarjovaara, Teemu; Kaario, Ossi; Hamalainen, Ismo; and Larmi, Martti. "Experimental Study of Conical Diesel Nozzle Orifice Geometry". In: *Atomization and Sprays* 25.6 (2015), pp. 519–538. DOI: 10.1615/AtomizSpr.2015010383 (cited on page 3).

Jakob, Markus et al. "Simultaneous high-speed visualization of soot luminosity and OH * chemiluminescence of alternative-fuel combustion in a HSDI diesel engine under realistic operating conditions". In: *Combustion and Flame* 159.7 (2012), pp. 2516–2529. DOI: 10.1016/j.combustflame.2012.03.004 (cited on pages 28, 68).

Jia, Tao Ming; Li, Guo Xiu; Yu, Yu Song; and Xu, Yang Jie. "Effects of ultra-high injection pressure on penetration characteristics of diesel spray and a two-mode leading edge shock wave". In: *Experimental Thermal and Fluid Science* 79 (2016), pp. 126–133. DOI: 10.1016/j.expthermflusci.2016.07.006 (cited on page 3).

Johnson, Timothy. "Vehicular Emissions in Review". In: *SAE International Journal of Engines* 9.2 (2016), pp. 1258–1275. DOI: 10.4271/2016-01-0919 (cited on page 1).

Jung, Yongjin; Manin, Julien; Skeen, Scott A; and Pickett, Lyle M. "Measurement of Liquid and Vapor Penetration of Diesel Sprays with a Variation in Spreading Angle". In: *SAE Technical Paper 2015-01-0946* (2015). DOI: 10.4271/2015-01-0946 (cited on pages 26, 70).

Kalghatgi, Gautam. "Is it really the end of internal combustion engines and petroleum in transport?" In: *Applied Energy* 225.April (2018), pp. 965–974. DOI: 10.1016/j.apenergy.2018.05.076 (cited on page 2).

Kamimoto, Takeyuki; and Bae, Myurng-hoan. "High Combustion Temperature for the Reduction of Particulate in Diesel Engines". In: *SAE Technical Paper 880423* (1988). DOI: 10.4271/880423 (cited on pages 138, 149).

Kastengren, Alan L et al. "Engine Combustion Network (ECN): Measurements of Nozzle Geometry and Hydraulic Behavior". In: *Atomization and Sprays* 22.12 (2012), pp. 1011–1052. DOI: 10.1615/AtomizSpr.2013006309 (cited on page 19).

Knox, Benjamin; and Genzale, Caroline L. “Effects of End-of-Injection Transients on Combustion Recession in Diesel Sprays”. In: *SAE International Journal of Engines* 9.2 (2016), pp. 1–18. DOI: 10.4271/2016-01-0745 (cited on page 64).

Knox, Benjamin W. “End-of-Injection Effects on Diesel Spray Combustion”. PhD thesis. Georgia Institute of Technology, 2016 (cited on page 28).

Kobori, S; Kamimoto, T; and Aradi, A A. “A study of ignition delay of diesel fuel sprays”. In: *International Journal of Engine Research* 1.29 (2000), pp. 29–39. DOI: 10.1243/1468087001545245 (cited on page 29).

Kook, Sanghoon; and Pickett, Lyle M. “Liquid length and vapor penetration of conventional , Fischer - Tropsch , coal-derived , and surrogate fuel sprays at high-temperature and high-pressure ambient conditions”. In: *Fuel* 93 (2012), pp. 539–548. DOI: 10.1016/j.fuel.2011.10.004 (cited on page 64).

Köylü, Ü Ö; Mcenally, C. S.; Rosner, D. E.; and Pfefferle, L. D. “Simultaneous measurements of soot volume fraction and particle size / microstructure in flames using a thermophoretic sampling technique”. In: *Combustion and Flame* 110.4 (1997), pp. 494–507. DOI: 10.1016/S0010-2180(97)00089-8 (cited on page 84).

Lahane, Subhash; and Subramanian, K. A. “Impact of nozzle holes configuration on fuel spray, wall impingement and NOx emission of a diesel engine for biodiesel-diesel blend (B20)”. In: *Applied Thermal Engineering* 64.1-2 (2014), pp. 307–314. DOI: 10.1016/j.applthermaleng.2013.12.048 (cited on page 31).

Lapuerta, Magín; Ramos, Ángel; Fernández-Rodríguez, David; and González-García, Inmaculada. “High-pressure versus low-pressure exhaust gas recirculation in a Euro 6 diesel engine with lean-NOx trap: Effectiveness to reduce NOx emissions”. In: *International Journal of Engine Research* 20.1 (2019), pp. 155–163. DOI: 10.1177/1468087418817447 (cited on page 1).

Le, Minh K. et al. “Effect of jet-jet interactions on soot formation in a small-bore diesel engine”. In: *Proceedings of the Combustion Institute* 36.3 (2017), pp. 3559–3566. DOI: 10.1016/j.proci.2016.07.025 (cited on page 32).

Lee, J W et al. “Effect of piezo-driven and solenoid-driven needle opening of common-rail diesel injectors on internal nozzle flow and spray development”. In: *International Journal of Engine Research* 7.6 (2006), pp. 489–502. DOI: 10.1243/14680874JER00806 (cited on page 19).

Lee, Jinwoo; Jeon, Jinwoog; Park, Jungseo; and Bae, Choongsik. "Effect of Multiple Injection Strategies on Emission and Combustion Characteristics in a Single Cylinder Direct-Injection Optical Engine". In: *SAE Technical Paper 2009-01-1354* (2010). DOI: 10.4271/2009-01-1354 (cited on page 3).

Lequien, Guillaume; Li, Zheming; Andersson, Oivind; and Richter, Mattias. "Lift-Off Length in an Optical Heavy-Duty Diesel Engine". In: *SAE International Journal of Engines* 8.5 (2015), pp. 2015–24–2442. DOI: 10.4271/2015-24-2442 (cited on pages 120, 138).

Lequien, Guillaume et al. "Effect of jet-jet interactions on the liquid fuel penetration in an optical heavy-duty di diesel engine". In: *SAE Technical Papers* 2 (2013). DOI: 10.4271/2013-01-1615 (cited on page 32).

Li, Feng; Lee, Chia Fon; Wang, Ziman; Pei, Yiqiang; and Lu, Guoxiang. "Impacts of duct inner diameter and standoff distance on macroscopic spray characteristics of ducted fuel injection under non-vaporizing conditions". In: *International Journal of Engine Research* (2020), pp. 1–12. DOI: 10.1177/1468087420914714 (cited on page 61).

Li, Tie; and Ogawa, Hideyuki. "Analysis of the Trade-off between Soot and Nitrogen Oxides in Diesel-Like Combustion by Chemical Kinetic Calculation". In: *SAE International Journal of Engines* 5.2 (2011), pp. 2011–01. DOI: 10.4271/2011-01-1847 (cited on pages 138, 149).

Li, Tie; Suzuki, Masaru; and Ogawa, Hideyuki. "Characteristics of Smokeless Low Temperature Diesel Combustion in Various Fuel-Air Mixing and Expansion of Operating Load Range". In: *SAE Technical Paper 2009-01-1449* (2009). DOI: 10.4271/2009-01-1449 (cited on pages 138, 149).

Lillo, Peter M; Pickett, Lyle M; Persson, Helena; Andersson, Oivind; and Kook, Sanghoon. "Diesel Spray Ignition Detection and Spatial/Temporal Correction". In: *SAE Paper 2012-01-1239* (2012), pp. 1–21. DOI: 10.4271/2012-01-1239 (cited on pages 29, 63).

Manin, J.; Bardi, M.; Pickett, L. M.; and Payri, R. "Boundary condition and fuel composition effects on injection processes of high-pressure sprays at the microscopic level". In: *International Journal of Multiphase Flow* 83 (2016), pp. 267–278. DOI: 10.1016/j.ijmultiphaseflow.2015.12.001 (cited on page 26).

Manin, Julien; Bardi, Michele; and Pickett, Lyle M. "Evaluation of the liquid length via diffused back-illumination imaging in vaporizing diesel sprays". In: *Comodia*. Fukuoka, 2012 (cited on pages 70, 107).

Manin, Julien; Bardi, Michele; Pickett, Lyle M; Dahms, R. N.; and Oefelein, J. C. "Microscopic investigation of the atomization and mixing processes of diesel sprays injected into high pressure and temperature environments". In: *Fuel* 134 (2014), pp. 531–543. DOI: 10.1016/j.fuel.2014.05.060 (cited on pages 26, 70).

Manin, Julien; Pickett, Lyle M; and Skeen, Scott A. "Toward quantitative spray measurements using high-performance high-speed video cameras". In: *ILASS Americas 2016* (2016), pp. 511–518 (cited on page 72).

Manin, Julien; Pickett, Lyle M.; and Skeen, Scott A. "Two-Color Diffused Back-Illumination Imaging as a Diagnostic for Time-Resolved Soot Measurements in Reacting Sprays". In: *SAE International Journal of Engines* 6.4 (2013), pp. 1908–1921. DOI: 10.4271/2013-01-2548 (cited on pages 70, 116).

Manin, Julien; Skeen, Scott A; and Pickett, Lyle M. "Two-color diffused back-illumination imaging as a diagnostic for time-resolved soot measurements in reacting sprays". In: *SAE Int. J. Engines* 6.4 (2013), pp. 1908–1921. DOI: 10.4271/2013-01-2548 (cited on pages 84, 132).

Martínez-López, Jorge. "Estudio computacional de la influencia del levantamiento de aguja sobre el flujo interno y el fenómeno de la cavitación en toberas de inyección Diesel". PhD thesis. Valencia: Universitat Politecnica de Valencia, 2013 (cited on pages 22, 24).

Meijer, Maarten et al. "Engine Combustion Network (ECN): Characterization and comparison of boundary conditions for different combustion vessels". In: *Atomization and Sprays* 22.9 (2012), pp. 777–806. DOI: 10.1615/AtomizSpr.2012006083 (cited on page 59).

Mersen-Boostec. *Online: https://www.mersen.com/products/graphite-specialties/boostec-silicon-carbide-sic, accessed on 21-01-2022* (cited on page 64).

Mingfa, Yao; Hu, Wang; Zunqing, Zheng; and Yan, Yue. "Experimental Study of Multiple Injections and Coupling Effects of Multi-Injection and EGR in a HD Diesel Engine". In: *SAE Technical Paper 2009-01-2807* (2009). DOI: 10.4271/2009-01-2807 (cited on pages 3, 23).

Molina, Santiago. "Influencia de los parámetros de inyección y la recirculación de gases de escape sobre el proceso de combustión en un motor diesel". PhD thesis. Barcelona, 2005 (cited on pages 22, 29).

Montanaro, Alessandro et al. “Schlieren and Mie Scattering Visualization for Single- Hole Diesel Injector under Vaporizing Conditions with Numerical Validation”. In: *SAE Technical Paper 2014-01-1406* (2014). DOI: 10.4271/2014-01-1406 (cited on page 64).

Musculus, Mark P B; Miles, Paul C; and Pickett, Lyle M. *Conceptual models for partially premixed low-temperature diesel combustion*. Vol. 39. 2-3. Elsevier Ltd, 2013, pp. 246–283. DOI: 10.1016/j.pecs.2012.09.001 (cited on page 3).

Musculus, Mark P.B. “Effects of the in-cylinder environment on diffusion flame lift-off in a di diesel engine”. In: *SAE Technical Papers* 724 (2003). DOI: 10.4271/2003-01-0074 (cited on page 123).

Naber, Jeffrey D; and Siebers, Dennis L. “Effects of Gas Density and Vaporization on Penetration and Dispersion of Diesel Sprays”. In: *SAE Paper 960034*. Vol. 105. 412. Society of Automotive Engineers, Inc., Warrendale, Pennsylvania, USA, 1996, pp. 82–111. DOI: 10.4271/960034 (cited on pages 26, 63, 110).

Neely, Gary D; Sasaki, Shizuo; Huang, Yiqun; Leet, Jeffrey A; and Stewart, Daniel W. “New Diesel Emission Control Strategy to Meet US Tier 2 Emissions Regulations”. In: *SAE Technical Paper 2005-01-1091* (2005). DOI: 10.4271/2005-01-1091 (cited on pages 138, 149).

Nerva, Jean-Guillaume; Genzale, Caroline L; Kook, Sanghoon; Garcia-Oliver, Jose Maria; and Pickett, Lyle M. “Fundamental Spray and Combustion Measurements of Soy Methyl-Ester Biodiesel”. In: *International Journal of Engine Research* 14.4 (2013), pp. 373–390. DOI: doi:10.1177/1468087412456688 (cited on page 64).

Nishida, Keiya; Jingyu, Zhu; Xianyin, Leng; and He, Zhixia. “Effects of microhole nozzle and ultra-high injection pressure on air entrainment, liquid penetration, flame lift-off and soot formation of diesel spray flame”. In: *International Journal of Engine Research* 18.1-2 (2017), pp. 51–65 (cited on pages 3, 30, 131).

O’Connor, Jacqueline; Musculus, Mark P B; and Pickett, Lyle M. “Effect of post injections on mixture preparation and unburned hydrocarbon emissions in a heavy-duty diesel engine”. In: *Combustion and Flame* 170 (2016), pp. 111–123. DOI: 10.1016/j.combustflame.2016.03.031 (cited on page 3).

Pachano, Leonardo. “CFD Modeling of Combustion and Soot Production in Diesel Sprays”. PhD thesis. Universitat Politècnica de València, 2020, pp. 1–157 (cited on page 84).

Pandurangi, Sushant S et al. “Onset and progression of soot in high-pressure n - Dodecane sprays under diesel engine conditions”. In: *International Journal of Engine Research* 18.5-6 (2017), pp. 436–452. DOI: 10.1177/1468087416661041 (cited on pages 132, 148).

Pastor, José V.; García, A.; Micó, C.; and García-Carrero, Alba A. “Experimental study of influence of Liquefied Petroleum Gas addition in Hydrotreated Vegetable Oil fuel on ignition delay, flame lift off length and soot emission under diesel-like conditions”. In: *Fuel* 260.July 2019 (2020), p. 116377. DOI: 10.1016/j.fuel.2019.116377 (cited on pages 28, 70, 81, 118).

Pastor, José V.; García-Oliver, José M.; Micó, Carlos; García-Carrero, Alba A.; and Gómez, Arantzazu. “Experimental study of the effect of hydrotreated vegetable oil and oxymethylene ethers on main spray and combustion characteristics under engine combustion network spray A conditions”. In: *Applied Sciences (Switzerland)* 10.16 (2020). DOI: 10.3390/APP10165460 (cited on pages 71, 84, 118, 133, 142, 148).

Pastor, Jose Vicente; Garcia-Oliver, Jose Maria; Garcia, Antonio; and Pinotti, Mattia. “Soot Characterization of Diesel/Gasoline Blends Injected through a Single Injection System in CI engines”. In: *SAE Technical Papers* 2017-Septe (2017). DOI: 10.4271/2017-24-0048 (cited on page 70).

Pastor, Jose Vicente; Garcia-Oliver, Jose Maria; Novella, Ricardo; and Xuan, Tiemin. “Soot Quantification of Single-Hole Diesel Sprays by Means of Extinction Imaging”. In: *SAE International Journal of Engines* 8.5 (2015), pp. 2068–2077. DOI: 10.4271/2015-24-2417 (cited on page 131).

Pastor, Jose Vicente; Garcia-Oliver, Jose Maria; Pastor, Jose Manuel; and Zapata, Luis Daniel. “Evaporating Diesel Spray Visualization using a Double-pass Shadowgraphy / Schlieren Imaging”. In: *SAE technical Paper 2007-24-0026* (2007). DOI: 10.4271/2007-24-0026 (cited on page 64).

Pastor, Jose Vicente; Lopez, Jose Javier; Garcia-Oliver, Jose Maria; and Pastor, Jose Manuel. “A 1D model for the description of mixing-controlled inert diesel sprays”. In: *Fuel* 87.13-14 (2008), pp. 2871–2885. DOI: 10.1016/j.fuel.2008.04.017 (cited on pages 5, 22, 63).

Pastor, Jose Vicente; Payri, Raul; Garcia-Oliver, Jose Maria; and Nerva, Jean-Guillaume. “Schlieren Measurements of the ECN-Spray A Penetration under Inert and Reacting Conditions”. In: *SAE Technical Paper 2012-01-0456* (2012). DOI: 10.4271/2012-01-0456 (cited on pages 64, 75, 132).

Payri, Francisco; Benajes, Jesus; Pastor, Jose Vicente; and Molina, Santiago. "Influence of the Post-Injection Pattern on Performance, Soot and NOx Emissions in a HD Diesel Engine". In: *SAE Technical Paper 2002-01-0502* (2002). DOI: 10.4271/2002-01-0502 (cited on page 3).

Payri, Francisco; Bermúdez, Vicente; Payri, Raul; and Salvador, Francisco Javier. "The influence of cavitation on the internal flow and the spray characteristics in diesel injection nozzles". In: *Fuel* 83.4-5 (2004), pp. 419–431. DOI: 10.1016/j.fuel.2003.09.010 (cited on pages 26, 110).

Payri, Francisco; and Desantes, Jose Maria. *Motores de combustion interna alternativos*. Editorial Universitat Politecnica de Valencia, 2011 (cited on pages 15, 22).

Payri, Francisco; Payri, Raul; Bardi, Michele; and Carreres, Marcos. "Engine combustion network: Influence of the gas properties on the spray penetration and spreading angle". In: *Experimental Thermal and Fluid Science* 53.September 2015 (2014), pp. 236–243. DOI: 10.1016/j.expthermflusci.2013.12.014 (cited on page 116).

Payri, Raul; Bracho, Gabriela; Gimeno, Jaime; and Bautista, Abian. "Rate of injection modelling for gasoline direct injectors". In: *Energy Conversion and Management* 166.February (2018), pp. 424–432. DOI: 10.1016/j.enconman.2018.04.041 (cited on page 100).

Payri, Raul; Bracho, Gabriela; Marti-Aldaravi, Pedro; and Viera, Alberto. "Near field visualization of diesel spray for different nozzle inclination angles in non-vaporizing conditions". In: *Atomization and Sprays* 27.3 (2017), pp. 251–267. DOI: 10.1615/AtomizSpr.2017017949 (cited on pages 24, 26, 70).

Payri, Raul; Bracho, Gabriela; Martí-Aldaraví, Pedro; and Viera, Alberto. "Nozzle geometry size influence on reactive spray development: from Spray B to heavy duty applications". In: *SAE Technical Paper 2017-01-0846* (2017), p. 12. DOI: 10.4271/2017-01-0846 (cited on page 30).

Payri, Raul; Climent, Hector; Salvador, Francisco Javier; and Favennec, A.-G. "Diesel Injection System Modelling. Methodology and Application for a First-generation Common Rail System". In: *Proceedings of the Institution of Mechanical Engineers, Part D: Journal of Automobile Engineering* 218.1 (2004), pp. 81–91. DOI: 10.1243/095440704322829191 (cited on page 100).

Payri, Raul; Garcia-Oliver, Jose Maria; Salvador, Francisco Javier; and Gimeno, Jaime. "Using spray momentum flux measurements to understand the influence of diesel nozzle geometry on spray characteristics". In: *Fuel* 84.5 (2005), pp. 551–561. DOI: 10.1016/j.fuel.2004.10.009 (cited on pages 19, 22, 49, 54, 56).

Payri, Raul; Gimeno, Jaime; Bardi, Michele; and Plazas, Alejandro Hernan. "Study liquid length penetration results obtained with a direct acting piezo electric injector". In: *Applied Energy* 106.JUNE (2013), pp. 152–162. DOI: 10.1016/j.apenergy.2013.01.027 (cited on pages 5, 24, 25, 107).

Payri, Raul; Gimeno, Jaime; Bracho, Gabriela; and Vaquerizo, Daniel. "Study of liquid and vapor phase behavior on Diesel sprays for heavy duty engine nozzles". In: *Applied Thermal Engineering* 107 (2016), pp. 365–378. DOI: 10.1016/j.applthermaleng.2016.06.159 (cited on pages 25, 63, 74, 107).

Payri, Raul; Gimeno, Jaime; Cardona, Santiago; and Ayyapureddi, Sridhar. "Measurement of Soot Concentration in a Prototype Multi-Hole Diesel Injector by High-Speed Color Diffused Back Illumination Technique". In: *SAE Technical Paper 2017-01-2255*. 2017, p. 11. DOI: 10.4271/2017-01-2255 (cited on pages 133, 138, 148).

Payri, Raul; Gimeno, Jaime; Cardona, Santiago; and Ayyapureddi, Sridhar. "Experimental study of the influence of the fuel and boundary conditions over the soot formation in multi-hole diesel injectors using high-speed color diffused back-illumination technique". In: *Applied Thermal Engineering* 158 (2019), p. 113746. DOI: 10.1016/J.APPLTHERMALENG.2019.113746 (cited on pages 70, 84).

Payri, Raul; Gimeno, Jaime; Cuisano, Julio; and Arco, Javier. "Hydraulic characterization of diesel engine single-hole injectors". In: *Fuel* 180 (2016), pp. 357–366. DOI: 10.1016/j.fuel.2016.03.083 (cited on page 5).

Payri, Raul; Gimeno, Jaime; Mata, Carmen; and Viera, Alberto. "Rate of injection measurements of a direct-acting piezoelectric injector for different operating temperatures". In: *Energy Conversion and Management* 154 (2018), pp. 387–393. DOI: 10.1016/j.enconman.2017.11.029 (cited on pages 19, 50, 52).

Payri, Raul; Gimeno, Jaime; Viera, Juan Pablo; and Plazas, Alejandro Hernan. "Needle lift profile influence on the vapor phase penetration for a prototype diesel direct acting piezoelectric injector". In: *Fuel* 113 (2013), pp. 257–265. DOI: 10.1016/j.fuel.2013.05.057 (cited on pages 19, 64).

Payri, Raul; Giraldo, Jhoan S.; Ayyapureddi, S.; and Versey, Z. "Experimental and analytical study on vapor phase and liquid penetration for a high pressure diesel injector". In: *Applied Thermal Engineering* 137.March (2018), pp. 721–728. DOI: 10.1016/j.applthermaleng.2018.03.097 (cited on page 61).

Payri, Raul; Hardy, Gilles; Gimeno, Jaime; and Bautista, Abian. "Analysis of counterbore effect in five diesel common rail injectors". In: *Experimental Thermal and Fluid Science* 107.February (2019), pp. 69–78. DOI: 10.1016/j.expthermflusci.2019.05.008 (cited on pages 20, 49, 58).

Payri, Raul; Martí-Aldavarí, Pedro; Montiel, Tomas; and Viera, Alberto. "Influence of aging of a diesel injector on multiple injection strategies". In: *Applied Thermal Engineering* 181.August (2020), p. 115891. DOI: 10.1016/j.applthermaleng.2020.115891 (cited on pages 20, 46, 50, 58).

Payri, Raul; Molina, Santiago; Salvador, Francisco Javier; and Gimeno, Jaime. "A study of the relation between nozzle geometry, internal flow and sprays characteristics in diesel fuel injection systems". In: *KSME International Journal* 18.7 (2004), pp. 1222–1235. DOI: 10.1007/BF02983297 (cited on page 26).

Payri, Raul; Salvador, Francisco Javier; Bracho, Gabriela; and Viera, Alberto. "Differences between single and double-pass schlieren imaging on diesel vapor spray characteristics". In: *Applied Thermal Engineering* 125 (2017), pp. 220–231. DOI: 10.1016/j.applthermaleng.2017.06.140 (cited on pages 63, 64, 74, 75).

Payri, Raul; Salvador, Francisco Javier; Garcia, Antonio; and Gil, Antonio. "Combination of visualization techniques for the analysis of evaporating diesel sprays". In: *Energy and Fuels* 26 (2012), pp. 5481–5490. DOI: 10.1021/ef3008823 (cited on page 64).

Payri, Raul; Salvador, Francisco Javier; Gimeno, Jaime; and Bracho, Gabriela. "A new methodology for correcting the signal cumulative phenomenon on injection rate measurements". In: *Experimental Techniques* 32.February (2008), pp. 46–49. DOI: 10.1111/j.1747-1567.2007.00188.x (cited on pages 52, 57).

Payri, Raul; Salvador, Francisco Javier; Gimeno, Jaime; and Bracho, Gabriela. "The effect of temperature and pressure on thermodynamic properties of diesel and biodiesel fuels". In: *Fuel* 90.3 (2011), pp. 1172–1180. DOI: 10.1016/j.fuel.2010.11.015 (cited on pages 50, 51).

Payri, Raul; Salvador, Francisco Javier; Gimeno, Jaime; and Peraza, Jesús E. "Experimental study of the injection conditions influence over n-dodecane and diesel sprays with two ECN single-hole nozzles. Part II: Reactive atmosphere". In: *Energy Conversion and Management* 126 (2016), pp. 1157–1167. DOI: 10.1016/j.enconman.2016.07.079 (cited on page 5).

Payri, Raul; Salvador, Francisco Javier; Gimeno, Jaime; and Viera, Alberto. "Effect of Injection Rate Shaping over Diesel Spray Development in Non-Reacting Evaporative Conditions". In: *10. Tagung Diesel- und Benzindirekteinspritzung 2016*. Ed. by Helmut Tschöke; and Ralf Marohn. 1. Springer Vieweg, 2016, pp. 133–152. DOI: 10.1007/978-3-658-15327-4 (cited on pages 74, 132).

Payri, Raul; Salvador, Francisco Javier; Manin, Julien; and Viera, Alberto. "Diesel ignition delay and lift-off length through different methodologies using a multi-hole injector". In: *Applied Energy* 162 (2016), pp. 541–550. DOI: 10.1016/j.apenergy.2015.10.118 (cited on pages 5, 28–30, 63, 115, 138).

Payri, Raul; Salvador, Francisco Javier; Martí-Aldaraví, Pedro; and Vaquerizo, Daniel. "ECN Spray G external spray visualization and spray collapse description through penetration and morphology analysis". In: *Applied Thermal Engineering* 112 (2017), pp. 304–316. DOI: 10.1016/j.applthermaleng.2016.10.023 (cited on page 64).

Payri, Raul; Tormos, Bernardo; Salvador, Francisco Javier; and Plazas, Alejandro Hernan. "Using one-dimensional modelling codes to analyse the influence of diesel nozzle geometry on injection rate characteristics". In: *International Journal of Vehicle Design* 38.1 (2005), pp. 58–78 (cited on page 45).

Payri, Raul; Viera, Juan Pablo; Gopalakrishnan, Venkatesh; and Szymkowicz, Patrick G. "The effect of nozzle geometry over internal flow and spray formation for three different fuels". In: *Fuel* 183 (2016), pp. 20–33. DOI: 10.1016/j.fuel.2016.06.041 (cited on page 3).

Payri, Raul; Viera, Juan Pablo; Gopalakrishnan, Venkatesh; and Szymkowicz, Patrick G. "The effect of nozzle geometry over ignition delay and flame lift-off of reacting direct-injection sprays for three different fuels". In: *Fuel* 199 (2017), pp. 76–90. DOI: 10.1016/j.fuel.2017.02.075 (cited on pages 29, 63).

Payri, Raul; Viera, Juan Pablo; Gopalakrishnan, Venkatesh; and Szymkowicz, Patrick G. "The effect of nozzle geometry over the evaporative spray formation for three different fuels". In: *Fuel* 188 (2017), pp. 645–660. DOI: 10.1016/j.fuel.2016.06.041 (cited on page 75).

Payri, Raul; Viera, Juan Pablo; Pei, Yuanjiang; and Som, Sibendu. "Experimental and numerical study of lift-off length and ignition delay of a two-component diesel surrogate". In: *Fuel* 158 (2015), pp. 957–967. DOI: 10.1016/j.fuel.2014.11.072 (cited on pages 28, 29, 63, 74).

Persson, Helena; Andersson, Öivind; and Egnell, Rolf. "Fuel effects on flame lift-off under diesel conditions". In: *Combustion and Flame* 158.1 (2011), pp. 91–97. DOI: 10.1016/j.combustflame.2010.07.020 (cited on pages 68, 121).

Pickett, Lyle M; Kook, Sanghoon; Persson, Helena; and Andersson, Öivind. "Diesel fuel jet lift-off stabilization in the presence of laser-induced plasma ignition". In: *Proceedings of the Combustion Institute* 32 (2009), pp. 2793–2800. DOI: 10.1016/j.proci.2008.06.082 (cited on pages 29, 30, 121).

Pickett, Lyle M et al. "Relationship Between Diesel Fuel Spray Vapor Penetration/Dispersion and Local Fuel Mixture Fraction". In: *SAE International Journal of Engines* 4.1 (2011), pp. 764–799. DOI: 10.4271/2011-01-0686 (cited on page 64).

Pickett, Lyle M.; Siebers, Dennis L.; and Idicheria, Cherian A. "Relationship Between Ignition Processes and the Lift-Off Length of Diesel Fuel Jets". In: *SAE Paper 2005-01-3843* 724 (2005). DOI: 10.4271/2005-01-3843 (cited on pages 27–30, 115, 138).

Plamondon, E.; and Seers, P. "Development of a simplified dynamic model for a piezoelectric injector using multiple injection strategies with biodiesel/diesel-fuel blends". In: *Applied Energy* 131 (2014), pp. 411–424. DOI: 10.1016/j.apenergy.2014.06.039 (cited on page 100).

Potter, Mike; and Durrett, Russell P. "High-Efficiency Clean Combustion Design for Compression Ignition Engines". In: *Diesel Engine-Efficiency and Emissions Research (DEER)*. Detroit, 2006 (cited on pages 138, 149).

Reitz, R. D. et al. "IJER editorial: The future of the internal combustion engine". In: *International Journal of Engine Research* 21.1 (2020), pp. 3–10. DOI: 10.1177/1468087419877990 (cited on page 2).

Ritchie, Hannah; and Roser, Max. *Emissions by sector*. 2020 (cited on pages 2, 3).

Rusly, Alvin M.; Le, Minh K.; Kook, Sanghoon; and Hawkes, Evatt R. "The shortening of lift-off length associated with jet-wall and jet-jet interaction in a small-bore optical diesel engine". In: *Fuel* 125 (2014), pp. 1–14. DOI: 10.1016/j.fuel.2014.02.004 (cited on pages 4, 31).

Salvador, Francisco Javier. "Estudio teórico experimental de la influencia de la geometría de toberas de inyección Diésel sobre las características del flujo interno y del chorro". PhD thesis. Valencia: E.T.S. Ingenieros Industriales. Universidad Politécnica de Valencia, 2003 (cited on pages 20, 58).

Salvador, Francisco Javier; De la Morena, Joaquin; Crialesi-Esposito, Marco; and Martínez-López, Jorge. "Comparative study of the internal flow in diesel injection nozzles at cavitating conditions at different needle lifts with steady and transient simulations approaches". In: *Proceedings of the Institution of Mechanical Engineers, Part D: Journal of Automobile Engineering* 232.8 (2018), pp. 1060–1078. DOI: 10.1177/0954407017725672 (cited on page 22).

Salvador, Francisco Javier; Gimeno, Jaime; Carreres, Marcos; and Crialesi-Esposito, Marco. "Fuel temperature influence on the performance of a last generation common-rail diesel ballistic injector. Part I: Experimental mass flow rate measurements and discussion". In: *Energy Conversion and Management* 114 (2016), pp. 364–375. DOI: 10.1016/j.enconman.2016.02.042 (cited on pages 20, 50–52).

Salvador, Francisco Javier; Martínez-López, Jorge; Caballer, M.; and De Alfonso, C. "Study of the influence of the needle lift on the internal flow and cavitation phenomenon in diesel injector nozzles by CFD using RANS methods". In: *Energy Conversion and Management* 66 (2013), pp. 246–256. DOI: 10.1016/j.enconman.2012.10.011 (cited on page 22).

Sayin, Cenk; Gumus, Metin; and Canakci, Mustafa. "Influence of injector hole number on the performance and emissions of a di diesel engine fueled with biodiesel-diesel fuel blends". In: *Applied Thermal Engineering* 61.2 (2013), pp. 121–128. DOI: 10.1016/j.applthermaleng.2013.07.038 (cited on pages 3, 31).

Settles, G. S. *Schlieren and Shadowgraph Techniques*. Berlin, Heidelberg: Springer Berlin Heidelberg, 2001, p. 376. DOI: 10.1007/978-3-642-56640-0 (cited on pages 63, 64).

Shi, J et al. "Using LES and x - ray imaging to understand the influence of injection hole geometry on Diesel spray formation". In: *THIESEL 2016 Conference on Thermo- and Fluid Dynamic Processes in Diesel EnginesConference on Thermo and Fluid Dynamic* (2016), pp. 1–21 (cited on page 3).

Siebers, Dennis L. "Liquid-Phase Fuel Penetration in Diesel Sprays". In: *SAE Technical Paper 980809* (1998), pp. 1–23. DOI: 10.4271/980809 (cited on pages 24, 25, 138).

Siebers, Dennis L. "Scaling liquid-phase fuel penetration in diesel sprays based on mixing-limited vaporization". In: *SAE Technical Paper 1999-01-0528* (1999). DOI: 10.4271/1999-01-0528 (cited on pages 24, 25, 107, 138).

Siebers, Dennis L; and Higgins, Brian. "Flame Lift-Off on Direct-Injection Diesel Sprays Under Quiescent Conditions". In: *SAE Technical Paper 2001-01-0530* 724 (2001) (cited on pages 28–31, 123, 124, 138).

Skeen, Scott A; Manin, Julien; Dalen, Kristine; and Pickett, Lyle M. "Extinction-based Imaging of Soot Processes over a Range of Diesel Operating Conditions". In: *8th US National Combustion Meeting*. Utah, USA, 2013, pp. 1–13 (cited on pages 83, 84, 132, 148).

Smyth, Kermit C.; and Shaddix, Christopher R. "The elusive history of m = 1.57 - 0.56i for the refractive index of soot". In: *Combustion and Flame* 107.3 (1996), pp. 314–320. DOI: 10.1016/S0010-2180(96)00170-8 (cited on page 84).

Som, Sibendu et al. "Effect of nozzle orifice geometry on spray, combustion, and emission characteristics under diesel engine conditions". In: *Fuel* 90.3 (2011), pp. 1267–1276. DOI: 10.1016/j.fuel.2010.10.048 (cited on page 49).

Sorensen, Christopher M. "Light Scattering by Fractal Aggregates: A Review". In: *Aerosol Science and Technology* 35.2 (2001), pp. 648–687. DOI: 10.1080/02786820117868 (cited on page 84).

Suh, Hyun Kyu; Park, Sung Wook; and Lee, Chang Sik. "Effect of piezo-driven injection system on the macroscopic and microscopic atomization characteristics of diesel fuel spray". In: *Fuel* 86.17-18 (2007), pp. 2833–2845. DOI: 10.1016/j.fuel.2007.03.015 (cited on page 19).

Taskiran, Ozgur Oguz; and Ergeneman, Metin. "Effect of nozzle dimensions and fuel type on flame lift-off length". In: *Fuel* 115 (2014), pp. 833–840. DOI: 10.1016/j.fuel.2013.03.005 (cited on pages 29, 30).

Taylor, Charles Fayette. *The internal-combustion engine in theory and practice*. 2nd ed. Cambridge: MIT Press, 1989 (cited on pages 15, 22).

Venegas, Oscar. "Estudio del fenómeno de la cavitación en la inyección diesel mediante la visualización del flujo interno en orificios transparentes." PhD thesis. Universitat Politècnica de València, 2014. DOI: 10.4995/Thesis/10251/37375 (cited on page 52).

Viera, Alberto. “Effect of multiple injection strategies on the diesel spray formation and combustion using optical diagnostics”. PhD thesis. Universitat Politècnica de València, 2019. DOI: 10.4995/Thesis/10251/123954 (cited on pages 5, 22, 24, 26, 30, 54, 78, 96).

Viera, Juan Pablo. “Experimental study of the effect of nozzle geometry on the performance of direct-injection diesel sprays for three different fuels”. PhD thesis. 2017. DOI: 10.4995/Thesis/10251/81857 (cited on pages 5, 19, 100).

Viera, Juan Pablo et al. “Linking instantaneous rate of injection to X-ray needle lift measurements for a direct-acting piezoelectric injector”. In: *Energy Conversion and Management* 112 (2016), pp. 350–358. DOI: 10.1016/j.enconman.2016.01.038 (cited on page 19).

Wan, Yuepeng; and Peters, Norbert. “Scaling of spray penetration with evaporation”. In: *Atomization and Sprays* 9.2 (1999), pp. 111–132. DOI: 10.1615/AtomizSpr.v9.i2.10 (cited on pages 26, 110).

Wang, Xiangang; Huang, Zuohua; Zhang, Wu; Abiola, Olawole; and Nishida, Keiya. “Effects of ultra-high injection pressure and micro-hole nozzle on flame structure and soot formation of impinging diesel spray”. In: *Applied Energy* 88.5 (2011), pp. 1620–1628. DOI: 10.1016/j.apenergy.2010.11.035 (cited on page 3).

Westbrook, C K et al. “The effects of pressure, temperature, and concentration on the reactivity of alkanes: Experiments and modeling in a rapid compression machine”. In: *International Symposium on Combustion* 27.1 (1998), pp. 371–378. DOI: 10.1016/S0082-0784(98)80425-6 (cited on page 27).

Williams, T.C.; Shaddix, C.R.; Jensen, K.A.; and Suo-Anttila, J.M. “Measurement of the dimensionless extinction coefficient of soot within laminar diffusion flames”. In: *International Journal of Heat and Mass Transfer* 50.7 (2007), pp. 1616–1630. DOI: 10.1016/j.ijheatmasstransfer.2006.08.024 (cited on page 83).

Wu, J. S.; Krishnan, S. S.; and Faeth, G. M. “Refractive indices at visible wavelengths of soot emitted from buoyant turbulent diffusion flames”. In: *Journal of Heat Transfer* 119.2 (1997), pp. 230–237. DOI: 10.1115/1.2824213 (cited on page 84).

Wu, K J; Su, C C; Steinberger, R L; Santavicca, D A; and Bracco, Frediano V. “Measurements of the spray angle of atomizing jets”. In: *Journal of fluids Engineering* 105.4 (1983), pp. 406–410. DOI: 10.1115/1.3241019 (cited on page 26).

Xi, Jun; and Zhong, Bei Jing. "Soot in diesel combustion systems". In: *Chemical Engineering and Technology* 29.6 (2006), pp. 665–673. DOI: 10.1002/ceat.200600016 (cited on page 29).

Xu, Qinglin et al. "Diesel Spray Characterization at Ultra-High Injection Pressure of DENSO 250 MPa Common Rail Fuel Injection System". In: *SAE Technical Paper*. SAE International, 2017. DOI: 10.4271/2017-01-0821 (cited on page 3).

Xuan, Tiemin. "Optical investigations on diesel spray dynamics and in-flame soot formation". PhD thesis. Universitat Politècnica de València, 2017. DOI: 10.4995/Thesis/10251/94626 (cited on pages 5, 70, 83, 84, 132, 133, 138, 142, 148).

Xuan, Tiemin et al. "In-flame soot quantification of diesel sprays under sooting/non-sooting critical conditions in an optical engine". In: *Applied Thermal Engineering* 149.301 (2019), pp. 1–10. DOI: 10.1016/j.applthermaleng.2018.11.112 (cited on page 84).

Yasutomi, Koji; and Skeen, Scott A. "Observations of soot optical property characteristics using high-speed, multiple wavelength, extinction imaging in heavy-duty diesel sprays". In: *10th U.S. National Combustion Meeting* 2017-April (2017), pp. 1–11. DOI: 10.4271/2018-01-0233.Abstract (cited on pages 83, 84).

Yon, J. et al. "Examination of wavelength dependent soot optical properties of diesel and diesel/rapeseed methyl ester mixture by extinction spectra analysis and LII measurements". In: *Applied Physics B: Lasers and Optics* 104.2 (2011), pp. 253–271. DOI: 10.1007/s00340-011-4416-4 (cited on page 84).

Zhou, L. Y. et al. "Measurements and analyses on the transient discharge coefficient of each nozzle hole of multi-hole diesel injector". In: *Sensors and Actuators, A: Physical* 244 (2016), pp. 198–205. DOI: 10.1016/j.sna.2016.04.017 (cited on pages 4, 31).

# Appendices

## Appendix A

# Graph Appendix

## A.1 KL maps

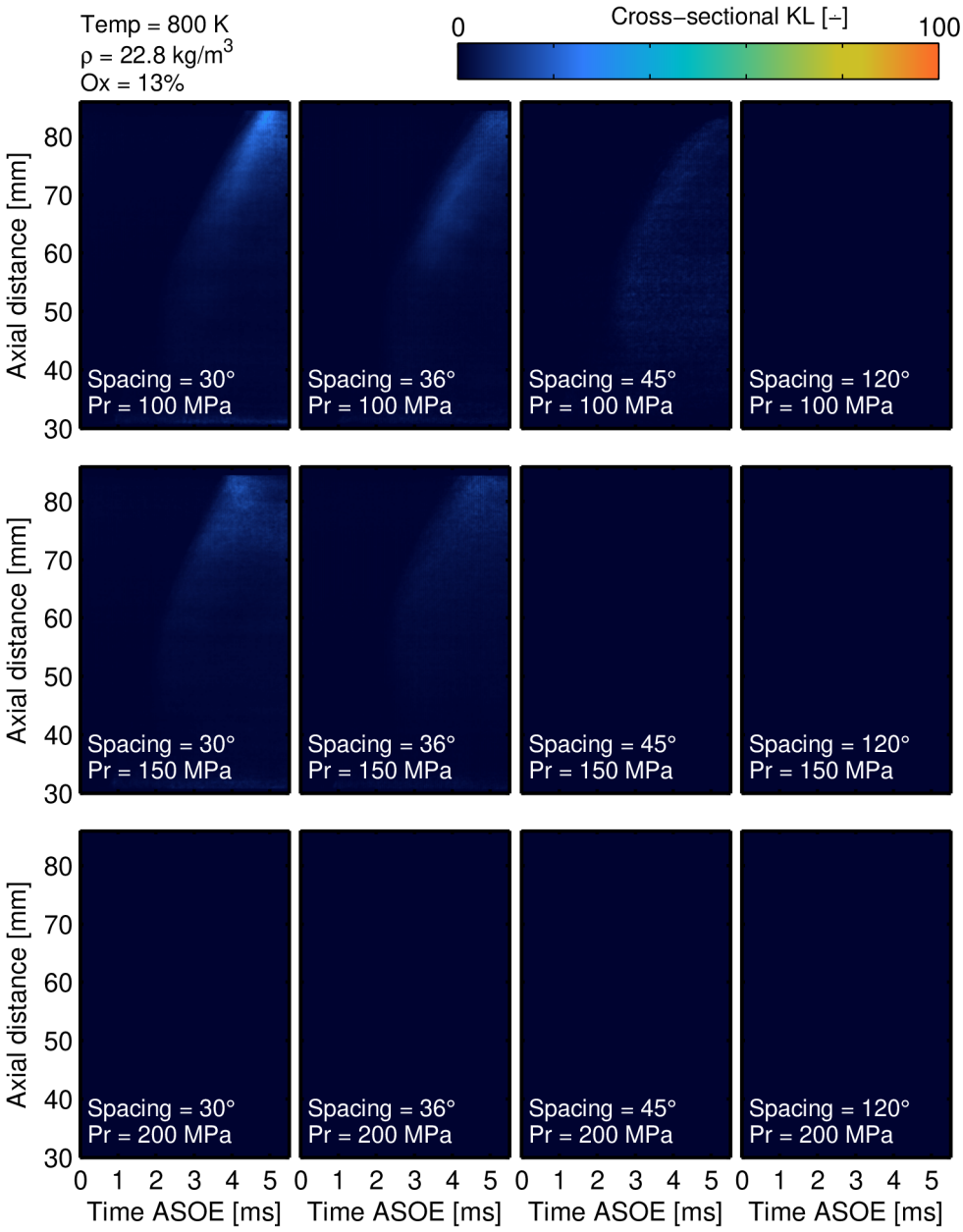


*Figure A.1: KL maps for every inter-jet spacing configuration and injection pressure. Ambient temperature = 800 K, ambient density = 22.8 kg/m$^3$, oxygen concentration = 13%.*

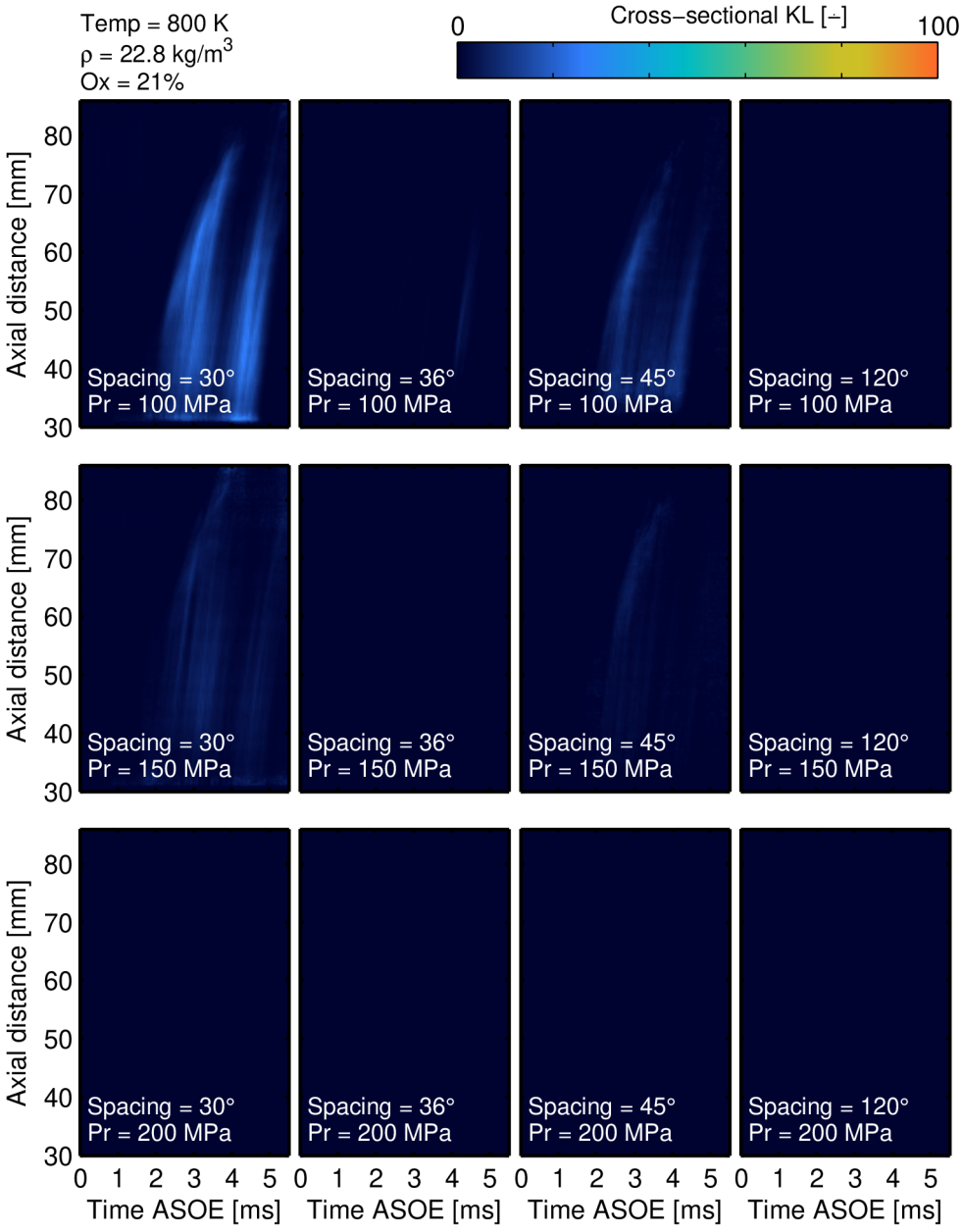


*Figure A.2: KL maps for every inter-jet spacing configuration and injection pressure. Ambient temperature = 800 K, ambient density = 22.8 kg/m$^3$, oxygen concentration = 21%.*

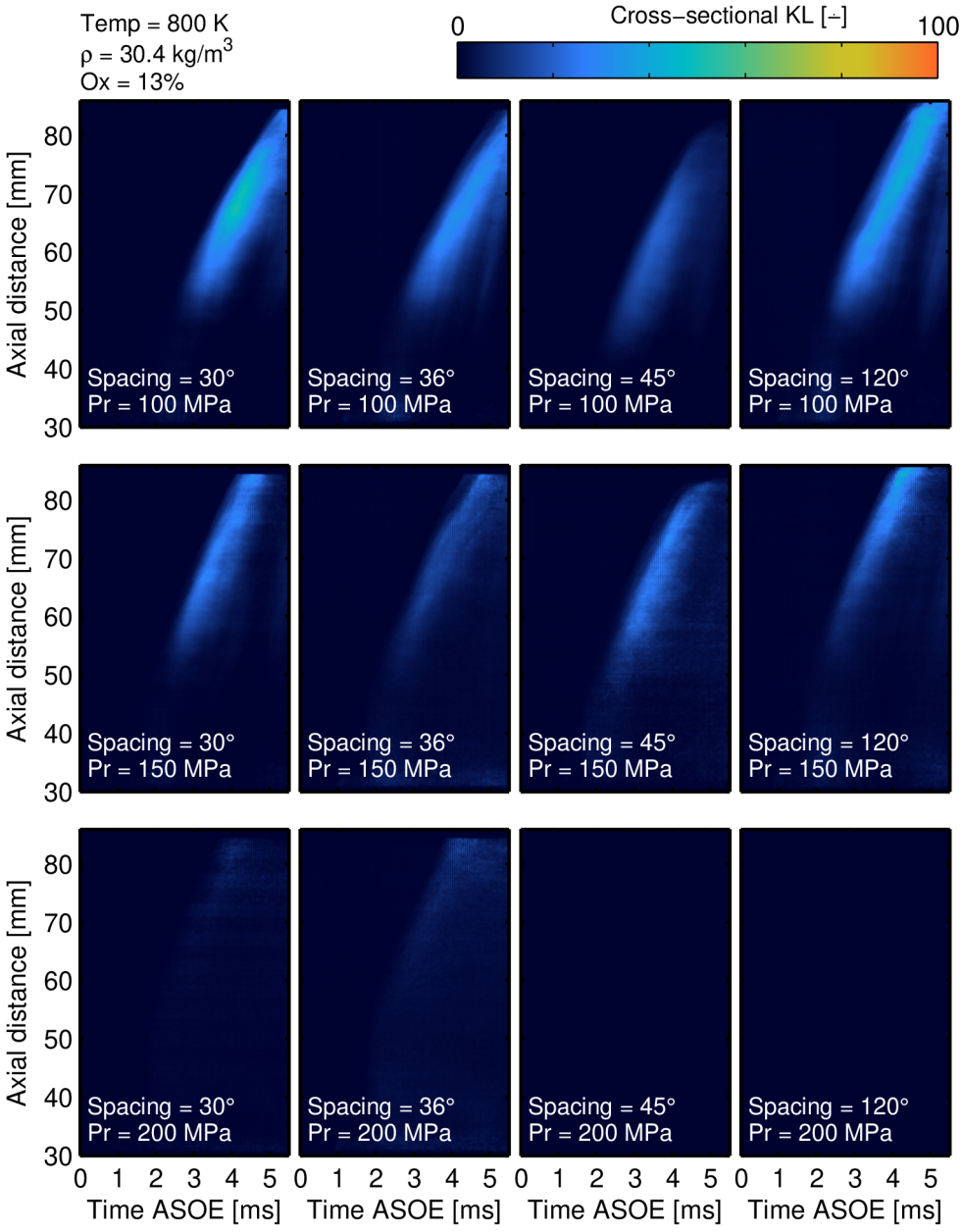


*Figure A.3: KL maps for every inter-jet spacing configuration and injection pressure. Ambient temperature = 800 K, ambient density = 30.4 kg/m$^3$, oxygen concentration = 13%.*

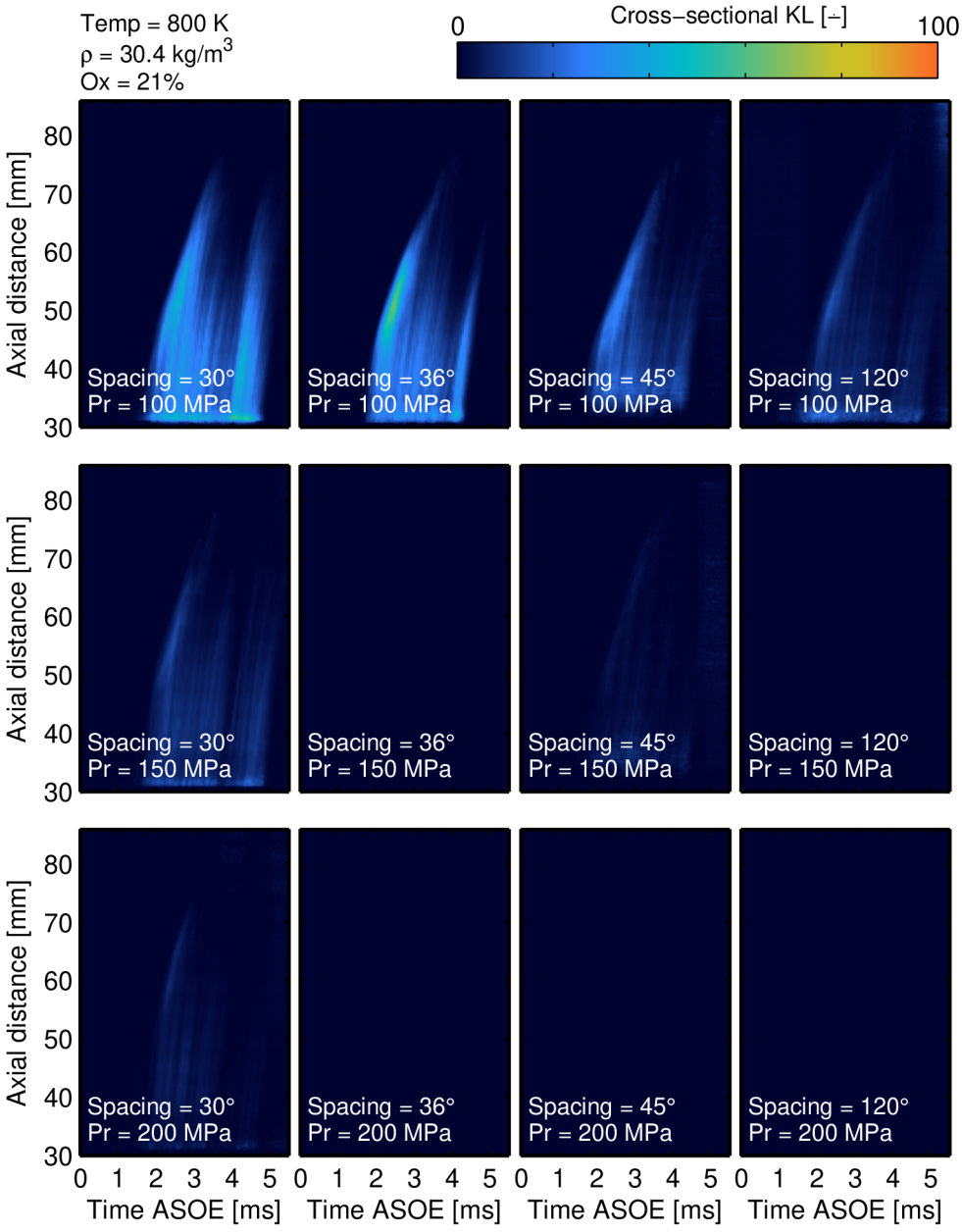


*Figure A.4: KL maps for every inter-jet spacing configuration and injection pressure. Ambient temperature = 800 K, ambient density = 30.4 kg/m$^3$, oxygen concentration = 21%.*

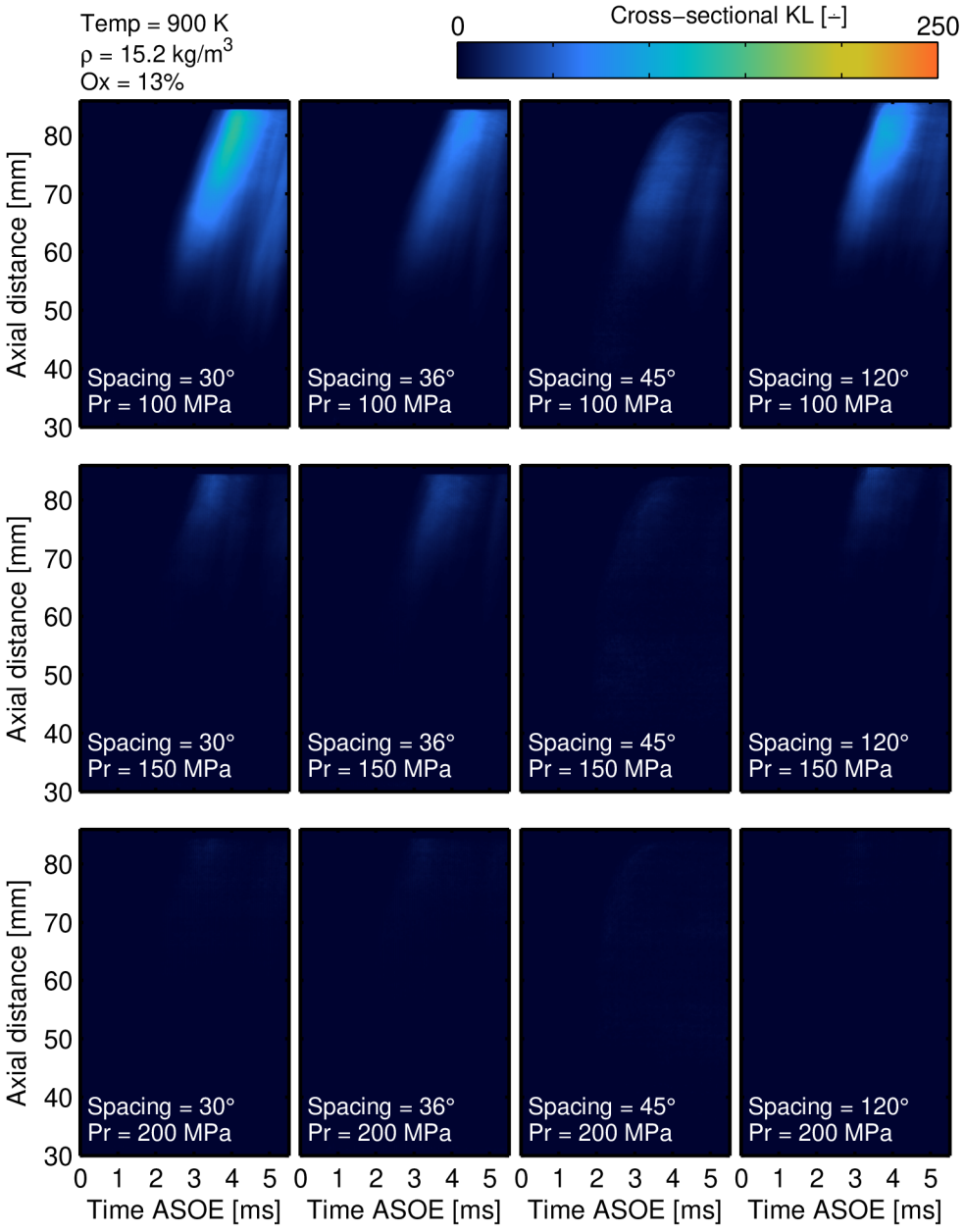


*Figure A.5: KL maps for every inter-jet spacing configuration and injection pressure. Ambient temperature = 900 K, ambient density = 15.2 kg/m$^3$, oxygen concentration = 13%.*

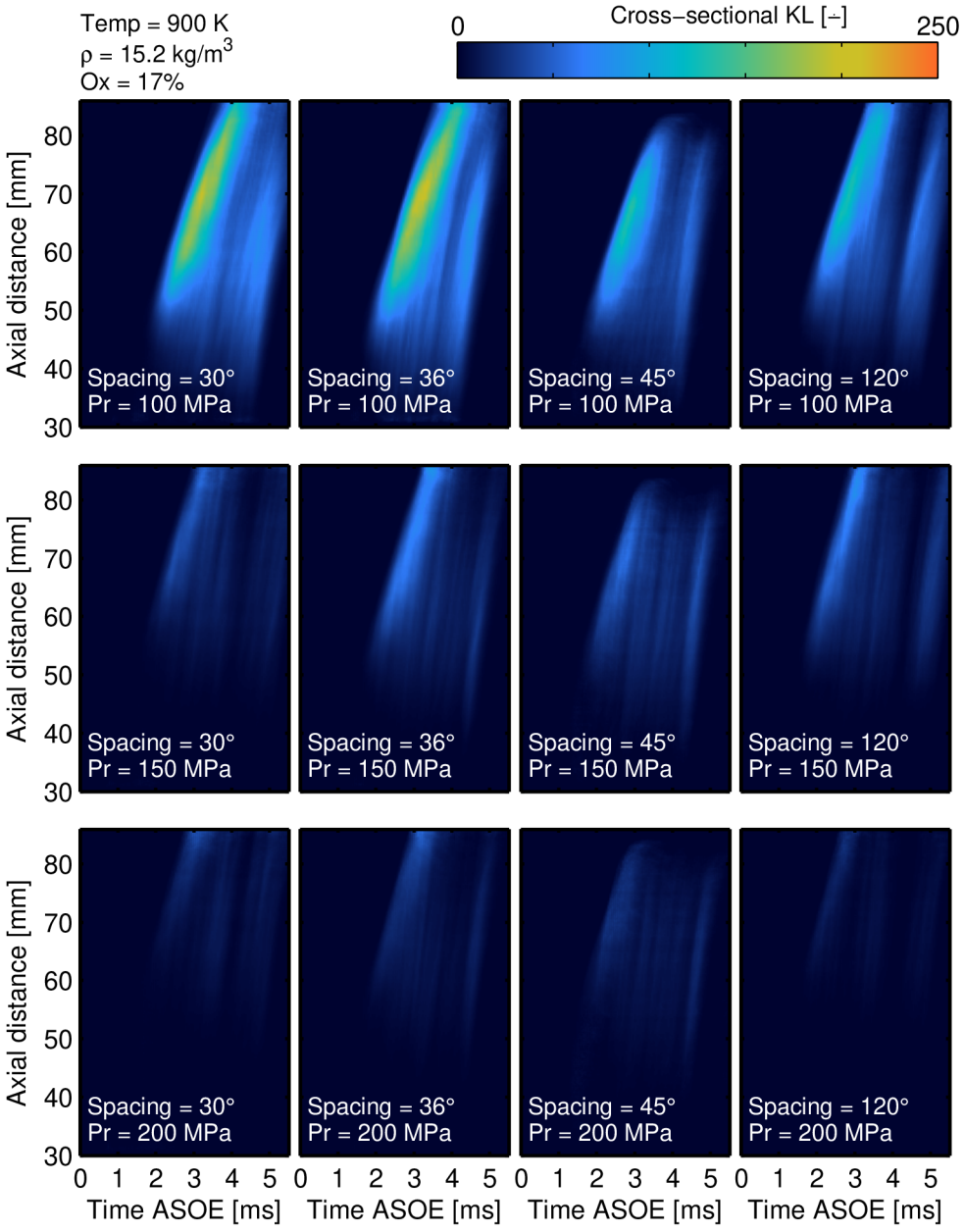


*Figure A.6: KL maps for every inter-jet spacing configuration and injection pressure. Ambient temperature = 900 K, ambient density = 15.2 kg/m$^3$, oxygen concentration = 17%.*

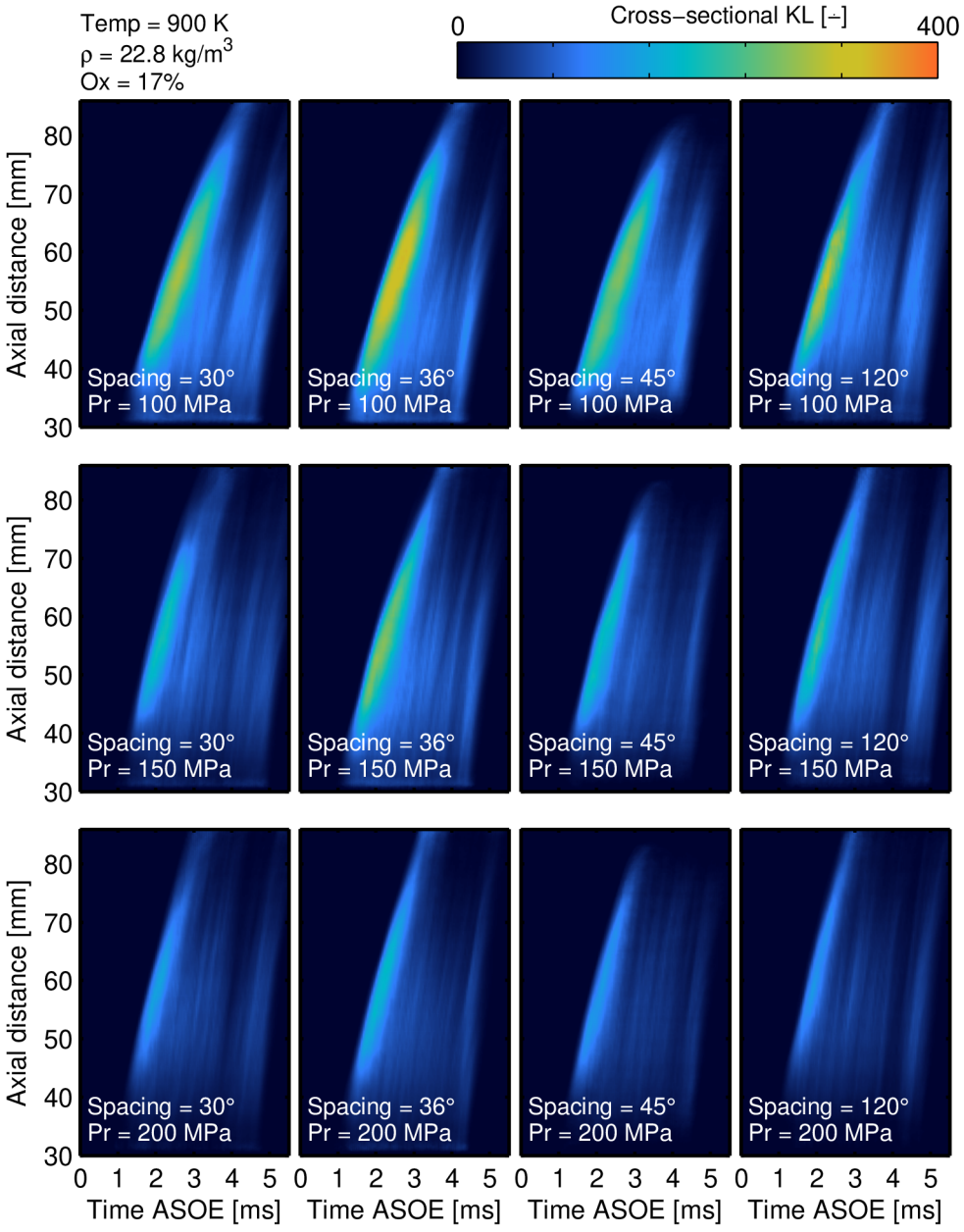


*Figure A.7: KL maps for every inter-jet spacing configuration and injection pressure. Ambient temperature = 900 K, ambient density = 22.8 kg/m$^3$, oxygen concentration = 17%.*

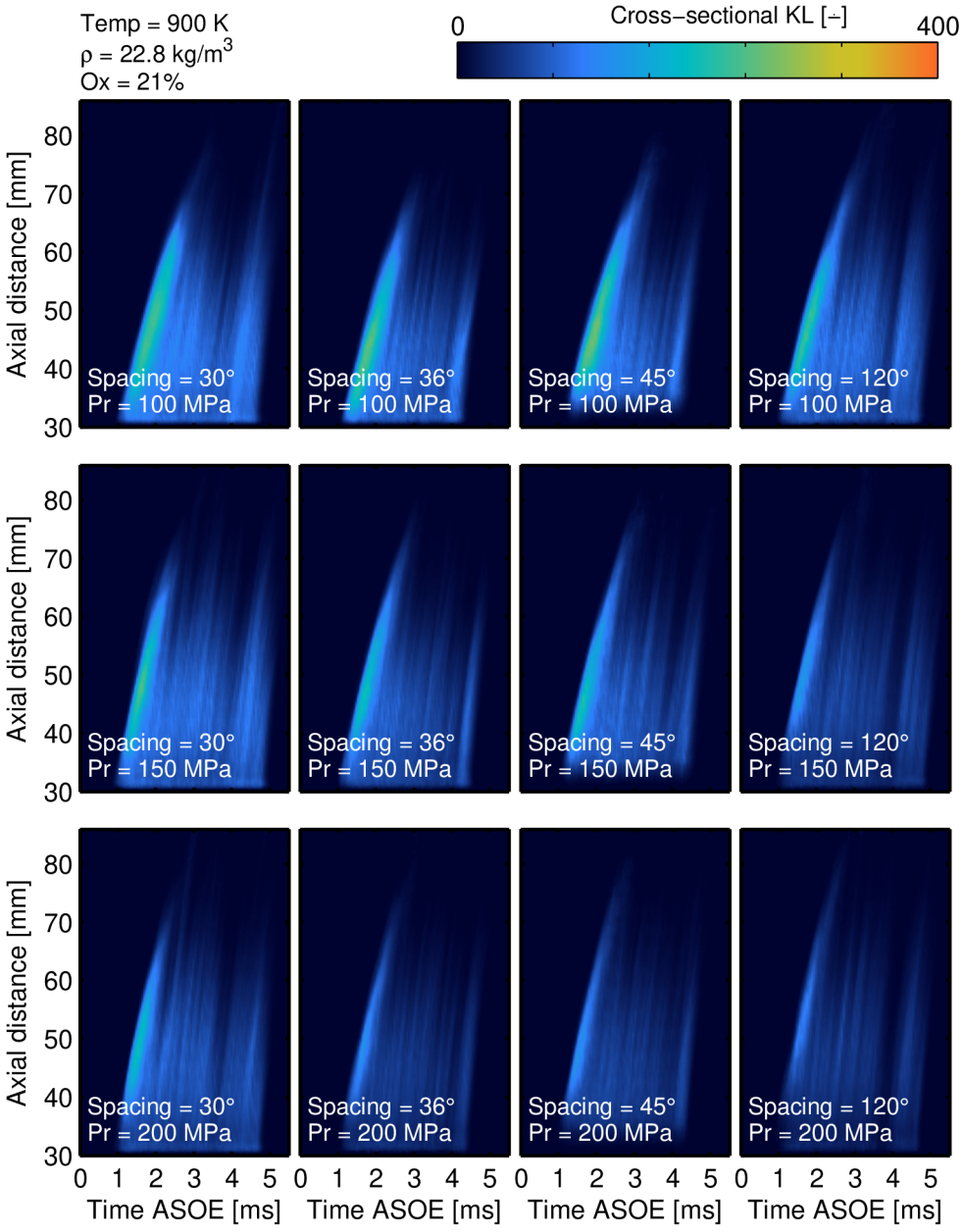


*Figure A.8: KL maps for every inter-jet spacing configuration and injection pressure. Ambient temperature = 900 K, ambient density = 22.8 kg/m$^3$, oxygen concentration = 21%.*

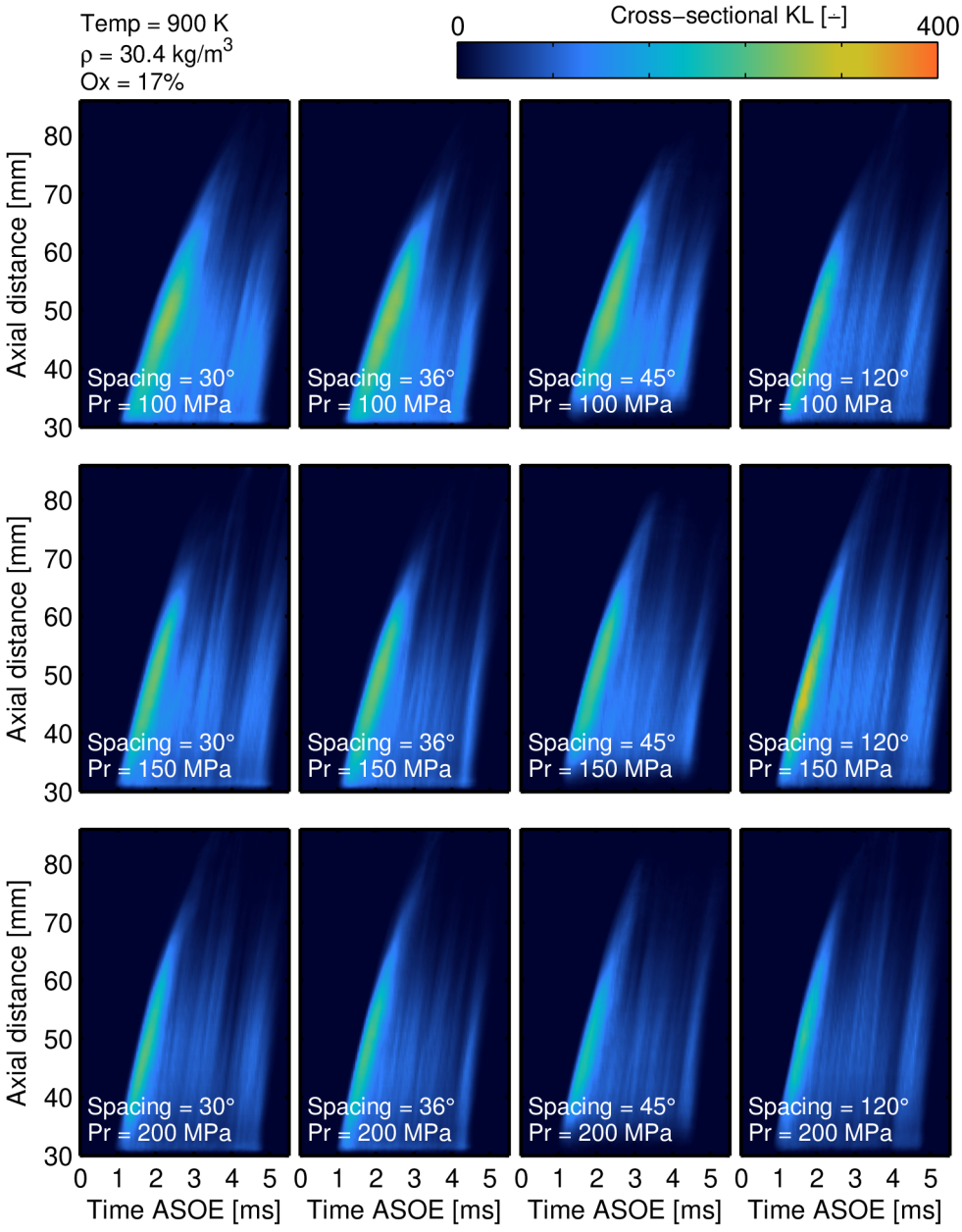


*Figure A.9: KL maps for every inter-jet spacing configuration and injection pressure. Ambient temperature = 900 K, ambient density = 30.4 kg/m$^3$, oxygen concentration = 17%.*

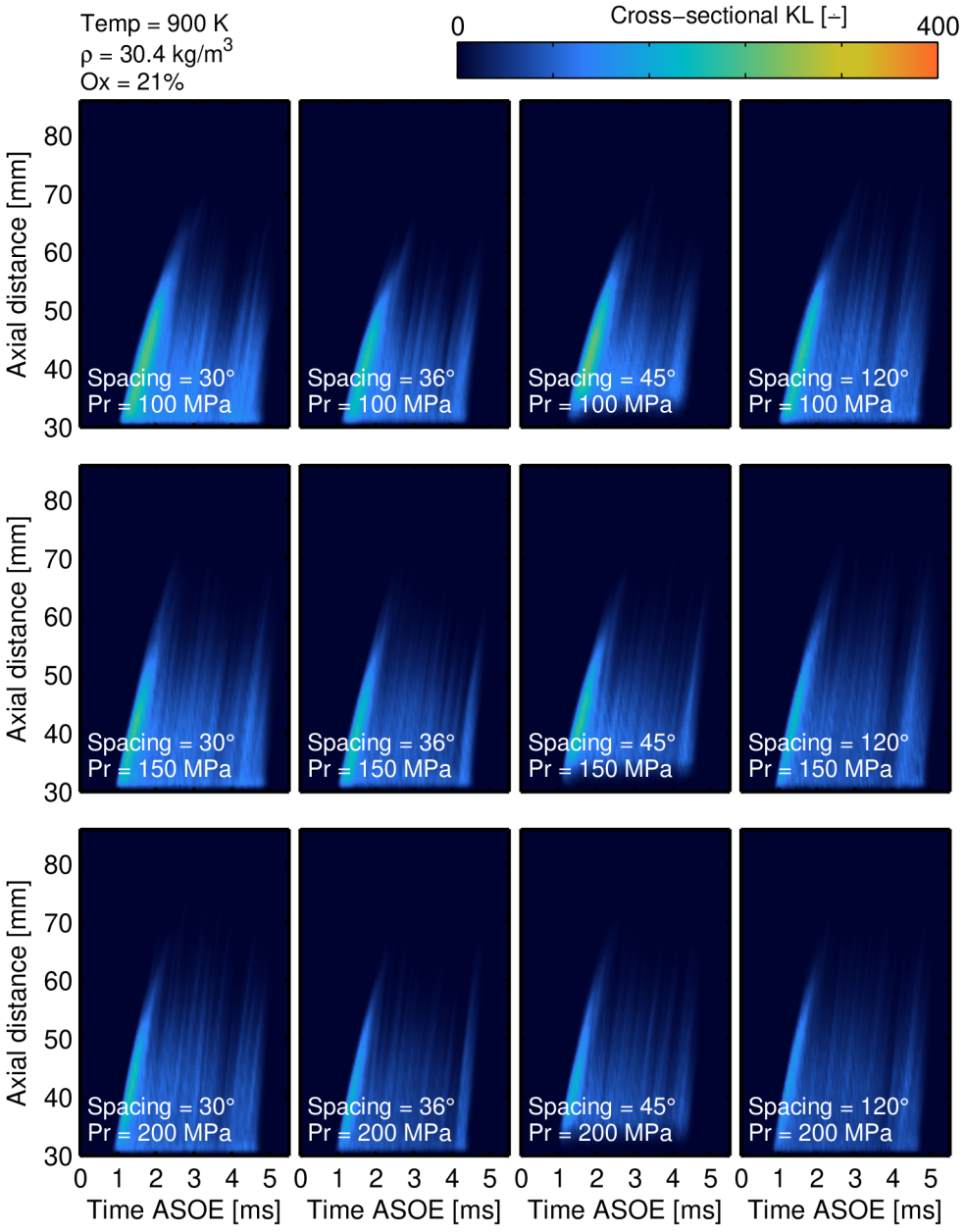


*Figure A.10: KL maps for every inter-jet spacing configuration and injection pressure. Ambient temperature = 900 K, ambient density = 30.4 kg/m$^3$, oxygen concentration = 21%.*

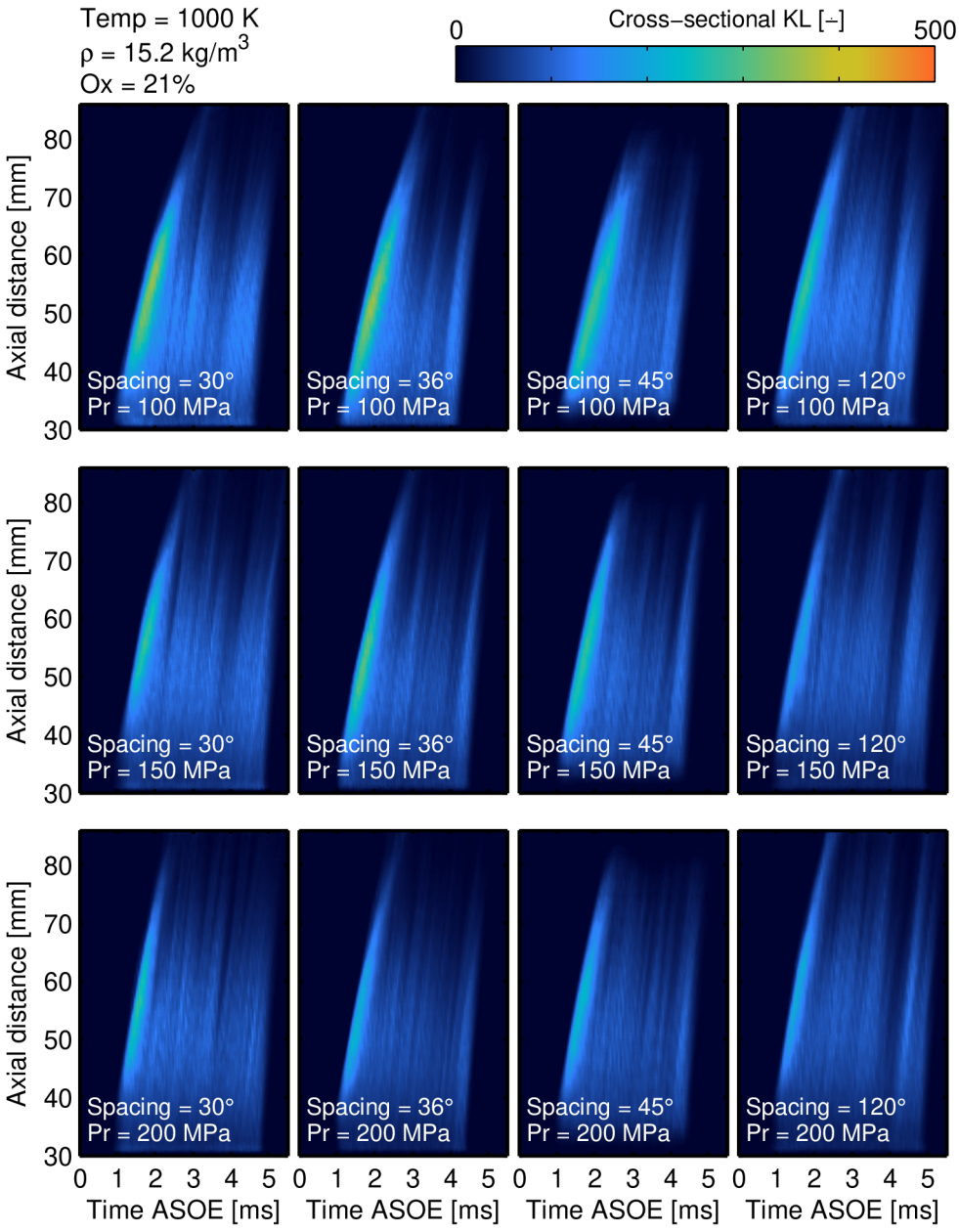


*Figure A.11: KL maps for every inter-jet spacing configuration and injection pressure. Ambient temperature = 1000 K, ambient density = 15.2 kg/m$^3$, oxygen concentration = 21%.*

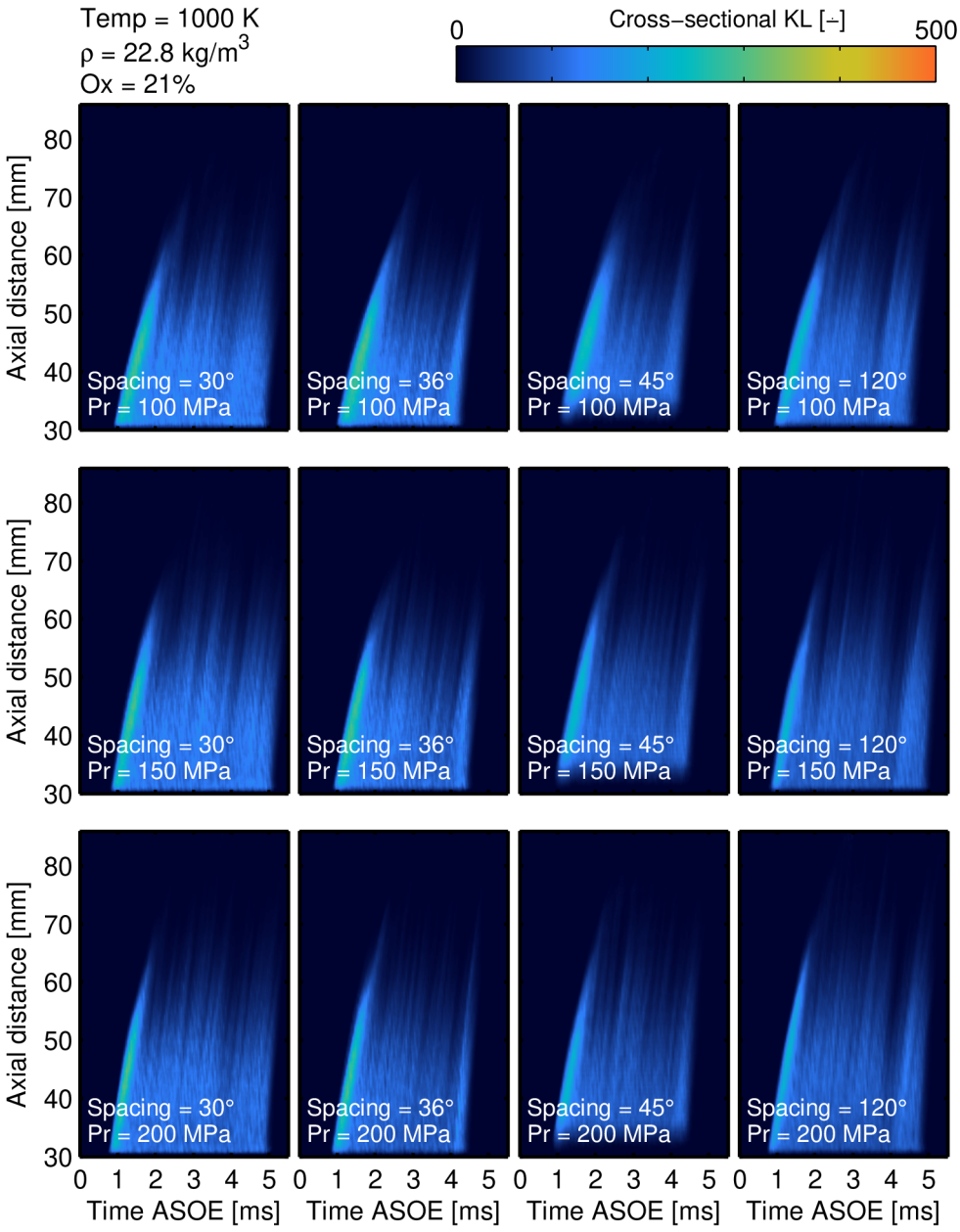


*Figure A.12: KL maps for every inter-jet spacing configuration and injection pressure. Ambient temperature = 1000 K, ambient density = 22.8 kg/m$^3$, oxygen concentration = 21%.*